

**STUDIES ON THE CHARACTERISTICS OF TROPOSPHERE  
AND LOWER STRATOSPHERE ASSOCIATED WITH THE  
PASSAGE OF TROPICAL CYCLONES**



*Thesis submitted to the*

**Cochin University of Science and Technology**

*in partial fulfillment of the requirement for the degree of*

**DOCTOR OF PHILOSOPHY**

*in*

**ATMOSPHERIC SCIENCE**

*By*

**MRUDULA G.**

**Department of Atmospheric Sciences**  
Cochin University of Science and Technology  
Lakeside Campus, Cochin – 682016

**MAY 2005**



**COCHIN UNIVERSITY OF SCIENCE AND TECHNOLOGY**  
**DEPARTMENT OF ATMOSPHERIC SCIENCES**

Lakeside Campus, Fine Arts Avenue, Cochin - 682 016, India.


**Dr. K. Mohankumar M.Sc., Ph.D.**  
Professor

**CERTIFICATE**

This is to certify that the thesis entitled ***Studies on the Characteristics of Troposphere and Lower Stratosphere Associated with the Passage of Tropical Cyclones*** is a bonafide record of the research work done by **Ms. Mrudula G., M.Sc**, in the Department of Atmospheric Sciences, Cochin University of Science and Technology. She carried out the study reported in this thesis, independently under my supervision. I also certify that the subject matter of the thesis has not formed the basis for the award of any Degree or Diploma of any University or Institution.

Certified that Ms. Mrudula G. has passed the Ph. D qualifying examination conducted by the Cochin University of Science and Technology in February, 2001.

Cochin- 682016  
May 21, 2005

  
K. MOHAN KUMAR  
Supervising Guide

## PREFACE

Tropical cyclones are most devastating weather phenomena which affect human life very much. They are violent whirls spiraling up from warm waters to great heights even above the tropopause. Many studies are going on around the world to determine the track and intensity of the cyclones, in which most studies are confined to middle and high latitudes. Very few studies are reported from tropical region. MST radar is an excellent tool for studying various features of the atmosphere from ground to mesospheric heights, as it can be operated continuously with good time and altitude resolution. This instrument can be used in cyclone studies to understand the characteristics of the atmosphere during the passage of cyclones.

In the present thesis work, an attempt has been made to study the characteristics of troposphere and lower stratosphere during the passage of tropical cyclones from a tropical station in India using MST radar. Special observations were carried out using MST radar at Gadanki (13.5°N, 79.2°E) during the years 2001-2004 for studying the atmospheric characteristics during cyclone passage.

The thesis consists of 8 chapters. An introduction to the study has been presented in chapter 1. Chapter 2 gives a brief review of literature obtained from published journals, reports and books. A description of the observation techniques and methods of data analysis is presented in Chapter 3.

Chapters 4 to 7 comprise the results obtained from the present work. Three cyclones are taken for the present study and they are categorized as overhead, nearby and far away passage. Chapter 4 describes the observed variations in the wind components in the troposphere and lower stratosphere associated with the passage of the three cyclones. The observation of multiple reflectivity

layers are presented in chapter 5. The fluctuations in the tropopause height associated with the passage of the cyclones are also reported in this chapter.

Chapter 6 deals with the generation of gravity waves associated with the passage of cyclones. This chapter includes the mean wind variations, detection of waves, determination of the period and vertical wavelength of the gravity waves and their direction of propagation. Chapter 7 describes a preliminary study of the stratosphere – troposphere exchange during the passage of cyclones. This chapter comprises of the study of horizontal momentum flux transport, mass flux transport and zonal and meridional body forces.

Major results of the present study are summarised in chapter 8. The prospects for future work in this area are also mentioned in this chapter. A list of the references used for the study is given in alphabetical order at the end of the thesis.

# ***CONTENTS***

<i>Certificate</i>	i
<i>Declaration</i>	ii
<i>Acknowledgements</i>	iii
<i>Preface</i>	iv
<i>Chapter 1: Introduction</i>	
1.1. Relevance of the Study	1
1.2. Earth's Atmosphere	2
1.3. Vertical Structure of the Atmosphere	3
1.3.1. Troposphere	3
1.3.2. Stratosphere	4
1.3.3. Mesosphere	5
1.3.4. Thermosphere	6
1.4. Probing of the Atmosphere	7
1.4.1. In-situ measurements	7
1.4.1a <i>Radiosonde</i>	7
1.4.1b <i>Rawinsonde</i>	8
1.4.1c <i>Meteorological rockets</i>	8
1.4.2. Remote sensing or indirect observations	9
1.4.2a <i>Lidar (Light Detection And Ranging)</i>	9
1.4.2b <i>Doppler lidar</i>	10
1.4.2c <i>Rayleigh lidar</i>	10
1.4.2d <i>Mie lidar</i>	11
1.4.2e <i>Raman lidar</i>	11
1.4.2f <i>Meteorological satellites</i>	11
1.5. Radar Remote Sensing of the Atmosphere	12
1.5.1. Doppler radar	12
1.5.2. MST radar	13

1.5.3. The radar equation	13
1.6. Tropical Cyclones	14
1.6.1. Formation and structure of tropical cyclones	15
1.6.2. Tropical cyclones over Indian region	18
1.6.3. Observation tools of tropical cyclones	19
1.6.3a Surface observations	19
1.6.3b Upper air observations	20
1.6.3c Satellite observations	21
1.6.4. Radar observations of tropical cyclones	22
1.6.4a Cyclone observations using MST radars	22
1.7. Objectives of the Present Study	23

## *Chapter 2: Literature Review*

2.1. MST Radar Technique and Observations	25
2.2. Tropical Cyclone Observations	33
2.3. Cyclone Observations using MST Radar	35
2.4. Tropopause Studies	36
2.5. Studies on Gravity Waves	38
2.6. Stratosphere –Troposphere Exchange	42

## *Chapter 3: MST Radar - System Description & Data Processing Techniques*

3.1. Introduction	48
3.2. Wind information from MST Radars	49
3.2.1. Doppler beam swinging method (DBS)	49
3.2.2. Spaced antenna drift (SAD) method	50
3.3. Indian MST Radar	50
3.3.1. Antenna array and feeder network	52
3.3.2. High power transmitter system	53
3.3.3. Receiver and signal processing system	55
3.3.4. Exciter and radar controller	56

3.4.	Atmospheric Data Processing	57
3.4.1.	Power spectrum Calculation	59
3.4.2.	Moments calculation	61
3.4.3.	Calculation of radial velocity and height	62
3.4.4.	Calculation of wind velocity vector (u, v, w)	64

*Chapter 4: Changes in the Circulation Pattern of the Troposphere and Lower Stratosphere During the Passage of Tropical Cyclones*

4.1.	Introduction	67
4.2.	Data Deduction Techniques	68
4.3.	Results and Discussion	69
4.3.1.	Overhead passage of cyclone	70
4.3.1a	<i>Synoptic features</i>	70
4.3.1.b	<i>Wind characteristics</i>	70
4.3.2.	Nearby passage of the cyclone	77
4.3.2a	<i>Synoptic features</i>	77
4.3.2b	<i>Wind characteristics</i>	78
4.3.3.	Far away passage of cyclone	83
4.3.3a	<i>Synoptic features</i>	83
4.3.3b	<i>Wind characteristics</i>	84
4.5.	Concluding Remarks	93

*Chapter 5: Fluctuations of the Tropopause and Other Reflectivity Layers Associated with the Passage of Tropical Cyclones*

5.1.	Introduction	94
5.2.	Data Deduction Techniques	96
5.2.1.	Determination of the tropopause and other reflectivity layers	96
5.2.2.	Experimental approach	101
5.3.	Results and Discussion	102
5.3.1.	Tropopause observations during the overhead cyclone passage	102
5.3.1a	<i>Determination of tropopause from SNR values</i>	103

5.3.1b	<i>Determination of tropopause from received echo power</i>	105
5.3.1c	<i>Tropopause variations from model profiles</i>	105
5.3.2.	Tropopause observation during the nearby cyclone passage	107
5.3.2a	<i>Determination of tropopause from SNR values</i>	108
5.3.2b	<i>Determination of tropopause from received echo power</i>	111
5.3.2c	<i>Tropopause variations from model profiles</i>	111
5.3.3.	Tropopause observations when the cyclone is Far away	113
5.3.3a	<i>Determination of tropopause from SNR values</i>	115
5.3.3b	<i>Determination of tropopause from received echo power</i>	115
5.3.3c	<i>Tropopause variations from model profiles</i>	117
5.4.	Concluding Remarks	118

## *Chapter 6: Generation of Gravity Waves during Tropical Cyclones*

6.1.	Introduction	119
6.2.	Theory of Atmospheric Gravity Waves	121
6.3.	Experimental approach	125
6.4.	Results and Discussion	125
6.4.1.	Generation of gravity waves during overhead passage of a cyclone	125
6.4.1a	<i>Disturbances in mean wind distribution</i>	125
6.4.1b	<i>Detection of wave generation</i>	127
6.4.1c	<i>Determination of the periodicity of gravity waves</i>	130
6.4.1d	<i>Characteristics of gravity waves generated due to storm passage</i>	131
6.4.2.	Generation of gravity waves during the nearby cyclone passage	134
6.4.2a	<i>Disturbances in mean wind distribution</i>	134
6.4.2b	<i>Detection of wave generation</i>	136
6.4.2c	<i>Determination of the periodicity of gravity waves</i>	136
6.4.2d	<i>Characteristics of gravity waves generated due to storm passage</i>	138
6.4.3.	Wave observations during far away passage	139
6.4.3a	<i>Variations in the mean wind distribution</i>	139
6.4.3b	<i>Detection of wave generation</i>	141



6.4.3c	<i>Determination of the periodicity of gravity waves</i>	141
6.4.3d	<i>Characteristics of gravity waves generated due to storm passage</i>	142
6.5.	Concluding Remarks	145

### *Chapter 7: Troposphere-Stratosphere Exchange During Tropical Cyclones*

7.1.	Introduction	146
7.2.	Momentum Flux, Mass Flux and Body Force	148
7.3.	Experimental Approach	149
7.4.	Stratosphere – Troposphere Exchange During Tropical Cyclones	150
7.4.1.	Case I – Overhead passage	150
7.4.1a	<i>Zonal and meridional momentum flux</i>	150
7.4.1b	<i>Mass flux transport</i>	152
7.4.1c	<i>Zonal and meridional body forces</i>	153
7.4.2.	Case II – Nearby passage	154
7.4.2a	<i>Zonal and meridional momentum fluxes</i>	154
7.4.2b	<i>Mass flux transport</i>	155
7.4.2c	<i>Zonal and meridional body forces</i>	155
7.4.3.	Case III- Far away passage	158
7.4.3a	<i>Zonal and meridional momentum fluxes</i>	158
7.4.3b	<i>Mass flux transport</i>	158
7.4.3c	<i>Zonal and meridional body forces</i>	169
7.5.	Concluding Remarks	163

### *Chapter 8: Summary and Conclusions*

8.1.	Major Outcome of the Study	164
8.2.	Scope of Future Studies	167

<i>References</i>	168
-------------------	-----

<i>List of Publications</i>	188
-----------------------------	-----

# Chapter #1

*Introduction*

## **1.1. Relevance of the Study**

Tropical cyclones affect people's life very much. Recently tropical cyclones, hurricanes and typhoons have been of great interest to many scientists and there is vast literature available on various aspects of tropical cyclones. All over the world many experiments were carried out to predict the cyclone track, intensity etc.

Lower tropospheric wind characteristics of the tropical cyclones are well known, whereas the three-dimensional structure of the cyclone extending upto the lower stratosphere is not properly understood due to the limitation on the resolution of the observational tools. Recent advances in the measurement techniques have enabled detailed observation of the three-dimensional structure of tropical cyclones. The MST (Mesosphere-Stratosphere-Troposphere) radar technique has a unique capability of measuring the background air motion. The MST radar is a powerful tool in observing the vertical structure of tropical cyclones.

Very limited VHF radar studies have been carried out on the wind characteristics in the entire troposphere and lower stratosphere associated with tropical cyclones. These observations have a potential to give a complete picture of three dimensional wind characteristics over the tropical cyclone region. The wind characteristics in the troposphere and lower stratosphere associated with a tropical cyclone over the Indian region has not yet been studied. In the present study, we report the characteristics of the troposphere and lower stratosphere using MST radar observations at Gadanki (13.5°N, 79.2°E) during the passage of various tropical cyclones over the station. These observations are the first of their kind from this latitude region.

## 1.2. Earth's Atmosphere

The Earth is surrounded by a blanket of air, which we call the *atmosphere*. It reaches over 560 kms from the surface of the Earth, so we are only able to see what occurs fairly close to the ground. Early attempts at studying the nature of the atmosphere used clues from the weather, the beautiful multi-coloured sunsets and sunrises, and the twinkling of stars. With the use of sensitive instruments from space, we are able to get a better view of the functioning of our atmosphere. Life on Earth is supported by the atmosphere, solar energy, and our planet's magnetic fields. The atmosphere absorbs the energy from the Sun, recycles water and other chemicals, and works with the electrical and magnetic forces to provide a moderate climate. The atmosphere also protects us from high-energy radiation and the frigid vacuum of space. The envelope of gas surrounding the Earth changes from the ground up.

The atmosphere is primarily composed of Nitrogen (78%), Oxygen (21%), and Argon (1%). A myriad of other very influential components are also present which include the water vapour (0 - 4%), and other major "greenhouse" gases, viz., Ozone (0 - 0.01%), Carbon dioxide (0.01-0.1%). These gases occupy 99.99% of the atmosphere by volume below 90 km. Nitrogen, oxygen and argon are constant in amount but carbon dioxide, ozone and water vapour vary both spatially and temporally. Water vapour comprises up to 4% of the atmosphere by volume near the surface, but is almost absent above 10-12 km. Ozone is concentrated mainly between 15 and 35 km and its content is low over the equator and high over areas poleward of 50<sup>0</sup> latitudes. Carbon dioxide enters the atmosphere mainly by the action of living organisms in the ocean and on the land. Photosynthesis helps to maintain a balance in the amount of global carbon dioxide by removing 3% of the world's total carbon dioxide annually. In addition to these gases, the atmosphere contains variable but significant quantities of aerosols. These are suspended particles of dust,

smoke, organic matter, sea salt, etc. coming from both natural and man-made sources. Water vapour, ozone, carbon dioxide and aerosols play important roles in energy distribution and exchanges within the atmosphere and between the earth's surface and the atmosphere.

### 1.3. Vertical Structure of the Atmosphere

Four distinct layers of atmosphere have been identified using thermal characteristics, chemical composition, movement, and density. The vertical structure of atmosphere is given in figure 1.1.

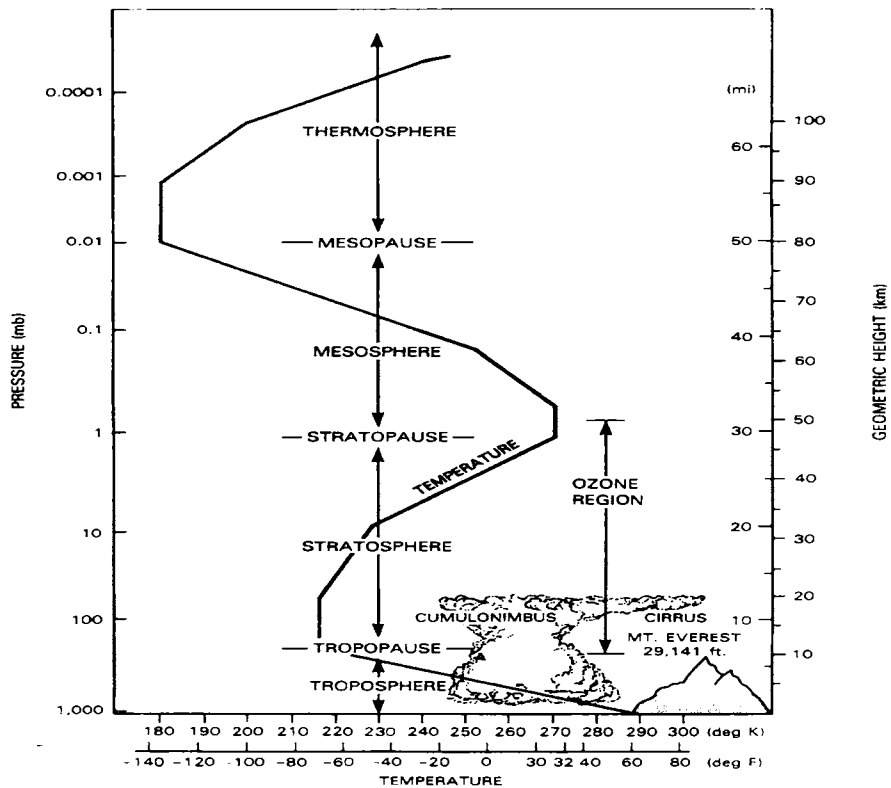


Figure 1.1. Vertical structure of the atmosphere

#### 1.3.1. Troposphere

The troposphere (from the Greek for "turning layer") starts at the Earth's surface and extends 8 kms in poles to 18 kms in tropics. This part of the atmosphere is the densest. As you climb higher in this layer, the temperature drops from about 300 to 210° K. The *troposphere* is where all weather takes

place; it is the region of rising and falling packets of air. The air pressure at the top of the troposphere is only 10% of that at sea level. If the temperature increases with increasing altitude in the troposphere, then a temperature inversion exists. The rate of temperature decrease is about 6.5 degrees Kelvin per 1 km (called the *lapse rate*). There is a thin buffer zone between the troposphere and the next layer, called the *tropopause*. The tropopause height is proportional to mean tropospheric temperature. The exchange of water vapor and other trace constituents between the troposphere and stratosphere through the tropopause is an important factor in understanding the problems of general circulation. The tropical troposphere is basically an unstable region and convective processes transport heat, water vapor and trace constituents to higher altitudes. Thus the exchange across the tropical tropopause merits special consideration. The tropical tropopause can be seen as a cap imposed on the deep tropospheric convection by the stable stratosphere aloft. The vertical transport of air and chemical species through the depth of tropical troposphere can occur on time scales as short as a few hours via moist convection (*Holton et al.*, 1995). The tropopause and the troposphere are known as the *lower atmosphere*. The variation in the height of tropopause is seen in figure 1.2.

### **1.3.2. Stratosphere**

The stratosphere starts just above the troposphere and extends to 50 kms high. It gets its name from the Greek meaning "stratified layer". Compared to the troposphere, this part of the atmosphere is dry and less dense. The layer is stratified with the denser, cooler air below the warmer, lighter air. This leads to an increase in temperature with height. The temperature in this region increases gradually to 270° K, due to the absorption of ultraviolet radiation. The ozone layer which absorbs the solar ultraviolet radiation is in this layer. The ozone then re-emits this energy in the form of heat into the stratosphere, warming it up in the mid-upper parts of the layer. The thin ozone layer in the upper stratosphere has a high concentration of ozone, a particularly

reactive form of oxygen. The formation of this layer is a delicate matter, since only when atomic oxygen is produced in the atmosphere can form the ozone layer and prevents an intense flux of ultraviolet radiation from reaching the surface, where it is quite hazardous to the evolution of life. Ninety-nine percent of "air" is located in the troposphere and stratosphere. The stratopause separates the stratosphere from the next layer.

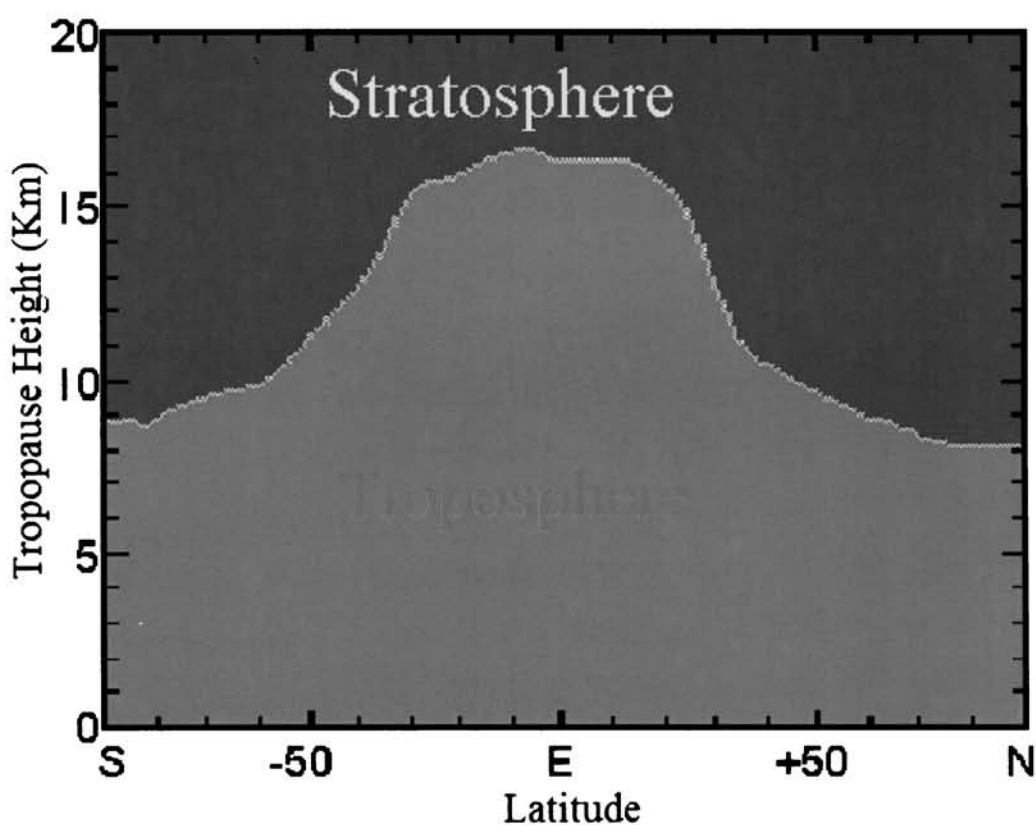


Figure 1.2. Tropopause height variations

### 1.3.3. Mesosphere

The mesosphere (middle layer) starts just above the stratosphere and extends to 85 kms high. In this region, the temperatures again fall with increase in altitude. The lowest temperature in the atmosphere is noted in this layer (around 180 degrees Kelvin). In the mesosphere, a small fraction of the neutral particles are ionized by the solar radiation forming the lowest layer, the D region (~ 60-90 km) of the ionosphere. The chemicals are in an excited state,

as they absorb energy from the Sun. In a manner of thinking, the mesosphere is a resumption of the troposphere after the rude interruption of the ozone layer in the stratosphere. The difference is that the mesosphere is not in contact with the forces mixing up the air in the troposphere, so it's much quieter up there. The mesopause separates the mesosphere from the thermosphere. The regions of the stratosphere and the mesosphere, along with the stratopause and mesopause, are called the *middle atmosphere*.

#### **1.3.4. Thermosphere**

The thermosphere starts just above the mesosphere and extends to 600 kms high. The temperatures go up with increase in altitude due to the absorption of intense solar radiation by the limited amount of molecular oxygen. Above 100 km from Earth's surface the chemical composition of air becomes strongly dependent on altitude and the atmosphere becomes enriched with lighter gases (atomic oxygen, helium and hydrogen). At these high altitudes, the constituent gases of the atmosphere become diffusively separated according to their atomic masses. In the thermosphere, a small but significant fraction of the neutral particles are ionized by the solar radiation forming the E and F regions of the ionosphere extending over 90 km to more than 1000 km. Chemical reactions occur much faster here than on the surface of the Earth. This layer is known as the *upper atmosphere*.

Above the thermosphere lies the exosphere ("outer layer"). The boundary between the two is very diffuse. Molecules in the exosphere have enough kinetic energy to escape the earth's gravity and thus fly off into space. The highest layers of the atmosphere, the mesosphere, the thermosphere, and the exosphere, differ significantly in composition from the lower regions, and also contain a significant proportion of ionized (electrically charged) gas atoms and molecules, which is called the ionosphere, since most of the molecules and atoms are ionized by the ultraviolet light and other high energy



particles at this height. The ionosphere is of practical importance because it makes possible long-distance radio communications. The upper regions of the atmosphere are also of practical importance because, although the atmospheric density is very low compared to that in the lower atmosphere, it still acts to slow down artificial satellites and limit the length of time a satellite can stay in low-altitude orbits around the Earth.

#### **1.4. Probing of the Atmosphere**

It has long been recognized that surface weather and weather forecasting are closely related to atmospheric conditions many kilometers above the ground. So the need to probe the atmosphere with various instruments was understood and instruments have been developed for the same purpose. Measurements of meteorological parameters, such as temperature, pressure, humidity and wind, are usually obtained by positioning the sensor instrumentation at the site where information is sought. The surface level observations of these parameters are done by thermometers, barometer, psychrometer and anemometer. The sensors are normally located in instrument shelters if surface observations are desired, or carried aloft in aircraft, kites, rockets, or as radiosondes if vertical structure is needed. Measurements made in this manner are termed *in-situ* measurements. Some of the in-situ instruments are described briefly below.

##### **1.4.1. In-situ measurements**

###### ***1.4.1a Radiosonde***

The radiosonde has become the standard instrument for upper-air measurements and today approximately 800 stations around the world release them on a regular basis-at 0000 GMT and 1200 GMT to provide regular measurements of meteorological parameters such as pressure, temperature, humidity and atmospheric wind upto 30 km from the surface. The instrument

is carried aloft by a hydrogen/helium filled balloon. The elevation and azimuth angles are determined by tracking the balloon at the ground using the receiver. The elevation is obtained from the recorded pressure. Because the balloon position is known at all times, its drift with the wind is used to measure the wind speed and direction. The signals are transmitted by different sensors, which are received by the receiver at the ground. The sensors are thermistors, hygrometers and aneroids to measure temperature, humidity and pressure respectively. Being lighter than air, unlike the aeroplane and rocket, it does not require an expenditure of energy to keep it flying but can float and remain aloft at great heights for long periods. Measurements at every 12 hours for these locations may be enough to define the large-scale weather patterns, but not sufficient to define small-scale weather events. Also these instruments have poor spatial and temporal resolutions.

#### ***1.4.1b Rawinsonde***

In rawinsondes, a radar is used to track the ascending balloon which is carried horizontally by the wind at its level, so that a series of observations of its position enable to measure the average wind over the layers traversed between successive observations. The tracking depends upon the reflection of radio waves transmitted from the ground station for which a reflector made of metal or metalised nylon mesh is suspended from the balloon. This method is not impeded by the presence of cloud or precipitation. Radar can be used to measure wind in addition to temperature and humidity using a balloon carrying both radar reflector and radiosonde apparatus.

#### ***1.4.1c Meteorological rockets***

The meteorological rockets involve a rocketsonde that is lowered by parachute after the rocket reaches the altitude of 80-90 km range. Rocketsonde is capable to measure temperature and pressure and also wind by measuring their horizontal drift. The drift of alkaline metal vapours that scatter

sunlight at twilight can be used to measure winds in the upper atmosphere. Besides, cloud chaff dipoles ejected by rockets upto 80-90 km are also used to measure wind by tracking the chaff particles using radar. Rocketsonde provides good vertical profiles of meteorological parameters like temperature in the middle atmosphere. Although large quantities of data are available, they are restricted mostly, to land areas of the Northern Hemisphere. Rocket observations are useful to calibrate and verify satellite-derived data and to formulate the climatology of the middle atmosphere over certain regions of the globe.

#### **1.4.2. Remote sensing or indirect observations**

The remote sensing system is a device that can, when placed in a given location, provide a description of the desired physical properties that characterize a second location. This technique is classified as active and passive and basically observes the target without disturbing it. Remote sensing techniques such as Sodar, Lidar, Radar and Satellites use quite similar sounding techniques. But the nature of the transmitted waves differs according to the instruments. In the case of Sodar it transmits acoustic waves into the atmosphere. Electromagnetic waves in various frequency ranges are used for other instruments. The different instruments are discussed briefly below.

##### ***1.4.2a Lidar (Light Detection And Ranging)***

Lidar techniques are widely used to study the structure and dynamics of the middle atmosphere. Lidars operate as optical frequency radars in which short, intense laser pulses are transmitted into the atmosphere and the back scattered signals are analysed to derive information about atmosphere using receivers. They use radiation in the form of visible or infra-red laser beams and detect scatterers. The laser properties, which make lidars useful for the exploration of the atmosphere, are their possibility to emit short pulses which allows to perform remote sounding without disturbing the medium with

high vertical resolution. By using a variety of scattering and absorbing processes it is possible to obtain a great deal of information about the atmosphere, its constituents and their changes in both time and space.

#### ***1.4.2b Doppler lidar***

The coherent Doppler lidar operates at optical and infrared wavelengths, from 0.3 to 100 $\mu$ . At these wavelengths the scatters are mainly particles which move with background wind. The Rayleigh scattering applies to spherical particles with diameters smaller than a wavelength. When the concentrations are very large, the aerosols scatter and attenuate the signal. The coherent lidar is limited to boundary layer research. The coherent Doppler lidar uses different scanning mode with one or two lidars (*Rothermel et al.*, 1985). Their horizontal range varies from 10-20 kms. Coherent Doppler lidar observations are very useful in boundary layer projects that do not involve clouds or precipitating weather systems. The susceptibility of the lidar beam to attenuation by water vapour and thick clouds remains a serious disadvantage.

#### ***1.4.2c Rayleigh lidar***

Rayleigh lidars operate to receive only Rayleigh scattering (i.e., at altitudes greater than 30 kms). The Rayleigh lidars observe the atmospheric density and temperature in the height region 30-80 kms with adequate height and time resolutions to study the atmospheric dynamics (*Chanin and Hauchecorne*, 1984). The scattering of the laser beam is due to the presence of air molecules irrespective of their nature and occurs at every altitude. The possibility to derive a density (and then temperature) measurement by Rayleigh Lidar is limited near the lower altitudes due to the presence of aerosols. Rayleigh lidar offers a powerful ground based method to measure temperature profile in the altitude region between 30 and 80 kms with adequate height and time resolution to study atmospheric dynamics.

#### ***1.4.2d Mie lidar***

To obtain the number density information of aerosols in the height range 4-35 km, Mie scattering is the sole method. The intensity of the scattering varies inversely as the fourth power of the probing wavelength in the case of Rayleigh scattering (whereas in Mie scattering, the dependence is less stronger) which is based on the size of the scatterers (aerosols).

#### ***1.4.2e Raman lidar***

Raman scattering results from the excitation of the vibrational or rotational transitions of molecules. This process involves the exchange of energy between the incident photons and the scattering constituents, resulting in a frequency shift between the incident and the scattered photons. This method has been successfully used to obtain temperature profile from N<sub>2</sub> and O<sub>2</sub> densities. In the first few kilometres of the atmosphere, it is used for measuring the water vapour contents. Raman lidar does not require a tunable laser is one of its advantages.

#### ***1.4.2f Meteorological satellites***

Remote sensing from space through satellites started way back in 1960, when the first TIROS 1 (Television and Infra Red Operational Satellite) was launched. Since then, a number of remote sensing satellites have been launched including the recent one, called TRMM (Tropical Rainfall Measuring Mission). Major advantages have been realised in atmospheric studies with the advent of satellites. Satellites are classified into two, namely, polar orbiting and geo-stationary satellites. In terms of resolution satellite data have relatively low resolution in horizontal and vertical directions. The advantage of satellites over other observing techniques is that they can monitor atmospheric conditions worldwide in a spatially continuous manner. Ground based remote sensors, like Light Detection And Ranging (LIDAR), Sound Detection And Ranging

(SODAR), Radio Detection And Ranging (RADAR) etc., are characterised by the continuous monitoring of the atmosphere, with time and height resolutions of 1-10 minutes and 100 m to a few km.

## **1.5. Radar Remote Sensing of the Atmosphere**

The acronym RADAR stands for Radio Detection And Ranging. Radar systems have been designed and are in use for a very broad spectrum of applications. The radar technology started around 1950's to study tropospheric radio propagation and over-the-horizon (OTH) radars. Depending on the target and probing frequency, radars can be classified into two types. Clear air radar gets echo from the fluctuations of atmospheric index of refraction associated with turbulence. Second type is the weather radar, which observes hydrometeors as its principal target. One of the major applications of the Radar system is in the atmospheric research, because of their simplicity, reliability and virtue of the fact a radar system provides a means of sampling the atmosphere at a rapid rate in a cost effective way. The Radar techniques make use of the fundamental properties of an electromagnetic (radio) wave. They are frequency, phase, amplitude and polarisation. Atmospheric radars derive information on the dynamical atmospheric phenomena by making use of the variations on the above four parameters of radio waves which are transmitted from the radar system, backscattered by the atmosphere and received by the radar system again. The tracer elements for the study of atmospheric dynamics using microwave radar are the hydrometeors (rain, snow, hail, etc.) and have the wavelength of a few centimetres.

### **1.5.1. Doppler radar**

A new generation of pulse Doppler radar systems has emerged which are probing the atmosphere and studying the dynamics of the atmosphere using the back scattered signals from clear air turbulence (CAT). The tracer elements for such radar system are the variations in the atmospheric

refractive index. Such radars have come to be known popularly as MST, the ST and the T radars depending on the height coverage of the radar corresponding to the three regions of the atmosphere viz. Mesosphere, Stratosphere and Troposphere. Because of the scale sizes of the refractive index variations, these radars operate at wavelengths of the order of a fraction of a meter to a few meters.

### **1.5.2. MST radar**

A major advance has been made in the radar probing of the atmosphere with the realisation in early seventies by *Woodman and Guillen* (1974) that it is possible to explore atmospheric dynamics upto a height of about 100 km by means of a high power VHF backscatter radar. It led to the concepts of MST (Mesosphere-Stratosphere-Troposphere) radar.

MST Radar is a highly sensitive high resolution pulse coded phase coherent radar operating in the lower VHF band, typically around 50 MHz, with average power aperture product exceeding about  $5 \times 10^7 \text{ Wm}^2$ . Radar operating in the higher frequencies or having smaller average power aperture products are termed ST (Stratosphere-Troposphere) radars. Analyses of the scattered signals enable measurements of the dynamical properties of the atmospheric wind, waves, turbulence and atmospheric stability throughout the atmosphere. The high resolution data in the vertical and temporal on a continuous basis is one advantage of this technique. One of most important parameters, which this radar can give, is the vertical wind component not directly available by any other technique (*Sienkiewicz and GalChen*, 1989; *Larsen et al.*, 1989).

### **1.5.3. The radar equation**

The scattering, reflection and mechanisms responsible for giving rise to radar echoes at VHF/UHF range are described by *Rottger and Liu*

(1978), *Gage and Balsley* (1980) and *Rottger* (1980). They are generally classified into three, turbulent scattering, fresnel scattering and thermal scattering. In these the turbulent and fresnel scattering are the important mechanisms for MST radar echoes. The radar equation relates the received signal strength  $p_r$  to the radar parameters.

The generalised radar equation can be written as

$$p_r = \left( \frac{p_t G_t \theta^2 A_e}{64 \pi r^4} \right) \sigma G_s$$

where,  $p_t$  is the transmitted power,  $G_t$  is the antenna gain equal to  $4\pi A_e / \lambda^2$  for a radar wavelength  $\lambda$ ,  $A_e$  is the effective antenna area,  $G_s$  may be thought as the gain of the scattering process in a particular direction relative to isotropic scattering element and  $\theta$  is the antenna beam width. The size of the volume reflectivity is expressed by the scattering cross section  $\sigma$  defined by  $\sigma = p_s / p_i$ .

## 1.6. Tropical Cyclones

Tropical cyclones are by far the most devastating of all natural disasters, in terms of both loss of human life and economic damage. These are occasionally very severe in the North Indian Ocean comprising of Bay of Bengal and the Arabian Sea. In the past out of 10 recorded cases of very heavy loss of life in the world due to tropical cyclones, 8 cases were in the Bay of Bengal. From the scientific point of view, very few atmospheric processes are as poorly understood as tropical cyclogenesis, i.e., the complex and interrelated dynamic and thermodynamic processes that lead to the formation and intensification of a tropical cyclone. This lack of knowledge is partly related to the fact that tropical cyclones spend most of their life time over remote tropical ocean areas where in situ observations are scarce or even lacking. Different stages of development of a cyclone/hurricane are given in figure 1.3.



A typical mature tropical cyclone is a warm core vortex in the atmosphere (anti-clockwise vortex rotation in the northern hemisphere and clockwise in the southern), cyclonic in the lower troposphere and anti-cyclonic in the upper troposphere. "Tropical cyclone" is the generic term for a low pressure system over tropical or subtropical waters with organized convection and a definite cyclonic surface wind circulation. Tropical cyclones are driven by the latent heat released by the condensation of immense amounts of water vapor within their convective rainbands. In tropical storms the winds are strongest from the surface up to 2–3 km. The circulation extends horizontally to some 1000 kms from the centre and vertically to about 1.5 km above sea level.

#### **1.6.1. Formation and structure of tropical cyclones**

Tropical cyclones form in the region of Inter-Tropical Convergence Zone (ITCZ) where the trade winds of the two hemispheres meet. This region receives a high radiant energy where, the atmosphere can absorb a large quantity of latent heat through evaporation from the sea surface. Disturbances such as easterly waves are quite common in the tropics and not all of them develop into tropical cyclone (TC). A trigger mechanism is required to transform these disturbances into a TC. The parameters affecting TC formation are threshold value of Earth's vorticity, low-level relative vorticity, vertical wind shear, SST and mixed layer depth, potentially unstable atmosphere and tropospheric humidity.

A fully grown cyclone is a violent whirl in the atmosphere 150 to 1000 kms across and 10-15s km high. Gale winds of the order of 150 to 250 km/hour spiral around a centre where the atmospheric pressure is 30 to 100 hPa below the normal sea level pressure. At the centre there is a cloud free region of calm winds called the "eye". The "eye" at the centre of the cyclone is of radius 5 to 50 kilometres. The eye is rain-free with light winds. Although the

winds are calm at the axis of rotation, strong winds may extend well into the eye. The eye is the region of lowest surface pressure and warmest temperatures aloft - the eye temperature may be 10°C warmer or more at an altitude of 12 km than the surrounding environment, but only 0-2°C warmer at the surface (*Hawkins and Rubsam, 1968*) in the tropical cyclone.

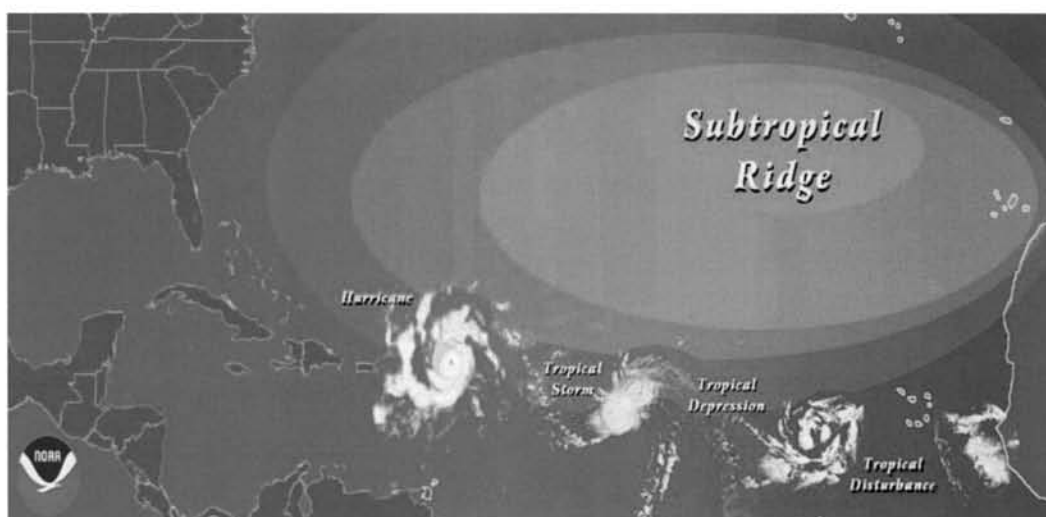


Figure 1.3. Different stages in development of a cyclone

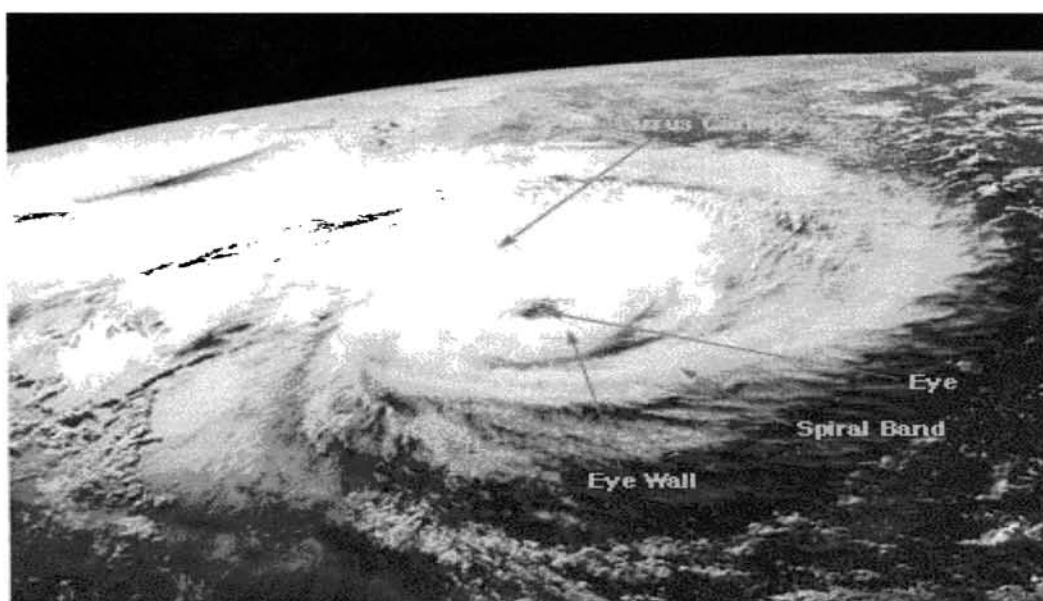


Figure 1.4. Mature cyclone

The eye is surrounded by the "**eyewall**", the roughly circular ring of deep convection which is the area of highest surface winds in the tropical cyclone. It is made up of tall cumulo-nimbus clouds rising upto an altitude of

15-18 km, the wall cloud thickness being about 10-15 km radially. The eye is composed of air that is slowly sinking and the eyewall has a net upward flow as a result of many moderate - occasionally strong - updrafts and downdrafts. The eye's warm temperatures are due to compressional warming of the subsiding air. Beyond the eyewall, surface wind speeds decrease gradually with the radial distance from the centre and rainfall is confined to the regions covered by the inward spiralling cloud-bands that are seen within a radial distance of about 400 km from the centre of the cyclone.

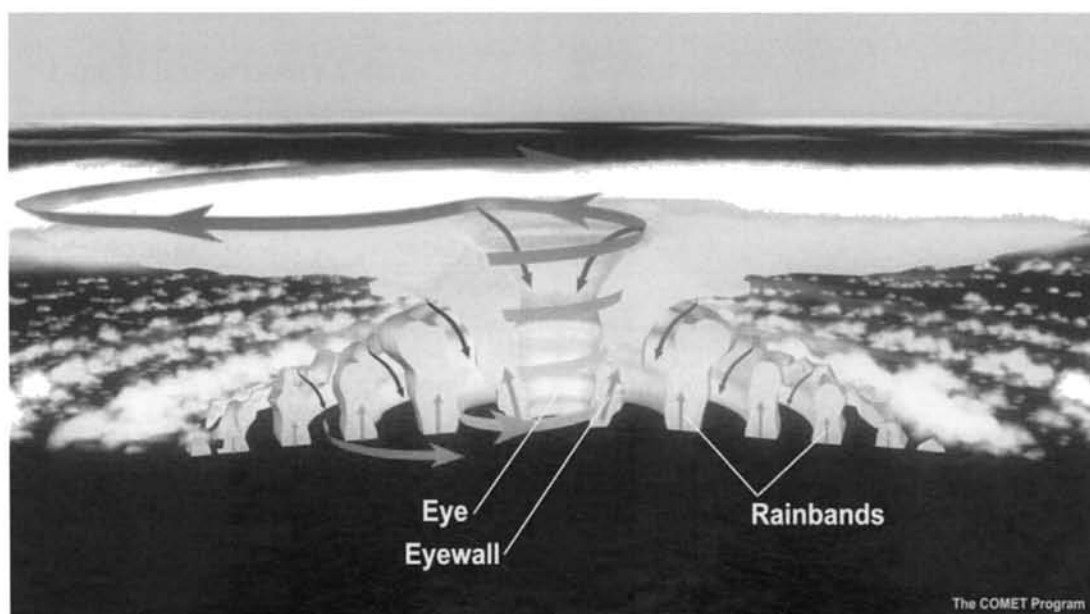


Figure 1.5. Structure of a cyclone

The sea level atmospheric pressure falls continuously from the periphery to the centre of the cyclone. The low level winds rich in moisture possess strong tangential and radial component causing the air parcels to spiral inwards from the peripheral regions of the cyclone towards its centre. The radial component of the wind converges large amounts of moisture to the central regions of the cyclone, which ascends and condenses in cloud formations there, keeping the central regions warmer than the surrounding tropical atmosphere. This warm anomaly, which reaches a maximum of about 15°C at 300-200 hPa level (9-12 km altitude), reduces the radial pressure

gradients at these high altitudes. The cyclonically rotating air parcels rising up in the central regions of the cyclone move outwards in the upper troposphere, under the action of unbalanced centrifugal forces (with reduced pressure gradients) and conserving angular momentum. These begin to reverse the cyclonic rotation as they move farther away from the centre. Tropical cyclones are classified according to their maximum sustained wind speeds at the surface. The classification followed by the India Meteorological Department (IMD) is given in Table 1.1.

Type of low pressure system	Highest surface wind (Speed in knots)
Low	Less than 17
Depression	17 to 27
Deep depression	28 to 33
Cyclonic storm	34 to 47
Severe cyclonic storm	48 to 63
Severe cyclonic storm with core of hurricane winds	64 to 119 knots
Super cyclone	120 knots and more

*1 knot=1.85 km/hour*

Table 1.1. Classification of low pressure systems in India

### 1.6.2. Tropical cyclones over Indian region

During the 100-year period 1891-1990, there have been 561 cyclones in the Indian seas with maximum winds of 34 knots or more. About 23% of these, intensified into hurricane strength with maximum winds of 64 knots or more. Cyclones over the Indian seas generally form between latitudes 5°N and 18°N during the pre-monsoon (April, May and early part of June) and post-monsoon (late September to December) seasons. During the monsoon period June to September, weaker systems (mostly depressions) form over the northern part of the Bay of Bengal (north of 18°N). Annual tropical cyclone

frequency in the Indian seas (Arabian Sea and Bay of Bengal) for the period 1891 to 1998 has varied with a prominent 36 year periodicity. Around 1970 cyclone frequency was about 7 per year. It gradually decreased to about 3 per year around 1990. The cyclone frequency is now on the increase and during the coming two decades we expect 5-8 cyclones per year in Indian Seas, about 80% of which is likely to occur in the Bay of Bengal. Therefore, there is urgency to strengthen Cyclone Disaster Mitigation Plans along the coasts of India.

### **1.6.3. Observation tools of tropical cyclones**

Intense tropical cyclones pose a particular observation challenge. As they are dangerous oceanic phenomena, weather stations are rarely available on the site of the storm, unless they pass over an island or a coastal area. Real time measurements are possible in the periphery of the cyclone. The cyclone can also be imaged remotely by radar and by weather satellites. Figure 1.6 shows a schematic diagram of cyclone observing tools.

#### ***1.6.3a Surface observations***

Tropical cyclones generally spend most of their life cycle over data-sparse ocean areas. In spite of the limited nature of the observations, a surface data network over the tropics is absolutely essential to monitor the broad-scale tropical atmosphere and ocean. Surface stations in the environment of a tropical cyclone provide valuable information on the intensity and structure (size) of the storm. Ships supplement the standard land-based measurements of atmospheric pressure, wind, temperature, dewpoint, cloud, visibility and weather phenomena with sea-surface temperature and wave data.

Instrumented ocean research vessels that observe both atmosphere and ocean have presented evidence on air-sea interactions with respect to tropical cyclones. Although deployment of drifting buoys

supplements the surface area network, relatively few buoys are located in the tropics. Drifting buoys have been deployed from aircraft in advance of a cyclone and successfully reported surface pressure, wind speeds at 1 metre elevation and ocean temperature at several levels throughout the passage of cyclone.

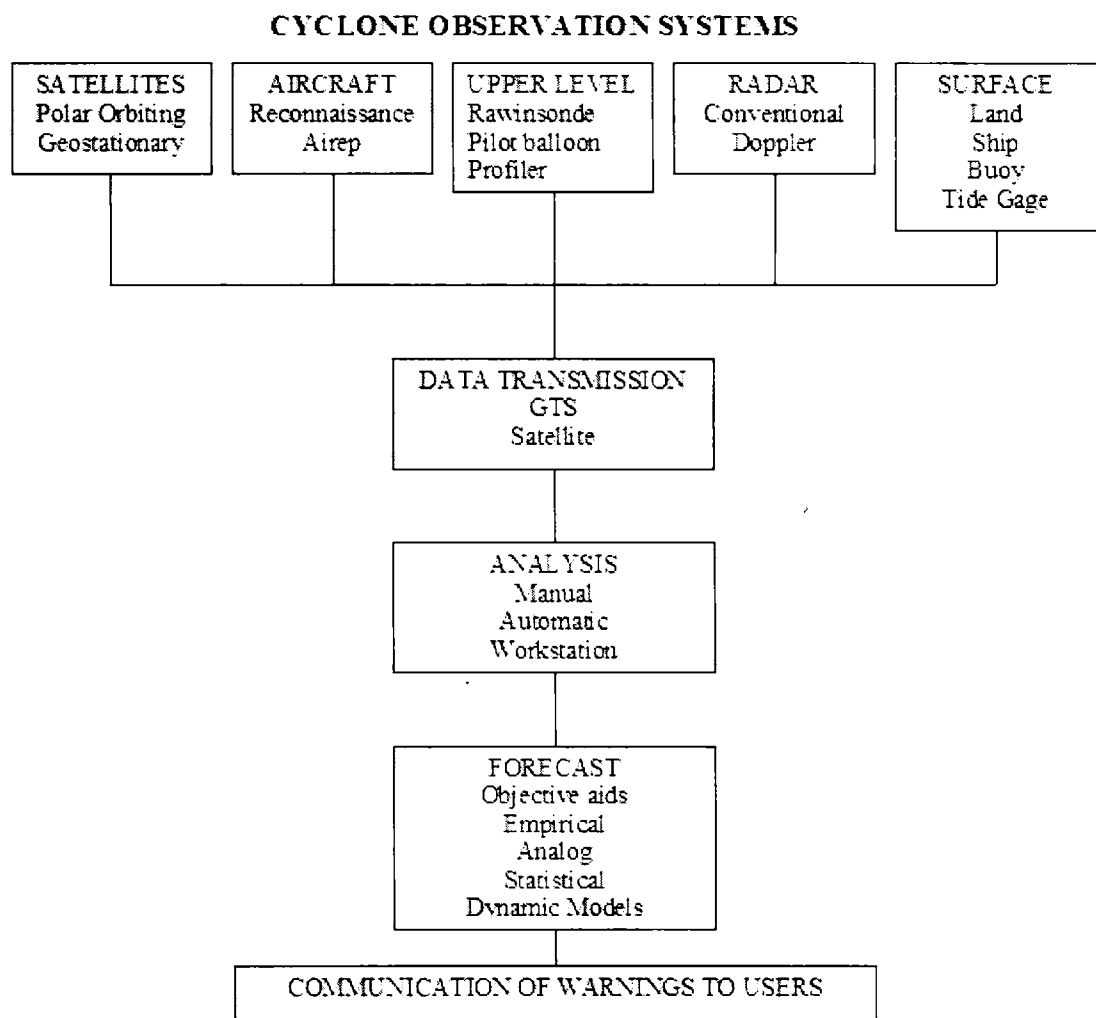


Figure 1.6. Cyclone observing tools

**1.6.3b Upper air observations**

Dynamical forecasts of tropical cyclone motion and intensity require knowledge of the vertical structure of both the tropical cyclone and the surrounding environment. The rawinsonde remains the principal instrument to sample upper-level temperature geopotential height, humidity and winds. The

availability of upper-level data to observe tropical cyclones is markedly less than surface data. Valuable data may also be lost as a tropical cyclone enters the radar range of an upper-air station and the cyclone tracking task takes precedence over the wind tracking task.

Another important source of upper-level data in the tropics is the aircraft reports (AIREP). These manually prepared and transmitted observations include flight-level wind, temperature turbulence and general flying conditions at designated reporting points about an hour apart along the flight route. Aircraft automatically transmit frequent and accurate observations of wind speed and direction, temperature and turbulence via satellite or High Frequency (HF) communication links. Aircraft reports of tropical cyclone location and intensity are considered to be the most reliable data source.

### ***1.6.3c Satellite observations***

The meteorological satellite has a tremendous impact on the global detection, analysis and forecasting of tropical cyclones. All significant tropical cloud clusters are now routinely observed through both geostationary and polar-orbiting satellites, and those showing signs of organization are closely monitored for intensification. In many regions, satellites provide the only observational evidence that a tropical cyclone exists and Dvorak technique has to be applied to estimate centre location and intensity.

The geostationary meteorological satellites currently in orbit provide global coverage of tropical cyclone activity. The Japanese Geostationary Meteorological Satellite (GMS), the US Geostationary Operational Environmental Satellite (GOES), the European Space Agency METEOSAT and the Indian INSAT transmit visible (VIS) and infrared (IR) imagery at hourly (and at times half-hourly) intervals. Polar-orbiting satellites such as the TIROS series (U. S.) and the METEOR series (Russia) provide VIS and IR imagery for locating tropical cyclones and making intensity estimates.

#### **1.6.4. Radar observations of tropical cyclones**

The structure of the tropical cyclone and of individual precipitation elements can be studied by radar. Radars can track the cyclone centre and precipitation bands. Pulsed Doppler radar is able to measure the component of velocity of clouds towards or away from the radar and thereby map the wind field of the cyclone. Radars enable precise location of the centre of the cyclone. Doppler radar can give the maximum wind in the cyclone.

Radar has been used to observe tropical cyclones since the mid-1940s (*Maynard, 1945; Wexler, 1947*). Radar data have enabled scientists to make detailed studies of key features of tropical cyclones such as the structure of the core and rain bands. Conventional weather radars, which typically have 5 cm (C band) or 10 cm wavelengths, may provide useful estimates of the storm center to a range of upto 400 km. In storms that do not possess a well-defined eye structure, a center position may be estimated by the superposition of spiral overlays on the rainbands echoes (*Senn and Hiser, 1957*).

It was not until the advent of Doppler radar the direct measurement of tropical cyclone wind fields was possible. In addition to mean returned power of the signal, which provides information on the reflectivity and hence the rainfall distribution, the Doppler radar also provides two other parameters, a frequency shift that gives the mean Doppler velocity, which is the radial wind with respect to the radar site and the spectrum width, which is a measure of the velocity dispersion or shear (turbulence) within the scattering volume.

##### ***1.6.4a Cyclone observations using MST radars***

Wind profilers and MST radars have been used to profile the winds in parts of the tropical cyclones in different basins. The Doppler radar wind profiler provides hourly (or more frequent) soundings of acceptable



quality in vertical steps of around 150 m through the depth of the troposphere and lower stratosphere.

The MST radars are a powerful tool in observing the vertical structure of tropical cyclones. Even though the MST radar observations are single stationed observations three dimensional structure of atmospheric disturbances can be studied if they passed by the radar site without remarkable modification in time. The first observation of a typhoon using the MST radar technique was made with the MU (middle and upper atmosphere) radar at Shigaraki, Japan (*Kato et al.*, 1984). *Sato et al.* (1991) have reported detailed wind observations of typhoons passing a radar wind profiler in Kyoto, Japan. These examples demonstrate the ability of profilers to provide useful wind measurements in tropical cyclones. If tropical cyclones are moving overhead or nearby the MST radar, these radars provide a wealth of information as they can be operated continuously with fairly good height resolution.

### **1.7. Objectives of the Present study**

The importance of tropical cyclones in the day to day life of human beings is well known. Still they remain one of the poor understood weather systems in terms of dynamics and forecasting. More and more studies are going on all around the world for a better understanding of such systems. MST radars provide valuable information regarding the structure of the tropical cyclones if it passed overhead or nearby the radar.

It can be noted that in North Indian Ocean, Bay of Bengal is the most affected area by tropical cyclones. In this basin, cyclones form during two seasons, during April-June and October – December. The main areas in India, where tropical cyclones usually make land fall is between north Tamil Nadu coast and West Bengal coast. As Indian MST radar is situated in this belt, it can be used for the purpose of studying tropical cyclones. The present study is the

first attempt to understand the tropical cyclone characteristics using MST radar in this region.

Special experiments using MST radar were conducted by Department of Atmospheric Sciences, CUSAT from 2001 onwards as and when the cyclone forms in the Bay of Bengal. Out of 4 cyclone cases observed, two cases were selected depending upon the data quality and position and intensity of the cyclones, one passed very close to the radar site (October 2001) and the other passed far away from the radar site (November 2002). A rare event of an exact overhead passage over Gadanki reported in 1994 is also considered. The common mode and special radar observations taken during these cyclones are used for studying various aspects of tropical cyclones.

The major objectives of the thesis are:

- *to find the wind characteristics in the troposphere and stratosphere during the passage of tropical cyclones, their relation to the position and movement of cyclone.*
- *to identify the multiple layers of reflectivity observed in the atmosphere during the cyclones.*
- *to study the tropopause characteristics during these cyclones and its dependence on cyclone position and intensity.*
- *to detect the waves present in the atmosphere. Prime importance has been given to gravity wave generation during the cyclone passage.*
- *to study the transport of momentum fluxes (both zonal and meridional), mass flux and body force during cyclone passage and*
- *to understand the stratosphere – troposphere exchange during the cyclone passage in terms of these parameters.*

## Chapter #2

*Literature Review*

## 2.1. MST Radar Technique and Observations

The history of radar studies of the clear atmosphere has roots in 1930s and has been well reviewed by *Hardy and Gage* (1990). In the mid 1930s the 10-200 m wavelength radars used for ionospheric studies, detected reflecting layers in the troposphere. *Friend* (1949) observed various types of echoes called “Angel echoes” or “Phantom echoes” or “Ghost echoes” and are considered to be induced by very strong gradients of refractive index associated with turbulence or atmospheric discontinuities. The decade of 1950 was a period of considerable activity in experiments and theoretical studies of over-the-horizon (OTH) radio propagation. The findings during this period were significant because the processes responsible for the tropospheric scatter observed on radio propagation links were also a factor in the backscatter of radar energy.

Theories were developed for the scattering of electromagnetic radiation in the troposphere by *Pekeris* (1947), *Booker and Gordon* (1950), *Tatarskii* (1961), etc. In the 1960s, a new generation of high-power, high frequency radars were developed for investigating atmospheric structures. During this period, long wavelength radars were effectively used to study clear air turbulence (CAT) and convective processes in the boundary layer. In 1970s, another type of radars using VHF band frequencies and large phased array antennas were developed, primarily for ionospheric research. However, *Woodman and Guillen* (1974) in their pioneering work at Jicamarca, Peru observed echoes from the lower atmosphere and mesosphere. This work led to the concept of Mesosphere-Stratosphere-Troposphere (MST) radar, and this class of radars has come to dominate the atmosphere radar scene over the past decade. The global distribution of MST radars is given in table 2.1.

<b>Radar</b>	<b>Location</b>	<b>Frequency (MHz)</b>	<b>Av.Power (Wm<sup>2</sup>)</b>	<b>Altitude Coverage</b>
Arecibo	Puerto Rico	46.8	$5 \times 10^7$	MST
Buckland Park	Australia	54.1	$3 \times 10^6$	ST
Chung-Li	Taiwan	52	$1 \times 10^7$	ST
EISCAT	N. Scandinavia	224	$2 \times 10^9$	ST
Equatorial radar	Indonesia	47	$4 \times 10^9$	MST
Fairbanks	Alaska	219	$1 \times 10^6$	ST
Flatland	Illinois	40.5	$4 \times 10^6$	ST
Gadanki	India	53	$7 \times 10^8$	MST
Jicamarca	Peru	49.9	$1 \times 10^{10}$	MST
Millstone Hill	Massachusetts	440	$5 \times 10^7$	ST
MU Radar	Japan	46.5	$4 \times 10^8$	MST
Penn State	Pennsylvania	49.9	$9 \times 10^5$	ST
Poker Flat	Alaska	49.9	$3 \times 10^9$	MST
Pohnpei	Christmas Island	49.8	$5 \times 10^6$	ST
PROUST	France	945	$7 \times 10^6$	ST
Provence	France	45-49	$5 \times 10^6$	ST
SOUSY	W. Germany	53.5	$7 \times 10^7$	MST
SOUSY Mobile	Norway etc.	53.5	$7 \times 10^7$	MST
Sunset	Colorado	40.5	$6 \times 10^6$	ST
UK-Radar	Wales	~50	$6 \times 10^7$	MST
Urbana	Illinois	40.9	$2 \times 10^7$	MST

Table - 2.1. Global Distribution of MST/ST Radars

The last few years have seen many significant advances in the field of middle atmospheric research using VHF radar techniques. Application for these instruments quickly developed and a large and successful community has been built up around them. Several successful international workshops have discussed scientific and technical aspects of the so-called MST techniques and have been summarised in MAP and STEP handbooks. Initial use of the MST radar technique was confined to the realm of atmospheric research rather than operational meteorology. However, *Larsen and Rottger* (1982) demonstrated the feasibility of employing MST radar for research in synoptic meteorology and indicated the potential of the technique for the investigation of synoptic-mesoscale interactions. Since, one of the primary purposes of all MST/ST radars is the measurement of atmospheric winds, the term “wind profiler” has gained acceptance with meteorologists. An additional consideration for wind profilers is that they must be sufficiently reliable to be operated continuously in unattended mode (*Ecklund et al.*, 1979; *Frisch et al.*, 1986). MST radar is an excellent tool for making high-resolution measurements of atmospheric winds, associated vertical shears of horizontal winds and various atmospheric turbulence parameters. However, most of such studies are confined to middle and high latitudes (*VanZandt et al.*, 1978; *Smith et al.*, 1983; *Nastrom et al.*, 1986) and only a few measurements are available at low latitudes (*Sato and Woodman*, 1982; *Tsuda et al.*, 1985; *Jain et al.*, 1995; *Rao et al.*, 1997).

Apart from wind profiling, several more diverse applications of MST radars, especially VHF radars, have arisen in the last few years. These include estimations of refractivity structure constant,  $C_n^2$ , eddy dissipation rate,  $\epsilon$ , fluxes of momentum and energy, rainfall intensity and raindrop size distributions. For the past few decades, the parameter  $C_n^2$ , known as refractivity turbulence structure constant, has been the focus of many radar measurements. It is recognised as the most appropriate parameter to specify the intensity of the refractivity turbulence. The vertical profile of the received power can be

converted into a vertical structure constant and also the eddy dissipation rate, which is a measure of intensity of turbulence. Doppler radars are used to observe clear-air turbulence with coherent techniques. Breaking of gravity waves, believed to be generated in the troposphere, is a source of turbulence in the atmosphere. These waves transport energy and momentum between different layers of the atmosphere and are major sources of turbulence. Observations of upward flux of horizontal momentum are useful to study such effects. *Vincent and Reid* (1983) measured the vertical flux of horizontal momentum using dual complementary coplanar Doppler beams using the Adelaide MF radar.

Since then several studies using VHF radar data explored application of this method for momentum flux computations. *Jain et al.* (1995) and *Rao et al.* (1997) carried out studies on  $C_n^2$  and vertical momentum flux using Indian MST radar. The received radar echo intensity is therefore aspect sensitive and this particular feature is utilised to determine the horizontal correlation length and the characteristics of the radar backscatterers giving rise to observed echo (*Hooper and Thomas*, 1995; *Jain et al.*, 1997). *Ghosh et al.* (2001) studied the height structure of  $C_n^2$  for different seasons using the long series of data from Indian MST radar. They also correlated changes in the height structure of  $C_n^2$  in relation to background atmospheric parameters such as horizontal winds and associated shears. Causative mechanism and characteristics of radar backscatterers at VHF were studied using simultaneous MST radar and radiosonde measurements at Gadanki by *Jain et al.* (2003). Using the same measurements *Ghosh et al.* (2003) determined various atmospheric turbulence parameters.

It was discovered that echoes received at vertical incidence were of a qualitatively different nature than echoes observed looking obliquely (*Gage and Green*, 1978; *Rottger and Liu*, 1978). The oblique echoes have been attributed to turbulent irregularities (*VanZandt et al.*, 1978) and the echoes

observed looking vertically have been attributed to partial reflections from stable layers (*Rottger and Liu, 1978; Gage and Green, 1978*). Comparisons of the magnitude of these specular echoes with balloon soundings have shown a very good correlation with atmospheric stability (*Green and Gage, 1980*). The observed correlation of echo intensity with stability permits the determination of the height of the tropopause (*Gage and Green, 1979; 1982a*). *Gage and Green (1979)* have demonstrated the ability of the VHF radar to detect the tropopause and to determine its height to within 1 km.

At VHF, the contributions from turbulent scattering will dominate for light rainfall rates, but the precipitation scattering will be of comparable magnitude when the rainfall is heavier. However, relatively a few studies have dealt with the use of VHF Doppler radar to observe precipitation. *Fukao et al. (1985c)* presented the first observations of rain echoes at VHF. *Larsen and Rottger (1987)* have also observed double peaks in the spectra corresponding to turbulence and precipitation during heavy rain followed by *Wakasugi et al. (1986)* and *Gossard (1988)*. Methods for using radar data to determine absolute precipitation rates and studies of the drop size distribution have become areas of research (*Sato et al., 1990; Rajopadhyaya et al., 1993; Maguire and Avery, 1994*). *Chilson et al. (1993)* performed experiments using two frequencies at 430 and 46.8 MHz to study precipitation at Arecibo. They found that the raindrop fall speeds and drop size distributions are unreliable in a turbulent environment. Similar dual-frequency studies have also been presented by *Maguire and Avery (1994)*. Precipitation studies using radar which are normally considered to be clear-air instruments have also to be proved quite interesting (*Ralph et al., 1996*) apart from cloud detection studies (*Kobayashi et al., 1999*).

Sudden changes in troposphere structure on time scales less than a few hours or so have been detected by MST radar (*Rastogi and Rottger, 1982; Nastrom et al., 1989*) and documented as tropopause break/folding. The



tropopause is associated with a large positive vertical gradient of signal-to-noise-ratio (SNR) (*Gage et al.*, 1986.; *Nastrom et al.*, 1989). *Jaya Rao et al.* (1994) observed multiple layered structures near the tropopause in the tropical atmosphere using the Indian MST radar. With the advent of clear-air Doppler radar it has become possible to continuously monitor the tropopause under all weather conditions. *Yamanaka et al.* (1996) found layered structure in the subtropics due to turbulence triggered by inertio-gravity waves. MST radars have successfully been used in detecting tropopause. *Mandal et al.* (1998) determined multiple layered structure near the tropopause and its "weakening". Their study emphasised more on the aspect of mass exchange between stratosphere and troposphere during weakening of tropopause.

However, new techniques and applications of the VHF radars have found application in many regions of the atmosphere from the troposphere into stratosphere and mesosphere. MF radar at Adelaide, Australia, with a narrow beam has performed experiments in regard to aspect sensitivity, gravity wave motions and momentum fluxes, turbulence measurements, long-term wind data, tidal and planetary wave studies (*Hocking*, 1979; *Lesicar et al.*, 1994). The observations of VHF radar are able to provide valuable information on tidal winds in the mesosphere and the lower stratosphere due to their very good height and time resolution. VHF radars are also being used in the field of lower ionospheric and the D region studies. The EISCAT radar operating at 224 MHz has been used in studies of the polar mesospheric summer echo and studies of D region turbulence (*Rottger et al.*, 1990; *Collis et al.*, 1992). Another area of application is in the field of equatorial spread F region (ESF) using coherent and incoherent mode of operation.

Several more diverse applications of VHF radars have arisen in recent years (*Caccia and Cammas*, 1998; *Nastrom, et al.*, 1998; *Gossard, et al.*, 1998). These include measurements of rainfall, frequency and spatial domain interferometry, rain drop size distribution and radio acoustic sounding system

(RASS). VHF radars can be effectively used in the area of lightning research. *Rottger et al.* (1995) have reported several interesting observations of lightning, including location and duration and possible generation of infrasound (*Hocking*, 1997). These radars have also been used to document the mesoscale environment associated with severe convection, including vorticity and divergence calculated from a triangle of radars (*Wilczak et al.*, 1992). Many studies have been carried out on lee waves and mountain waves using VHF radar measurements (*Prichard et al.*, 1995; *Caccia et al.*, 1997; *Rechou et al.*, 1999; *Worthington*, 1999; *Rottger*, 2000). *Raja et al.* (1999) observed layered clouds in the Indian monsoon region using the Indian MST radar. *Krishnamurthy et al.* (2002) studied the equatorial waves in the temperature from 4 to 70 km. *Reddy et al.* (2002) studied Chung-Li VHF radar returns from hydrometeors and reflectivity fluctuations associated with “showery” precipitating cloud systems in detail.

With the development of wind profiling radar technology by *Woodman and Guillen* (1974) and *Green et al.* (1975), the first measurements of the vertical velocity with a time resolution of the order of a minute became possible. Some other experiments computed the temperature of the troposphere, stratosphere and mesosphere, even though the techniques differ in each regime, without using additional equipment like RASS. *Gage and Green* (1982a, b) used measurements of backscattered power to deduce temperature profile in the troposphere. Many studies were carried out on vertical motions of large-scale system (*Nastrom et al.*, 1985; *Larsen et al.*, 1988; *Sato*, 1990). Results from case studies of vertical motions reveals that synoptic or sub-synoptic scale vertical motions can be observed using VHF radars (*Nastrom et al.*, 1994; *Warnock et al.*, 1994). *Revathy et al.* (1996) used measurements of vertical velocity spectra from Indian MST radar to identify the vertical profile of Brunt-Vaisala frequency in order to compute the temperature profile with good accuracy. Recent studies on vertical velocities addressed several problems and found new techniques from VHF/MST radar observations (*Nastrom and*

*VanZandt, 1996; Cifelli et al., 1996; Nastrom et al., 1998). Muschinski et al. (1999) compared vertical velocities taken from observations with a very high frequency (VHF) radar using (i) the standard Doppler technique and (ii) the frequency domain interferometry (FDI); in addition, vertical velocity estimates from (iii) a regional numerical weather prediction model (NWPM) were considered.*

Atmospheric gravity waves transport energy and momentum from the lower altitudes and can deposit it into the middle atmosphere. This can be measured with MST radars by observing the altitude variation of vertical velocity fluctuations and the covariance of vertical and horizontal velocity due to these waves as well as its connection to mean wind velocity variations. Many case studies of ST (stratosphere-troposphere) radar observations of gravity wave generation by shear and convective instability have been performed (*Fritts and Rastogi, 1985*). The propagation and dissipation of these waves and the corresponding energy dissipation and momentum fluxes have been studied explicitly for lee or mountain waves (*Nastrom and Fritts, 1992; Prichard and Thomas, 1993*). Many studies proved that gravity waves are major dynamic processes which affect the small-scale structure, such as turbulence (*Hocking, 1985; 1996*), as well as the large-scale dynamics, namely the global circulation of the atmosphere (*Palmer et al., 1986*). Frontal systems, convection, wind shear and topography are thought to be significant sources of gravity wave activity. *Sato (1989)* detected an inertio-gravity wave generated near the tropopause due to shearing instability when a synoptic scale pressure trough passed over the radar site. *Fritts and Nastrom (1992)* have attempted to identify various tropospheric sources of gravity waves. In spite of significant advancements, there have been very few studies of gravity wave activity in the tropical troposphere using radar observations. *Chang et al. (1997)* used ST radar data from Christmas Island (1.95°N, 157.30°W) to study tropospheric gravity waves. Wind observations made using Indian MST Radar have been

analyzed to study gravity wave activity in the troposphere and lower stratosphere (*Dutta et al.*, 1999).

## 2.2. Tropical Cyclone Observations

A tropical cyclone (TC) is a warm-core vortex. The winds that swirl about the center decrease with height, but typically fill the depth of the troposphere (*Haurwitz*, 1935). This inner region, termed the cyclone "core" contains the spiral bands of precipitation, the eyewall, and the eye that characterise tropical cyclones in radar and satellite imagery (e.g. *Wexler*, 1947; *Dvorak*, 1975). The inner region winds can become intense, and in extreme cases reach  $90 \text{ ms}^{-1}$  just outside the eye. As a tropical cyclone approaches land, the outer winds begin to be modified. Intense convection tends to form ahead of the TC center and to its right in the frictional convergence where onshore winds reach the coast (*Parrish et al.*, 1982; *Burpee and Black*, 1989). This asymmetric heating tends to induce a track acceleration toward the enhanced convection by forcing vortex asymmetries as described theoretically by *Willoughby* (1992). Once a TC has passed onshore increased roughness leads to an immediate reduction of surface winds (e.g., *Powell*, 1982; 1987).

Tropical cyclones can be thought of as engines that require warm, moist air as fuel (*Emanuel*, 1987). In 1948, *Erik Palmén* observed that tropical cyclones required ocean temperatures of at least  $26.5^{\circ}\text{C}$  for their formation and growth. *Gray* (1979) also pointed out the need for this warm water to be present through a relatively deep layer (50 m) of the ocean. Above this temperature deep convection can occur, but below this value the atmosphere is too stable and little to no thunderstorm activity can be found (*Graham and Barnett*, 1987).

The general mechanisms by which the eye and eyewall are formed in tropical cyclones are not fully understood, although observations have shed some light on the problem. The calm eye of the tropical cyclone

shares many qualitative characteristics with other vortical systems such as tornadoes, waterspouts, dust devils and whirlpools. Given that many of these lack a change of phase of water (i.e. no clouds and diabatic heating involved), it may be that the eye feature is a fundamental component to all rotating fluids. It has been hypothesized that supergradient wind flow (i.e. swirling winds that are stronger than what the local pressure gradient can typically support) present near the radius of maximum winds (RMW) causes air to be centrifuged out of the eye into the eyewall, thus accounting for the subsidence in the eye (e.g. *Gray and Shea 1973; Gray 1991*). However, *Willoughby (1990b; 1991)* found that the swirling winds within several tropical storms and hurricanes were within 1-4% of gradient balance.

Another feature of tropical cyclones that probably plays a role in forming and maintaining the eye is the eyewall convection. Convection in tropical cyclones is organised into long, narrow rainbands which are oriented in the same direction as the horizontal wind. Because these bands seem to spiral into the center of a tropical cyclone, they are called "spiral bands". Along these bands, low-level convergence is a maximum, and therefore, upper-level divergence is most pronounced above. A direct circulation develops in which warm, moist air converges at the surface, ascends through these bands, diverges aloft and descends on both sides of the bands. The spiral bands are noted to move towards the center and encircle it and the eye and eyewall form (*Willoughby, 1979; 1990a; 1995*). Some of the most intense tropical cyclones exhibit concentric eyewalls, two or more eyewall structures centered at the circulation center of the storm (*Willoughby et al., 1982; Willoughby, 1990a*).

In several of world oceans the frequency, origin point and movement of tropical cyclone have been observed varying with the El Niño/Southern Oscillation (ENSO) Cycle (*Evans and Allen, 1992; Lander, 1994; Basher and Zheng, 1995*). Early studies served to indicate that the advection and conservation of high Potential Vorticity (PV) stratospheric air within a

narrow intrusion down to tropospheric levels can establish an upper-level PV anomaly and help trigger cyclogenesis (*Bleck and Mattocks, 1984; Boyle and Bosart, 1986*). Also the production of diabatically-induced potential vorticity at intermediate and low-tropospheric levels within or in the neighbourhood of a maturing cyclone can result in a lower-level positive PV anomaly (*Gyakum, 1983; Boyle and Bosart, 1986*). *Rossa et al (2000)* studied the growth and decay of the PV-tower for one major event of cyclogenesis in the central North Atlantic.

The time and spatial evolution of gravity-wave characteristics are analysed using wavelets in vertical profiles of temperature and winds at Tromelin Island during the passage of the intense tropical cyclone Hudah in the Southern Ocean Indian Basin in 2000 (*Chane-ming et al., 2002*). Inertia-gravity waves were observed in the upper troposphere and lower stratosphere with dominant vertical wavelengths of 1.5–3 km, horizontal wavelengths <2000 km and periods of 0.6–1.6 days. Large amounts of gravity-wave energy were detected during landfalls of the tropical cyclone. *Dickinson and Molinari (2002)* provided evidence for equatorial modes, under the right conditions can supply precursor disturbances for repeated formation of tropical cyclones.

### **2.3. Cyclone Observations using MST Radar**

The MST radar technique has a unique capability of the measuring background air motion. Although the horizontal coverage of these radars is usually limited by a large antenna aperture, which is hard to steer at low elevation angles, they can observe above the tropopause height and motions in a clear sky continuously in time. The MST radars can be a powerful tool in observing the vertical structure of tropical cyclones. The first observation of a typhoon using the MST radar technique was made with the MU radar at Shigaraki, Japan (*Kato et al., 1984*). The Chung Li radar at Taiwan has an ideal location to study typhoons in their developing stage since

it is on the middle of a typical course of typhoon. A short observation of the vector wind field accompanied with a typhoon by Chungli radar is reported by *Hung et al.* (1988).

A clear turning of the wind velocity associated with the typhoon was observed up to a height of around 18 km, in which short-period wind fluctuations showed strong effects associated with the typhoon up to 24 km (*Sato et al.*, 1991). Prominent waves with vertical wavelength of 2-4 km were found throughout the observation period. These waves propagated both upward and downward from around the layer of a temperature inversion, suggesting the generation of these waves from that layer. *Rottger et al.* (1991) studied a typhoon passage using Chungli VHF radar. It was observed that during the closest approach of the typhoon the winds in the altitudes above 5 km rotated suddenly from northeasterly to northwesterly direction. After the passage the zonal component recovered but the meridional component changed to southerly direction, resulting in a southeasterly wind. *Sato* (1993) found that the typhoon is significant as an energy source of gravity waves. Some of the gravity waves were generated so as to decelerate strong cyclonic wind of the typhoon although the estimated drag was only several percent of surface friction. The gravity waves associated with the typhoon appeared to the top of the observed height region, and hence, they may reach the upper- atmospheric region. *Dhaka et al.* (2003) studied the gravity wave generation in the lower stratosphere due to passage of the typhoon 9426 (Orchid) observed by the MU radar.

#### **2.4. Tropopause Studies**

In recent years, the tropopause region has received much attention because there is a growing necessity of knowing the temporal and spatial structure of meteorological parameters within the transition zone between the troposphere and the stratosphere. In order to estimate the stratospheric-tropospheric exchange of mass, water, and chemical constituents

it is necessary to have precise knowledge about the meteorological conditions of the tropopause. Of particular interest is the tropical tropopause, since it is widely accepted that most water vapour enters the stratosphere here; hence, tropical tropopause conditions have a strong influence on the stratospheric water vapour distribution. Recently, *Mote et al.* (1995) showed that tropical stratospheric air appears to retain information about tropopause conditions that it encountered during more than a year as it rises through the stratosphere.

The detection of stable atmospheric layers by means of partial specular reflection with monostatic VHF radars provides a direct and simple method for determining the height of the tropopause. When the tropopause is well defined and consists of a pronounced discontinuity in atmospheric stability, its height is given by the height at which the magnitude of the radar echo from the vertically directed antenna starts to increase appreciably (*Gage and Green*, 1978). The coherency of tropical tropopause height variations at several widely separated geographic locations was explored by *Reid and Gage* (1985). It was found that the interannual variations of tropopause height were positively correlated indicating a global signal in the tropopause height variations. This result is consistent with the idea that the tropical tropopause is formed as a result of the most intense tropical convective activity and that local (less intense) convection may play a minor role. The tropical tropopause is thought to be formed as the direct result of the deepest and most active convection in the tropics. As a consequence, the variability of the tropical tropopause can be directly attributed to variations in tropical convective activity, and the climatology of the tropical tropopause can provide a proxy climatology of tropical convective activity. The hypothesis that systematic increases in tropical tropopause potential temperatures occur away from major centres of convection was tested by looking for systematic zonal gradients in tropopause potential temperature across the western Pacific network (*Gage and Reid*, 1987).



The sensitivity of the tropopause height to various external parameters has been investigated using a global circulation model (GCM). The tropopause was found to be strongly sensitive to the temperature at the earth's surface, less sensitive to the ozone distribution, and hardly sensitive at all to moderate changes in the earth's rotation rate (*Thuburn and Craig, 1997*). *Sato and Dunkerton (2002)* observed double tropopause structure, which is related to the existence of a strong westerly jet around 11 km, and the appearance of a lower tropopause corresponds to the southward shift of the westerly jet. *Zhou (2000)* showed that the tropical tropopause is affected by the stratospheric quasibiennial oscillation (QBO) and the tropospheric El Niño - Southern Oscillation (ENSO). The QBO signature in the tropical tropopause is mainly zonally symmetric and has smaller amplitudes than the ENSO signature. It is argued that certain aspects of tracer patterns and related stirring by the flow in the extratropical tropopause region can be understood in terms of a transition between dynamically active and passive tracer advection, called *active to passive tracer transition*. In the framework of surface quasi-geostrophic dynamics a specific initial value problem is defined and investigated (*Wirth et al., 2005*).

## **2.5. Studies on Gravity Waves**

Many theoretical and observational studies have shown that gravity waves play an important role in the global atmospheric circulation, redistributing momentum in the atmosphere through their generation, propagation and breaking. Although the majority of studies have emphasized the role of gravity waves in the global circulation of middle and high-latitude regions, some theoretical studies suggest the importance of gravity waves for the mechanism of the quasi-biennial oscillation (QBO) and semi-annual oscillation (SAO) of the mean zonal wind in the equatorial stratosphere and mesosphere. Gravity waves in the equatorial region are considered to be mainly excited by convection through various generation mechanisms. The importance

of gravity waves lies in the fact that they are the major components of the total flow and also contribute to the temperature variability fields in the mesosphere. Moreover, they are associated with the fluxes of momentum that communicate stress over very large distances. In order for these waves to exert a net drag on the atmosphere it must get saturated and attenuated. The saturation of gravity waves takes place near the mesosphere region due to the wave breaking mechanism.

*Hines* (1960) first suggested that irregular motions observed in the upper atmosphere might be interpreted in terms of internal gravity waves. Gravity wave processes are now recognized to be important for the dynamics of the atmosphere (*Holton*, 1975; *Andrews et al.*, 1987). *Cadet and Teitelbaum*, (1979) presented observational evidence for the presence of short vertical wavelength waves propagating westward and upward in the tropical upper troposphere and stratosphere which are identified as internal inertia-gravity waves. It is now confirmed that the gravity waves are mainly excited in the troposphere due to various reasons like: interaction of surface winds with topography, wind shear associated with jet-streams, geotropic adjustment, cumulonimbus convection, and various meteorological disturbances such as frontal systems, thunderstorms or typhoons (e.g. *Fritts et al.*, 1984).

Gravity waves transport energy and momentum from the lower atmosphere to the middle and upper atmosphere producing the dynamical stress which is required to maintain the general circulation (*Lindzen*, 1981). Subsequent theoretical and observational studies have confirmed these predictions and provided evidence of a zonal drag of  $\sim 50 - 100 \text{ ms}^{-1} \text{ day}^{-1}$  and a corresponding strong meridional circulation (*Holton*, 1982; *Dunkerton*, 1982; *Nastrom et al.*, 1982; *Vincent and Reid*, 1983, *Fritts*, 1984, *Garcia and Solomon*, 1985; *Miyahara et al.*, 1986; *Fritts and Vincent*, 1987). Small-scale waves such as gravity waves cannot be directly resolved in the major existing atmospheric general circulation models and therefore they have to be

parameterized (*McLandress*, 1998). The data from meteorological rocketsonde and high-resolution radiosonde observations enabled *Hirota* (1984), *Hamilton* (1991), *Eckermann et al.* (1995) and *Allen and Vincent* (1995) to draw up a climatology of gravity waves in the middle and the lower atmosphere. Recent works on the characteristics of gravity wave parameters, wave spectra and the temporal evolution are mainly based on radar measurements (*Nakamura et al.*, 1993; *Kuo and Lue*, 1994; *Connor and Avery*, 1996).

The use of aircraft data in the study of gravity waves were examined by *Metcalf* (1975). *Alexander and Pfister* (1995) developed a method to calculate the vertical fluxes of horizontal momentum flux carried by short period horizontal scale gravity waves ( $\lambda=10-100$  km) using aircraft measured winds in the lower stratosphere. Lidar techniques provide suitable measurements with high spatial and temporal resolution for the study of gravity waves at heights between 30 km and 80 km using a Rayleigh lidar (*Chanin and Hauchecorne*, 1981; *Shibata et al.*, 1986), between 10 km and 30 km using a Raman lidar (*Keckhut et al.*, 1990; *Hauchecorne et al.*, 1992) and at heights  $85\pm 105$  km using a Na lidar (*Gardner and Voelz*, 1987).

Gravity wave variances as a function of altitude, season and latitude are now well understood at mid- latitude continental observations (*Eckermann*, 1995; *Alexander*, 1998). The time and spatial localization of gravity waves, their characteristics and the activity are poorly documented (*Vincent*, 1984; 1990). *Chane-ming et al.* (2000) studied gravity waves in the tropical middle atmosphere over La Reunion Island (21°S, 55°E) with lidar using wavelet techniques. *Dunkerton and Butchart* (1984) examined longitudinally asymmetric features of gravity wave propagation in a sudden warming using geostrophic wind fields in the stratosphere for three days of winter 1979. *Alexander et al.* (2002) studied the latitudinal variations observed in gravity waves with short vertical wavelengths. *Beres et al.* (2002) examined the effects of tropospheric wind shear on the spectrum of convectively

generated gravity waves. The effect of deep convection on the intensities of gravity waves and turbulence during the summer at White Sands, New Mexico, is investigated by *Hansen et al.* (2002) using 50-MHz Mesosphere – Stratosphere – Troposphere (MST) radar observations and surface weather reports.

Both *Fovell et al.* (1992) and *Alexander et al.* (1995) have described general features associated with gravity waves evolved in their 2-dimensional meso-scale models including the dominance of high frequency (periods of few tens of minutes) with short horizontal wavelengths (less than 100 km). *Sato et al.* (1991) also indicated similar disturbances in a typhoon case at midlatitude using MU radar. A more recent study by *Lane et al.* (2001a, b), using a 3-dimensional numerical model, resolved successfully both the meso-scale cloud clusters, and the generation of gravity waves in the lower stratosphere. These gravity waves are important because they can significantly interact with the dynamical systems (*Takahashi, 1999; Beres et al., 2002*). *Alexander and Holton* (1997) have addressed some of the issues relating to the qualitative and quantitative contribution these gravity waves can make to the quasi-biennial oscillation (QBO). Their study suggested that about 25 percent of the required momentum fluxes attributed to the QBO originate from these gravity waves.

Some interesting observed features of the gravity wave generated during thunderstorms were presented in the stratosphere by *Dewan et al.* (1998) using satellite data. From investigations based on numerical simulations and observations, it was suggested that these gravity waves evolved as circularly symmetric waves in the lower stratosphere. *Dhaka et al.* (2001) reported high frequency gravity waves (wave periods of less than one hour), in some of the experiments conducted in the tropics, using MST radar at Gadanki, India, during summer monsoon. Increases in momentum fluxes due to these gravity waves in the tropospheric and lower stratospheric regions and a high magnitude

of vertical winds (with some sudden bursts in the order of  $8\text{--}10\text{ ms}^{-1}$ ) were noted during the convection event. *Shibagaki et al.* (2000) also reported strong vertical winds inside a precipitating cloud extending up to an altitude of 14 km using MU radar and other co-located meteorological radars. These large magnitude vertical winds were measured during the occurrence of a meso-scale convective complex (MCC) system. Gravity wave generation due to convection specifically in the tropics, has attracted serious attention in attempts to understand the mechanism and evolved characteristics of such wave disturbances (*Dhaka et al.*, 2002).

## **2.6. Stratosphere –Troposphere Exchange**

Stratosphere–troposphere exchange (STE) is important for the chemical composition of both the lowermost stratosphere (LS) and the troposphere. Modifications in a changing climate may significantly affect stratospheric ozone depletion (*Butchart and Scaife*, 2001) and the oxidizing capacity of the troposphere (*Lelieveld and Dentener*, 2000). However, STE is still poorly understood and inadequately quantified, due to the involvement of physical and dynamical processes on local to global scales (*Holton et al.*, 1995), and conceptual problems. On a long-term and global scale and in the zonally averaged sense, there is slow ascent from the troposphere to the stratosphere in the tropics, quasi-isentropic transport to the extratropics in the stratosphere and downward flow from the stratosphere to the troposphere in middle and higher latitudes (*Brewer*, 1949; *Plumb*, 1996; *Mote et al.*, 1996; *Waugh*, 1996). This circulation is related to the dissipation of extratropical planetary and gravity waves in the stratosphere (*Haynes et al.*, 1991).

Based upon calculations of the monthly averaged hemispheric mass flux into the LS and of the mass of the LS, the monthly mean net mass flux across the tropopause can be evaluated (*Appenzeller et al.*, 1996; *Rosenlof*, 1995). Actual STE is highly episodic, associated with strong mesoscale

perturbations of the tropopause (*Appenzeller and Davies, 1992*), and occurs in both directions. In situ and remote sensing observations have produced evidence for the existence of layers of originally tropospheric air in the midlatitude LS (*Hintsa et al., 1998; Vaughan and Timmis, 1998*), and stratospheric intrusions into the troposphere (*Danielsen, 1968; Stohl and Trickl, 1999*). *Holton et al., (1995)* summarized and extended arguments showing that the net mass flux through the tropical tropopause is controlled non-locally by angular momentum forcing in the extratropical stratosphere. Figure 2.1 shows the dynamical aspects of STE.

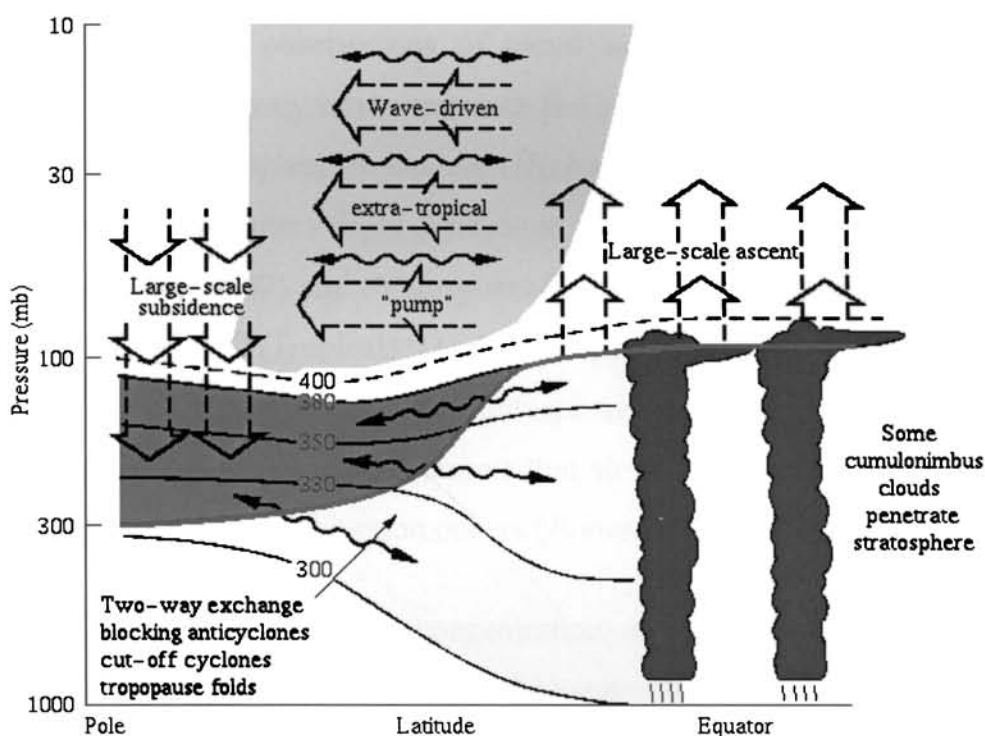


Figure 2.1. Dynamical aspects of stratosphere-troposphere exchange. (*Holton et al., 1995*).

In the figure the tropopause is shown by the thick line. Thin lines are isentropic or constant potential temperature surfaces labelled in Kelvins. Heavily shaded region is the "lowermost stratosphere" where isentropic surfaces span the tropopause and isentropic exchange by tropopause folding occurs. The region above the 380K surface is the *overworld*, in which isentropes lie entirely in the stratosphere. Yellow shading in the overworld

denotes wave-induced forcing (the extratropical *pump*). The wiggly double headed arrows denote meridional transport by eddy motions, which include tropical upper-tropospheric troughs and their cut-off cyclones as well as their mid-latitude counterparts including folds. Not all eddy transports are shown; and the wiggly arrows are not meant to imply any two-way symmetry. The broad arrows show transport by the global-scale circulation which is driven by the extratropical pump. This global scale circulation is the primary contribution to exchange across isentropic surfaces (e.g., the ~380 K surface) that are entirely in the overworld.

Satellite observations of cloud top temperatures suggest that optically thick clouds very rarely approach the height (inferred from brightness temperature) of the tropical tropopause (*Highwood and Hoskins, 1998*). Data from the NASA Water Vapor Exchange Experiment (*Kley et al., 1982; Knollenberg et al., 1982*) and Stratosphere-Troposphere Exchange Program tropical mission (STEP/Tropical) (*Danielsen, 1993*) demonstrated that cumulo - nimbus clouds can penetrate the stratosphere and mix irreversibly with stratospheric air. It has long been known that air enters the stratosphere at low latitudes, where net upward motion occurs (*Brewer, 1949; Dobson, 1956*).

The observed low concentration of water vapour can not be explained unless tropospheric air enters the stratosphere dominantly across the tropopause (*Brewer, 1949*). The failure of freeze drying at the mean tropical tropopause temperature to dehydrate the stratosphere to observed water vapour mixing ratio led *Newell and Gould-Stewart (1981)* to propose the stratospheric fountain hypothesis. According to this hypothesis the tropospheric air enters the stratosphere preferentially in the areas where the tropical tropopause temperatures are below their annual and longitudinal mean values. The fountain region is mainly over the western pacific with a little variation of season.

The role of jet stream frontal zone clear air turbulence as a mechanism for exchange of air and chemical trace constituents as between the troposphere and stratosphere. The observations reveal that tropopause folds are mixing regions whose chemical characteristics lies somewhere between those of the troposphere and the stratosphere. It was first suggested by *Molina and Rowland* (1974) that the transport of chlorofluoromethanes in to the stratosphere would lead to the depletion of ozone within the UV-absorbing ozone layer of the atmosphere. Correlation between stratospheric temperature, total ozone and tropospheric weather systems were studied by *Petzoldt et al.* (1994).

Recently, a few attempts to measure the momentum flux and the implied accelerations in the lower atmosphere have been done by *Fukao et al.* (1987), *Mc Afee et al.* (1989), and *Fritts et al.* (1990). They have attributed the observed flux primarily to either mesoscale and convective motions or to the wind and terrain alignment. Momentum flux observations by *Fritts et al.* (1990) indicated largely zonal accelerations below the tropospheric jet and deceleration above it.

Dynamical, chemical, and radiative coupling between the stratosphere and troposphere are among the many important processes that must be understood for prediction of global change. Of special significance is the transport of trace chemical species, natural and anthropogenic, between the stratosphere and the troposphere. For instance, anthropogenic species transported from the troposphere into the stratosphere initiate much of the chemistry responsible for stratospheric ozone depletion, according to a large body of evidence (e.g., *WMO*, 1995). Conversely, downward transport from the stratosphere not only constitutes the main removal mechanism for many stratospheric species, including those involved in ozone depletion, but also represents a significant input of ozone and other reactive species into the tropospheric chemical system (e. g., *Levy II et al.*, 1980). It is now widely



appreciated that the dynamics of the troposphere and the stratosphere are, in principle, inseparable (e.g., *Hoskins et al.*, 1985). Chemical effects from stratosphere–troposphere exchange (STE) can, in turn, influence the radiative flux balance in the troposphere and lower stratosphere, and can do so in more than one way (e.g., *Ramaswamy et al.*, 1992; *Toumi et al.*, 1994). STE can therefore have a significant role in the radiative forcing of global climate change.

As stated by *Holton et al.* (1995), deformations of the tropopause can be rapid and are mostly reversible, thus possibly irrelevant for stratosphere–troposphere exchange. In such circumstances the presence of waves can make the transport effective. The waves found here, even those of long period which induce quasi-horizontal displacements of air parcels, can contribute to the transport between the stratosphere and the troposphere by additionally deforming the tropopause. But even this transport could be reversible. However, other waves of shorter wavelength and probably also of shorter period, induced by nonlinear interaction or simply directly generated by the meteorological conditions identified above, can render the transport truly irreversible. Such a mechanism but of a different scale has been invoked by *Danielsen et al.* (1991) to explain that the transport through the tropopause by planetary waves can become irreversible by mixing induced by internal waves of short vertical wavelength. Inertial–gravity waves could play a very important role in mixing and transport. *O’Sullivan and Dunkerton* (1995) have shown that these waves are more relevant for mixing of constituents than for momentum transport. The transport takes place not only by the direct displacement of air parcels but also by instabilities, which can appear in the wave field (*Dunkerton*, 1984).

It has been shown by *Shapiro* (1980) from the analysis of data obtained by a research aircraft, turbulence can also be a mechanism for stratosphere–troposphere exchange. *Sherwood and Dessler* (2000) presented a

hypothesis on the dehydration and transfer of air from the tropical troposphere into the stratosphere based on the existence of a thick tropopause layer, in which vertical and horizontal mixing are both significant. *Sherwood and Dessler (2001)* described a model for convective and advective transport across the tropical tropopause. They found that for reasonable parameter settings, the combined action of convection, isentropic mixing, and advection by the large-scale circulation in the model can produce realistic water vapor and ozone profiles while balancing the energy budget.

Convective tropical cyclones initiate exchanges of mass and energy between the troposphere and stratosphere. A tropical cyclone is characterized by extremely violent horizontal winds, convergent in the cyclonic direction in the lower layers, divergent in the anticyclonic direction in the high troposphere. Disturbances in the tropopause above the most active cloud masses can be the origin of transfer from the high troposphere to the low stratosphere. When the cyclone is particularly strong, which was the case for cyclone Marlene, its influence can extend to the outer environment of the cyclone, where mesoscale stratosphere - troposphere transfers are possible. a direct transport of the mesoscale air masses, induced by strong ageostrophic movements generated in the upper troposphere around the convective area (*Barray et al., 1999*). *Zeng and Pyle (2005)* studied influence of El Nino Southern Oscillation on stratosphere/ troposphere exchange and the global tropospheric ozone budget.

## Chapter #3

*MST Radar - System Description & Data  
Processing Techniques*

### 3.1. Introduction

The technique of using sensitive pulsed Doppler radar to investigate the atmosphere on continuous basis with good height and time resolution, in the height range from near ground to about 100 km is known as MST Radar technique. The MST (Mesosphere-Stratosphere-Troposphere) technique, which uses sensitive radars in the frequency range 30-3000 MHz to examine the optically clear atmosphere below roughly 100 km, can be considered as having evolved from the pioneering work of *Woodman and Guillen* (1974). They reported for the first time echoes from mesosphere and also from stratosphere. They showed that these echoes are due to scattering from turbulence of scale size of nearly half of the wavelength. To increase the detectability of the signal as well as to reduce the computational requirements, they introduced coherent pre-integration of the data. The origin of the echoes in these regions was determined to be Bragg scattering from refractive index fluctuations associated with turbulent irregularities of scale sizes nearly half of the radar wavelength. Because such turbulence is virtually ubiquitous in the atmosphere, it can be used as a tracer of the clear air motion, provided that it moves with the mean flow.

Studies of *Woodman and Guillen* (1974) triggered the evolution of a new generation of VHF/UHF radars for atmospheric research. The first of this type of radar was built near Boulder, Colorado at Sunset (*Green et al.*, 1975) followed by the SOUSY (SOUnding SYstem) VHF radar in West Germany (*Czechowsky et al.*, 1976). Since then a number of radars capable of sensing turbulence in the neutral atmosphere have been built and operated throughout the world. The detailed explanation of these radars are reported elsewhere (Poker Flat radar in Alaska has been described by *Balsley et al.* (1980); MU radar near Kyoto, Japan by *Fukao et al.* (1985a, b); Buckland Park radar near Adelaide, Australia by *Vincent et al.* (1982; 1987); Arecibo 50 MHz radar by *Rottger et al.* (1981); Chung-Li radar in Taiwan by *Chao et al.* (1986);

Equatorial radar at Indonesia by *Fukao et al.* (1990) and the Indian MST radar at Gadanki, India by *Rao et al.* (1995)). *Hocking* (1997) described some of the existing MST/ST radars in his review article.

Since one of the primary purposes of all MST/ST radars is the measurement of atmospheric winds, the term “wind profiler” has gained acceptance with meteorologists. Initially the use of MST radar technique was confined to the realm of atmospheric research rather than operational Meteorology. But nowadays it is used regularly for synoptic purposes also (*Larsen and Rottger*, 1982). An additional consideration for wind profilers is that they must be sufficiently reliable to be operated continuously in unattended mode (*Ecklund et al.*, 1979; *Frisch et al.*, 1986).

### **3.2. Wind information from MST Radars**

There are two basic techniques to extract the vector wind information from the MST radar returns. They are the following.

#### **3.2.1. Doppler beam swinging method (DBS)**

This technique uses a large antenna array with correspondingly narrow radiation patterns and with a minimum of three beams pointing in different non-coplanar directions to measure the wind velocities. These three directions generally include one at zenith and other two at off-zenith angles. The velocity vectors are computed from the line of sight velocities from these directions. The DBS technique assumes that the vector wind field is steady in time and uniform in space over the volume containing the range cells used. For Indian MST radar oblique beams with zenith angle  $10^\circ$  are utilised for wind estimation in place of  $15^\circ$  as  $15^\circ\text{N}$  beam is almost orthogonal to the earth's geomagnetic field at Gadanki where the radar is located. Estimation of vertical and horizontal velocities is done from the radar return through signal processing. For a preset condition of Doppler resolution and maximum Doppler

shift, the percentage error in velocity determination decreases with increasing velocity.

### **3.2.2. Spaced antenna drift (SAD) method.**

This method uses three or more spaced antennas and the received signals are cross-correlated to determine the horizontal velocity components. In this method the transmitter beam is pointed vertically while the signal is received at three (or more) spaced antennas (receivers) and the horizontal velocity is obtained from the time delays as the signal pattern drifts past the spaced antennas. The vertical velocity can be determined either from the phase information or from the Doppler shift. Apparently it appears that the two techniques are different but they are closely related and the difference is only in the experimental sense. The DBS method uses a narrow beam at an angle  $\theta$  and measures the Doppler shift, which is a measure of the radial velocity. The SAD method on the other hand receives energy returned over a range of angles around zenith and measures the movement of the amplitude pattern over the ground which moves at velocity twice that of the scatters.

### **3.3. Indian MST Radar**

A VHF radar has been established under the Indian Middle Atmosphere Program (IMAP) program at Gadanki (13.5°N, 79.2°E) in southeastern part of India, as a national facility to probe the tropical atmosphere. This radar commonly known as the Indian MST radar is highly sensitive, monostatic, pulse coded, coherent VHF phased array radar operating at 53MHz with a average power-aperture product of  $7 \times 10^8 \text{ Wm}^2$  (Rao *et al.*, 1995; Jain *et al.*, 1995). The system design specification of Indian MST radar is given in table 3.1. Figure 3.1a and b show the location of Indian MST radar and the functional block diagram of the radar system. The functioning of the various radar subsystems is described briefly in the following paragraphs.

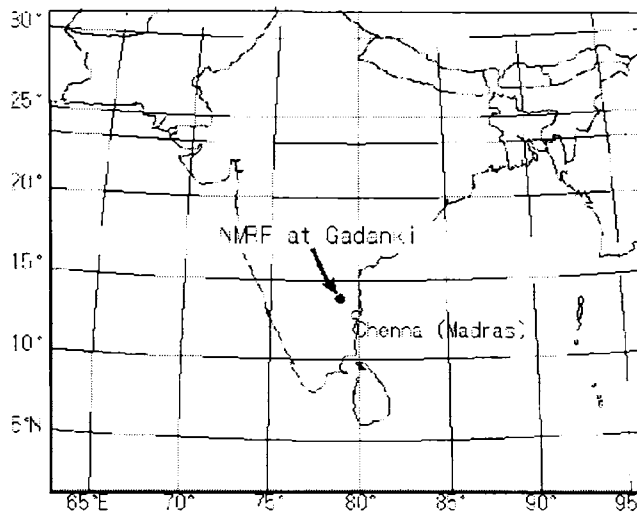


Figure 3.1a. Location of Indian MST radar

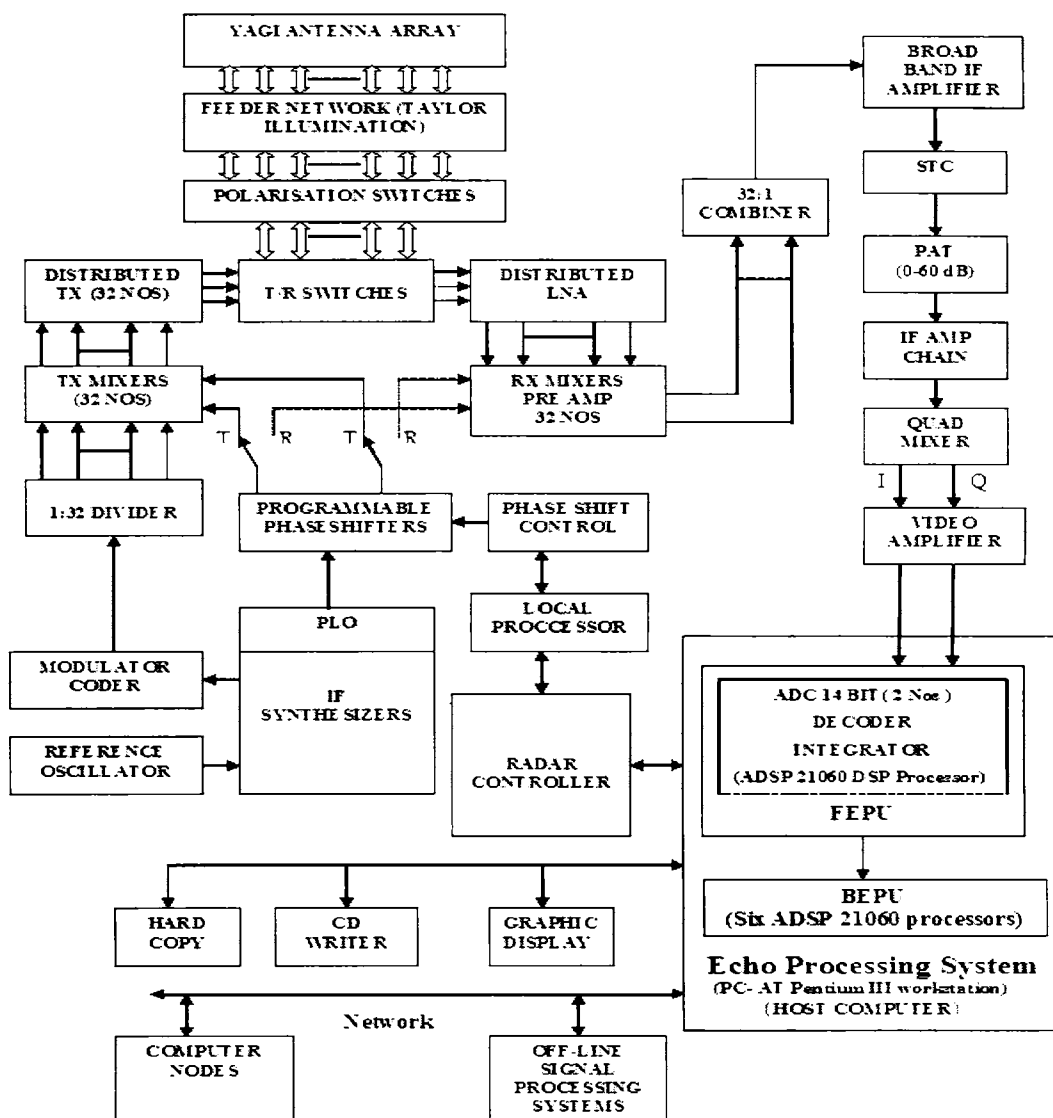


Figure 3.1b. Functional block diagram of Indian MST Radar

### 3.3.1. Antenna array and feeder network

The phased array consists of two orthogonal sets, one for each polarization of 1024 three element Yagi-Uda antennas arranged in a 32x32 matrix over an area of 130x130 m. The two sets are co-located with pairs of crossed yagis mounted on the same sets of poles. The array is aligned along the geomagnetic N-S and E-W directions to enable the radar beam to be pointed perpendicular to the Earth's magnetic field for ionosphere backscatter applications. The inter-element spacing in the matrix grid is  $0.7\lambda$ . These allow grating lobe free array beam scanning up to scan angle of about  $20^\circ$  from zenith. The array is illuminated in either of the polarizations using 32 transmitters of varying power each feeding a linear sub-array of 32 antennas. The feeder network consists of two orthogonal sets, one for each polarization of 32 parallel runs of centered series structures. Figure 3.2a shows the feeding scheme for one linear sub-array of 32 antennas.

The power distribution across the array follows an approximation of modified Taylor distribution in both principle directions. The distribution function was arrived at to realize a  $-20$  dB level for the first side lobe of the radiation pattern (*Elliot*, 1985). Figure 3.2b shows the amplitude distribution along one sub-array of 32 antennas. The desired power distribution across the array is accomplished in one principle direction by the differential powers of the transmitters and the other direction by the appropriate coupling coefficients of the series feed network (*Sarkar et al.*, 1988). The far field array pattern for the aperture distribution shown in figure 3.2b was computed using the expression similar to that given by *Ma* (1988) for a planar array. Figure 3.2c shows the array pattern for the E-plane. The beam pointing accuracy of antenna is better than  $0.2^\circ$  and 3 dB beam width is in the range of  $2.8^\circ$  to  $3^\circ$ . The radar beam can be positioned at any look angle over arrange of  $\pm 20^\circ$  from zenith in the EW and NS planes with a resolution of  $1^\circ$  by using the 8-bit phase shifters.



PARAMETERS	SPECIFICATIONS
Location	Gadanki (13.45° N, 79.18° E)
Frequency	53 MHz
Peak power	2.5 MW
Peak power aperture product	$3 \times 10^{10} \text{ Wm}^2$
Maximum duty ratio	2.5 %
Number of Yagi antennae	1024
Beam width	3°
Angular coverage of beam scans	$\pm 20^\circ$
Pulse width	1 to 64 $\mu\text{s}$ (coded/uncoded)
Pulse repetition frequency	62.5 Hz - 8 k Hz
Maximum number of coherent integrations	512
Maximum number of range bins	512
Maximum number of FFT points	1024
Radar controller	PC-AT P-III featuring programmable experiment specification file
Computer system	DSP processors for data acquisition and processing

Table 3.1. System specification of Indian MST radar

### 3.3.2. High power transmitter system

The total peak power transmitted is about 2.5 MW is achieved by 32 transmitters, whose output power range from 120 kW to 15 kW, each feeding a sub-array of 32 yagis. A typical transmitter system has four power amplifier stages and associated power monitoring and controlling, and safety interlock circuits. The 32 transmitters are distributed in four huts, one contiguous pair on the north side and the other on the south side of the array. One local processor (LPC), which is linked to the remotely located radar controller, serves a group of eight transmitters. The LPC controls all operations of the transmitters and also provide controls to the duplexers, polarization switches and 8-bit phase shifter. The transmitters can operate upto a duty cycle of 2.5%, limiting the total power average of about 60 kW. It is possible to transmit both coded and uncoded pulses with pulse repetition frequency (PRF) in the range of 62.5 Hz to 8 kHz, keeping the duty cycle from exceeding the limit. The uncoded pulsewidth can vary from 1 to 64  $\mu\text{s}$  in multiple of 1. The

coded pulses are 4, 8, 16, 32, 64 baud bi-phase complimentary pair with a baud length of 1  $\mu$ s, providing a range resolution of 150 m. The output of transmitter is fed to an antenna sub-array through a transmit-receive (T/R) duplexer switch and polarization selection switch.

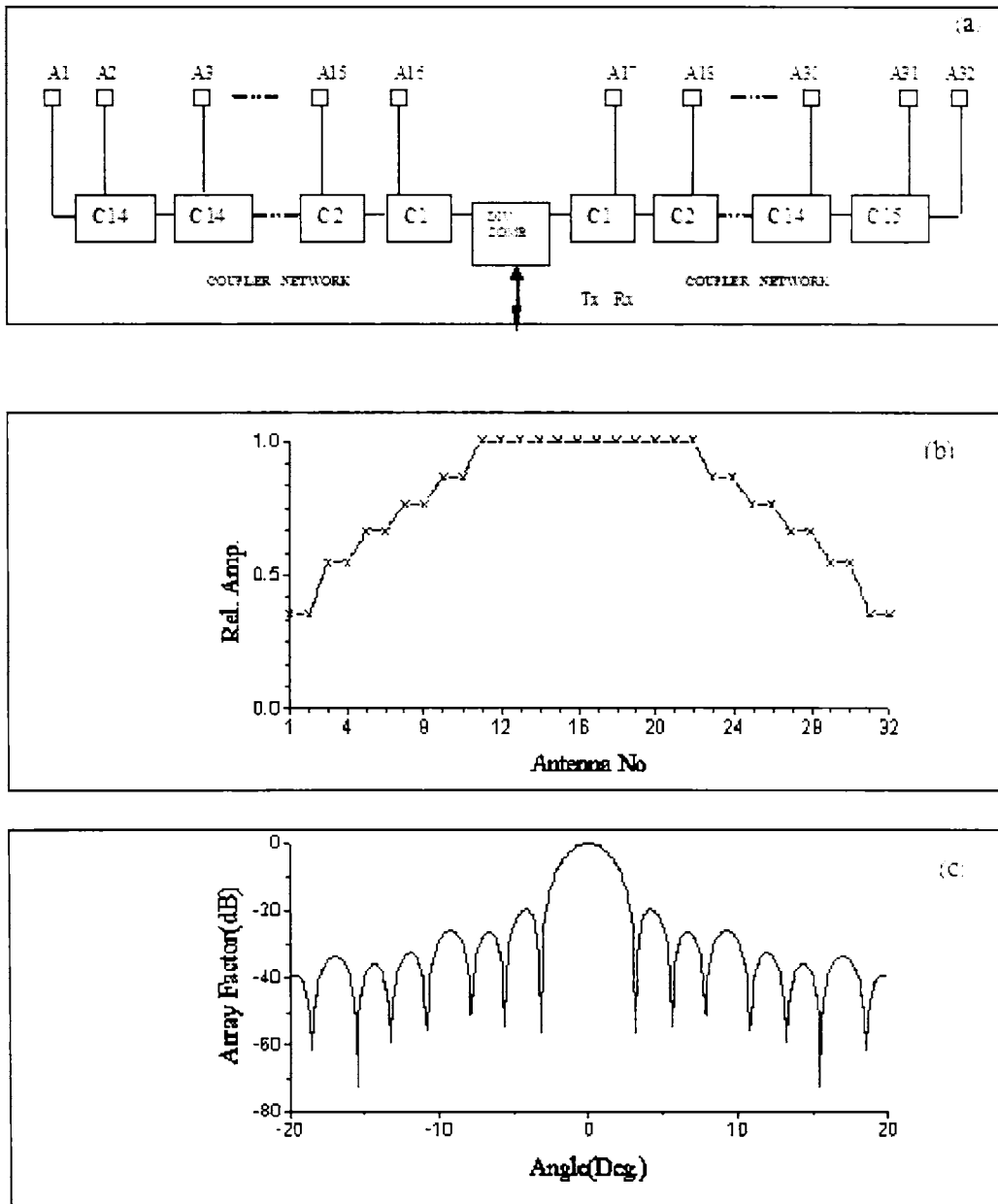


Figure 3.2. (a) Feeder line configuration for one linear subarray of 32 antennas (b) A step-wise approximation to modified Taylor distribution for the amplitude along one sub-array of 32 antennas & (c) Far field array pattern computed for the amplitude distribution shown in Figure 3.2b.

### 3.3.3. Receiver and signal processing system

The phase coherent receiver with quadrature channels, having an overall gain of 120 dB, a dynamic range of 70 dB, and a bandwidth matched to the baud length of the coded pulse, detects the weak back scattered signals. T/R switches using hybrid couplers and PIN diodes accomplish the switching of the antenna array between the transmitter and receiver. The IF outputs from the 32 channels are combined, after having been Taylor weighed in order that the receiver beam has the same characteristics as the transmit beam. A broadband modular amplifier having a gain of 15 dB amplifies the combined IF signal. The signal then goes through a sensitivity time control (STC) circuit providing a fixed attenuation of 20 dB up a selectable range over which the signal tends to be saturated. The output of the STC passes through a programmable attenuator of 0-60 dB with 10 dB steps and as IF amplifier chain with a gain of 60 dB and a bandwidth of 1.7 MHz. The IF signal is now split into and applied to a pair of quadrature mixers, which mix them with 5 MHz locked oscillator (LO) signals having quadrature phase of  $0^0$  and  $90^0$ . The quadrature signals from the mixers are then fed to two identical channels of low pass filters (LPF) and video amplifier to obtain the two bipolar video signals of  $A\cos\theta$  and  $A\sin\theta$  at the output. The receiver has an overall gain of about 120 dB and a dynamic range of 70 dB.

The quadrature (I and Q) outputs of the receiver are limited to  $\pm 5$  volts and given to the I and Q channels of acquisition card in the Echo Processing System. On the falling edge of IPP, the SHARC processor is interrupted and sampling, digitization, decoding follows sequentially. The analog signal in each channel is sampled at 1 MHz rate. The decoding operation essentially involves cross correlating the incoming signal from the ADC with the replica of transmitted code. The obtained data is now stored in SIM modules. Coherent adding is a processing step introduced to reduce the data volume by adding a specified number of pulse samples when the Doppler

shifts are quite low. It would mean a limitation, however, when the Doppler shifts are high, since it would not only restrict the unambiguous Doppler range but also distorts the signal spectra. The coherent integration is implemented in double buffer mode using two RAM memory banks as buffers. At any time, while the data are being collected for the current integration period in one bank, the data already stored in the other memory bank from the previous integration period is accessible for transfer. Multi-tasking signal processing software is written for multiprocessor environment. The processed data or the unprocessed data (in case of raw data) is transferred to the host computer in the next beam cycle while the data archival is going on. Design supports the data collection and processing time as low as zero which implies that, the second beam can start without any time overhead from the acquisition / processing side as soon as the first beam run is completed.

#### **3.3.4. Exciter and radar controller**

The exciter unit generates the entire RF and timing and control signal for various sub-systems of the radar. It comprises of a master reference oscillator, a two-channel frequency synthesizer, a phase-locked oscillator, a  $\mu$ P controlled bi-phase coder and a timing signal generator. The master reference is a 5 MHz oven controlled crystal oscillator with a short-term stability better than 1 part in  $10^{10}$ . The two channel synthesizer provides two 5 MHz channels with programmable relative amplitude and phase. It provides LO signals to the receiver, IF signals to the transmitter coder and reference and simulator signals for phase calibration. The phase locked oscillator (PLO) operating at 48 MHz, serves as LO for up conversion while transmitting and down conversion while receiving. The bi-phase coder generates a 5 MHz complimentary coded pulse taken from the 5 MHz signals to the two-channel synthesizer and the complimentary code sequence from an 8085A processor. The timing signal generator (TSG) is a programmable multi channel pulse generator, supplying control signals for synchronizing the operations of various subsystems of the

radar. The output from the TSG includes Tx and Rx gate signals, duplexer signal, coder and ADC sample clocks, and control signals to preprocessor and signal simulator. The main function of the RC is to set up, control and synchronize the operations of various sub-systems viz., TSG, bi-phase coder, preprocessor, host computer and four satellite processor located in the transmitter huts during the normal operation of the radar. Once the radar parameters are specified in the form of experiment specification file (ESF), the RC takes over the automatic data acquisition and completes the run.

### 3.4. Atmospheric Data Processing

The MST radar data is usually processed in two stages; on line and off-line. Figure 3.3 shows the data processing sequence. The online processing significantly compresses the data volume by time averages and usually produces power spectra and the off-line calculations for parameter extraction (*Farley, 1985*).

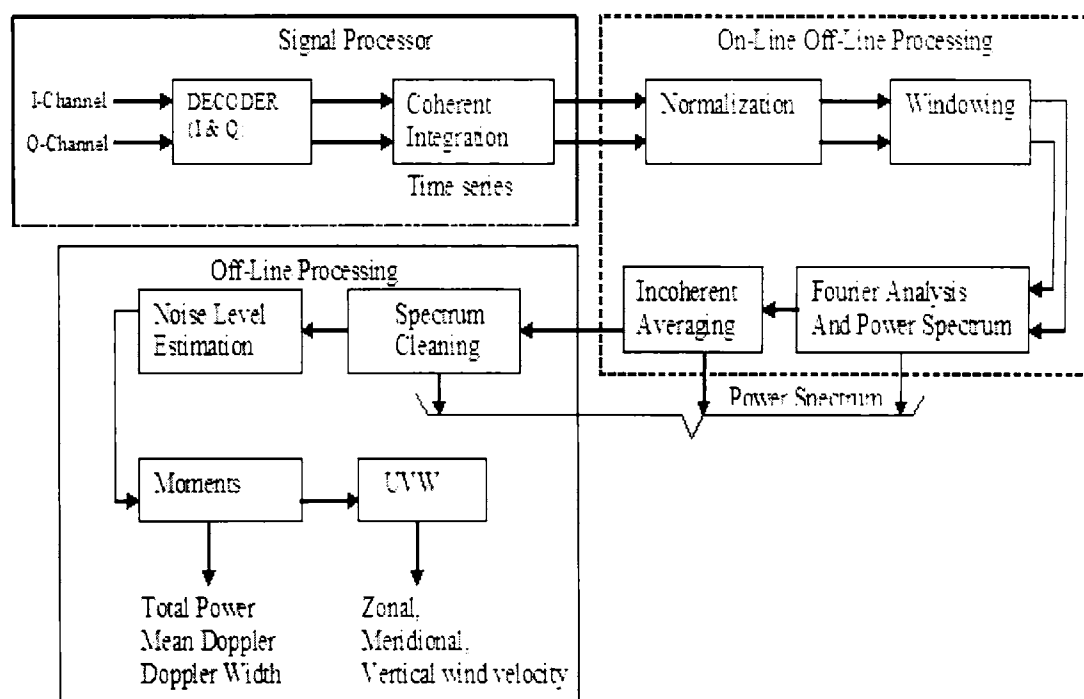


Figure 3.3. Signal and data processing sequence for extraction of spectral Moments and U, V and W

The input to the data processing system is the preprocessed data after decoding and coherent integration in the complex format. Coherent integration is the technique that filters much of the wide band noise and reduces the data volume to the signal processor without distorting the information that is contained in the radar returns. The detected quadrature signals are integrated for many pulses over a period in order to increase Signal to Noise Ratio (SNR). This is coherent integration. The complex time series of the samples are subjected to Fast Fourier Transform (FFT) for online computation of the Doppler power spectrum for each range bin of the selected range window. The Doppler spectra are recorded and transmitted for off-line processing. There is a provision, however to record raw data (complex time series samples) directly for any application, if so desired. Figure 3.4 shows the Doppler spectra plot from a typical six beam scan.

The off-line data processing for parameterisation of the Doppler spectrum is carried out following the method given by *Riddle* (1983), as suitably modified by *Anandan* (1996). In this method it defines the number of spectra peaks for the same range gate and tries to extract the best peak, which satisfies the criteria chosen before the estimation. This method involves the following steps. The DC contribution, which is arising either from nonfading clutter or uncancelled system biases or both and is eliminated by replacing the spectral point at zero frequency value with the average of two adjacent points (3 point DC removal) or with the four adjacent points (5 point DC removal). The data are further edited to remove if any interference band, that might run through the entire range window and is subtracted out by estimating it in a range bin where it dominates the real signal. After removing the interference from the spectra, suitable incoherent integration can also be done off-line to improve the signal detectability and better estimate of spectral parameters. The spectral parameters *viz.* total signal power, mean Doppler velocity and velocity variance are obtained from the three lower order moments of the spectrum. A typical spectrum is given in figure 3.5.

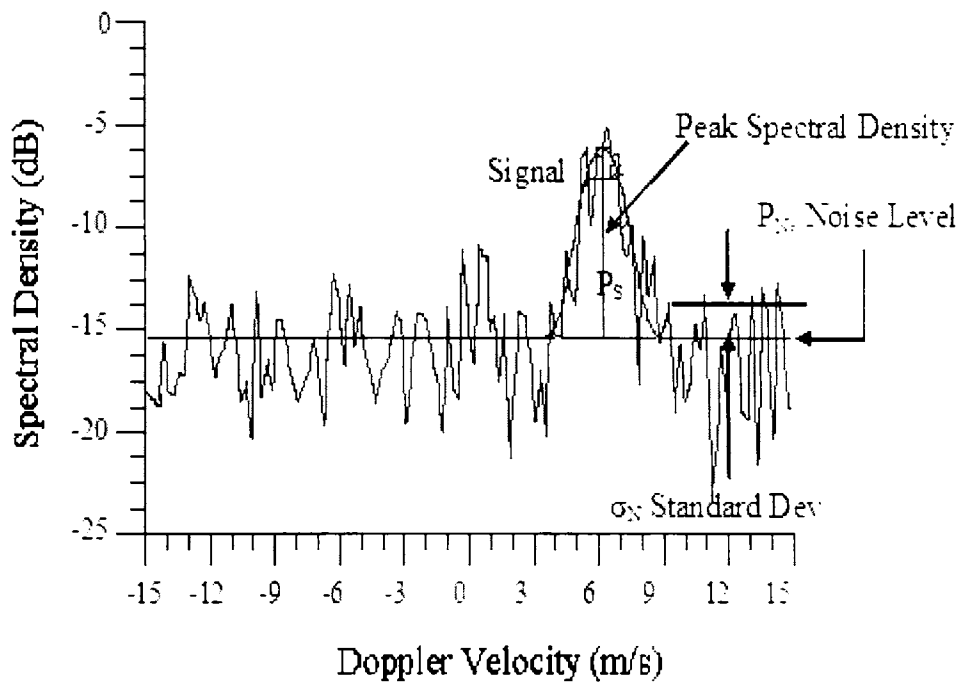


Figure 3.5. A typical example of a Doppler velocity spectrum in the lower atmosphere at  $10^\circ$  off-zenith.

The spectrum may contain noise as background and it needs to be removed as a first step to compute the moments. The average noise value for each range bin is estimated following the objective method of *Hildebrand and Sekhon* (1974). Now, the median noise level is calculated and subtracted from all the range bins of the spectral frame. For each range bin, the highest peak in the spectrum is recognized as the signal and its spectral window is determined by noting all the contiguous points that are above zero level. The three low order ( $0^{\text{th}}$ ,  $1^{\text{st}}$  and  $2^{\text{nd}}$ ) are computed through numerical integration using the expression given by *Woodman* (1985). The three lower order moments are estimated from the spectrum using the equations below for each range bin.

### 3.4.1. Power spectrum calculation

Each of the coherently integrated complementary pulse pair is decoded by cross-correlating it with the transmitted binary code denoted by  $S_m$ , where  $m$  is the baud index and varies over the code length 1 to  $M$ .

For one of the pulses (say odd pulse), the operation may be expressed as

$$\begin{aligned}
 Z_{ik}^0 &= \sum_{m=1}^M C_{(i+m-1)k}^0 \cdot S_m \\
 &= \sum_{m=1}^M x_{(i+m-1)k}^0 \cdot S_m + j \sum_{m=1}^M y_{(i+m-1)k}^0 \cdot S_m \\
 &= X_{ik}^0 + jY_{ik}^0
 \end{aligned} \quad \text{--- 3.1}$$

Similarly, for even pulse of the code

$$Z_{ik}^e = X_{ik}^e + jY_{ik}^e \quad \text{--- 3.2}$$

The final integrated and decoded signal for the  $i^{\text{th}}$  gate and  $k^{\text{th}}$  integration is given as:

$$\begin{aligned}
 Z_{ik} &= Z_{ik}^0 + Z_{ik}^e \\
 &= (X_{ik}^0 + X_{ik}^e) + j(Y_{ik}^0 + Y_{ik}^e) = X_{ik} + jY_{ik}
 \end{aligned} \quad \text{--- 3.3}$$

The decoded signal for any range gate represented by the complex time series  $Z_k$  (suppressing range index I) is subject to Discrete Fourier Transform (DFT) to obtain the frequency spectrum of the signal. The coefficient of the  $n^{\text{th}}$  harmonic component  $A_n$  ( $n=0$  to  $k-1$ ) is given by

$$\begin{aligned}
 A_n &= \frac{1}{k} \sum_{k=0}^{k-1} Z_k W^{kn} \\
 &= \frac{1}{k} \left( \sum_{k=0}^{k-1} X_k W^{kn} + j \sum_{k=0}^{k-1} Y_k W^{kn} \right) \\
 &= a_n + jb_n
 \end{aligned} \quad \text{--- 3.4}$$

where,  $W = \exp(-i2\pi T_i / T_s) = \exp(-i2\pi / k)$ . It may be noted that  $A_{n+k} = A_{n-k} = A_n$ , because  $W^k = 1$ . Hence the unambiguous frequency window of the DFT is of width  $f_k$  with the range  $-f_k/2$  to  $f_k/2$ , where,  $f_k = k/T_s$ . The frequency resolution of the DFT is given by  $1/T_s$ . The signals with frequencies outside  $\pm f_k/2$  contaminate the signal within the fundamental range through



aliasing. However, because of the weighting introduced by the coherent integration filter, the contribution due to the aliasing components is greatly reduced (Tsuda, 1988). The DFT computation is usually carried out by means of a fast Fourier Transform (FFT) algorithm for the significant advantage that it offers (Brigham, 1988). From the DFT, an estimate of power spectrum is given as

$$P_i = (1/k)(A_i A_i^*) = (1/k)(a_i^2 + b_i^2) \quad \text{--- 3.5}$$

The power spectrum thus obtained is usually quite noisy and at times several estimates of it need to be averaged to reduce the fluctuation of the noise and thereby improve the signal detectability. This process, known as incoherent integration, when performed for  $N_s$  spectra reduce the standard deviation of the noise spectral density and the signal detectability is enhanced by a factor  $(N_s)^{1/2}$ .

### 3.4.2. Moments calculation

The discrete average power spectrum  $P_i$  is used to compute the first three low order spectral moments through numerical integration using the expressions given by Woodman (1985). These moments provide the total signal power  $P_s$ , the mean Doppler frequency  $f_d$  and the spectral width  $f_w$  as follows:

$$P_s = m_0 = \sum_{i=m}^n P_i \quad \text{--- 3.6}$$

$$f_d = m_1 = \frac{1}{m_0} \sum_{i=m}^n P_i f_i \quad \text{--- 3.7}$$

$$f_w^2 = m_2 = \frac{1}{m_0} \sum_{i=m}^n P_i (f_i - m_1)^2 \quad \text{--- 3.8}$$

where,  $m$  is the number of spectra that were averaged in spectral averaging and  $n$  is the number of coherent integration.

Signal to Noise Ratio is calculated in dB as

$$SNR = 10 \log \left\{ \frac{M_0}{N \times L} \right\} \quad \text{--- 3.9}$$

where, N and L are the total number of Doppler bins and average noise level respectively, and NxL therefore gives the total noise over the whole signal window bandwidth. Doppler width, which is taken to be the full width of the Doppler spectrum, is calculated as

$$\text{Doppler width (Full)} = 2\sqrt{M_2} \text{ Hz} \quad \text{---3.10}$$

The moments calculated above at times suffer from the non-fading DC clutter and un-cancelled system biases. They are eliminated by notching out the zero frequency and averaging the two adjacent Doppler bins to interpolate for a new zero frequency value. The noise level estimation is then done following the method by *Hilderbrand and Sekhon* (1974). The noise level thus determined is subtracted from the received power for each Doppler bin. At times, some interference band might run through the entire range window corrupting the data. Such interference is subtracted out by estimating it in a range bin where it dominates the real signal. Then, for each range bin the highest peak in the spectrum is recognized as the signal and its window is determined by noting all the continuous points that are above zero level. The low order spectral moments are then computed by the equations 3.6-3.8. Figure 3.6 shows the height profiles of the spectral moments.

### 3.4.3. Calculation of radial velocity and height

The moments calculated above is used to calculate the radial or line of sight velocity and the range bins are adjusted in terms of height. The radial velocity  $V_d$  corresponding to the Doppler shift  $f_d$  is given as

$$V_d = \left( \frac{C \times f_d}{2 \times f_c} \right) \text{ or } \frac{\lambda}{2} f_d \text{ ms}^{-1} \quad \text{--- 3.11}$$

Date: 11 March 1999, Time: 17:15 IST

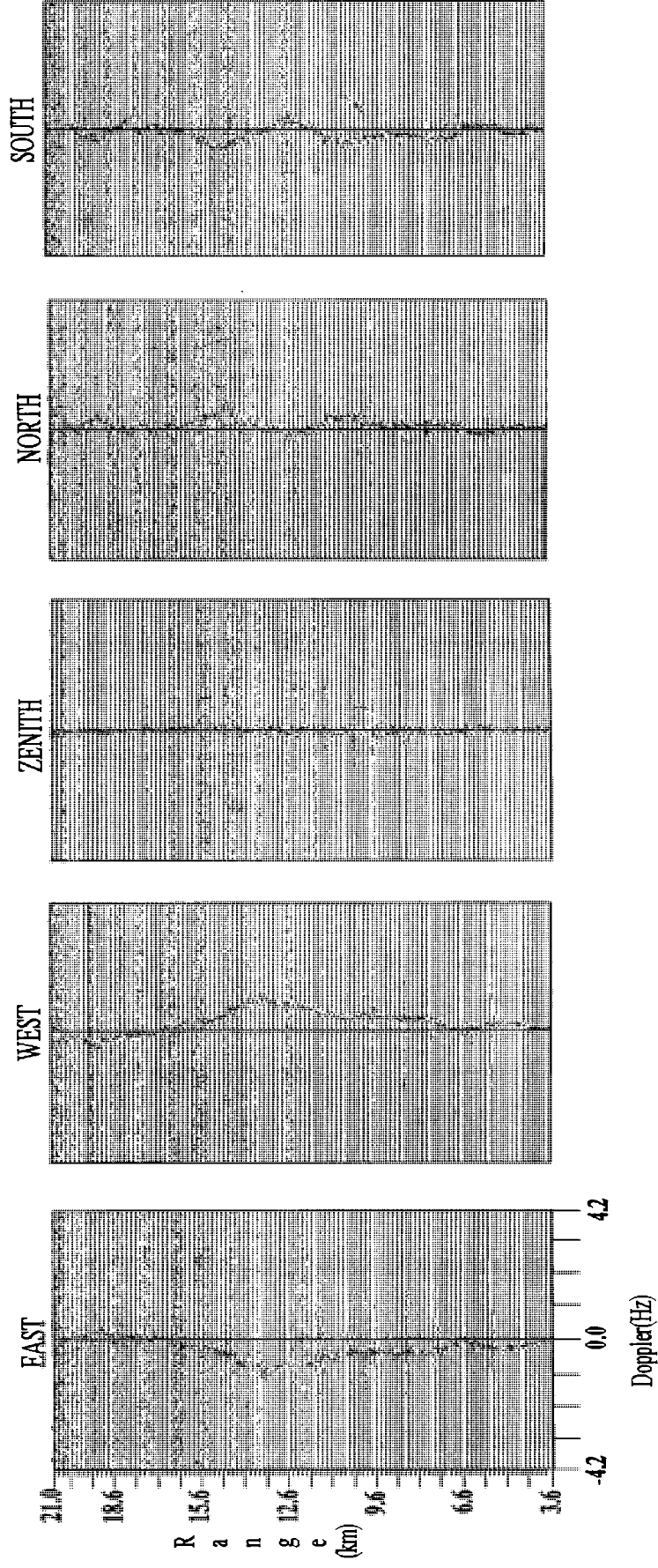


Figure 3.4: Doppler spectra of typical five-beam scan using 16  $\mu$ s coded pulses (Oblique beams are at 10° off-zenith)

The vertical height  $H$  corresponding to the range time delay  $t_r$  is given by

$$H = \frac{C \times t_r \cos \theta}{2} \text{ m} \quad \text{--- 3.12}$$

where  $C$  is velocity of light,  $f_d$  is Doppler frequency,  $f_c$  is carrier frequency,  $\lambda$  is carrier wavelength (5.86m),  $\theta$  is beam tilt angle of the radar beam or line of sight angle and  $t_r$  is range time delay.

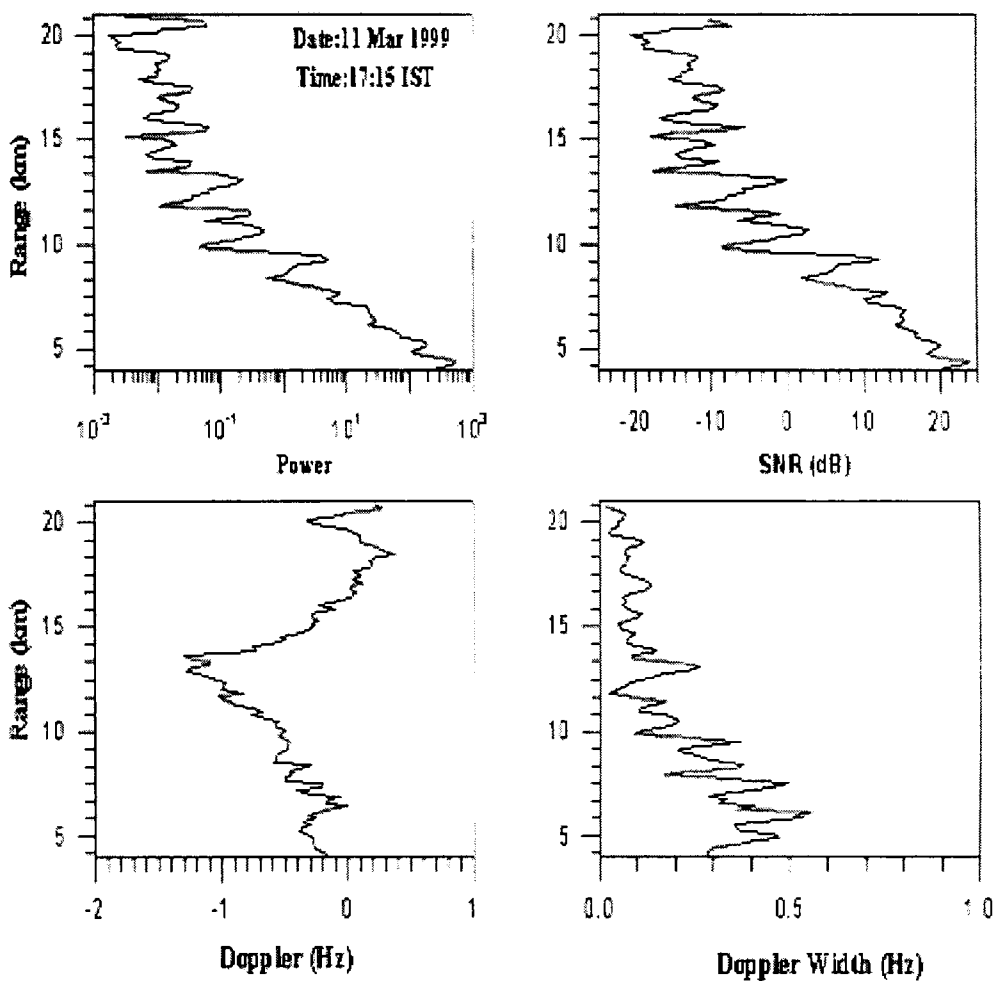


Figure 3.6. Height profiles of spectral moments

#### 3.4.4. Calculation of wind velocity vector ( $u, v, w$ )

The calculation of wind velocity vector using the radar beams is based upon the assumption that the velocity field is invariant over the spatial separation of the radar beams at a given height and over the time it takes to

cover the measurements for one complete cycle. After computing the radial velocity for different beam positions, the absolute wind velocity vector can be calculated. To compute UVW, at least three non co-planar beam radial velocity data is needed. If higher number of different beam data is there, then the computation will give an optimum result in the least square method. The line of sight component  $V_d$ , of the velocity vector  $V = (V_x, V_y, V_z)$  at a given height is expressed as

$$V_d = V \cdot i = V_x \cos \theta_x + V_y \cos \theta_y + V_z \cos \theta_z \quad \text{--- 3.13}$$

where,  $i$  is the unit vector along the radar beam and X, Y and Z directions are aligned to East-West, North-South and Zenith, respectively.  $\theta_x$ ,  $\theta_y$  and  $\theta_z$  are the angles that radar beam makes with the X, Y and Z axes. Applying least square method (Sato, 1989)

$$\varepsilon^2 = (V_x \cos \theta_x + V_y \cos \theta_y + V_z \cos \theta_z - V_{Di})^2 \quad \text{--- 3.14}$$

where,  $V_{Di} = f_{Di} \times \lambda / 2$  and  $i$  represents the beam number. To satisfy the minimum residual,  $\partial \varepsilon^2 / \partial V_k = 0$ , K corresponds to X, Y and Z.

$$\vec{V}_d = \vec{V} \cdot \vec{i} = V_x \cos \theta_x + V_y \cos \theta_y + V_z \cos \theta_z \quad \text{-- 3.15}$$

$$\begin{bmatrix} V_x \\ V_y \\ V_z \end{bmatrix} = \begin{bmatrix} \cos \theta_{x1} & \cos \theta_{y1} & \cos \theta_{z1} \\ \cos \theta_{x2} & \cos \theta_{y2} & \cos \theta_{z2} \\ \cos \theta_{x3} & \cos \theta_{y3} & \cos \theta_{z3} \end{bmatrix}^{-1} \times \begin{bmatrix} V_{d1} \\ V_{d2} \\ V_{d3} \end{bmatrix} \quad \text{--- 3.16}$$

where  $V_d = -f_d \lambda_R / 2$ .

where  $\theta_{x1}$ ,  $\theta_{y1}$  and  $\theta_{z1}$  are the angles between  $i_1$  and  $x$ ,  $y$  and  $z$  directions respectively and  $V_{d1}$ ,  $V_{d2}$  and  $V_{d3}$  are the components of velocity along  $i_1$ ,  $i_2$  and  $i_3$  respectively. By solving the above equation, we can derive  $V_x$ ,  $V_y$

and  $V_z$ , which correspond to U (zonal), V (meridional) and W (vertical) components of wind velocity. If we observe more than three directions, then the estimate of V can be determined in a least squares manner, with which the residual given by the following is minimized.

$$\varepsilon_v^2 = \sum_{i=1}^m (v_x \cos \theta_{x_i} + v_y \cos \theta_{y_i} + v_z \cos \theta_{z_i} - v_{d_i})^2 \quad \text{--- 3.17}$$

where m is the number of beam directions. The necessary condition for V to give minimum is that the partial derivatives of  $\varepsilon_v^2$  with respect to all three components of V are zero.

$$\frac{\partial \varepsilon_v^2}{\partial v_j} = 0, \quad (j = x, y, z)$$

This set of equations can be solved in terms of V as

$$v = \begin{pmatrix} \sum \cos^2 \theta_{x_i} & \sum \cos \theta_{x_i} \cos \theta_{y_i} & \sum \cos \theta_{x_i} \cos \theta_{z_i} \\ \sum \cos \theta_{y_i} \cos \theta_{x_i} & \sum \cos^2 \theta_{y_i} & \sum \cos \theta_{y_i} \cos \theta_{z_i} \\ \sum \cos \theta_{z_i} \cos \theta_{x_i} & \sum \cos \theta_{z_i} \cos \theta_{y_i} & \sum \cos^2 \theta_{z_i} \end{pmatrix}^{-1} \begin{pmatrix} \sum v_{d_i} \cos \theta_{x_i} \\ \sum v_{d_i} \cos \theta_{y_i} \\ \sum v_{d_i} \cos \theta_{z_i} \end{pmatrix} \quad \text{--- 3.18}$$

Typical height profiles of U, V and W are given in Figure 3.7.

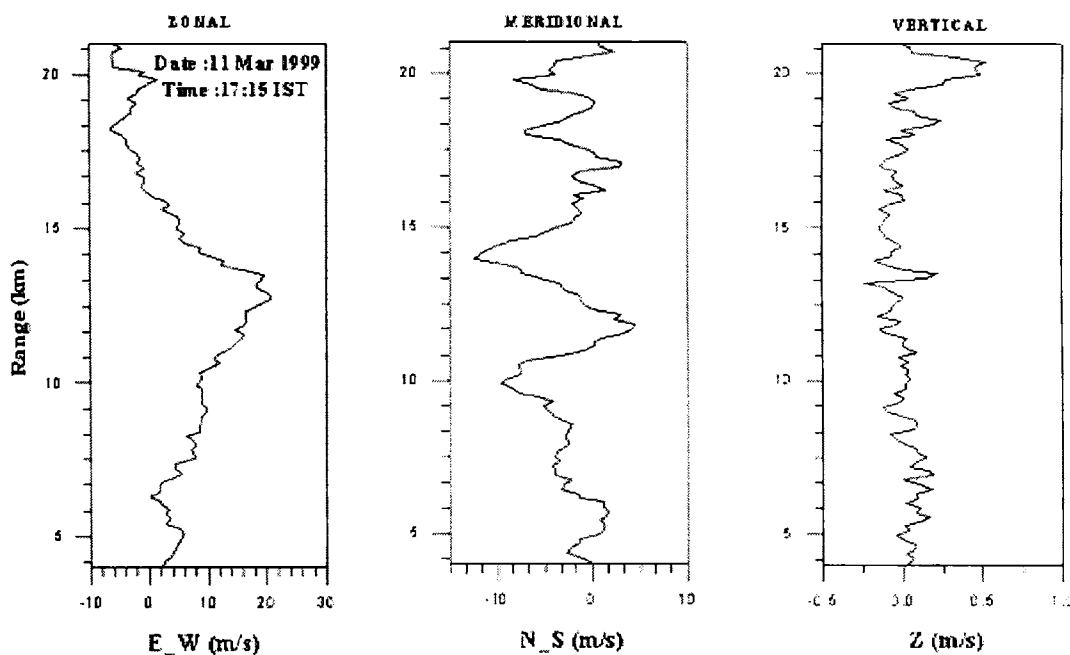


Figure 3.7. Typical height profiles of zonal (U), meridional (V) and vertical (W) wind velocity

## Chapter #4

*Changes in the Circulation Pattern of the  
Troposphere and Lower Stratosphere During  
the Passage of Tropical Cyclones*

## 4.1. Introduction

A large number of recent observational studies of mesoscale systems have been signifying a renewed interest in tropical cyclone systems and their impact on the general atmospheric circulation and hence the global climate. Observational studies of tropical cyclones are crucial for understanding their internal processes and also for quantifying their interactions with the large-scale environment. Tropical cyclones and their associated dynamics in the upper troposphere and lower stratosphere are not much studied.

Tropical cyclones are large, cyclonically swirling cloud systems, usually originating equatorward of  $30^{\circ}$  latitude in each hemisphere. They are violent whirls spiraling upward from ocean surface to great heights, sometimes upto the tropopause height. The circulation and cloud mass of the tropical cyclone extend vertically upward from the surface through the troposphere, although the circulation typically becomes anticyclonic in the upper troposphere. Horizontal wind fields exceeding  $15 \text{ ms}^{-1}$  are found above the ground near the centre. They tend to move westward following prevailing easterly winds in the tropical troposphere.

Lower tropospheric wind characteristics of the cyclonic system are well known, whereas the three-dimensional structure of the tropical cyclone extending upto the lower stratosphere is not properly understood. Recent advances in the measurement techniques have enabled detailed observation of three-dimensional structure of tropical cyclones. The MST (Mesosphere-Stratosphere-Troposphere) radar technique has a unique capability of measuring the background air motion. The MST radar is a powerful tool in observing the vertical structure of tropical cyclones.

*Sato et al.* (1991) studied the wind characteristics in the troposphere and lower stratosphere using MU radar associated with the passage



of a typhoon 100 km away from the radar site at Shiga, Japan (35.0°N, 136.0°E). A clear reversal of the zonal wind direction from easterly to westerly in the lower troposphere and from westerly to easterly in the upper troposphere is noted during the time of storm passage. An upward flow of about  $2 \text{ ms}^{-1}$ , which continued for about three hours around the time of storm passage at the height range of 8 – 12 km, is also observed. *Rottger et al* (1991) investigated the wind field and reflectivity variations with the Chung-Li VHF radar located at northern Taiwan (24.6°N, 121.0°E) associated with the passage of a typhoon. During the time of approach of the typhoon the winds in the altitudes above 5 km changed suddenly from northeasterly to northwesterly. After the passage of the system the zonal component recovered but the meridional wind changed to southerly.

Very limited VHF radar studies have been carried out on the wind characteristics in the entire troposphere and lower stratosphere associated with tropical cyclones. These observations have a potential to give a complete picture of three dimensional wind characteristics over the tropical cyclone region. The wind characteristics in the troposphere and lower stratosphere associated with a tropical cyclone over the Indian region has not yet been studied. In the present study, we report the three dimensional wind characteristics in the troposphere and lower stratosphere extending from 4 – 21 km using MST radar observations at Gadanki (13.5°N, 79.2°E) during the passage of various tropical cyclones over the station. These observations are first of their kind from this latitude region.

## **4.2. Data Deduction Techniques**

The Indian MST radar is highly sensitive, pulse coded, coherent VHF phased array radar operating at 53 MHz with a peak power-aperture product of  $3 \times 10^{10} \text{ Wm}^2$ . Detailed description of the Indian MST radar is

reported elsewhere (*Rao et al.*, 1995; *Jain et al.*, 1995). The details of deriving the wind components from the MST radar data are described in chapter 2.

The MST radar observations were made using 6 beams (East, West, North and South at 10° beam angle and Zenith X and Zenith Y) with a pulse width of 16  $\mu$ s (coded). The upper height limit varies from observation to observation. The data from 4 to 20 km is used for the study depending on the data quality. The altitude resolution of the data is 150 m. Since there were no continuous observations in 1994, available data is used for the study. In 2001 and 2002 special experiments were carried out at the MST radar site in Gadanki. From the radar observations, the three components of wind  $u$ ,  $v$  and  $w$  were calculated and used for studying the atmospheric characteristics due to the passage of the tropical cyclone over Indian subcontinent.

### 4.3. Results and Discussion

In the present study, three cyclone cases were considered, one each in 1994 (27 October – 1 November), 2001 (14-17 October) and 2002 (22-29 November). Details of the cyclones studied in this chapter are given in table 4.1. In 2001 October, the cyclone passed very near (~ 60 km) to the radar site in which special experiments were carried out by CUSAT team. In 2002 November, the cyclone was formed in the Bay of Bengal about 700 km away from the radar site and special observations were also carried out by us during this period.

Serial No.	Cyclone dates	Time and Date of Nearest approach	Distance From the radar site
1	26 October- 02 November 1994	1500 hrs, 31-10-94	Overhead
2	14-17 October 2001	0530 hrs, 16-10-01	60 km
3	23-28 November 2002	0300 hrs, 24-11-02	700 km

Table 4.1. Details of tropical cyclones considered for the study

### **4.3.1. Overhead passage of cyclone**

#### ***4.3.1a Synoptic features***

The depression formed over southwest bay was centred on 29<sup>th</sup> October, 1994 near 9.5°N and 84.5°E at 0830 hrs LT, about 520 km east-southeast of Nagapattinam. It intensified into a deep depression and lay centred within half a degree of 10.5°N and 84.5°E at 1730 hrs LT of the same day, about 500 km east of Nagapattinam. Moving in a northwesterly direction, it further intensified into a cyclonic storm and lay centred near 12.0°N and 82.0°E at 0830 hrs LT on 30<sup>th</sup> October (225 kms southeast of Chennai). Further moving in a west-northwesterly (WNW) direction it intensified into a severe cyclonic storm. The severe cyclonic storm further intensified into a core of hurricane winds on 31<sup>st</sup> October at 0530 hrs LT. The landfall occurred north of Tamil Nadu coast, near Chennai around 0700 hrs LT. After landfall it weakened into cyclonic storm which lay about 50 kms northwest of Chennai at 1730 hrs LT on 31<sup>st</sup> October. Further it rapidly weakened into a well marked low pressure area. The track of the cyclone as reported by India Meteorological Department (IMD) is given in figure 4.1.

#### ***4.3.1b Wind characteristics***

Zonal wind observed three days prior to the overhead passage of the storm is illustrated in figure 4.2a. It can be noted that weak easterlies are prevailing in the lower and middle troposphere upto 14 km. A narrow band of westerlies is seen from 17 to 19 km. Easterlies are strengthening as we go up in the atmosphere. Very strong easterlies are noted around the tropopause height. The maximum easterly wind strength is  $\sim 35 \text{ ms}^{-1}$ . The overhead passage of the storm was around 1300 hrs LT on 31<sup>st</sup> October. Unfortunately there were no observations taken during that time. The available data are nearly four hours after the passage of the storm. Zonal wind observed from 1700 hrs LT to 1820 hrs LT on 31<sup>st</sup> October is given in figure 4.2b.

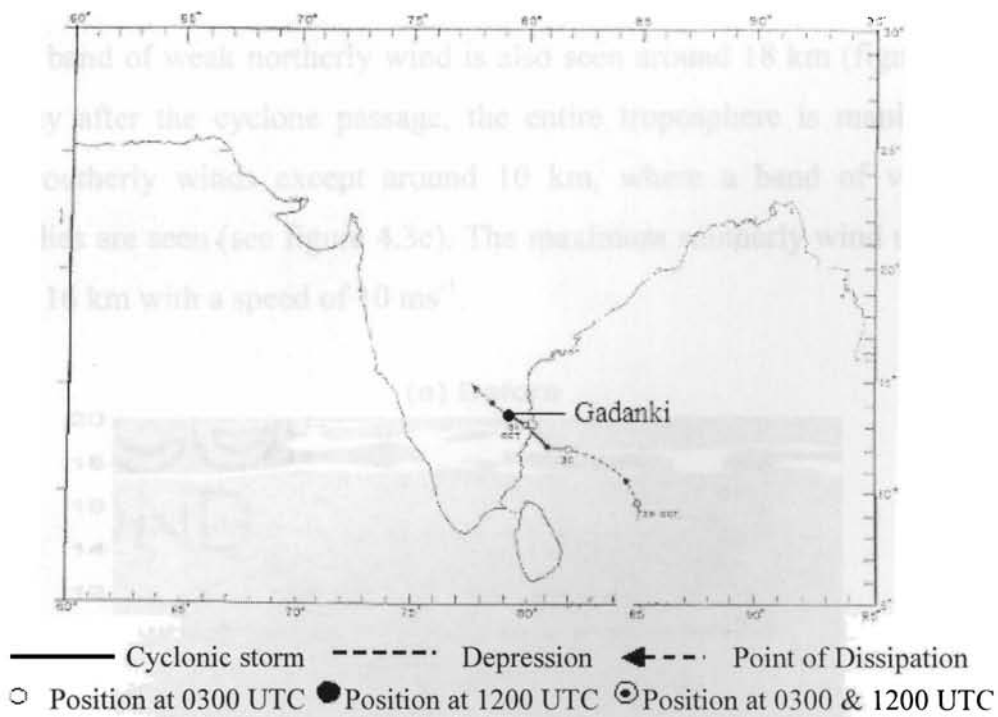


Figure 4.1. Track of the cyclone during 27<sup>th</sup> October to 01<sup>st</sup> November, 1994

After the passage of the storm, the zonal wind reversed from easterlies to westerlies from 4 to 11 km. Above this region strong easterlies are replaced by weak easterlies. One day after the passage of the cyclonic storm, weakening of westerlies is noted (figure 4.2c).

Before the passage of the storm, easterlies are noted upto 17 km. After the passage the wind changes its direction to westerlies. Above 12 km, though the wind is still easterly, the band of strong wind gets shifted upward. It can also be noted that just after the passage of the storm the winds in the lower levels (westerlies) are strong and one day after the passage of the storm the westerly winds became very weak.

Figure 4.3a-c show the meridional wind observed during the overhead passage of the cyclone. Before the passage of the cyclonic storm, southerlies are seen prevailing from 4 to 20 km (figure 4.3a). The southerly wind is seen strengthening above 14 km and a narrow layer of very strong southerly wind is noted around 16 km with a core speed of  $40 \text{ ms}^{-1}$ . Just after

the cyclone passage southerlies shifted to northerlies from 4 to 13 km. A narrow band of weak northerly wind is also seen around 18 km (figure 4.3 b). One day after the cyclone passage, the entire troposphere is manifested by weak southerly winds except around 10 km, where a band of very weak northerlies are seen (see figure 4.3c). The maximum southerly wind strength is around 16 km with a speed of  $10 \text{ ms}^{-1}$ .

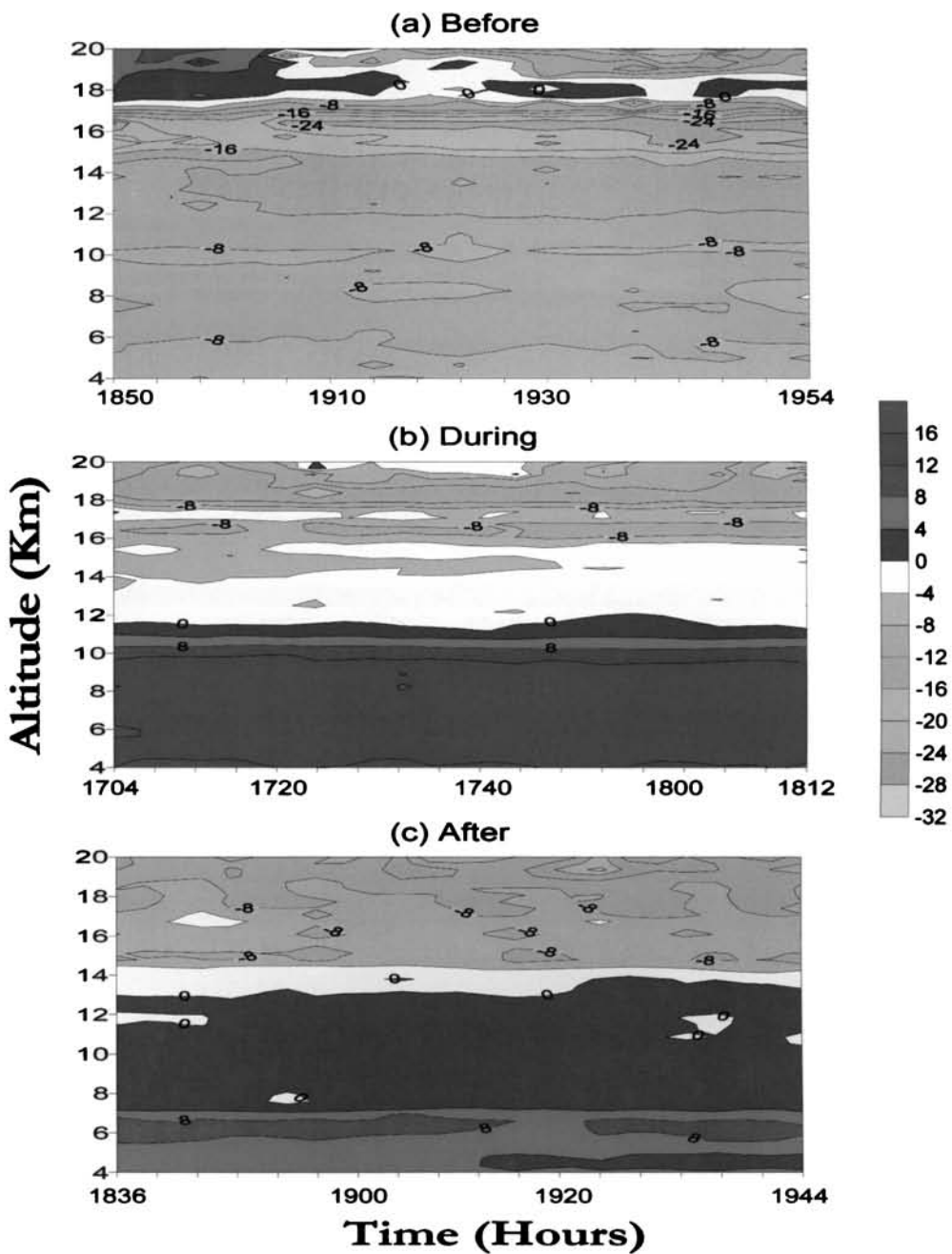


Figure 4.2 Contour plots of zonal wind on a) before, b) during and c) after the cyclone passage

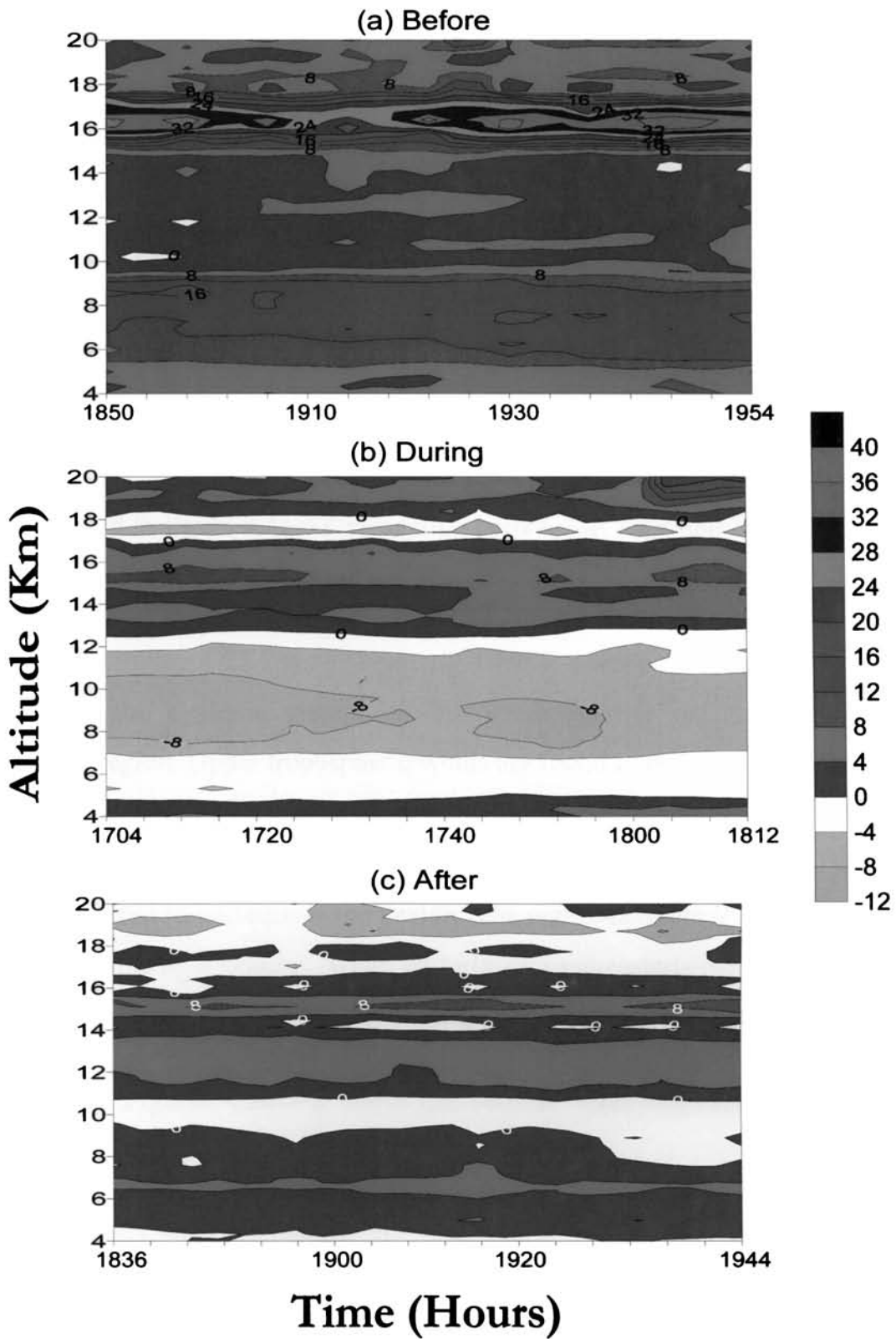


Figure 4.3 Contour plots of meridional wind on a) before, b) during and c) after the cyclone passage

Marked changes in the direction and speed of the meridional wind are noted in the entire troposphere and lower stratosphere associated with the passage of the storm. The southerly wind observed before the passage of the storm changes its direction to northerly just after the passage of the cyclone. It is very interesting to note that one day after the passage of the storm, the wind direction changes back to southerly in the lower levels upto 10 km.

For a better understanding of the horizontal wind characteristics with height and its special features, vector plots of horizontal wind with height are illustrated in figure 4.4a-c representing before, just after and one day after the passage of the cyclonic storm.

From 4-20 km southeasterly wind is seen prevailing before the passage of the cyclonic system. Strong southeasterlies are noted in the tropopause region. Upper tropospheric winds are found to be very weak (figure 4.4a). Just after the overhead passage, the southeasterly winds in the lower levels have reversed in direction to northwesterlies upto 9 km. The wind strength is noted to decrease in this region. The region between 9 and 12 km is very calm with light winds. Weak easterly or southeasterly winds are seen above 12 km (figure 4.4 b). One day after the passage the winds became weak.

Figures 4.5a - c show the vertical wind observations before, during and one day after the cyclonic storm. The wind is generally weak and downward. Strong downdraft is seen in the tropopause level (fig 4.5a). During the passage of the storm, upward wind is found above 10 km. It can be noted that wind is upward in the lower and middle troposphere, with a maximum around 13 km (see fig 4.5 b). One day after the passage the vertical wind became very weak and variable (fig 4.5 c).

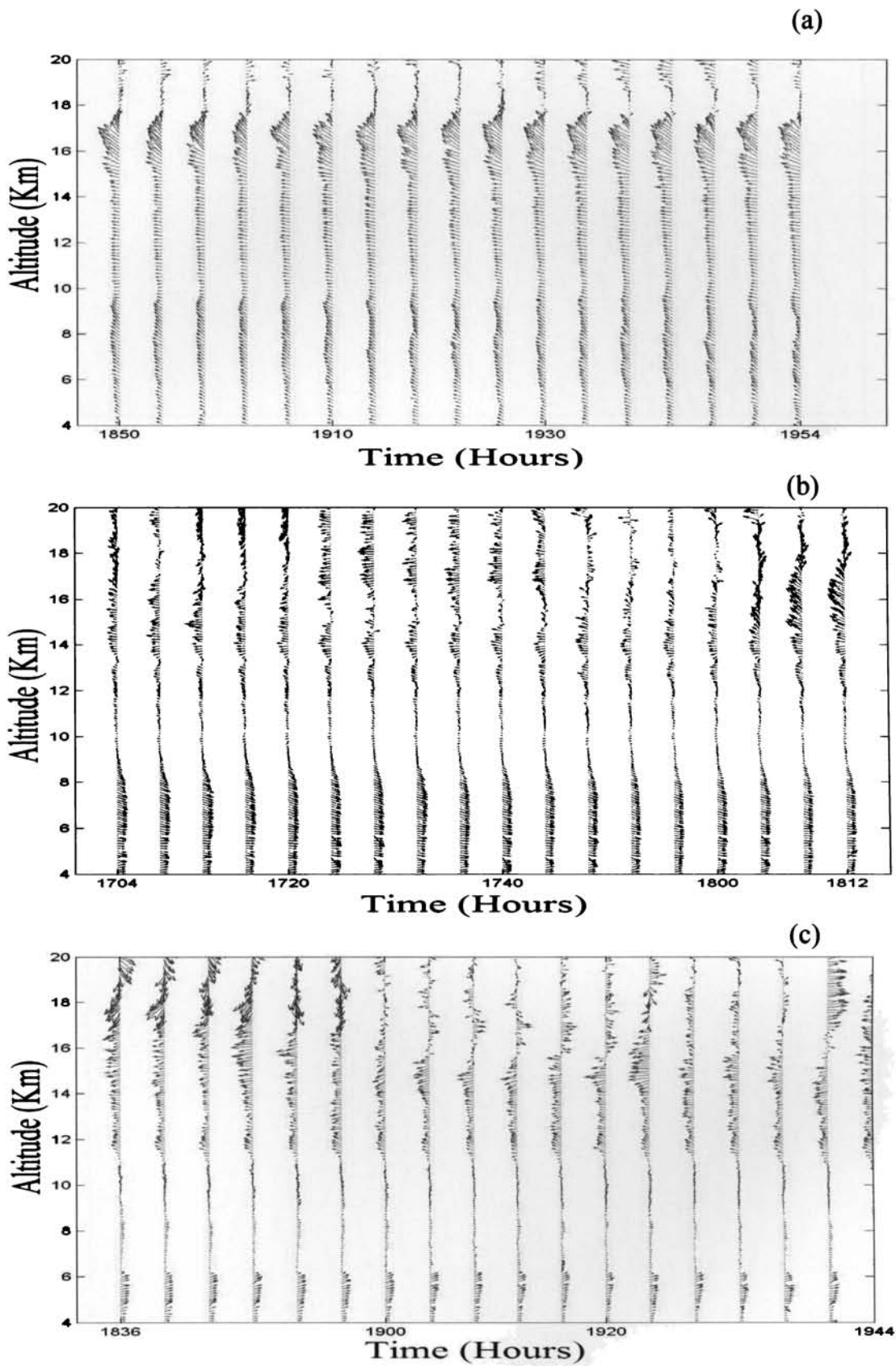


Figure 4.4 b & c. Horizontal wind vector distribution before, during & one day after the storm passage



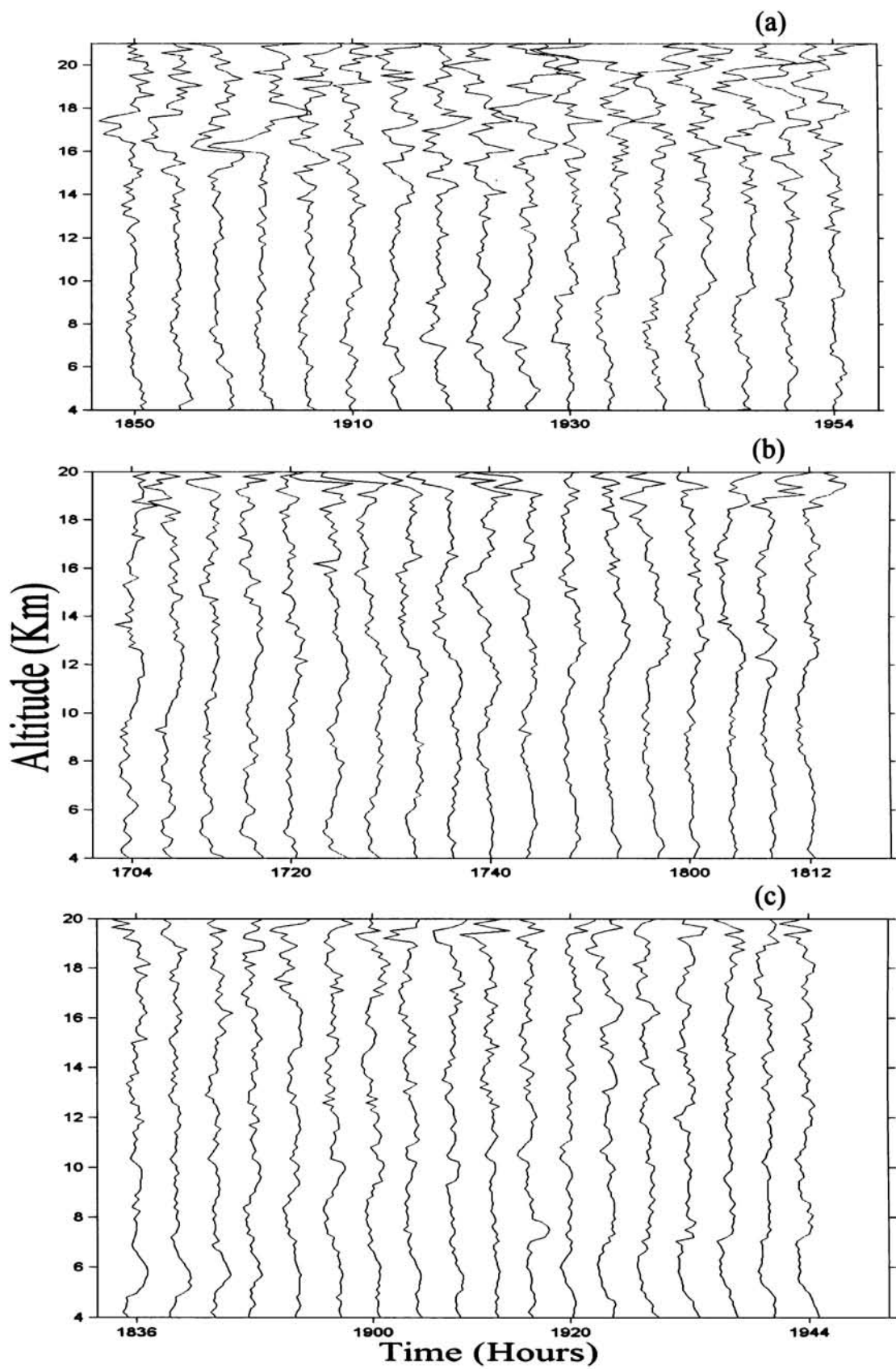


Figure 4.5. Altitude profile of vertical velocity (a) before, (b) during and (c) one day after the passage of the storm

### 4.3.2. Nearby passage of the cyclone

#### 4.3.2a Synoptic features

A low-pressure area formed in the west central bay on 14<sup>th</sup> October 2001 morning, became well marked on the same day evening. It concentrated into a depression over west central and adjoining SW Bay and lay centred near 13.5°N, 83.0°E at 0830 hrs LT on 15<sup>th</sup> October and intensified into a depression at 1430 hrs LT. The depression further intensified into a cyclonic storm around 1730 hrs LT and centred near 14.0°N, 81.5°E, about 170 km east-southeast of Nellore. Moving west-northward, it crossed the south Andhra coast in the morning of 16<sup>th</sup> October, and was lying centred 80 km northeast of Gadanki at 0830 hrs LT. It moved slowly westward and weakened into a depression at 0230 hrs LT on 17<sup>th</sup> October. It further weakened into a well-marked low-pressure area over central parts of Andhra Pradesh at 0830 hrs LT. The cyclone centre was most nearer (~60 km) to the station nearly at 0500 hrs LT on 16<sup>th</sup> October 2001. The track of the cyclone given by IMD is shown in figure 4.6.

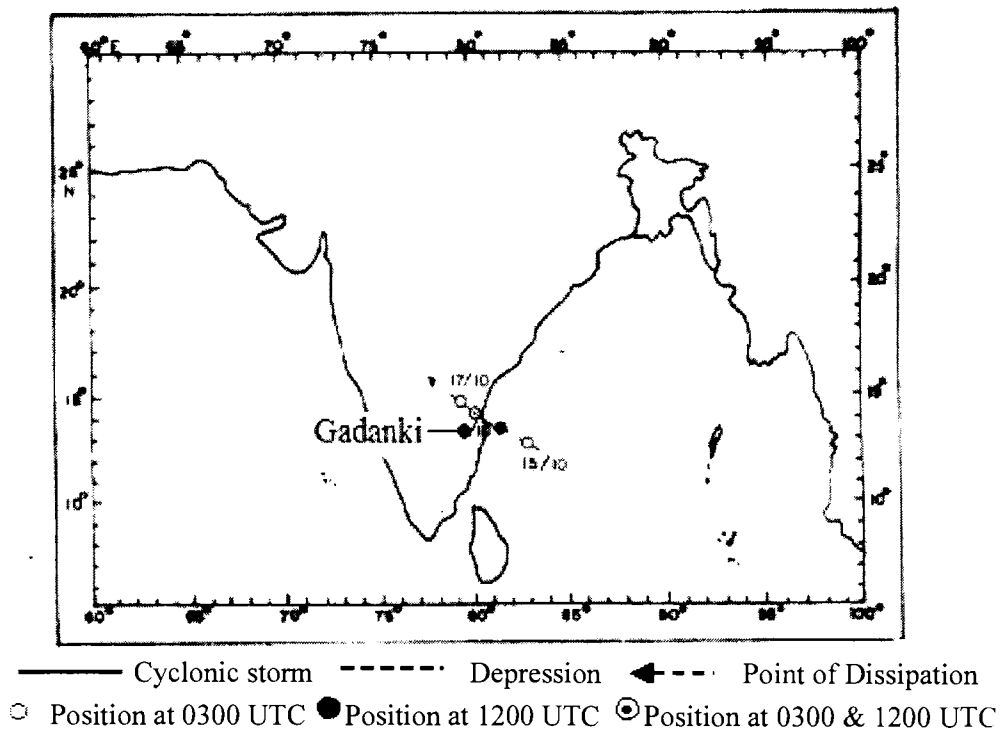


Figure 4.6. Cyclone track (14<sup>th</sup> October – 17<sup>th</sup> October 2001

#### *4.3.2b Wind characteristics*

Special cyclone experiments were carried out to study wind characteristics. These special observations were analysed using Atmospheric Data Processor (ADP) available at NMRF, Gadanki and figure 4.8a illustrates the contour plots of daily observations of zonal (u) wind components from 11-21 October 2001.

Vertical structure of the zonal wind shows that weak easterlies are generally prevailing over the entire troposphere and lower stratosphere during the period (Fig. 4.7a). When the tropical cyclone approaches the station the easterlies start strengthening in the upper troposphere and near tropopause region and reached a maximum of the order of  $25 \text{ ms}^{-1}$  at 16.5 km altitude on 16<sup>th</sup> October, the day on which the tropical cyclone reached over the station. After that the easterly wind components gradually decreased and returned to the normal strength.

Figure 4.7b shows the zonal wind just after the closest approach of the cyclone derived from the high-resolution data (at 4-minute interval) from 0930 hrs LT to 1200 hrs LT on 16<sup>th</sup> October 2001 (just after the passage of the cyclone centre). The zonal wind is easterly at all altitudes during the first half of the observation period. It is interesting to note that as the cyclone passes over the station the easterly wind changes to westerly in lower altitudes from 4 to 9 km. Very strong easterlies are noted around 16 km. The maximum wind is  $\sim 30 \text{ ms}^{-1}$  around 16.5 km. It is also seen that after the cyclone passage, the wind speed decreased.

Prior to the arrival of tropical cyclone, northerlies are prevailing in the entire troposphere (fig.4.8a). Intense northerly flow of wind with a core speed of  $20 \text{ ms}^{-1}$  is noted at 16 km on 16<sup>th</sup> October, the day of nearest passage of the cyclonic storm over Gadanki. After the tropical cyclone passage, the entire troposphere is manifested by southerly winds.

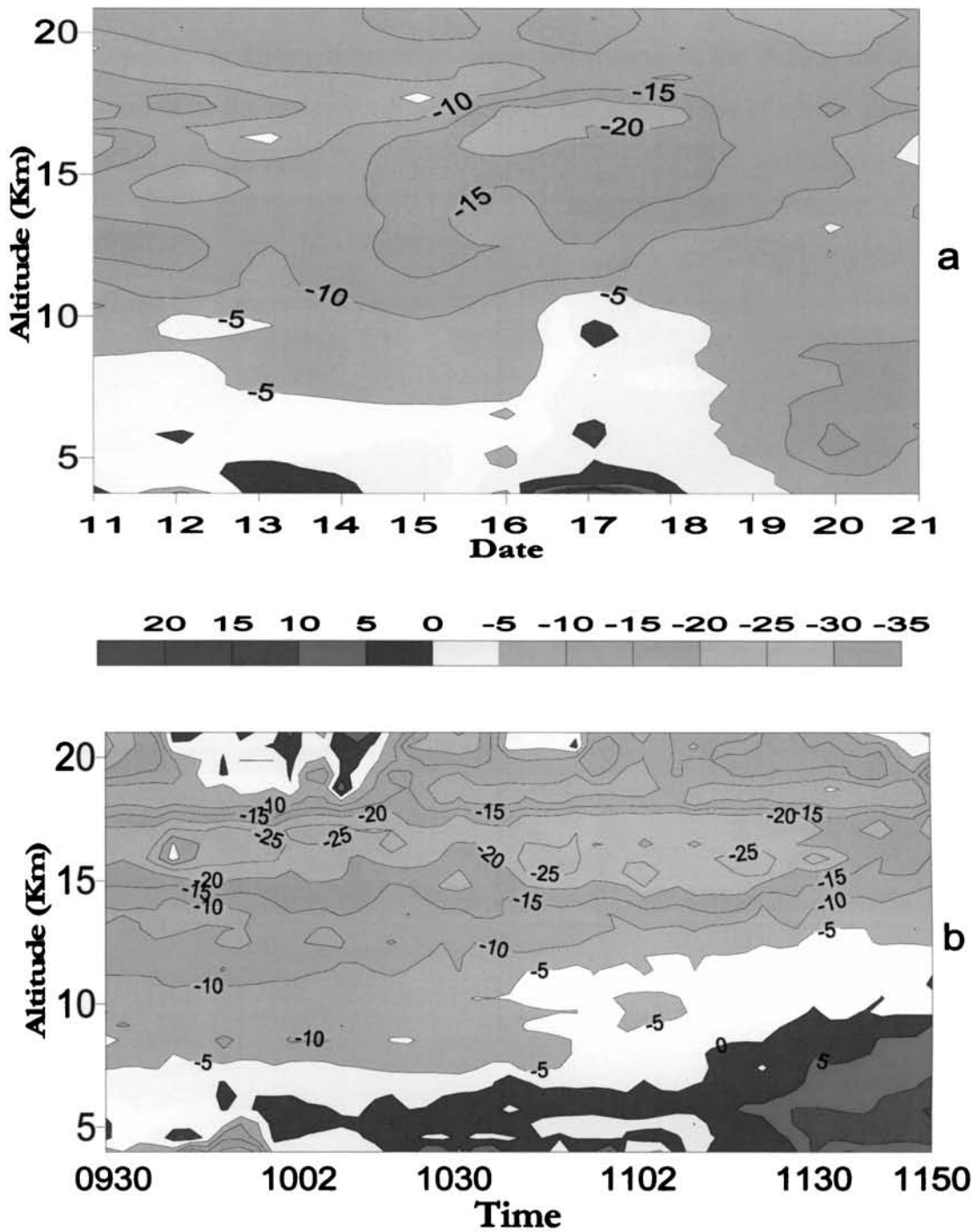


Figure 4.7. Zonal wind distributions a) from 11-21 October 2001 and b) for 2½ hours just after the passage of the cyclonic storm

Meridional wind, just after the nearest passage of the cyclone, derived from the high-resolution data (at 4-minute interval) from 0930 hrs LT to 1200 hrs LT on 16<sup>th</sup> October 2001 is shown in figure 4.8b. Northerlies are seen in the entire altitude range from 4 to 21 km during the first half of the

observation period. Strong northerlies are noted around 16 km during the entire period. Soon after the passage of the cyclone, the wind at lower levels changed to southerlies upto 12 km.

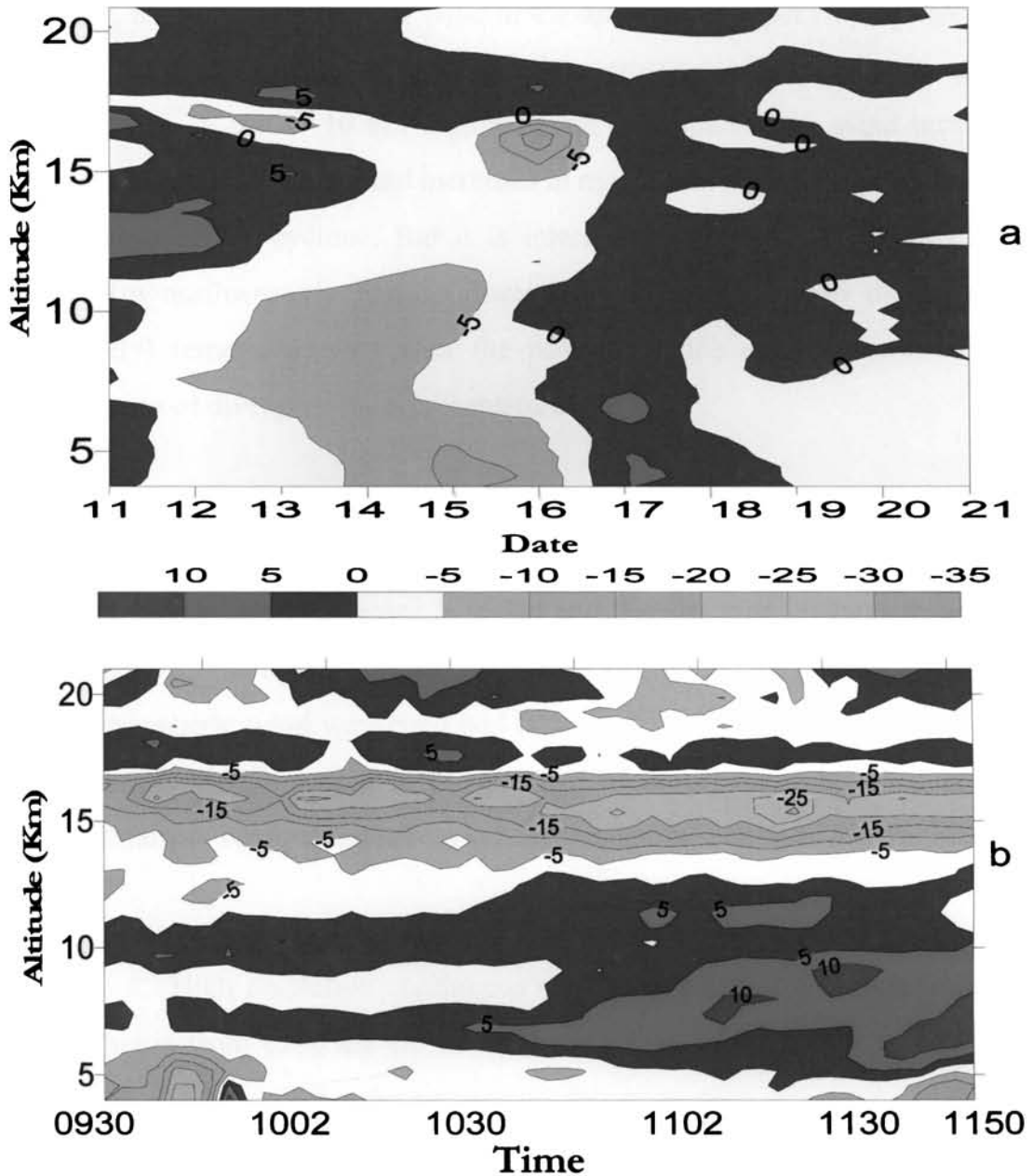


Figure 4.8. Meridional wind distributions a) from 11-21 October 2001 and b) for 2½ hours just after the passage of the cyclonic storm

Special observations were taken continuously for 32 hours at 1-hour interval from 0930 hrs LT on 15<sup>th</sup> October to 1630 hrs LT on 16<sup>th</sup> October 2001. Vertical distribution of the horizontal wind vector from these continuous 1-hour observations is illustrated in figure 4.9a. Vertical arrow in the bottom of

the figure indicates the time of nearest passage of the cyclonic centre over the station and the box in this figure indicates the period in which high-resolution wind data observed at 4-minute interval just after the cyclone passage. From the figure, it can be seen that the wind in the middle and upper troposphere are generally easterly or northeasterly before the crossing of the cyclonic storm over Gadanki. In the 4 -10 km region of the troposphere, the wind turns to north-northeasterly direction and increases in magnitude about 2-6 hours before the approach of the cyclone. But it is interesting to note that the direction changes (to northwesterly and southwesterly in the lower and upper part, respectively) remarkably just after the passage of the cyclonic storm. The source region of divergence is seen centred at 5.5 km.

The magnitude of the horizontal wind is very weak in the troposphere upto 13 km during and just after the nearest passage of the cyclone. The northeasterly wind increases in speed and the direction changes to north-northwesterly in the upper troposphere (14-16 km). It is also observed that the upper tropospheric wind weakened and became northerly after the crossing of the system. During the time of the passage of the cyclonic storm over the station, a narrow band of easterly wind component is seen near the tropopause region.

High resolution continuous wind data taken at 4-minute interval for 2½ hours from 0930 hrs LT to 1200 hrs LT on 16<sup>th</sup> October showed the reversal of wind soon after the passage of the storm (fig. 4.9 b). A region of calm wind exists at lower altitudes between 4 and 8 km. A level of divergence can be seen near to 9 km altitude for one hour from 0930 hrs LT, which disappear afterwards. There exists a level of convergence at 11.5 km at 0930 hrs LT, which remains more or less in the same position for 30 minutes. Afterwards it is seen to be shifting upward as time elapses. Strong northeasterlies are seen in the tropopause region, which is seen to be extending downwards. A narrow band of easterly wind is observed throughout this period

around 17 km. The change in wind direction at lower troposphere soon after the passage of the cyclonic storm can be clearly identified (see fig 4.9b).

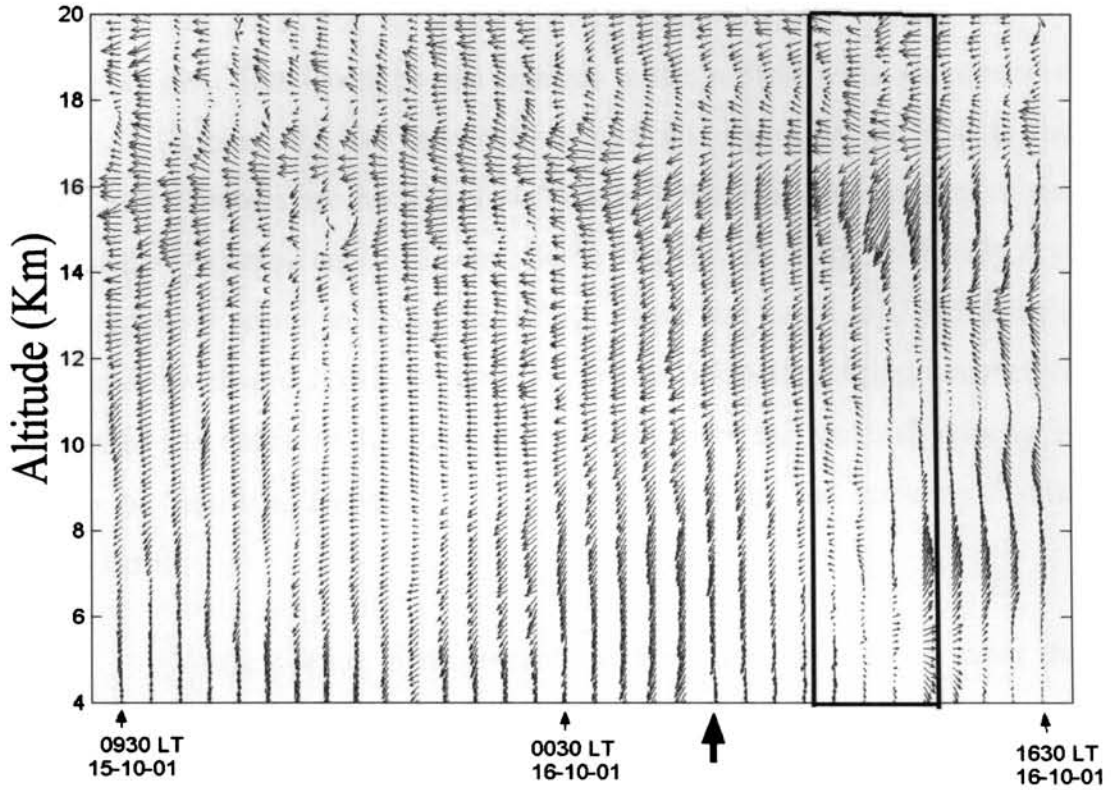


Figure 4.9a. Horizontal wind vector for 32 hours (from 0930 hrs LT on 15<sup>th</sup> October 2001 at 1-hour interval)

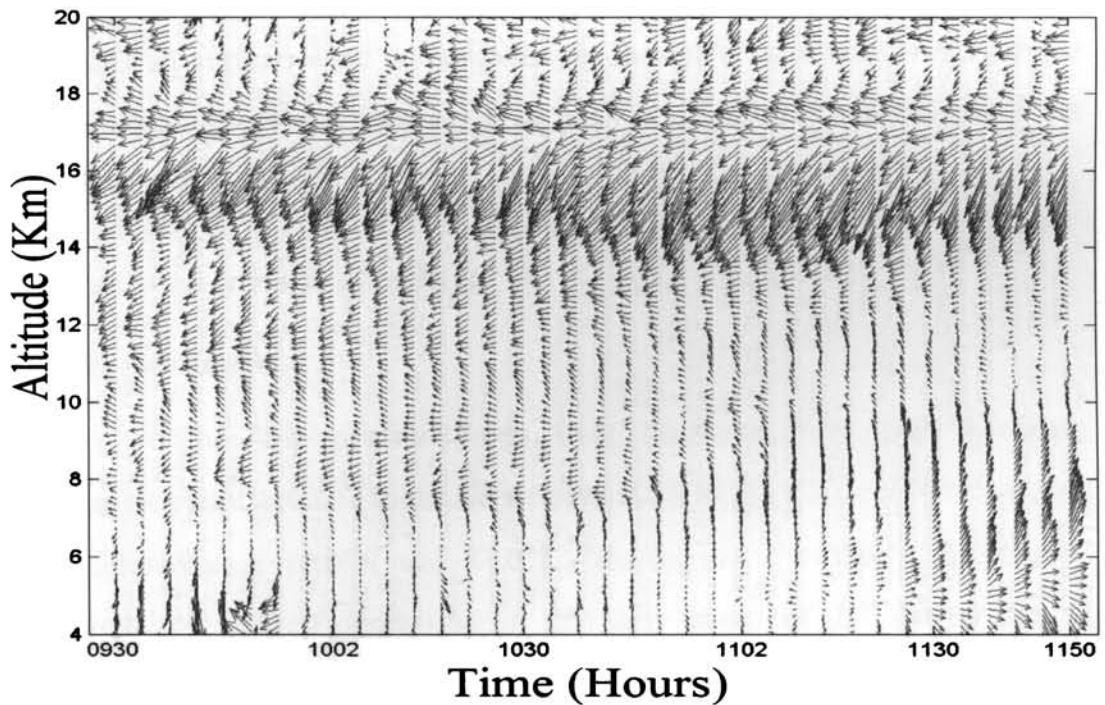


Figure 4.9b. Horizontal wind vectors for 2½ hours just after the passage

Figure 4.10a shows the height profiles of vertical wind during 11-21 October 2001. The vertical wind is generally very weak. As the cyclonic storm approaches the station the vertical wind in the lower levels are generally downward in direction. Considerable changes in the vertical wind are observed only on 16<sup>th</sup> October, the day in which the cyclonic storm passed near to the station. Large changes are noted below 12 km. Intense upward motion of the order of  $1 \text{ ms}^{-1}$  is noted around 12 km. Since this altitude range is already dry, this upward flow seems to be forced lifting above the cloud top. More rapid upward and downward flows are observed below 6 km suggesting convective activities. In the entire middle and upper troposphere the vertical velocity is found to be positive. Downward wind prevailed after the crossing of the cyclonic storm.

Vertical wind measurements at 4-minute interval, just after the nearest passage of the cyclone (from 0930 hrs LT to 1200 hrs LT) are shown in Figure 4.10b. Strong upward flow of nearly  $1.5 \text{ ms}^{-1}$  is noted near 12 km. Intense downward flow is seen around 6 km. As time elapses the downward flow is seen extending upto 8 km and upward flow is noted upto 17 km. It is also noted that vertical wind is weakening as the cyclone moves away from the radar site. Strong upward flow is noted in the middle troposphere during the entire observation period.

### **4.3.3. Far away passage of cyclone**

#### ***4.3.3a Synoptic features***

The low pressure area over southeast Bay and adjoining Andaman Sea concentrated into a depression at 0830 hrs LT on 23<sup>rd</sup> November 2002 centered near  $10.0^{\circ}\text{N}$  and  $87.0^{\circ}\text{E}$ . Moving in a northerly direction it intensified into a deep depression in the early hours of 24<sup>th</sup> November. It further intensified into a cyclonic storm over west central and adjoining southeast Bay centred near  $13.0^{\circ}\text{N}$  and  $87.0^{\circ}\text{E}$  on 24<sup>th</sup> November at 0830 hrs



LT. It further moved into the northerly direction till 26<sup>th</sup> November 1430 hrs LT and started recurving thereafter. It was located over central parts of Bay near 16.5°N and 90.0°E at 0830 hrs LT on 27<sup>th</sup> November 2002. The track of the cyclone is illustrated in figure 4.11.

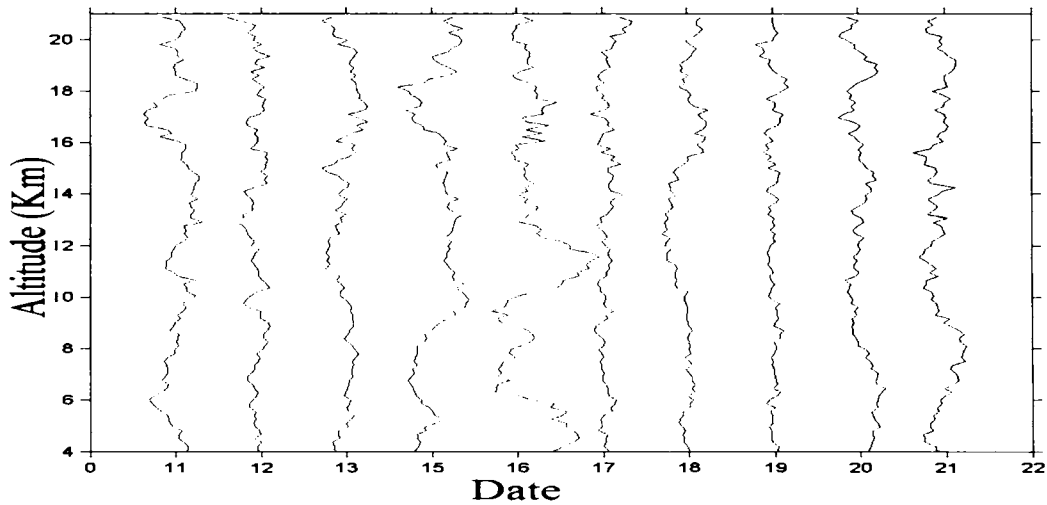


Figure 4.10a. Height profiles of vertical wind from 11-21 October

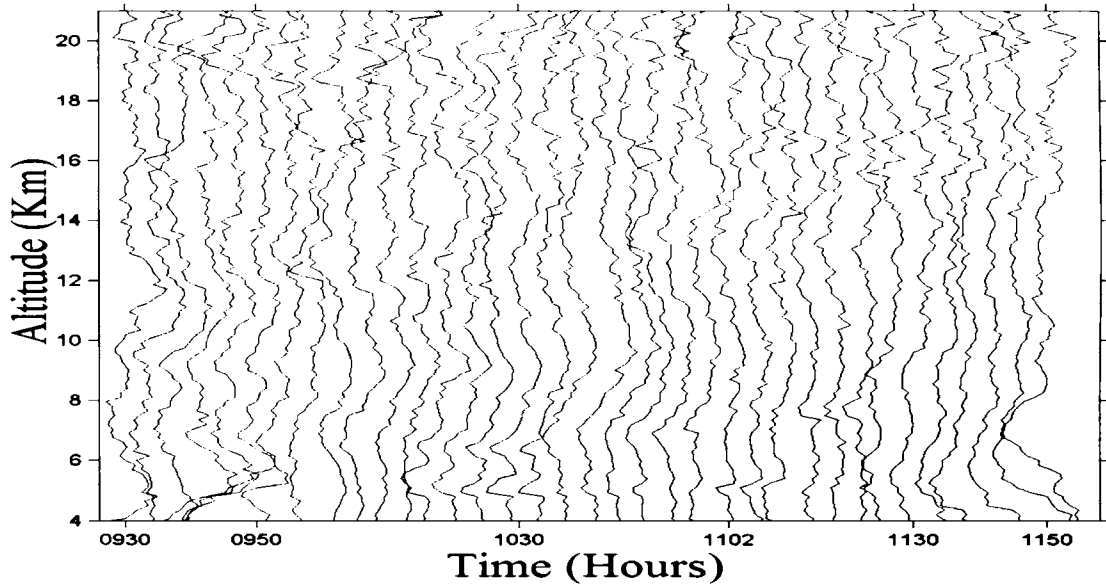
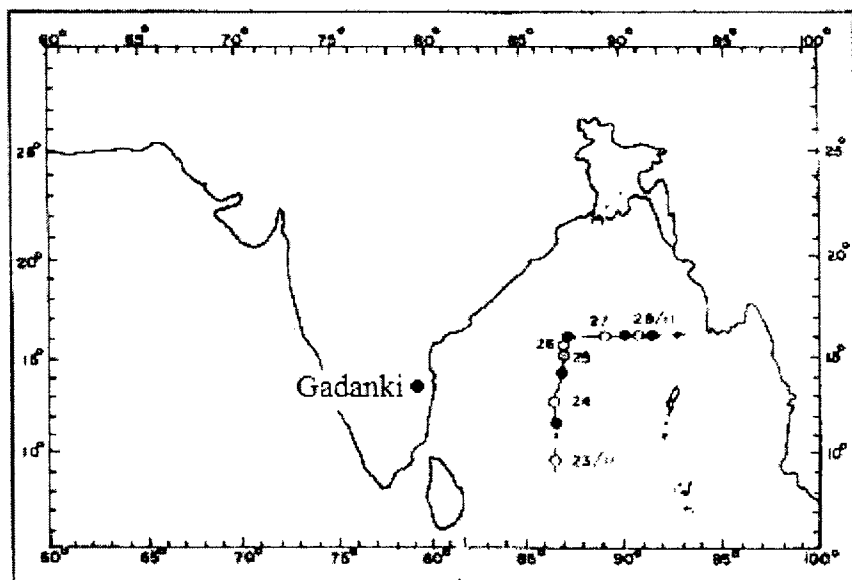


Figure 4.10b. Vertical wind profiles for 2½ hours after storm passage

#### 4.3.3b Wind characteristics

Special cyclone experiments were also carried by the Department of Atmospheric Sciences, CUSAT during November, 2002. Figure 4.12a shows the distribution of zonal wind for 29 hours at 1-hour interval from 2000 hrs LT

on 23<sup>rd</sup> November to 0000 hrs LT on 25<sup>th</sup> November 2002. This cyclone was nearest to the station (around 700 km) from 0000 hrs LT to 1000 hrs LT on 24<sup>th</sup> November. The arrow in the figure shows the time of nearest passage of the cyclone. Easterlies are noted at all altitudes between 4 and 20 km, prior to the approach of the cyclone. During the time of nearest position of the cyclone, westerly wind start appearing around 7 km, which spreads both upward and downward and increase in strength. The wind strength is seen decreasing when the cyclone moves away from the radar site. Above and below the region of westerlies, easterlies prevail throughout the observation period. The easterlies are seen strengthening when the cyclone is nearest to the station with a maximum speed around 14 km just after the passage.



— Cyclonic storm    - - - - - Depression    ← - - - Point of Dissipation  
 ○ Position at 0300 UTC    ● Position at 1200 UTC    ⊙ Position at 0300 & 1200 UTC

Figure 4.11. Cyclone track (23-28 November 2002)

High-resolution wind data of 4-min interval for 2½ hours before the nearest passage of the storm is shown in figure 4.12b. Easterlies are seen prevailing at all altitudes from 4 to 20 km. Very strong easterlies with speed of the order of  $\sim 25 \text{ ms}^{-1}$  is noted around 14 km. High-resolution wind data for 2 hours just after the nearest passage of the storm is shown in fig 4.12c. It is interesting to note that in the region between 7 and 10 km, easterlies are

replaced by westerlies. At all other altitudes easterlies are seen prevailing. It can also be seen that the easterly wind strength increases around 14 km and a maximum strength of the order of more than  $30 \text{ ms}^{-1}$  is noted.

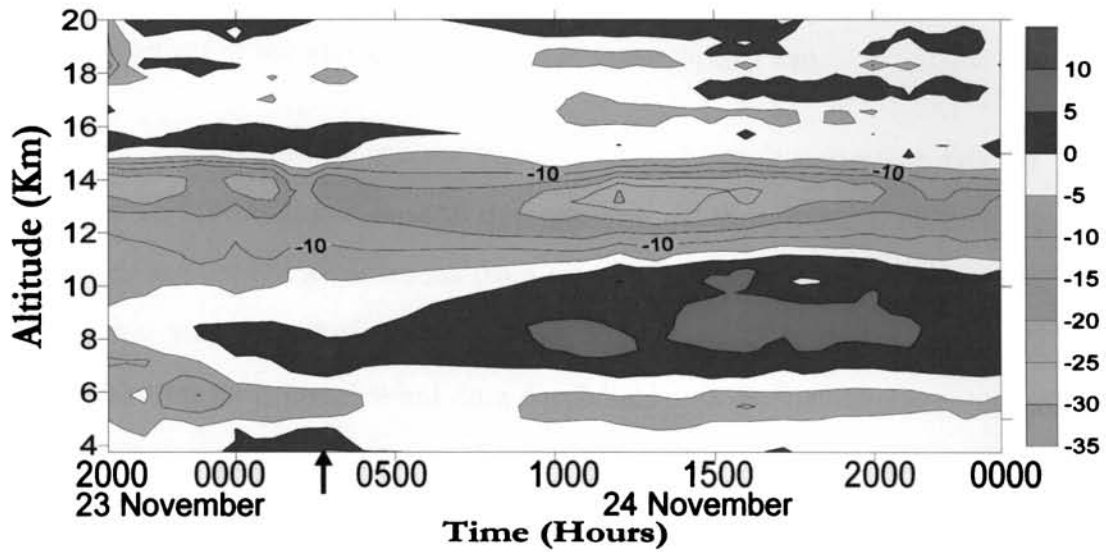


Figure 4.12a. Zonal wind for 29 hours from 2000 hrs LT on 23<sup>rd</sup> November

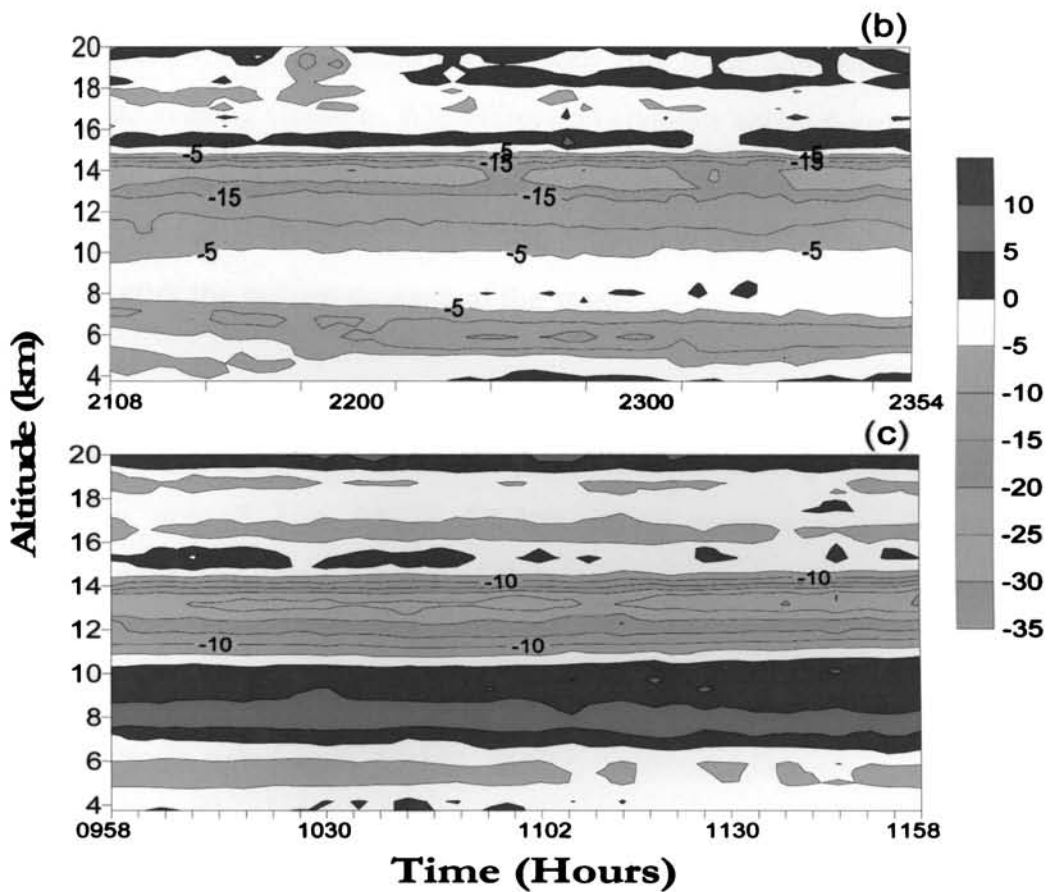


Figure 4.12b & c. Zonal wind distributions for 2½ hours before & 2 hours after the passage

Figure 4.13a shows the meridional component of wind for 29 hours at 1-hour interval from 2000 hrs LT on 23<sup>rd</sup> November. While the cyclone approaches the station, southerlies are prevailing at all altitudes between 6 and 22 km. Weak northerly wind is noted below 6 km. During the nearest position of the storm, northerlies are seen upto 7 km.

Figure 4.13b is a contour plot of high-resolution wind data for 2½ hours on 23<sup>rd</sup> November before the passage of the storm. In this figure southerlies are seen at all altitudes from 6 to 22 km. No marked change is noted in the wind structure during this period. Figure 4.13c is the contour plot of high-resolution meridional wind data for 2 hours on 24<sup>th</sup> November, just after the nearest passage of the storm. The meridional wind is not much changed except bands of northerly wind appearing around 16 and 20 km.

The horizontal wind vector plot for 29 hours at 1-hour interval is shown in figure 4.14. Northeasterlies are seen upto 6 km and persisting for 29 hours with decreasing strength. Wind direction changes above 6 km. Above 12 km, the wind is southeasterly upto 15 km. These winds are very strong compared to the wind at all other altitudes. There is a decrease in windspeed at all altitudes after the nearest passage of the storm.

Figure 4.15a is the horizontal vector wind plot for 2 hours before the nearest passage of the storm. The wind is northeasterly upto 6 km and southeasterly upto 8 km. Above 12 km strong southeasterly wind with increasing strength is noted. Figure 4.15b is the horizontal vector wind plot for 2 hours just after the passage of the storm. The wind is northeasterly upto 7 km similar to that observed before the passage of the storm. Above 7 km change in wind direction is noted upto 13 km. Strong southeasterlies are noted in the region between 12 and 15 km. In the tropopause region, the wind is northeasterly/easterly. Marked changes in wind direction occur in the middle troposphere associated with the passage of the cyclone.

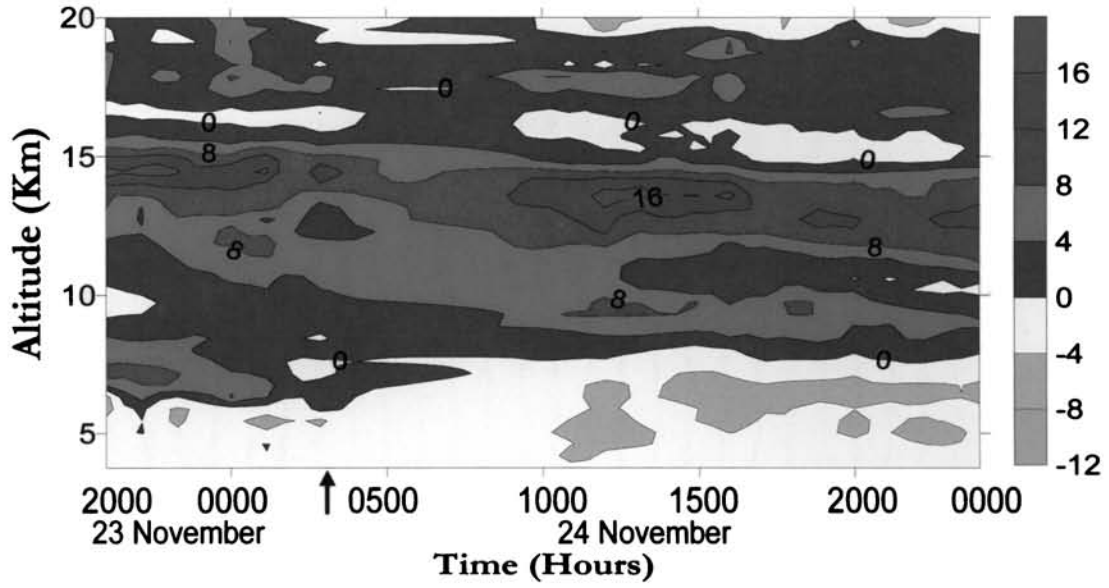


Figure 4.13a. Meridional wind distributions for 29 hours

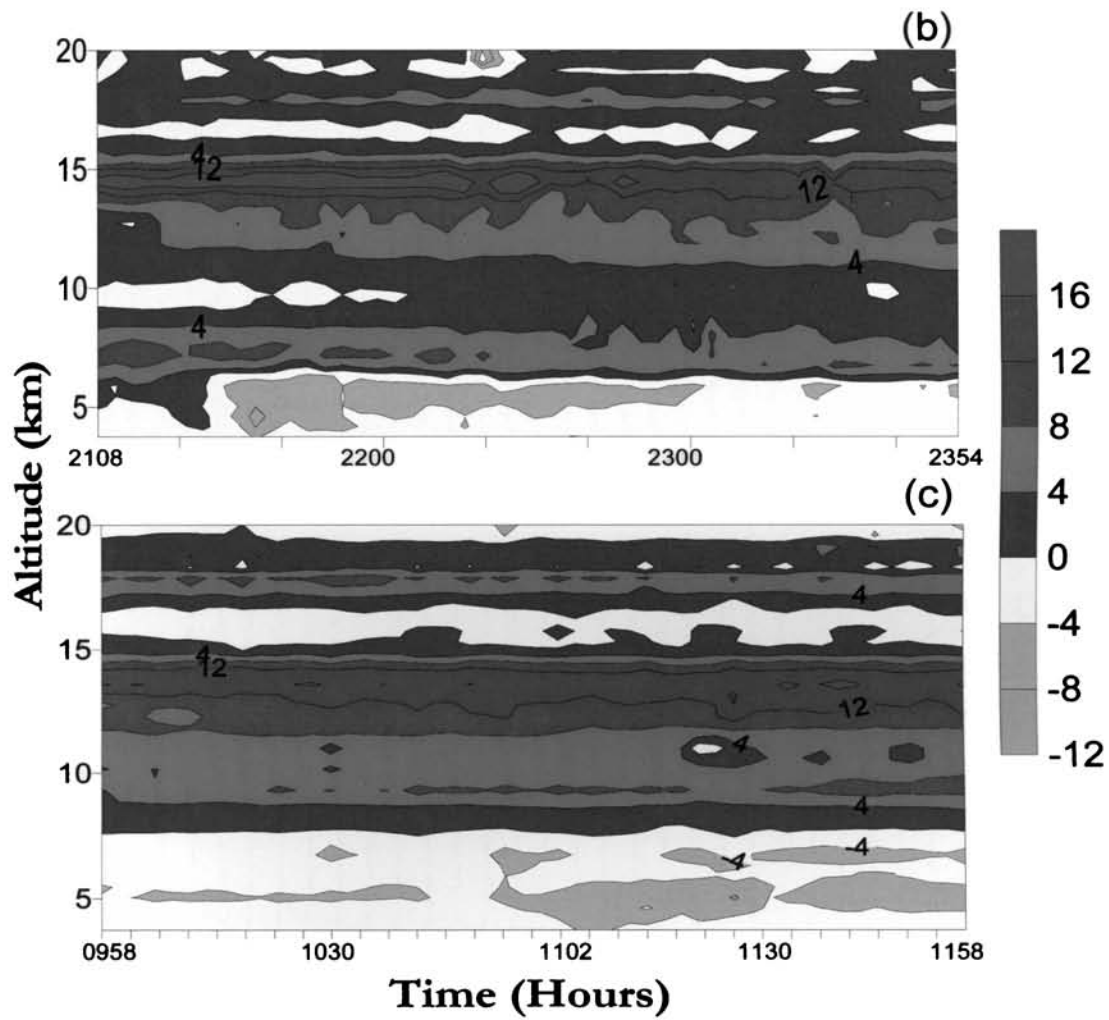


Figure 4.13b & c. Meridional wind distributions for 2½ hours before & 2 hours after the passage

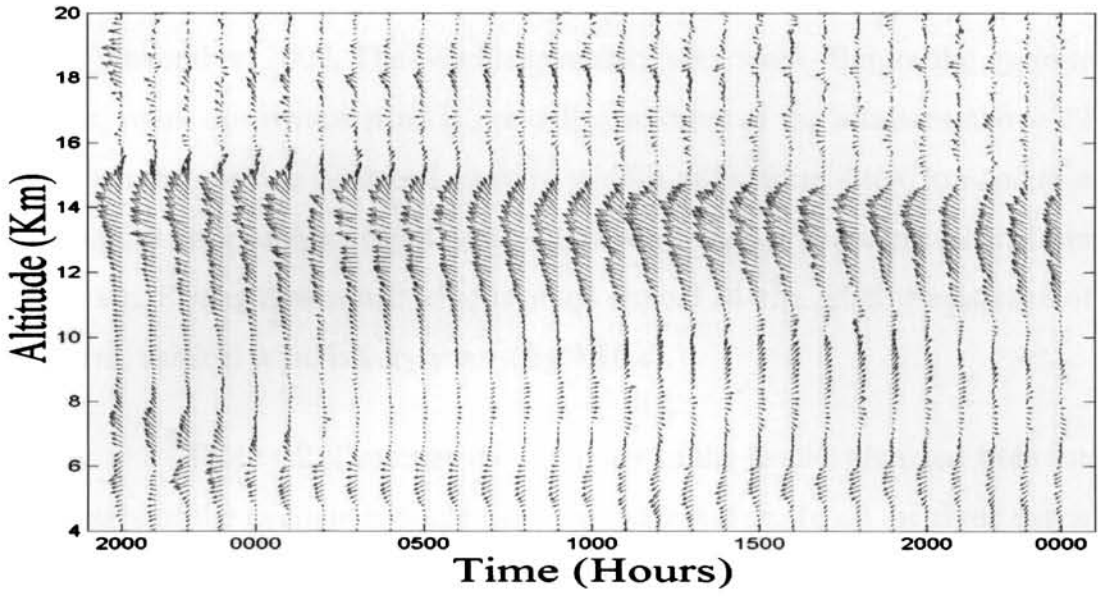
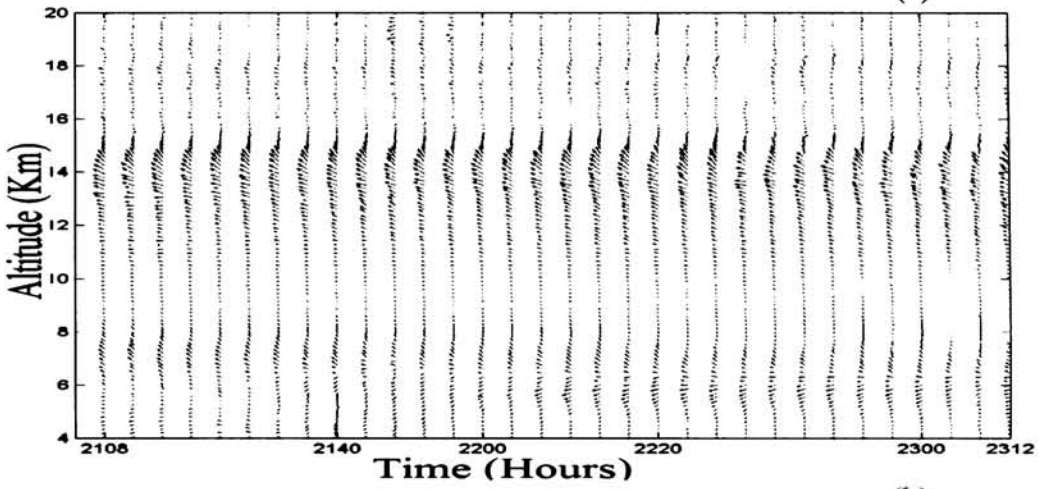


Figure 4.14. Horizontal wind vector distribution for 29 hours

(a)



(b)

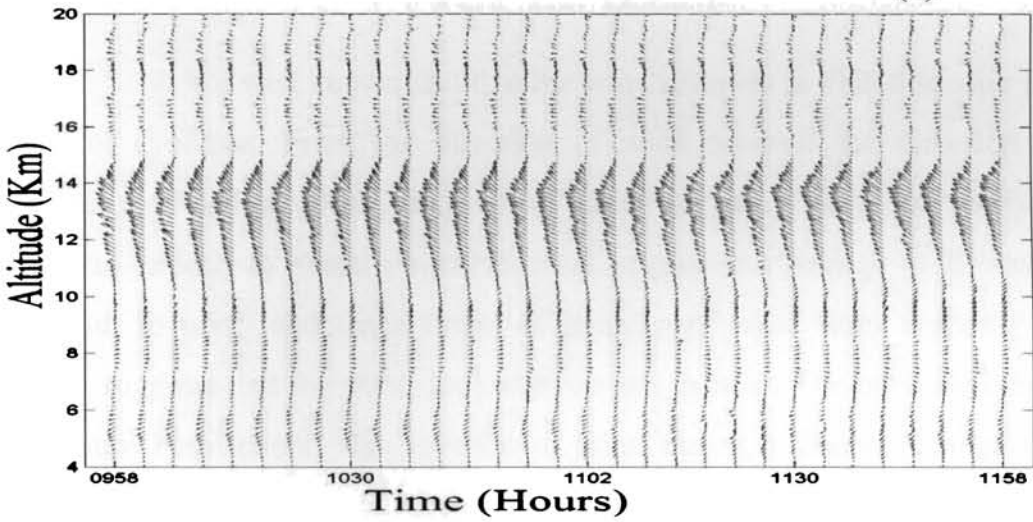


Figure 4.15 a & b. Horizontal wind vectors before & after the storm passage

Figure 4.16a shows the vertical wind profiles from 2000 hrs LT on 23<sup>rd</sup> November, 2002. The wind is generally very weak. Before the cyclone passage, weak downward wind is prevailing at most of the altitudes above 12 km. When the cyclone is nearest, upward wind is noted from 4 to 6 km and also in the middle troposphere (fig 4.16b). Downward wind is more prevalent from 4 to 22 km. Strong downward wind is noted around 14 km. After the passage of the storm, vertical wind is very weak (fig 4.16 c).

Table 4.2 illustrates the summary of the results obtained from the three cases of the cyclone passage over the radar station. In all the three cases, the wind reversal has taken place in the lower and middle troposphere associated with the passage of cyclones. During this period, strengthening of the easterly components in the upper troposphere and lower stratosphere is observed. In the case of overhead and nearby passage, reversal is noted both in zonal and meridional wind. But in the case of far away passage, reversal is found only in zonal wind. Both in nearby and overhead passage, the zonal wind reversed from easterly to westerly and the meridional wind from northerly to southerly, suggesting that the cyclone had passed from southeast to northwest of the radar site. In the case of far away passage, easterly wind is noted to change in direction to westerly, which implies that the cyclone had passed from south to north of the radar site.

It is a well known fact that the wind reverses in direction after the passage of cyclones. From the direction of wind reversal the direction of movement of cyclones can be studied (*Sato et al.*, 1991). In northern hemisphere easterly to westerly wind reversal suggests the passage of the storm from south to north and the reversal of meridional wind from northerly to southerly suggests that the storm moved from east to west. The opposite is true for southern hemisphere. The reversal of wind during typhoon passage has been observed by MU radar in Japan (*Sato et al.*, 1991) and by Chungli radar in Taiwan (*Rottger et al.*, 1991).

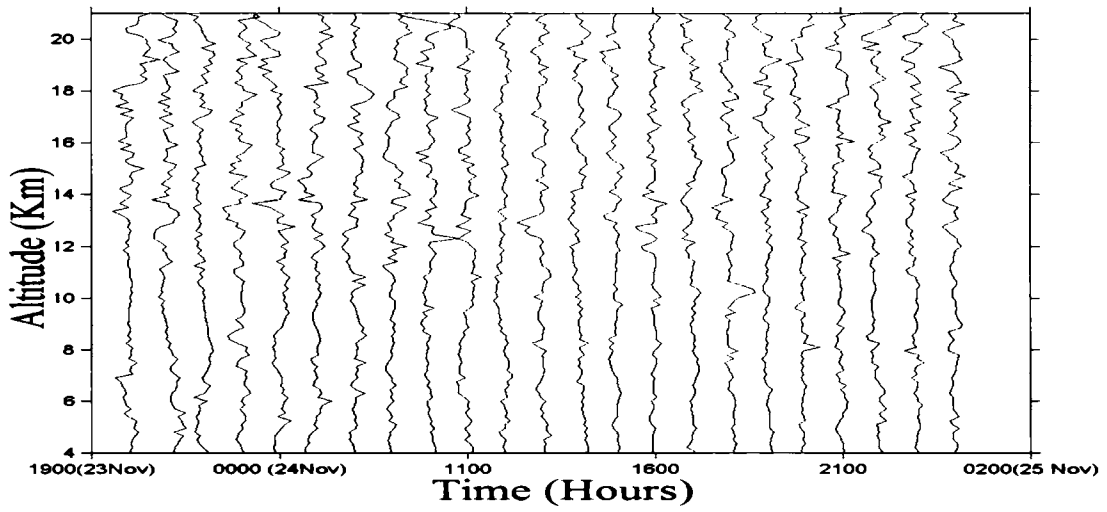


Figure 4.16a. Vertical wind profiles for 29 hours

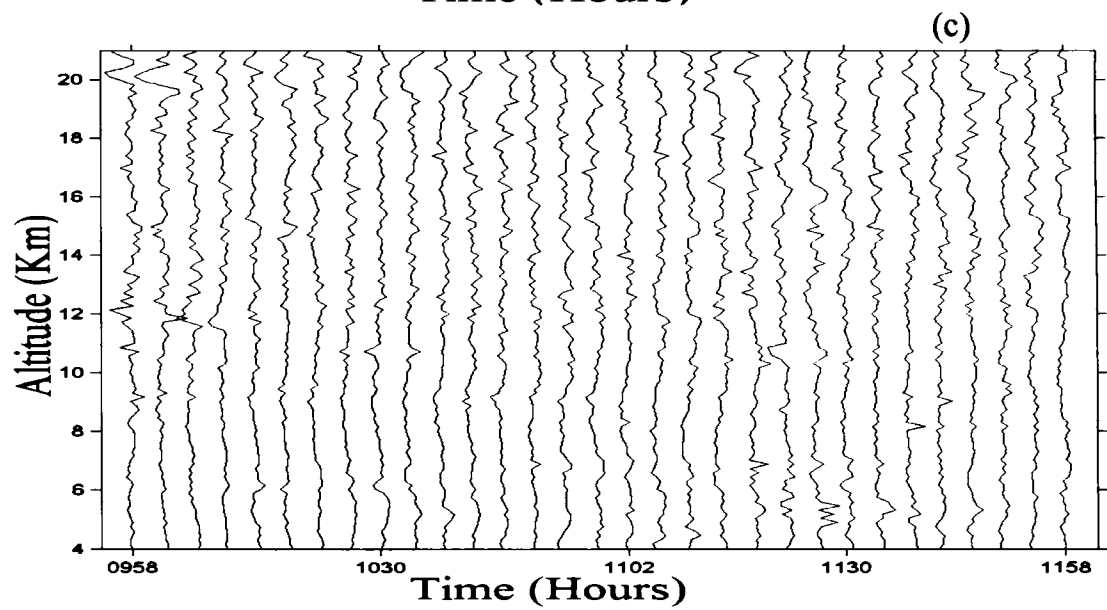
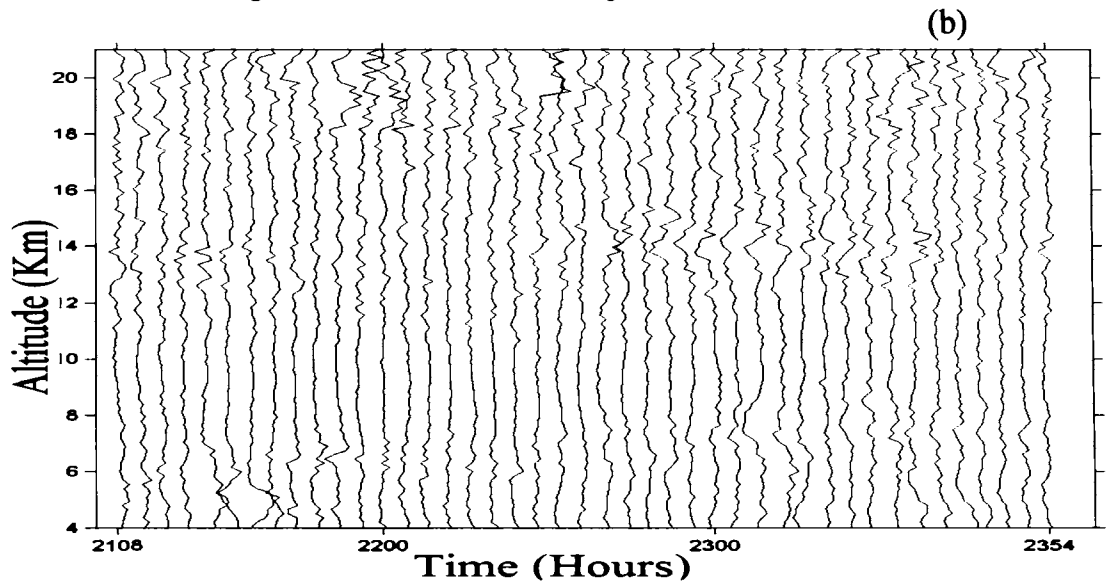


Figure 4.16 b & c. Vertical winds before & after storm passage



Cyclone Cases	Height Region	Horizontal wind Vector			Vertical Wind		
		Before	During	After	Before	During	After
<b>OVERHEAD PASSAGE</b>	<i>4-8 km</i>	<i>SE</i>	<i>NW</i>	<i>SW</i>	<i>Downward</i>	<i>Downward</i>	<i>Weak Variable</i>
	<i>8-12 km</i>	<i>SE</i>	<i>Light E</i>	<i>NE</i>	<i>Downward</i>	<i>Upward</i>	<i>Weak Variable</i>
	<i>12-16 km</i>	<i>SE</i>	<i>SE</i>	<i>SE</i>	<i>Downward</i>	<i>Downward</i>	<i>Weak Variable</i>
	<i>Above 16 km</i>	<i>SE</i>	<i>SE</i>	<i>SE</i>	<i>Downward</i>	<i>Downward</i>	<i>Weak Variable</i>
<b>NEARBY PASSAGE</b>	<i>4-8 km</i>	<i>NNE</i>	<i>N</i>	<i>SW</i>	<i>Weak Downward</i>	<i>Weak Downward</i>	<i>Weak Downward</i>
	<i>8-12 km</i>	<i>NE</i>	<i>E</i>	<i>NW</i>	<i>Weak Downward</i>	<i>Weak Downward</i>	<i>Strong Upward</i>
	<i>12-16 km</i>	<i>NE</i>	<i>NE</i>	<i>NNE</i>	<i>Weak Downward</i>	<i>Weak Downward</i>	<i>Weak Downward</i>
	<i>Above 16 km</i>	<i>E</i>	<i>E</i>	<i>E</i>	<i>Weak Downward</i>	<i>Weak Downward</i>	<i>Weak Downward</i>
<b>FAR AWAY PASSAGE</b>	<i>4-8 km</i>	<i>NE</i>	<i>Weak NE</i>	<i>Weak NE</i>	<i>Upward</i>	<i>Downward</i>	<i>Downward</i>
	<i>8-12 km</i>	<i>E / SE</i>	<i>W / SW</i>	<i>SW</i>	<i>Upward</i>	<i>Downward</i>	<i>Downward</i>
	<i>12-16 km</i>	<i>SE</i>	<i>SE</i>	<i>SE</i>	<i>Downward</i>	<i>Upward</i>	<i>Downward</i>
	<i>Above 16 km</i>	<i>WEAK</i>	<i>WEAK</i>	<i>WEAK</i>	<i>Downward</i>	<i>Downward</i>	<i>Downward</i>

(E- Easterly, W- Westerly, N-Northerly, -Southerly, NE- Northeasterly, NW- Northwesterly, SE- Southeasterly, SW- Southwesterly, NNE- North-northeasterly)

Table 4.2. Summary of the observational findings associated with the passage of tropical cyclones

The horizontal wind vectors clearly indicate the time of passage of the storm and the change in wind behaviour associated with the passage. Strong upward flow is noted around 12 km during and just after the passage of the storm. *Sato et al.* (1991) also identified similar behaviour between 8 and 12 km during the passage of the storm using MU radar. This level is identified as level of maximum convective outflow.

It was also observed that during and just after the passage of the storm, the horizontal winds are very weak in the lower and middle troposphere. After the passage of the storm the winds are seen strengthening. The vertical winds are very calm in the entire troposphere and lower stratosphere soon after the passage of the cyclonic storm.

#### **4.5. Concluding Remarks**

The wind characteristics before, during and after the passage of different cyclones are studied in detail. Marked changes in wind speed and direction are noted during the passage of all these three cases, depending on the intensity and position of the cyclones. In the case of cyclone in 2002, even though the cyclone was away from the radar, the effect is felt at the radar site. Reversal of wind is noted in all the cases. The wind reversal is observed both in zonal and meridional wind for the overhead and nearby passage, whereas only the zonal wind reversed for the far away passage of the cyclone.

Chapter #5

*Fluctuations of the Tropopause and Other  
Reflectivity Layers Associated with the  
Passage of Tropical Cyclones*

## 5.1. Introduction

In recent years, the tropopause region has received much attention because there is a growing necessity of knowing the temporal and spatial structure of meteorological parameters within the transition zone between the troposphere and the stratosphere. In order to estimate the stratospheric-tropospheric exchange of mass, water and chemical constituents, it is necessary to have precise knowledge about the meteorological conditions of the tropopause. *Reid and Gage (1996)* revealed the statistics of tropical tropopause using radiosonde data taken at Truk Island. The meridional and zonal variations in the tropopause height and temperature reflect the global jet stream structure (*Hoinka, 1999*). It has been reported that under cyclonic influence, the tropopause is lower than the normal and the stratification above the tropopause is less stable than average (*Zangl and Wirth, 2002*).

Long-wavelength radars are extremely sensitive to stratification in temperature structure of the atmosphere and it has been shown by *Rottger (1980)* and *Green and Gage (1980)* that radars operating in the VHF regime can be used to determine the height of the tropopause. Many investigators have studied about the stable layer structures associated with the tropical tropopause using VHF radar (*Gage and Green, 1979; Larsen and Rottger, 1983*). The method to determine the height of the tropopause is then modified by considering the modified Fresnel scattering model for VHF radar observations (*Gage et al., 1986*). A practical algorithm for online determination of the height of the tropopause using VHF radar was developed by *Riddle et al. (1983, 1984)*.

*Jordan and Jordan (1954)*, in their study of the mean thermal structure of tropical cyclones, found a general increase in the height of the tropopause toward the central region of the storm. Their mean radial height profile at 100 hPa indicated a decrease in height towards the core. Another U-2

probe made into hurricane Isbell in October 1964 was also studied by *Penn* (1966) who found that the tropopause was inclined upward into the eye and cloud-tops were found extending to 68 hPa (19 km) to the north side of the storm.

*Koteswaram* (1967) studied the structure of hurricanes in the troposphere and lower stratosphere using rawinsonde data. He found that the tropopause generally bulges upward and is coldest near the hurricane core, the bulge being more prominent in intense hurricanes than in weak ones. It lowers and is warmer at the axis of the peripheral ridge and again rises and becomes colder at the outer rim of the peripheral ridge and again lowers as shown in figure 5.1.

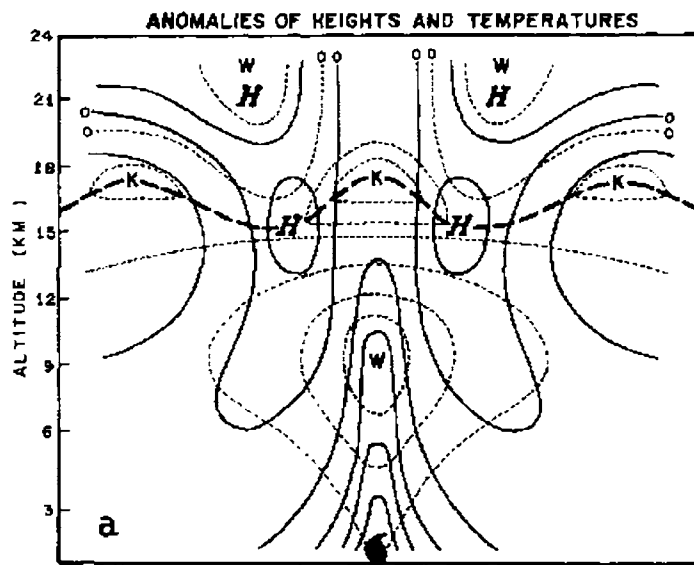


Figure 5.1. Tropopause structure during a hurricane (from *Koteswaram*, 1967)

The Indian MST radar used in the ST mode with spatial resolution of 150 m and temporal resolution of 72 s showed interesting results on the tropopause structure and stable layers in the lower atmosphere (*Kumar et al.*, 1994). Sharp enhancement in power and Signal to Noise Ratio (SNR) is noted at tropopause height, which has been verified using the radiosonde data at Chennai (*Jayarao et al.*, 1994). The 90-year climatological mean tropopause at Gadanki for October and November are 16.4 km and 16.6 km, respectively.

A large number of recent observational studies of mesoscale systems have been signifying a renewed interest in tropical cyclone systems and their impact on the general atmospheric circulation and hence the global climate. Observational studies of tropical cyclones are crucial for understanding their internal processes and also for quantifying their interactions with the large-scale environment. The MST radar is a powerful tool in observing the vertical structure of tropical cyclones. In this chapter the observation of tropical tropopause and other high reflectivity layers using MST radar during the passage of Bay of Bengal tropical cyclones nearer to MST radar site are included. These observations are first of their kind from this latitude region.

## **5.2. Data Deduction Techniques**

The Indian MST Radar at Gadanki, India is highly sensitive, pulse coded, coherent VHF phased array radar operating at 53MHz with a peak power-aperture product of  $3 \times 10^{10} \text{ Wm}^2$ . Detailed description of the Indian MST radar is reported in chapter 2 of the thesis.

### **5.2.1. Determination of the tropopause and other reflectivity layers**

VHF radars are used to observe specular echoes at vertical incidence. These echoes arise primarily from the stable layers of the atmosphere. The ability to detect stable atmospheric regions from enhanced echoes using VHF radars provides a direct and simple technique for determining the height of the tropopause, since a pronounced discontinuity is an indication of the tropopause (*Gage and Green, 1979*). We can detect the layers of the atmosphere from the height profiles of Signal to Noise Ratio (SNR) observed with vertical antenna of the MST Radar. The method to determine the height of the tropopause, developed by *Gage et al. (1986)* for mid-latitude stations is modified considering the climatology of the thermal structure at tropical latitudes and used in this study. If the radar echo arises due

to Fresnel reflection/scattering, the back scattered power can be expressed in terms of radar parameters and the power reflection coefficient ( $P_r$ ) of the probing volume as (Gage and Green, 1982a)

$$P_r = \frac{\alpha^2 P_t A_e^2}{4\lambda r^2} |\rho|^2 \quad \text{--- 5.1}$$

where,  $\alpha$  is the efficiency factor of the antenna,  $P$  is the peak transmitted power,  $A$  is the effective antenna aperture,  $\lambda$  is the radar wavelength and  $r$  is the radar range and  $|\rho|^2$  is the power reflection coefficient.  $|\rho|^2 = 0.25\Delta r M^2 F_1^2(\lambda) e^{(z_0-z)/H}$ , where,  $M$  is the gradient of radio refractive index (Gage et al., 1985).

The range corrected echo power  $S_v (= P_r r^2)$  can be expressed as

$$S_v = \frac{BP^2}{T^4} \left[ \Gamma d + \frac{dT}{dz} \right]^2 e^{(z_0-z)/H} \quad \text{--- 5.2}$$

where,  $M = M_d$  (for dry air) =  $-0.77 \times 10^{-6} \frac{p}{T^2} \left[ \Gamma d + \frac{dT}{dz} \right]$ . Here  $B$  is a constant.

The WMO criteria of the tropopause height is *the level above 500 mb at which the temperature lapse rate drops to  $2^\circ \text{K km}^{-1}$  and stays below that value for at least 2 km*. The determination of tropical tropopause at Gadanki involves three steps mentioned below.

- i. The estimation of model power profile corresponding to the lower stratospheric mean temperature gradient. i.e.,  $\frac{dT}{dz} = 3.5^0 \text{ K km}^{-1}$
- ii. The estimation of model power profile corresponding to  $\frac{dT}{dz} = 0^0 \text{ K km}^{-1}$ ,
- iii. The estimation of model power profile corresponding to  $\frac{dT}{dz} = -2^0 \text{ K km}^{-1}$

The atmospheric pressure (P) decreases exponentially with height. Therefore, it can be expressed as

$P = P_0 e^{(z_0 - z)/H}$ , where,  $P_0$  is the pressure at the reference level  $z_0$  and H is the scale height.

The mean temperature gradient in the tropical stratosphere deviates significantly from  $0^\circ \text{ K km}^{-1}$ . Therefore the temperature in the lower stratosphere at tropical latitudes can be expressed as

$$T = T_0 \left[ 1 + \frac{1}{T_0} \frac{dT}{dz} (z - z_0) \right]$$

where,  $T_0$  is the temperature corresponding to a reference level  $z_0$ .

The temperature at tropical latitudes is noted to vary significantly in the lower stratosphere. The scale height is also varying as it is proportional to mean temperature. So the variation in scale height can be expressed as

$$H = H_0 \left[ 1 + \frac{1}{H_0} \frac{dH}{dz} (z - z_0) \right]$$

where,  $H_0$  is the scale height corresponding to the height level  $z_0$ . Considering the values of P, T and H, the range corrected echo power can be expressed as

$$\log(S_v) = Q - \left[ \frac{1.3029}{H_0} + \frac{1.7372}{T_0} \frac{dT}{dz} \right] (z - z_0) \quad \text{---- 5.3}$$

Equation 5.3 represents a straight line between  $\log(S_v)$  and  $z$ , Q is a constant for the height range under consideration and it is given by

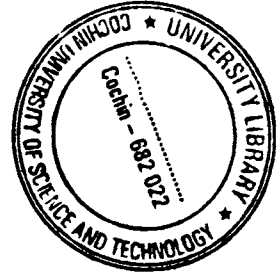
$$Q = \log \left( \frac{BP_0^2}{T_0^4} \right) + \log \left[ \Gamma d + \frac{dT}{dz} \right]^2$$



The tropopause is the region of transition which separates the troposphere with negative lapse rate and stratosphere with positive lapse rate. So the lapse rate will be  $0^{\circ} \text{ K km}^{-1}$  near the tropopause. It can also be noted that at  $z = z_0$ , i.e., in the lower stratosphere  $\log(S_v) = Q$ . To determine the value of  $Q$  in the lower stratosphere, a best fit line can be constructed for climatological mean stratospheric temperature gradient. The intercept ( $Q$ ) at  $z = z_0$  represents the observed power in the lower stratosphere. We can get the value of  $Q$  corresponding to  $dT/dZ = 0^{\circ} \text{ K km}^{-1}$  ( $Q_0$ ) once we get the intercept  $Q$ .  $Q$  can be expressed as

$$Q = Q_0 + 2 \log \left[ \frac{\Gamma_d + \frac{dT}{dz}}{\Gamma_d} \right],$$

$$\text{where, } Q_0 = \log \left[ \frac{BP_0^2}{T_0^4} \right] + \log(\Gamma_d^2)$$



Using mean temperature gradient in the tropical stratosphere,  $Q$  and  $Q_0$  can be expressed as

$$Q = Q_0 + 2 \log (13.3/9.8) = Q_0 + 0.26525$$

Thus the model power profiles corresponding to temperature lapse rates in the lower stratosphere, around the tropopause and also for  $dT/dZ = -2^{\circ} \text{ K km}^{-1}$ , the conventional lapse rate to determine the tropopause can be obtained. The model profile corresponding to  $dT/dZ = 0^{\circ} \text{ K km}^{-1}$  can be expressed as

$$\log(S_v) = Q_0 - \left[ \frac{1.3029}{H_0} \right] (z - z_0) \quad Q \quad \text{--- 5.4}$$

$Q$  corresponding to  $dT/dZ = -2^{\circ} \text{ K km}^{-1}$  ( $Q_{-2}$ ) can be expressed in terms of  $Q_0$  as

$$Q_{-2} = Q_0 + 2 \log \left[ \frac{\Gamma_d - 2}{\Gamma_d} \right] = Q_0 - 0.2$$

So, the model profile corresponding to  $dT/dZ = -2^0 \text{ K km}^{-1}$  can be expressed as

$$\log(S_v) = Q_{-2} - \left[ \frac{1.3029}{H_0} + \frac{3.4744}{T_0} \right] (z - z_0)$$

and, the profile corresponding to  $dT/dZ = 3.5^0 \text{ K km}^{-1}$  in the lower stratosphere can be expressed as

$$\log(S_v) = Q_s - \left[ \frac{1.3029}{H_0} + \frac{1.7372}{T_0} \frac{dT}{dz} \right] (z - z_0)$$

where,  $Q_s = Q_0 + 2\log(13.3/9.8) = Q_0 - 0.26525$ .

The height of the tropopause can then be obtained by determining the height at which the model profile  $S_v$ , corresponding to  $dT/dZ = -2^0 \text{ K km}^{-1}$  intersects with the radar observed  $S_v$  profile. The discrepancy in altitude of the tropopause is less than  $1/3^{\text{rd}}$  of the altitude resolution taken. The error analysis shows that a maximum of  $\pm 500 \text{ m}$  variation in the altitude may occur when the range resolution is  $1 \text{ km}$  (*Gage and Green, 1982a*).

Figure 5.2 demonstrate the algorithm of tropopause determination, using the observed power profile, predicted power profile in lower stratosphere which corresponds to an average lapse rate of  $3.5^0 \text{ K km}^{-1}$ , and the constructed power profile for  $dT/dZ = -2$ , that determines the tropopause for a normal day. The horizontal bar represents the height of the tropopause reported by radiosonde and the arrow represents the radar tropopause. Previous studies of tropopause using the Indian MST radar indicates that the height of the tropopause determined by the radar shows good agreement with the radiosonde observations with a correlation coefficient of 0.7 which is significant at 0.1% level. Also it is mentioned that the contribution of isotropic scattering to the vertical beam echo power is less than 6%, which makes no significant change in the determination of the height of the tropopause and therefore can be neglected.

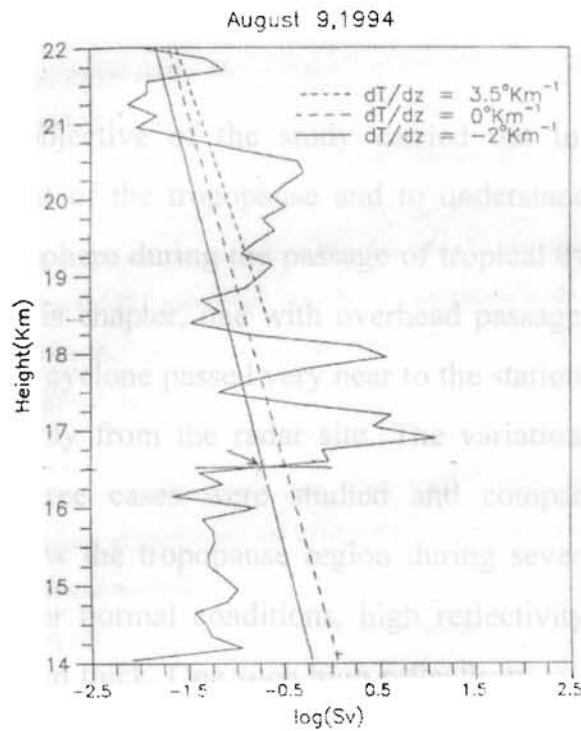


Figure 5.2. Determination of tropopause from model profiles

### 5.2.2. Experimental approach

Observations were made using 6 beams (East 10, West 10, North 10, South 10, Zenith X and Zenith Y) and single vertical beam (Zenith) with a pulse width of  $16\mu\text{s}$  (coded) during tropical cyclone passage in various years. The algorithm to determine the height of the tropopause is based on Fresnel scattering model. The model explains the radar observed echo power at vertical incidence in terms of meteorological parameters. The percentage of occurrence of the height of the tropopause under normal circumstances at Chennai, the nearest radiosonde station to the radar, above the height of 14 km is 99% (*Ramanatham et al.*, 1969). But to know whether the tropopause goes below 14 km during the passage of tropical cyclones, the lowest level for the determination of height of the tropopause is taken as 12 km. In 1994, already available data was used. The observations were taken from 4 – 21 km with an altitude resolution of 150 m. Only zenith beam data is used for determining the tropopause and other reflectivity layers in the atmosphere.

### **5.3. Results and Discussion**

The objective of the study carried out in this chapter is to determine the height of the tropopause and to understand the various layers present in the atmosphere during the passage of tropical cyclones. Three cases are considered in this chapter, one with overhead passage of the cyclone, the second one with the cyclone passed very near to the station and the third, when the cyclone was away from the radar site. The variations in the tropopause height for these three cases were studied and compared. Appearance of multiple layers below the tropopause region during severe weather events is also observed. Under normal conditions, high reflectivity regions are in the form of layers 1-2 km thick. One such high reflectivity layer is always present near tropopause level at 17 km. Below the tropopause, there is a bunch of such high reflectivity layers, generally 3-4 in number, between 4 and 11 km. The atmosphere between 11 and 15 km is generally free from high reflectivity layers during normal conditions. Only during severe weather conditions like cyclones and thunderstorms, reflectivity layers form in this region.

#### **5.3.1. Tropopause observations during the overhead cyclone passage**

In 1994, a cyclone passed overhead the radar station on 31<sup>st</sup> October. The low pressure area in the Bay of Bengal on 27<sup>th</sup> October intensified into a deep depression near to 10.5°N and 84.5°E at 1730 hrs LT of 29<sup>th</sup> October. Moving in a northwesterly direction, it further intensified into a cyclonic storm and lay centred at 1730 hrs LT on 30<sup>th</sup> October near 12.3°N and 81°E about 120 km southsoutheast of Chennai. It moved in a northwesterly direction and further intensified into a severe cyclonic storm with a core of hurricane winds at 0530 hrs LT of 31<sup>st</sup> October and crossed north Tamilnadu coast, near Chennai between 0630 hrs to 0730 hrs LT of 31<sup>st</sup> October. It weakened into severe cyclonic storm which lay about 50 kms northwest of Chennai at 0530 hrs LT of 31<sup>st</sup> October. It rapidly weakened into a well marked

low pressure area on 1<sup>st</sup> November evening. The satellite picture of the storm at the landfall of the cyclone is given in figure 5.3.

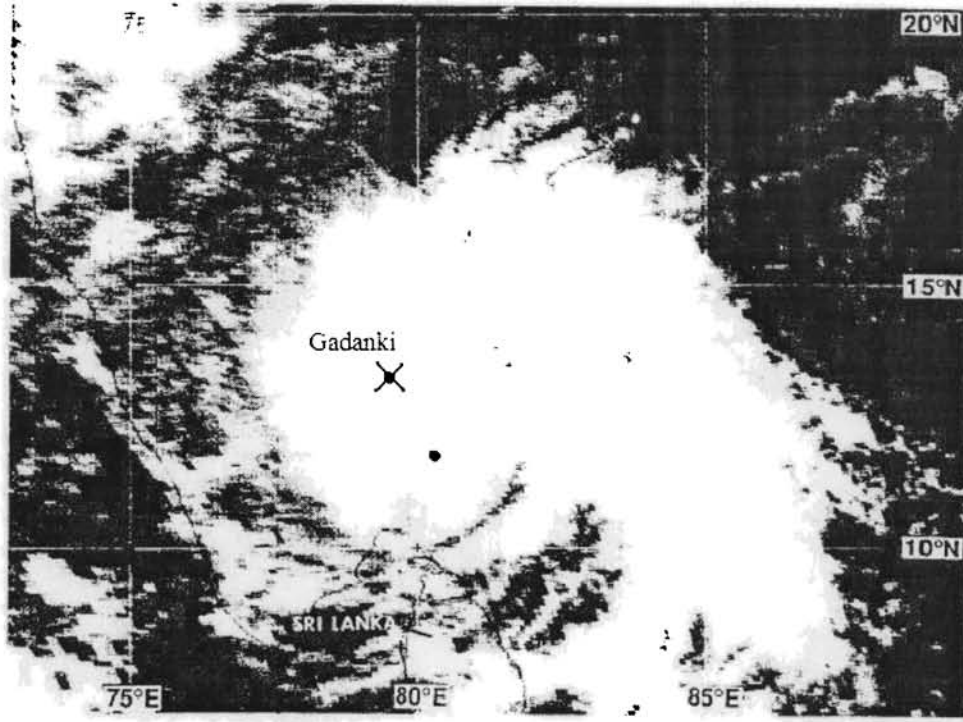


Figure 5.3. Cyclone approaching south India on 31<sup>st</sup> October, 1994

### *5.3.1a Determination of tropopause from SNR values*

In 1994, the cyclone passed overhead of the station around 1300 hrs LT of 31<sup>st</sup> October. Unfortunately there was no observation during the time of exact overhead passage of the cyclone. Figure 5.4a-d show the Range-Time-Intensity (RTI) plots of SNR on 27<sup>th</sup> October, three days prior to cyclone, 31<sup>st</sup> October at 1700 hrs and 2025 hrs LT ( 4 hours and 8 hours after overhead passage) and on 1<sup>st</sup> November, one day after the passage. Multiple layers are observed three days before the cyclone passage, when it was in the form of a low pressure area in the Bay.

Very thick layer of high SNR is found around 18 km (fig 5.4a). Another two layers are found around 16 km. A thin layer of low SNR in comparison with that at 16 and 18 km is found near to 15 km. The region from 11 – 14 km is free from high reflectivity layers, i.e., the region is having weak

SNR signals. It can be noted that the number of layers present in the atmosphere has increased, 4 hours after the overhead passage. The thickness of the layer around 16 km is seen increased. At the same time the layer at 18 km is thicker than the other observed layers. No layers are present between 13 and 15 km. But very thin layers are seen in between 11 and 13 km (fig 5.4b). The presence of such layers may be due to convective activity.

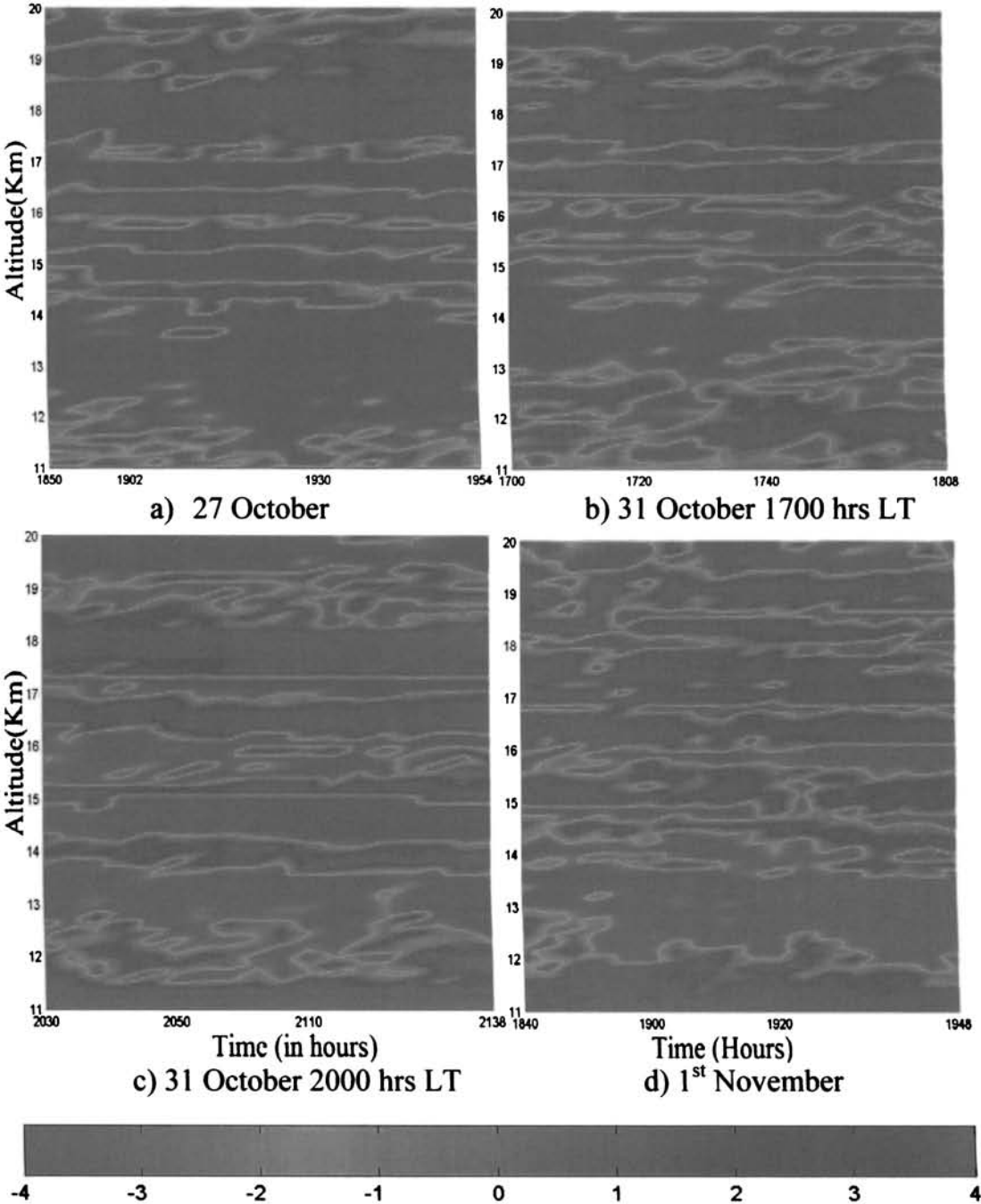


Figure 5.4 a-d. RTI Plots of Signal to Noise Ratio (SNR)

Eight hours after the overhead passage, distinct layers are present nearly at all altitudes from 11 to 20 km. In figure 5.4c, we can find very thick layer around 18 km. Well marked layers are noted around 14, 15 and 17 km. One day after the storm passage, high reflectivity layers are distinct in the upper troposphere and lower stratosphere. From 12 to 15 km the SNR values are very weak (fig.5.4 d).

Before the passage of the storm, there were no distinct layers present below the tropopause. But on the day of overhead passage, a well-marked layer is seen below the tropopause. One day after the passage, this layer is seen weakening again. These observations suggest that a severe weather system was present over the station on 31<sup>st</sup> October 1994, which can be due to the effect of the cyclone passage.

### ***5.3.1b Determination of tropopause from received echo power***

Figure 5.5 a-d show the height of the tropopause from the radar data determined from the model profiles derived from received echo power (as explained in section 5.2.1) before, during and one day after the passage of the cyclone. The data is averaged for 1 hour. Before the passage of the storm, the tropopause is located at 15.4 km (fig 5.5a). Four hours after the overhead passage, the tropopause is situated nearly at 15.1 km (fig 5.5b). After 4 hours, the tropopause is found to be lowered to 14.1 km (see fig 5.5c). On 1<sup>st</sup> November, one day after the passage of the cyclone, the tropopause returned to 16.4 km as seen in figure 5.5d.

### ***5.3.1c Tropopause variations from model profiles***

Tropopause height variations derived from model profiles at every 4-minute interval for 1 hour duration, during, 4 hours, 8 hours and 21 hours after the passage of the storm, respectively are shown in figures 5.6a-d.

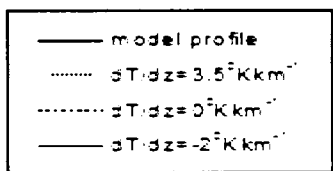
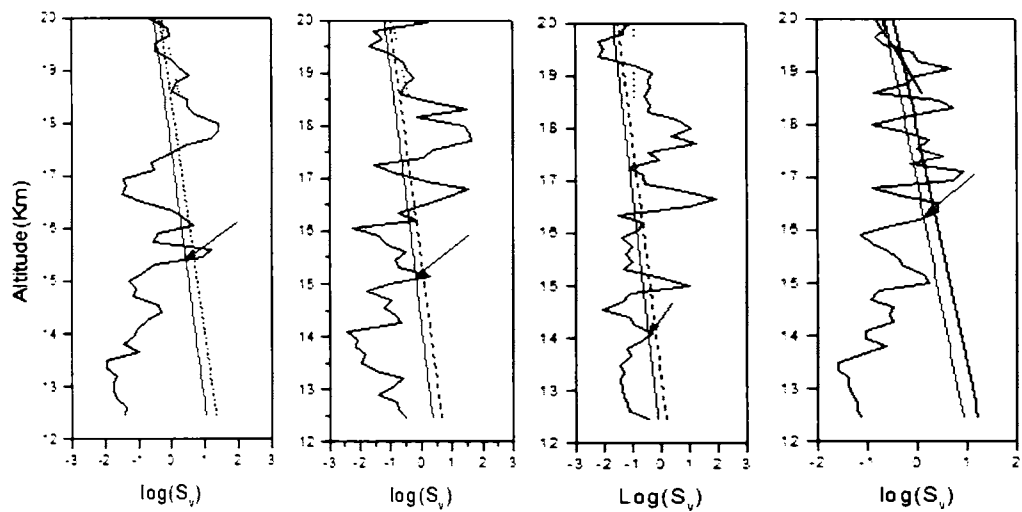
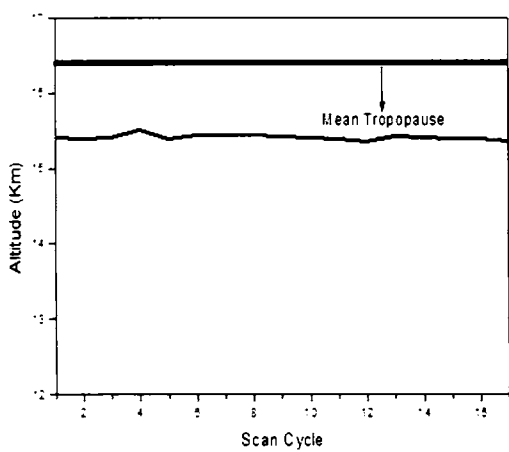
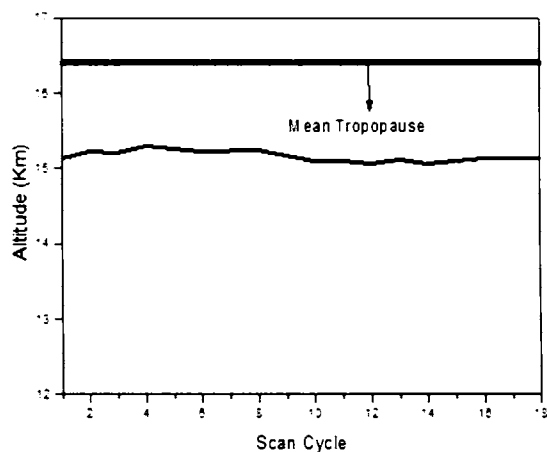


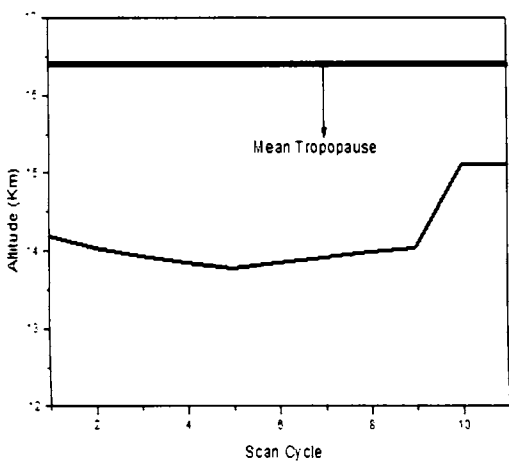
Figure 5.5a-d. Tropopause determination from model profile (using received echo power) on a) 27<sup>th</sup> October, b) 31<sup>st</sup> October at 1700 hrs LT, c) 31<sup>st</sup> October 2000 hrs LT and d) 1<sup>st</sup> November



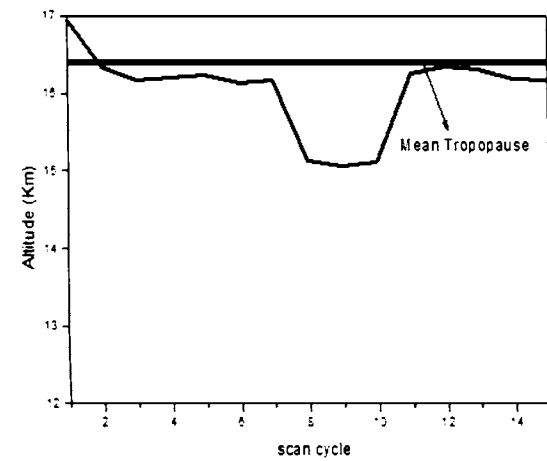
a) 27 October



b) 31 October 1700 hrs LT



c) 31 October 2025 hrs LT



d) 01 November

Figure 5.6. Tropopause height derived from model profile



From figure 5.6a & b it can be noted that the tropopause is seen around 15.3 km, which is 1 km lower than the climatological mean tropopause height. The tropopause remains nearly stationary upto 4 hours after the overhead passage. Eight hours after the storm passage, we can see that the tropopause is lowered and is observed between 13.5 and 14 km (fig 5.6 c). One day after the passage of the storm, it is observed that the tropopause swings back to 16 km which is nearly the same as the climatological mean value (see fig 5.6 d).

It can be deduced that as the cyclone passes over the station, the tropopause has lowered first and then raised. As there is no data during the exact overhead passage (passage of the cyclone centre) the tropopause height at the exact time of overhead passage could not be identified. But when the periphery of the cyclone is over the radar site, it can be noted that the tropopause is lowered. This is in accordance with the observations of *Koteswaram* (1967). After the passage of the storm the tropopause raises to its mean position. Continuous observations may expect to show the exact variations in the tropopause height associated with tropical cyclone passage.

### **5.3.2. Tropopause observation during the nearby cyclone passage**

Satellite pictures received from EUMETSAT during 2001 October cyclone is shown in figure 5.7. The satellite pictures are at the interval of one hour from 0000 hrs LT to 1400 hrs LT on 16<sup>th</sup> October. The deep depression centred near 13.5°N, 82.0°E at 1430 hrs LT on 15<sup>th</sup> October 2001, intensified into a cyclonic storm at 1730 hrs LT on the same day centred near 14.0°N, 81.5°E. Moving west-northward, it crossed the south Andhra coast near Gadanki in the morning of 16<sup>th</sup> October. From there, it moved slowly westward and weakened into a depression at 0230 hrs of 17<sup>th</sup> October 2001.

### *5.3.2a Determination of tropopause from SNR values*

Continuous observations were carried out during the storm passage in October 2001. This storm passed nearly overhead of the radar site. Figure 5.8a shows the RTI plot of SNR for 32 hours continuously from 15<sup>th</sup> October 0930 hrs LT (one day before the storm) to 16<sup>th</sup> October 1630 hrs LT (after the storm) at 1-hour interval. A sharp enhancement of SNR is seen at 16 km at 0930 hrs LT on the previous day, which is inferred as tropopause height. As time progresses the tropopause is seen shifting upwards. The tropopause is observed near 17 km in the early morning hours of 16<sup>th</sup> October 2001. High reflectivity layers are not present in the region from 11 to 16 km, till 0930 hrs LT on the day of cyclone passage. There are high reflectivity layers found above the tropopause region. At 0930 hrs LT on 16<sup>th</sup> October 2001 (which is just before the crossing of the cyclonic storm over the station), SNR enhancement is seen around 16 km. A very high reflectivity layer is observed below 15 km from 0930 hrs LT and disappears after 1330 hrs LT.

It can be inferred that the high reflectivity layer appears when the cyclone crossed near to the station. The cyclone was most near to the station around 0500 hrs LT. The raising of tropopause is observed when the cyclonic centre passed above the radar site and lowering of tropopause is noted when the radar site is in the periphery of the cyclone.

RTI plot of SNR for nearly 1 hour from 0450 hrs LT during the closest approach of the cyclonic storm at 4-minute interval based on special observations is illustrated in figure 5.8b. A well-distinguished layer of high reflectivity is noted around 17 km. Several thin patches of high reflectivity are also identified in the region between 11 and 16 km.

RTI plot of SNR for 2½ hours from 0930 hrs LT to 1200 hrs LT, soon after the passage of the storm at 4-minute interval, is illustrated in figure 5.8c. A broad layer of high reflectivity is found in between 11 and 15 km,

which is seen to be lowering as time elapses. This layer corresponds to the tropopause. The tropopause reaches its lowest limit around 1030 hrs LT. At this time, the periphery of the cyclone was passing over the station. After 1130 hrs LT (after the overhead passage of cyclone periphery) tropopause is seen to be rising again.

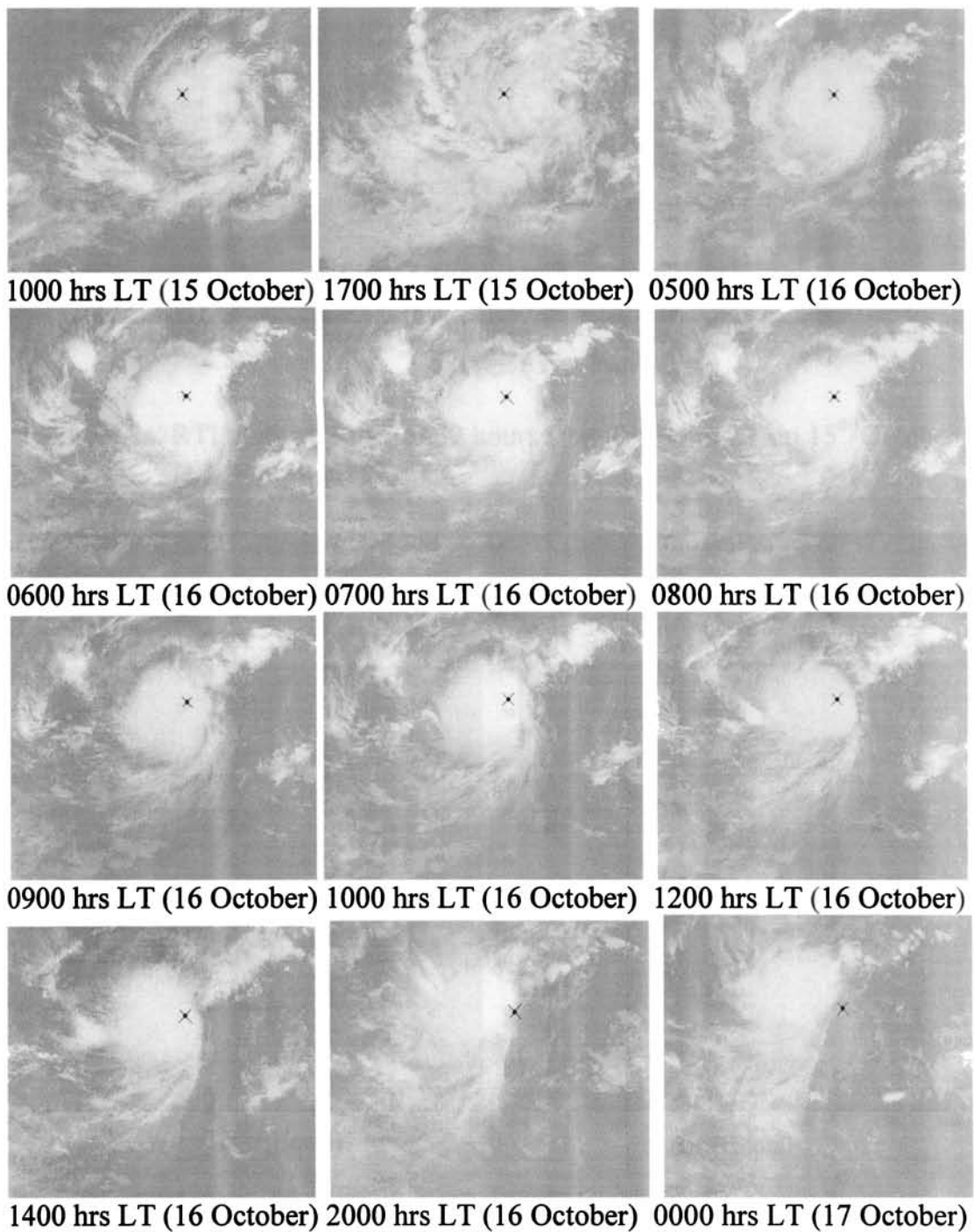


Figure 5.7. Satellite pictures of the cyclone during October 2001

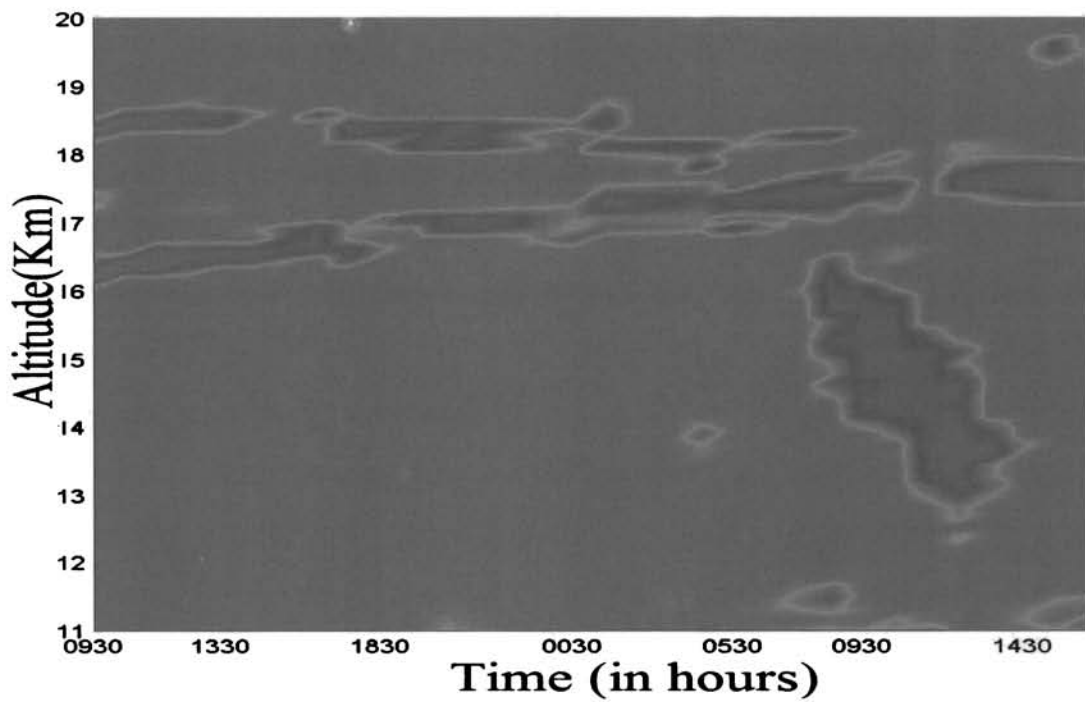


Figure 5.8a. RTI plots of SNR for 32 hours from 0930 hrs LT on 15<sup>th</sup> October at 1-hour interval

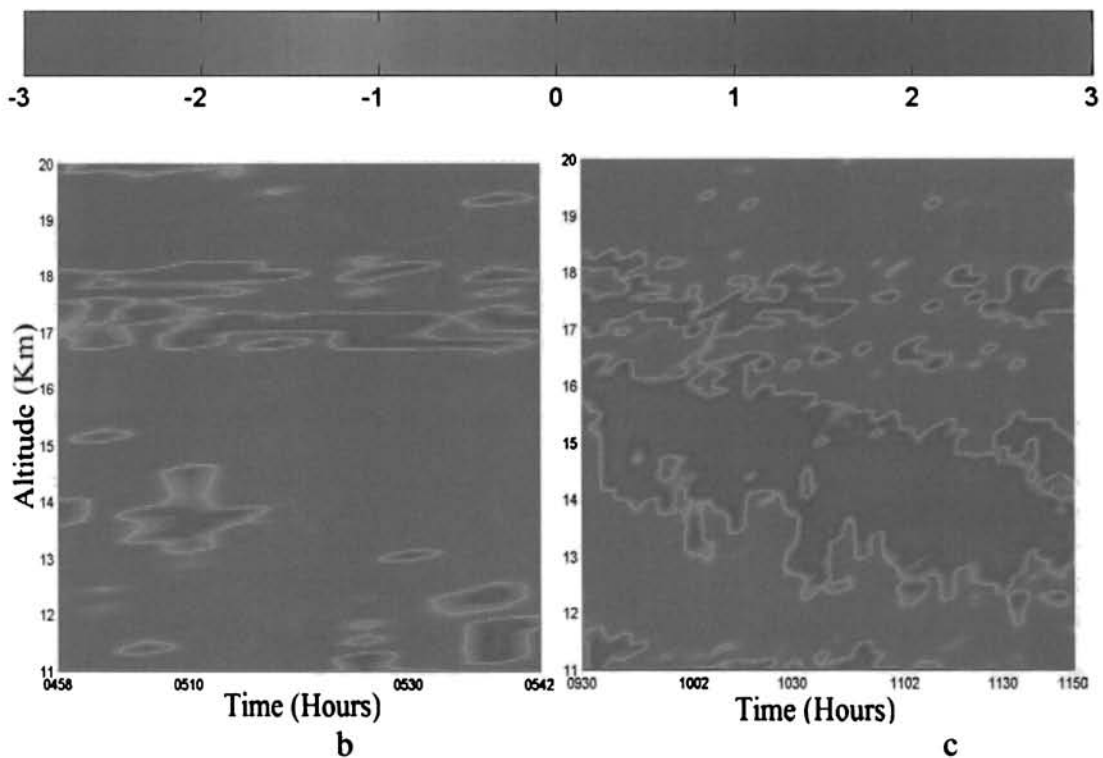


Figure 5.8b &c. RTI plots of SNR for 1 hour from 0450 hrs LT on 16<sup>th</sup> October and for 2 ½ hours from 0930 hrs LT on 16<sup>th</sup> October (at 4 minute-interval)

### ***5.3.2b Determination of tropopause from received echo power***

Figures 5.9 a-d show the height of the tropopause from the radar data determined from the model profile before, during and after the closest approach of the cyclone in 2001. From figure 5.9a, we can note the tropopause is at 16.2 km near to the climatological mean value, before the approach of the storm. At the time of nearest approach of the centre of the cyclone, the tropopause has raised a little and is around 16.8 km (fig 5.9b). Soon after the passage, the tropopause is noted to be around 14 km. At this time the periphery of the cyclone was passing over the radar site (see fig 5.9c). At 1630 hrs LT of the same day, as seen from figure 5.9d, the tropopause is seen to be rising again and is found to be near 17 km, which is well above the climatological mean tropopause.

### ***5.3.2c Tropopause variations from model profiles***

Figure 5.10a shows the tropopause derived from received echo power for 32 hours from 0930 hrs LT on 15<sup>th</sup> October to 1630 hrs LT on 16<sup>th</sup> October 2001. A day before the cyclone over the station, the tropopause shows only minor variations. The tropopause is observed to be around 16 km upto 1230 hrs LT, which slightly goes upto 16.3 km and remains there till sunset. When the cyclonic centre is near, the tropopause is seen shifting upwards. As the cyclone moves over the radar site the tropopause height decreases. A sudden drop in the tropopause height (about 4 km) is observed after the cyclone crosses over the station. The tropopause swings back to the normal position gradually and even overshoots the climatological mean height.

The height of the tropopause derived from received echo power at 4-minute interval for a period of nearly 1 hour during the time of closest approach of the cyclonic storm over the radar site is shown in figure 5.10b. It can be observed that the tropopause is above the climatological mean value. At this time the centre region (eye) of the cyclone is very close to the radar site. It

can be noted that the tropopause is fluctuating between 16.5 and 17 km. The tropopause observed at this time is slightly higher than that observed before the passage of the cyclone. The raising of the tropopause height is due to the passage of the core region of the cyclone above the station.

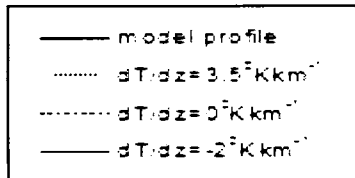
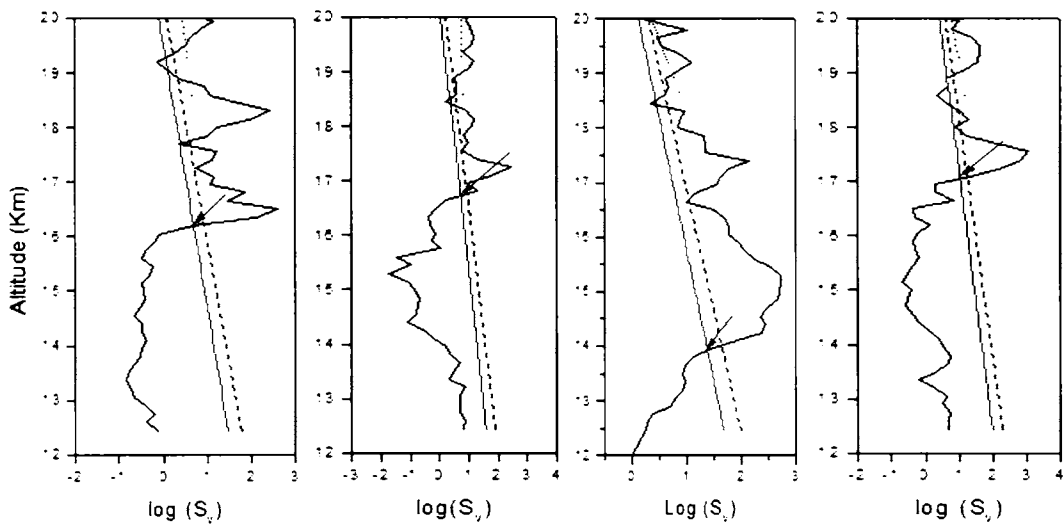


Figure 5.9a-d. Tropopause determination from model profile (using received echo power) on a) 15<sup>th</sup> October 1730 hrs LT, b) 16<sup>th</sup> October at 0530 hrs LT, c) 16<sup>th</sup> October 1030 hrs LT and d) 16<sup>th</sup>

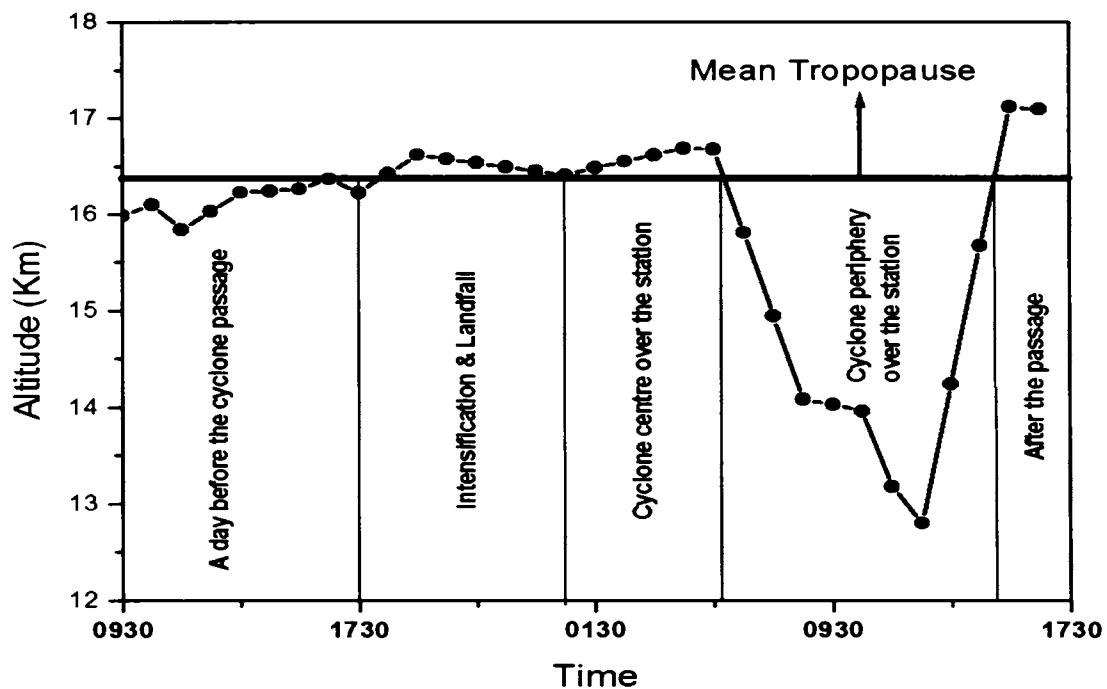


Figure 5.11 a. Tropopause height from received echo power at 1-hour interval

The height of the tropopause for 2½ hours at 4-minute interval, just after the nearest approach of the cyclonic storm over the radar site is shown in Figure 5.10c. The tropopause height fell suddenly to 14 km and is found to be fluctuating. Within two hours, it further drops down to the lowest position at 12.5 km. Afterwards tropopause height is found to be gradually increasing. The periphery of the cyclone was over the radar station for 1 - 2 hours, about 5 hours after the passage of the centre. The drop in the tropopause height can be attributed to the passage of the periphery of the cyclonic storm over the station.

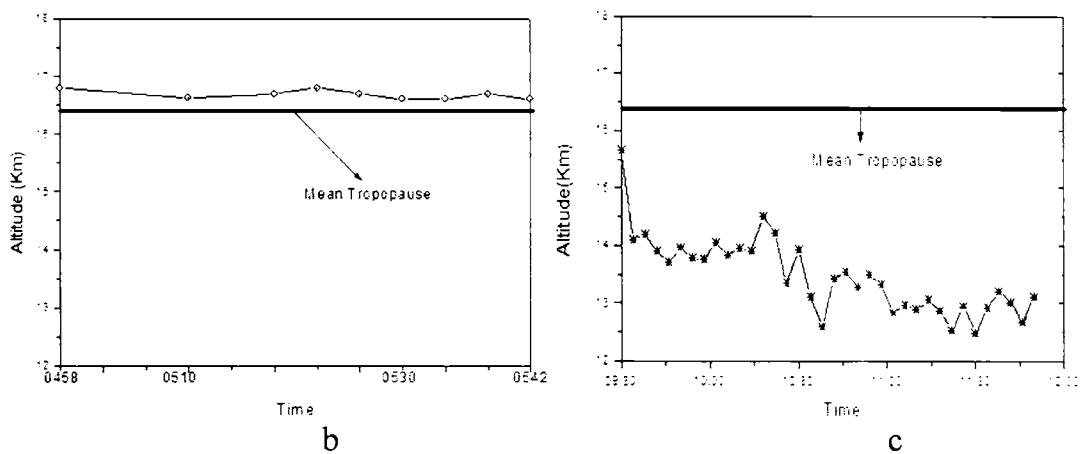


Figure 5.10b & c. Tropopause Height derived from received echo power during and just after the storm passage(At 4- minute Interval)

### 5.3.3. Tropopause observations when the cyclone is far away

A low pressure area was developed over the southeast bay on 22<sup>nd</sup> November 2002. Moving in a northerly direction it was centred at 1730 hrs LT of 23<sup>rd</sup> November near 12.0°N and 87.0°E and intensified into a deep depression in the early hours of 24<sup>th</sup> November 2002. It further intensified into a cyclonic storm over west central and adjoining southeast bay, centred near 13.0°N and 87.0°E at 0830 hrs LT on 24 November and near 14.5°N and 87.5°E at 1730 hrs LT. This cyclone was near to the radar site in the early morning hours of 24<sup>th</sup> November. In this case, only the spiral bands passed over the station. Satellite pictures received from EUMETSAT during this cyclone passage on 23<sup>rd</sup> and 24<sup>th</sup> November 2002 are shown in figure 5.11.

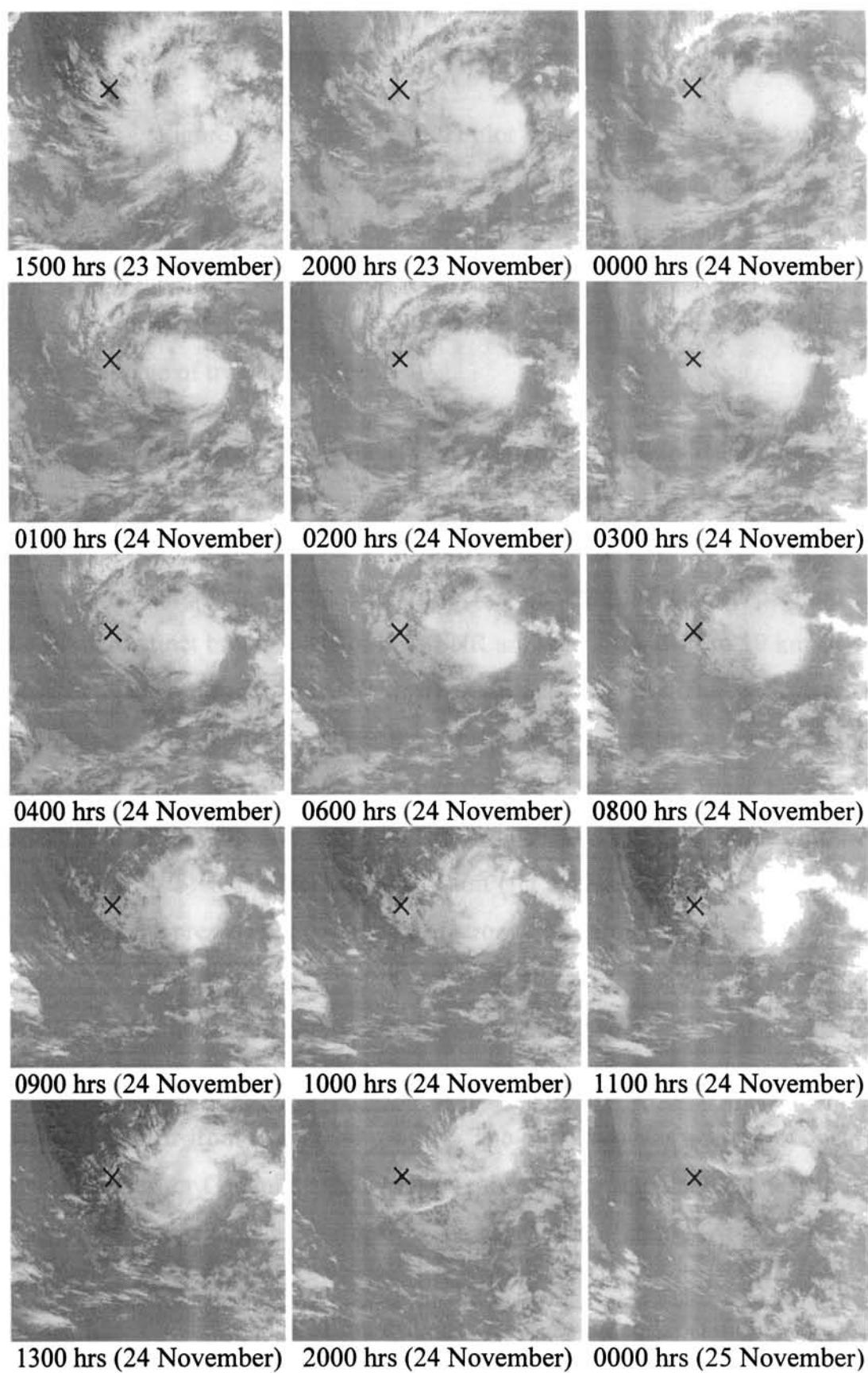


Figure 5.11. Satellite pictures during the cyclone passage (23-25 November'02)



### ***5.3.3a Determination of tropopause from SNR values***

Figure 5.12a shows the RTI plot for 29 hours associated with the far away passage of the storm. High reflectivity layers are present in the atmosphere for the entire 29 hours. Well-marked layers are noted in the upper troposphere and lower stratosphere. The layer at 14 km is more pronounced in the early morning hours of 24<sup>th</sup> November 2002. This coincides with the nearest passage of tropical cyclone.

High reflectivity layers between 16 and 18 km are seen as very distinct layers, before the passage of the storm. Layers of high reflectivity are noted around 14 km below the tropopause. These layers are very weak. Such layers are noted above 18 km also (fig 5.12b). During the nearest position of the storm, distinct broad layers of high SNR are seen around 17 to 19 km. Also weak layers are noted below 14 km (see fig 5.12 c & d). The layers above tropopause are much thicker than those observed during the cases mentioned above (see figs. 5.4 and 5.8). Just after the nearest passage, these layers are observed, but they became narrow. The layer at 14 km is seen vanishing. A layer of strong SNR is noted around 11 km (fig 5.12 e). An important feature observed is the presence of two layers of strong SNR around 12 and 14 km.

### ***5.3.3b Determination of tropopause from received echo power***

Figure 5.13a-f show the height of the tropopause from the radar data determined from the model profiles. The climatological mean tropopause for November for Gadanki is 16.6 km. The tropopause is at 16.2 km near to the climatological mean value before the passage of the storm. At the time of passage, we can note that the tropopause has lowered and is around 14.1 km. At this time the outer edge of the cyclone was over the radar station. After the passage of the storm, the tropopause is seen returning to the normal position.

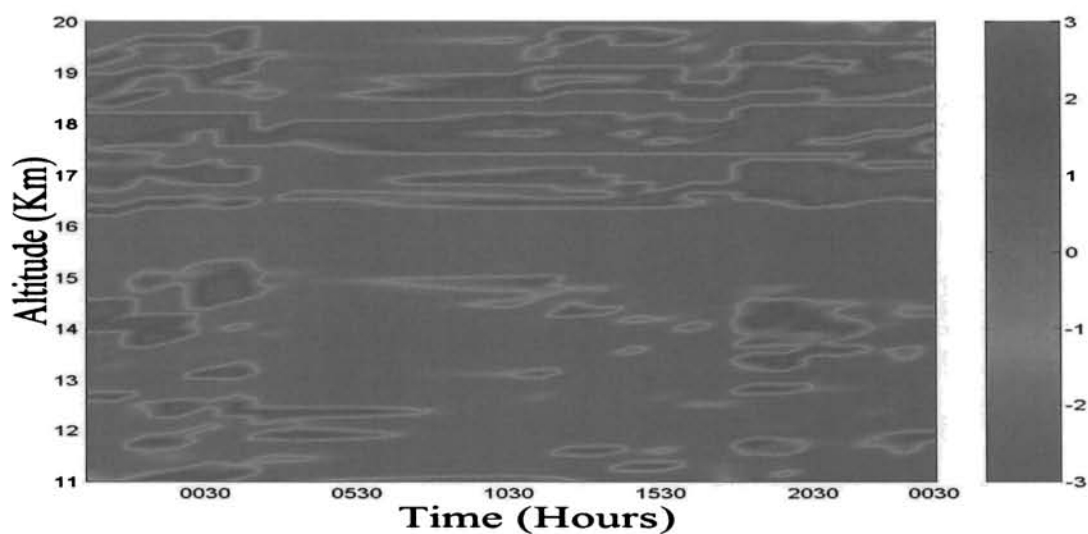
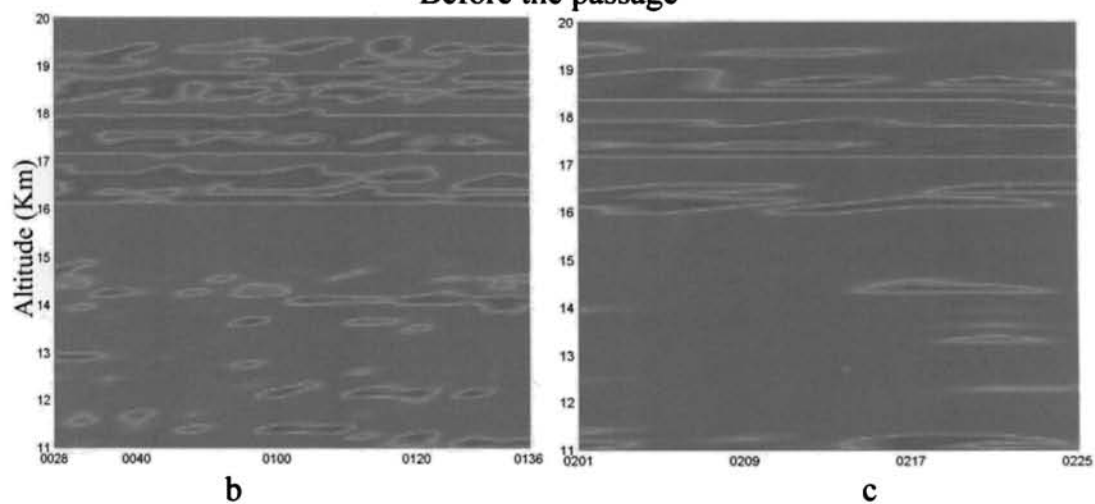


Figure 5.12a. RTI plot of SNR for 29 hours

Before the passage



After the Passage

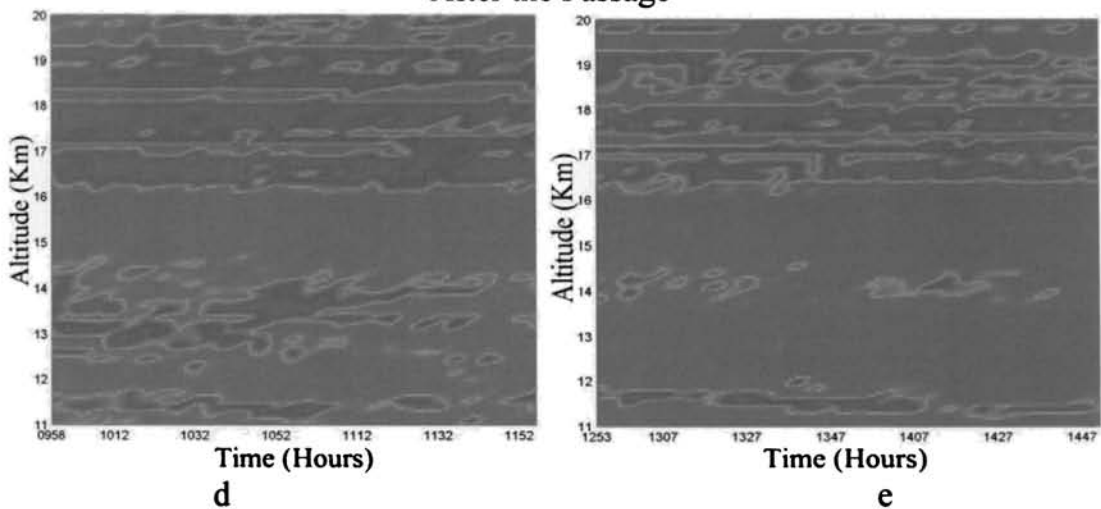
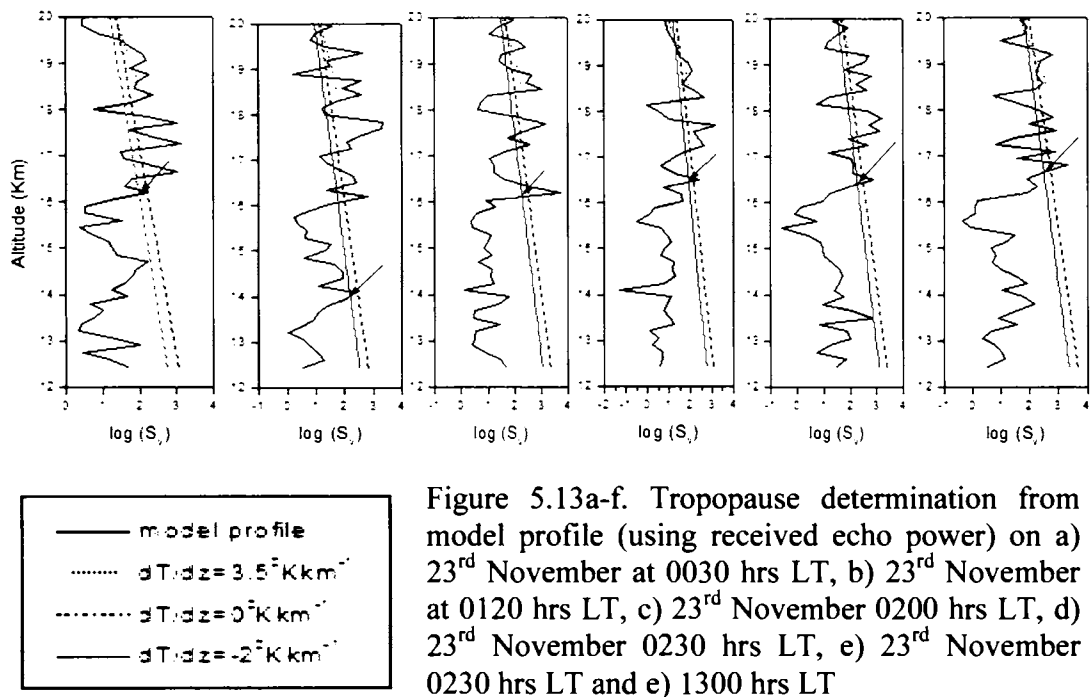


Figure 5.12b-5.12 e. RTI plots of SNR at 4 - minute interval at 0000 hrs LT, 0200 hrs LT, 1000 hrs LT and 1200 hrs LT



### 5.3.3c Tropopause variations from model profiles

Figure 5.14a is the tropopause height derived from received echo power for 29 hours from 2000 hrs LT on 23<sup>rd</sup> November. It can be noted that the tropopause which was around 16.7 km before the passage of the storm, lowers to 16 km during the passage. Afterwards, it returns to its normal position. Figure 5.14 b and c are the tropopause heights before the cyclone passage. A drop in tropopause height from 16.2 to 14 km is noted for nearly 20 minutes. Afterwards it is seen returning gradually to 16.5 km. Just after the passage of the storm, we can see that the tropopause is around 16.5 km, very near to the climatological mean tropopause (figs. 5.14 d&e).

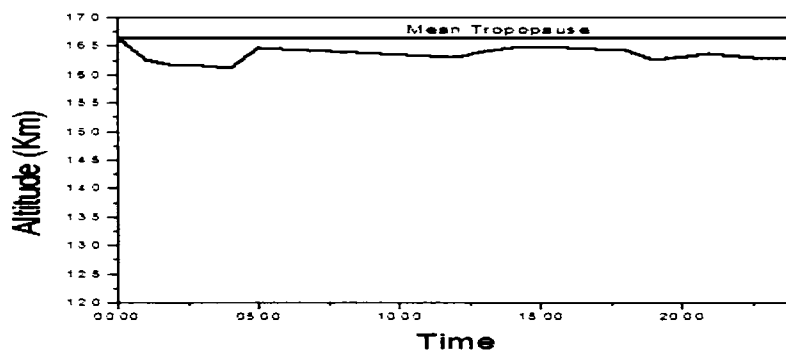


Figure 5.14a. Tropopause height for 29 hrs (23-25 November 2002)

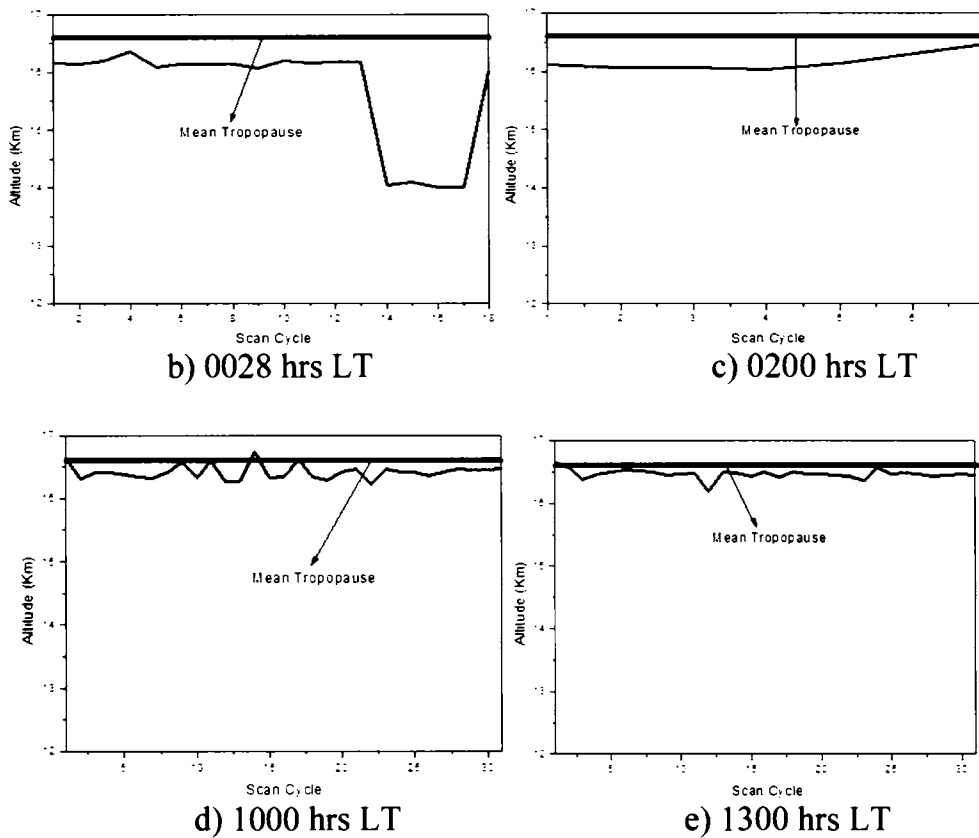


Figure 5.14 b-e. Tropopause height on 24<sup>th</sup> November

#### 5.4. Concluding Remarks

Layers of reflectivity and tropopause height variations are studied during the passage of various cyclones using the MST radar. The important factor observed in all the three cases considered for the study, is the appearance of high SNR layers below the tropopause in between 11 and 15 km, during and soon after the passage of tropical cyclones. The appearance of these layers greatly depends on the intensity and position of the cyclone with respect to the radar station. Rising of the tropopause is observed during the overhead or nearby passage of the centre of the tropical cyclones. Lowering of the tropopause is noted during the passage of periphery of the cyclone in all the three cases. The lowering of the tropopause is more evident during the nearby passage of the cyclone.

## Chapter #6

*Generation of Gravity Waves During  
Tropical Cyclones*

## 6.1. Introduction

Atmospheric gravity waves are thought to play an important role in the observed dynamical processes in the ionosphere, as well as in the middle and lower atmosphere. Ever since *Hines* (1960) first recognized the importance of gravity waves in the middle atmosphere, their influence on the large and small scale dynamics of the lower atmosphere has become increasingly apparent. Gravity waves play a very intriguing role in transporting momentum and energy right from the troposphere to upper atmosphere, which contribute to the shaping and structure of the atmospheric circulation (*Eliassen and Palm*, 1960; *Gossard*, 1962; *Bretherton*, 1969a; 1969b). The gravity wave drag effect on the large-scale flow is important for the dynamic coupling of the troposphere and stratosphere. Vertically propagating gravity waves are accompanied by a vertical flux of horizontal momentum with horizontal momentum transferred to the mean flow whenever the wave transient or experience attenuation (by means of dissipation, saturation, wave breaking, or absorption at a critical level). Momentum deposition by internal gravity waves in the middle and upper atmosphere provides significant forcing to the mean flow. Also, break down of gravity waves and resulting turbulence has shown that this mechanism is crucial in understanding the general circulation of the middle atmosphere (*Lindzen*, 1981; *Holton*, 1982; *Matsuno*, 1982). Three-dimensional general circulation models are, however, sensitive to the details of the geographical and temporal distribution of wave activity and so require a more detailed description of the gravity waves and their sources. To the present day, frontal systems, cyclones, convection, wind shear and topography have been thought to be the source of gravity wave activity in the troposphere. Especially, tropical cyclones are believed to be one of the major sources for the generation of gravity waves.

One of the important issues on gravity waves is the energy sources and generation mechanisms. Observational studies of gravity waves have been performed widely since 1950s. *Uccellini and Koch* (1987) reviewed the earlier studies using conventional tools and suggested that shearing instability and geostrophic adjustment in synoptic-scale wind systems are the possible source mechanisms. Due to limitations on resolution of the observational tools, however, the analyses have been restricted to gravity waves with comparatively large scales (horizontal wavelengths of tens to hundreds of kilometers). Recently advanced MST radars (VHF/UHF clear-air Doppler radars) provide wind velocities with fine time and height resolution, which enable us to investigate detailed structures of small-scale gravity waves in a wide range of frequency and vertical wave number spectra. With the aid of the MST radars, several kinds of gravity waves were detected and the relation to synoptic-scale atmospheric phenomena was discussed in some studies (e.g. *Hirota and Niki*, 1986; *Fukao et al.*, 1989; *Sato*, 1989).

Tropical cyclones are fascinating mesoscale energy sources of gravity waves. They have been examined in relation to gravity waves especially for the formation of spiral rainbands, which are conventionally explained to be a manifestation of internal gravity waves (e.g., *Yamamoto*, 1963; *Abdullah*, 1966; *Kurihara*, 1976; *Xu* 1983). Recent studies with aircraft observations (*Willoughby et al.*, 1984) and a three-dimensional numerical model (*Yamasaki*, 1986) show that not all features of the spiral bands are consistent with gravity waves, while some propagating bands are considered to be due to inertio-gravity waves. Gravity waves have various horizontal and vertical scales in a wide range. *Black* (1977, 1983) analyzed stereoscopic photographs from Skylab of a hurricane and detected small-scale structures like gravity waves with wavelength of 1.5-13 km on the periphery of a deep convective cloud around the tropopause. *Matsumoto and Okamura* (1985) detected a sharp pressure dip accompanied with a typhoon using data from a dense network of surface meteorological observations and a Doppler radar

around the Kanto District in Japan, and showed that the structure of the pressure dip is consistent with an internal gravity wave. *Hung et al.* (1988) made wind observations by an MST radar located at Chung Li, Taiwan, for about one hour and detected some gravity waves. *Sato* (1993) studied small-scale gravity waves using MU radar during the passage of Typhoon Kelly.

In India, most of the gravity wave studies are theoretical in nature using atmospheric models. In this chapter the observation of gravity waves during the passage of different cyclones are studied using the MST radar located at Gadanki. This is the first study of cyclone induced gravity waves using Indian MST radar.

## 6.2. Theory of Atmospheric Gravity Waves

Various forces act upon the actual atmosphere. It ranges from the molecular interactions (giving rise to viscosity, diffusivity etc.) to the forces due to pressure and temperature gradients, gravity and inertia. To study atmospheric gravity waves, however, it is convenient to consider an unbounded, non-rotating, non-ionized atmosphere without molecular viscosity and thermal conductivity (This assumption eliminates the dynamic processes like gyroscopic or inertial waves, viscosity waves and heat conduction waves resulting, respectively, from the Coriolis forces and the dissipative terms in equation of momentum and energy). Under these conditions the wave motions in the atmosphere is governed by the equation of motion or the Bernoulli's equation

$$\rho \frac{\partial \vec{U}}{\partial t} + \vec{\nabla} p - \rho \vec{g} = 0 \quad \text{--- 6.1}$$

The continuity or mass conservation equation

$$\frac{\partial \rho}{\partial t} + \vec{U} \cdot \vec{\nabla} \rho + \rho \vec{\nabla} \cdot \vec{U} = 0 \quad \text{--- 6.2}$$



where, 
$$\frac{d\rho}{dt} = \frac{\partial\rho}{\partial t} + \vec{U} \cdot \vec{\nabla} \rho$$

and the equation of adiabatic processes in the atmosphere

$$\frac{dp}{dt} = \frac{\gamma p}{\rho} \frac{d\rho}{dt}, \text{ which can be written as}$$

$$\frac{\partial p}{\partial t} + \vec{U} \cdot \vec{\nabla} p = \frac{\gamma p}{\rho} \left[ \frac{\partial \rho}{\partial t} + \vec{U} \cdot \vec{\nabla} \rho \right] \quad \text{--- 6.3}$$

where  $\rho$ ,  $p$  and  $\vec{U}$  are density, pressure and velocity of the fluid respectively.  $\gamma = c_p/c_v$  is the specific heat ratio. The linearised scalar equations governing the atmospheric oscillations under the assumption of two dimensional wave propagation are

$$\rho_0 \frac{\partial U_x}{\partial t} = -\frac{\partial p}{\partial x}, \quad \rho_0 \frac{\partial U_z}{\partial t} = -\rho g - \frac{\partial p}{\partial z} \quad \text{--- 6.4}$$

$$\frac{\partial p}{\partial t} + U_z \frac{d\rho_0}{dz} + \rho_0 \left( \frac{\partial U_x}{\partial x} + \frac{\partial U_z}{\partial z} \right) = 0 \quad \text{--- 6.5}$$

$$\frac{\partial p}{\partial t} + U_z \frac{d\rho_0}{dz} = C^2 \left( \frac{\partial p}{\partial x} + U_z \frac{\partial \rho_0}{\partial z} \right) \quad \text{--- 6.6}$$

Equations 6.4, 6.5, and 6.6 represent the most general perturbation equation for the waves in the atmosphere. The detailed theory for gravity waves is given by Hines (1960). The general solution to the wave equations 6.4-6.6 can be found in the complex Fourier form such that

$$\frac{p - p_0}{p_0 P} = \frac{\rho - \rho_0}{\rho_0 R} = \frac{U_x}{X} = \frac{U_z}{Z} = A e^{i(\omega t - K_x x - K_z z)} = \Phi \quad \text{--- 6.7}$$

where, P, R, X, Z are constants to be determined. A is a constant and  $\omega$  is the angular frequency of the wave;  $K_x$  and  $K_z$  are the corresponding constant complex wave numbers. Substituting the solution equation 6.7 for p,  $\rho$ ,  $U_x$  and  $U_z$  in terms of  $\Phi$  in equations 6.4-6.6, we get

$$\begin{aligned} \frac{C^2}{\gamma} K_x P + 0 \cdot R - \omega X + 0 \cdot Z &= 0 \\ \left(\frac{C^2}{\gamma} i K_x + g\right) P - g R + 0 \cdot X - i \omega Z &= 0 \\ i \omega P - \gamma i \omega R + 0 \cdot X + \frac{\gamma - 1}{H} Z &= 0 \\ 0 \cdot P - i \omega R + i K_x X + \left(i K_z + \frac{1}{H}\right) Z &= 0 \end{aligned}$$

These four sets of linear homogeneous equation will have a non-zero solution for P, R, X, Z only if the determinants of the coefficients are zero. This gives on expanding

$$\omega^4 - \omega^2 C^2 (K_x^2 + K_z^2) + (\gamma - 1) g^2 K_x^2 + i \gamma g \omega^2 K_z = 0 \quad \text{--- 6.8}$$

and the constants,  $P = \gamma \omega^2 K_z - i \omega^2 / H$ ,  $R = \omega^2 K_z + i(\gamma - 1) g K_x^2 - i \omega^2 / H$ ,  $X = C^2 \omega K_x K_z - i \omega g K_x$  and  $Z = \omega^3 - \omega C^2 K_x^2$  are called the polarization relations which determine the relative magnitudes and phases of the pressure and density variations and of the horizontal and vertical components of the atmospheric motion.

In the absence of gravity ( $g=0$ ) the dispersion relation 6.8 gives  $\omega^2 = C^2 (K_x^2 + K_z^2)$  which governs the sound waves with speed C and wave numbers  $K_x$  (horizontal) and  $K_z$  (vertical) propagating in an arbitrary direction making an angle  $\theta$  with the x-axis given by  $\theta = \tan^{-1} (K_x / K_z)$ . In the presence of gravity, however, equation 6.8 has no solution for which both  $K_x$  and  $K_z$  are purely real and non-zero. So we seek a solution for which  $K_x$  is real ( $= k_x$ , say) then  $K_z$  is either purely imaginary or else  $K_z = k_z + i/2H$ , where,  $H = C^2 / \gamma g$ .

Then the solution equation  $\Phi = Ae^{z/2H} e^{i(\omega t - k_x x - k_z z)}$  gives rise to the dispersion relation 6.8 as

$$\omega^4 - \omega^2 C^2 (k_x^2 + k_z^2) + (\gamma - 1)g^2 k_x^2 - \frac{\gamma^2 g^2}{4C^2} \omega^2 = 0 \quad \text{--- 6.9}$$

If we substitute  $\omega_a = \gamma g / 2C$  and  $\omega_b = (\gamma - 1)^{1/2} g / C$ , where,  $\omega_a$  is called acoustic resonance and  $\omega_b$  the buoyancy or Brunt- Vaisala resonance respectively. Then the dispersion relation gives

$$k_z^2 = \left(1 - \frac{\omega_a^2}{\omega^2}\right) \frac{\omega^2}{C^2} - k_x^2 \left(1 - \frac{\omega_b^2}{\omega^2}\right) \quad \text{--- 6.10}$$

It can be noticed that  $\omega_a > \omega_b$  since  $\gamma$  is always less than 2. Since  $k_x$  and  $k_z$  must both be real in a propagating wave, two distinct sequences of internal wave may occur. When  $\omega > \omega_a$  it is called acoustic range and when  $\omega < \omega_b$  it is called the gravity wave range. For  $\omega_b \leq \omega \leq \omega_a$ , the waves are evanescent and do not propagate. From equation 6.16, when  $\omega^2 \ll C^2 k_x^2$  thus removing the effect of compressibility, we get

$$k_z^2 = k_x^2 \left( \frac{\omega_b^2}{\omega^2} - 1 \right) \quad \text{--- 6.11}$$

which represents a pure gravity wave. As the waves can propagate only when both  $k_x$  and  $k_z$  are real and positive, requiring that  $\omega < \omega_b$ . The phase propagation of these waves is at an elevation angle  $\theta = \tan^{-1}(\lambda_x / \lambda_z) = \tan^{-1}(k_z / k_x)$ , which in this case is given by

$$\theta = \tan^{-1} \left( \frac{\omega_b^2}{\omega^2} - 1 \right)^{1/2} \quad \text{--- 6.18}$$

In an acoustic wave the speed is determined by properties of the propagation medium, and selecting a frequency fixes the wave length but not the direction of travel. In the gravity wave, however, the frequency fixes the propagation angle but neither the velocity nor the wavelength.

### **6.3. Experimental Approach**

Observations were made using 6 beams (East, West, North and South at 10° beam angle and Zx and Zy) and single beam with a pulse width of 16μs (coded) during tropical cyclone passage on various years. The observations were taken from 4 – 21 km with an altitude resolution of 150 m. Only single beam data is used for determining the tropopause and other layers. The exact overhead passage of a tropical cyclone over Gadanki had occurred in 1994. There were no continuous observations using MST radar during this cyclone period. Common mode data and other available data are used for the present study. During the nearby passage of the cyclone in October 2001, special observations were carried out by CUSAT team and therefore continuous data is available. In all other years considered here the data was before and after the cyclone passage.

### **6.4. Results and Discussion**

#### **6.4.1. Generation of gravity waves during overhead passage of a cyclone**

##### ***6.4.1a Disturbances in mean wind distribution***

To understand the influence of overhead passage of a cyclonic storm on the horizontal and vertical winds at various levels in the troposphere and lower stratosphere, mean height profiles of zonal, meridional and vertical winds are plotted as shown in figure 6.1 for three days before, during and one day after passage. The horizontal bars represent standard deviation.

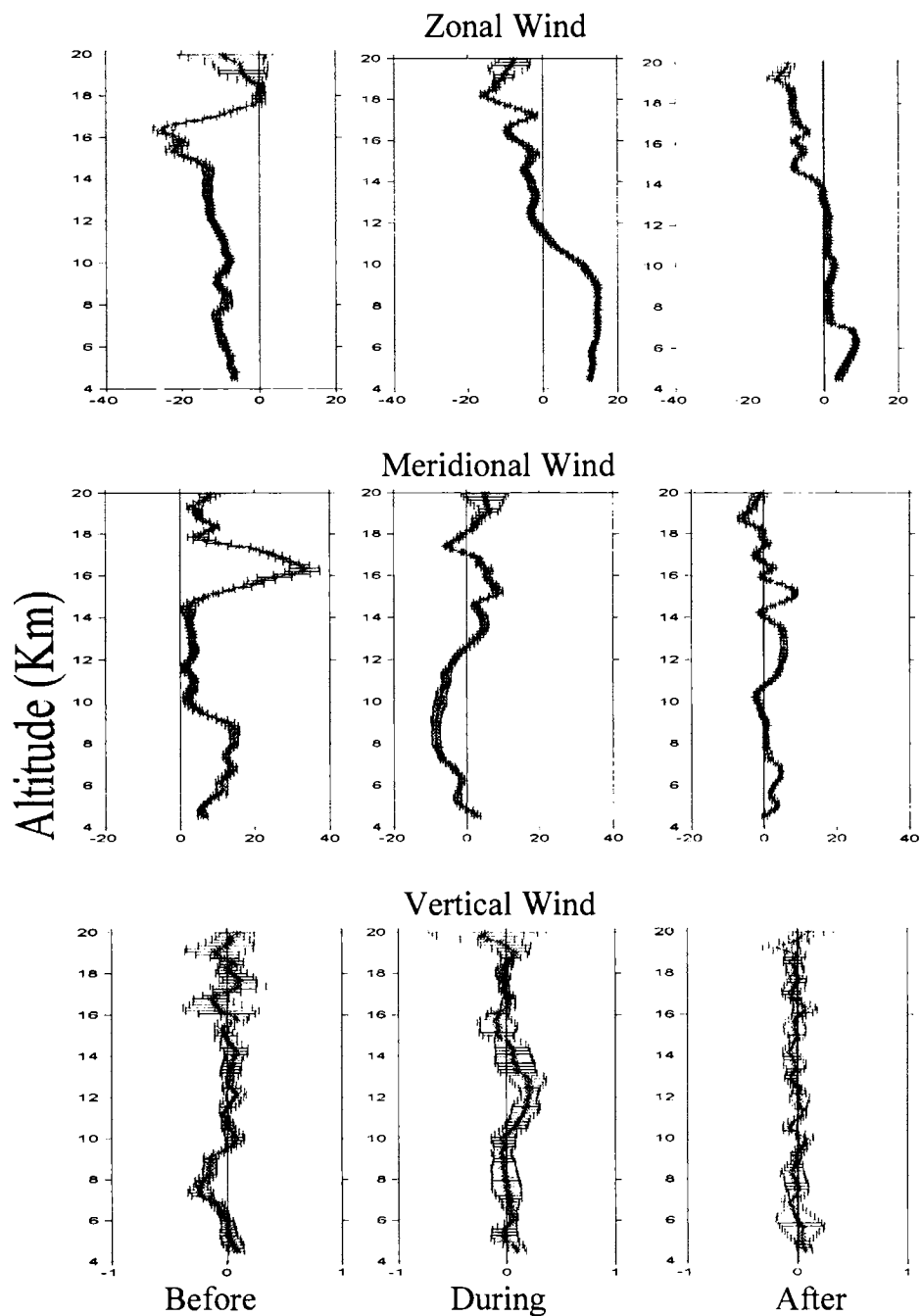


Figure 6.1. Mean height profiles of a) zonal, b) meridional and c) vertical wind.

From figure 6.1 a, it can be noted that zonal wind shows marked changes before and after the passage of the cyclonic storm. The important thing to be noted is the reversal of wind to westerly from easterly in the lower and middle troposphere. On 27<sup>th</sup> October, three days before the overhead passage of the cyclone, the easterly wind is noted in the atmosphere upto 20 km. Strong

easterlies with the strength of more than  $30 \text{ ms}^{-1}$  are noted around 16 km. On 31<sup>st</sup> October, just after the overhead passage of the cyclonic storm, it can be seen that the easterlies decrease in strength and reverses the direction to westerlies in the lower and middle troposphere upto 11 km. Above this altitude the winds are still easterly with lesser strength. It is interesting to note that the wind is very weak or no wind is present in the region between 7 and 14 km, one day after the passage of the cyclonic storm.

In the case of meridional wind, the reversal of wind is from southerly to northerly as the cyclone moves over the station. Before the approach of the cyclone, southerly wind persists from 4 to 20 km with the maximum wind speed of the order of  $40 \text{ ms}^{-1}$  at 16 km. Just after the passage of the cyclone, the wind changes in direction to northerly from 4 to 13 km and at 17 km. The strength of the winds is also decreased. One day after the passage of the cyclonic storm, the winds in the lower levels have returned to southerly, but with less speed.

The vertical wind does not show much variation (see figure 6.1c). On 27<sup>th</sup> October downward wind speed of the order of  $0.4 \text{ ms}^{-1}$  is noted around 8 km. On 31<sup>st</sup> October, wind is weak in the lower levels. Most part of the atmosphere from 4 to 22 km is dominated by upward winds. On 01<sup>st</sup> November the wind is weak in strength and variable in direction.

#### ***6.4.1b Detection of wave generation***

The waves generated in the atmosphere due to a cyclonic disturbance can be detected by plotting the winds with respect to time at different altitude levels. Time series of zonal wind on 3 days before, 4 hours, 8 hours and 21 hours after the storm passage are illustrated in figure 6. 2a - d respectively. In each case the observations were taken at 4 minute intervals for 18 cycles (72 minutes) continuously. Though the observation period is short,

the presence of waves can be clearly noted from these figures. Before the passage of the cyclonic storm, the waves can be seen in the lower stratosphere. On the day of passage of the cyclone, the waves can also be noted in the troposphere and wave features are more prominent 8 hours after the overhead passage (fig 6.2c). One day after the storm, the waves are confined to the lower stratosphere.

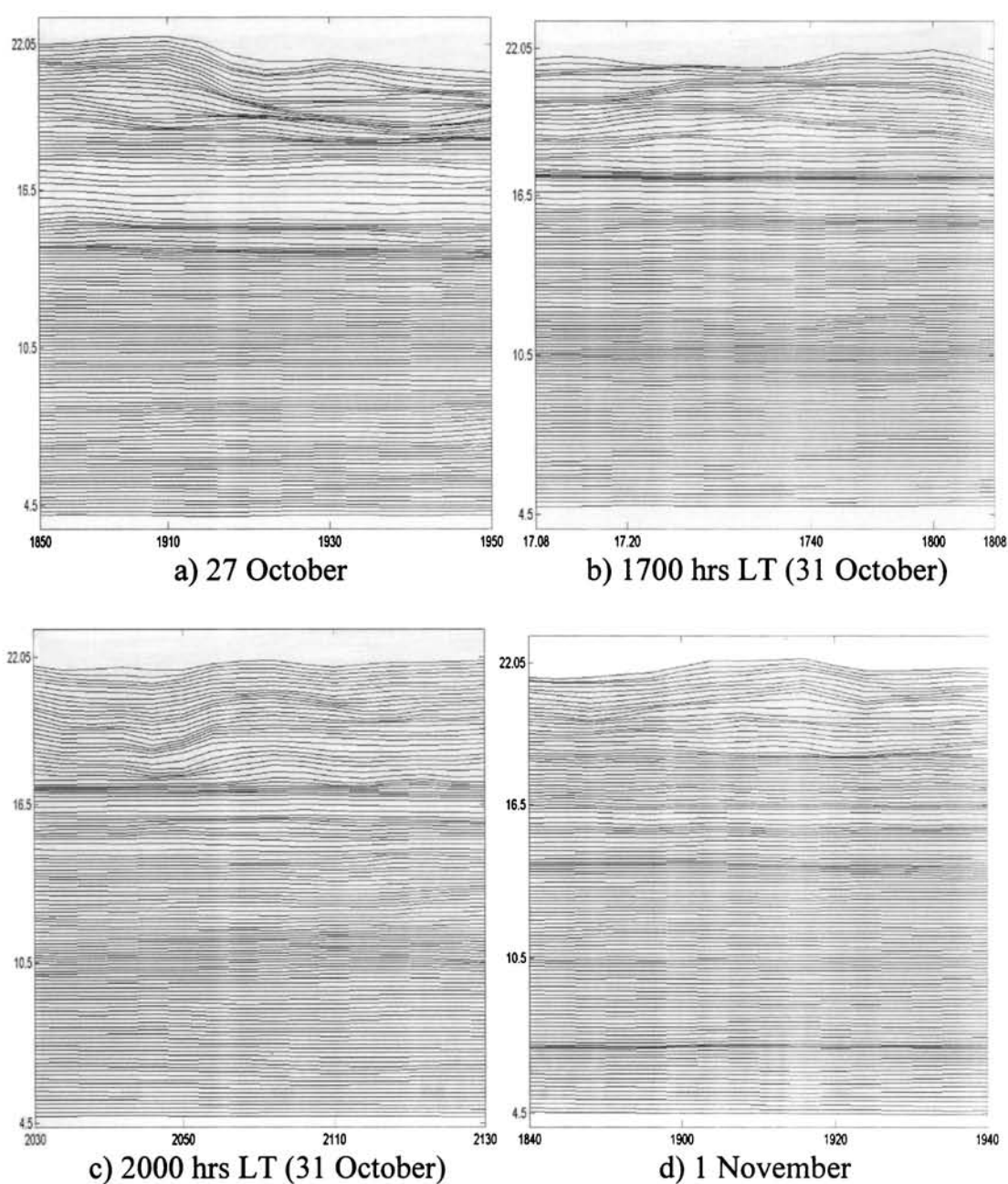


Figure 6.2. Time series of zonal wind with height

Time series of meridional wind 3 days prior, 4 hours, 8 hours and 1 day after the passage of the overhead passage of the storm is shown in figure 6.3a-d. Waves present in the lower stratosphere are more dominant. More wave features are noted before the passage of the storm. Figures 6.4a-d is the time series data of vertical wind in the troposphere and lower stratosphere. Waves are dominant in the lower stratosphere than in the troposphere.

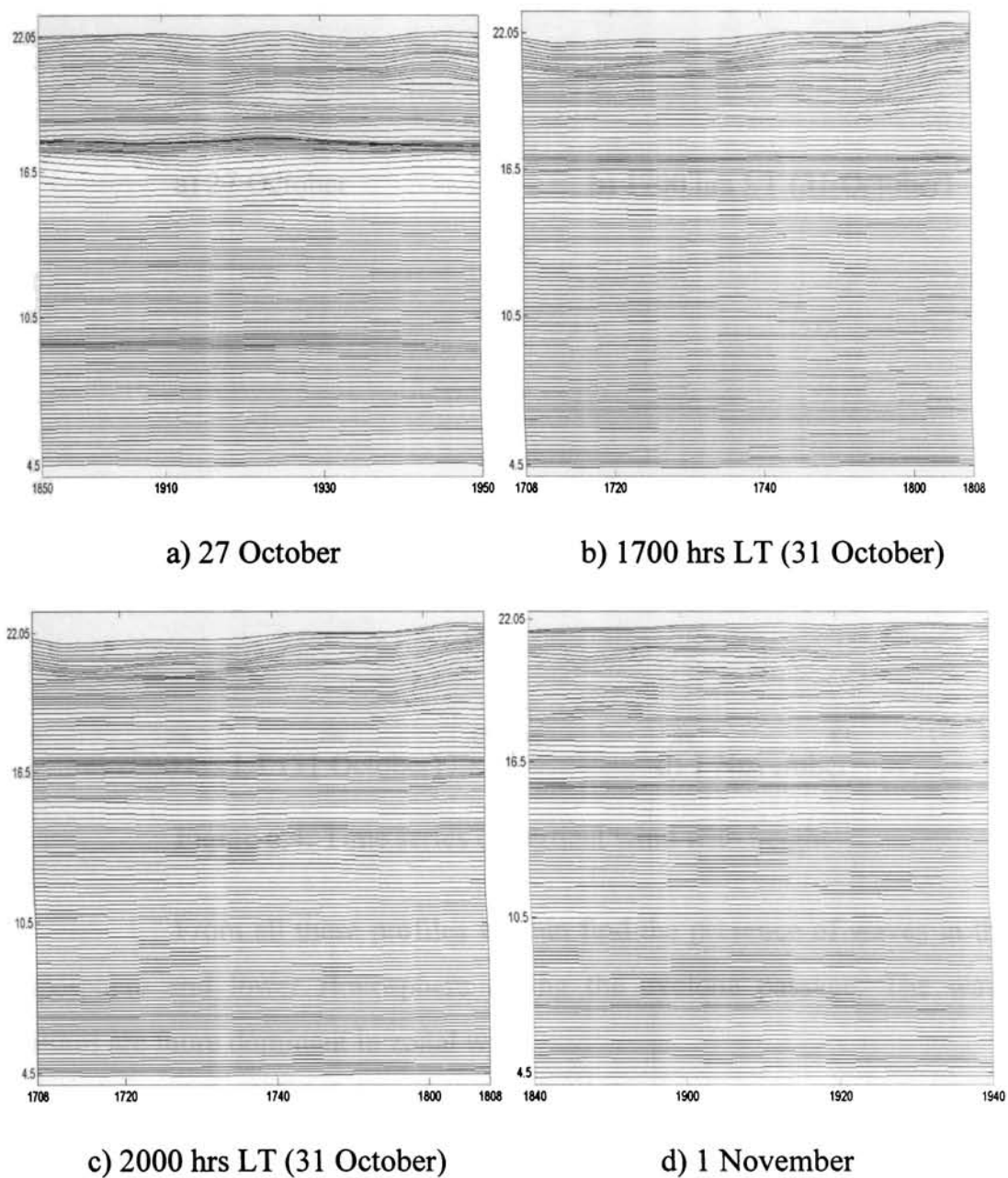


Figure 6.3. Time series of meridional wind with height during the storm in 1994



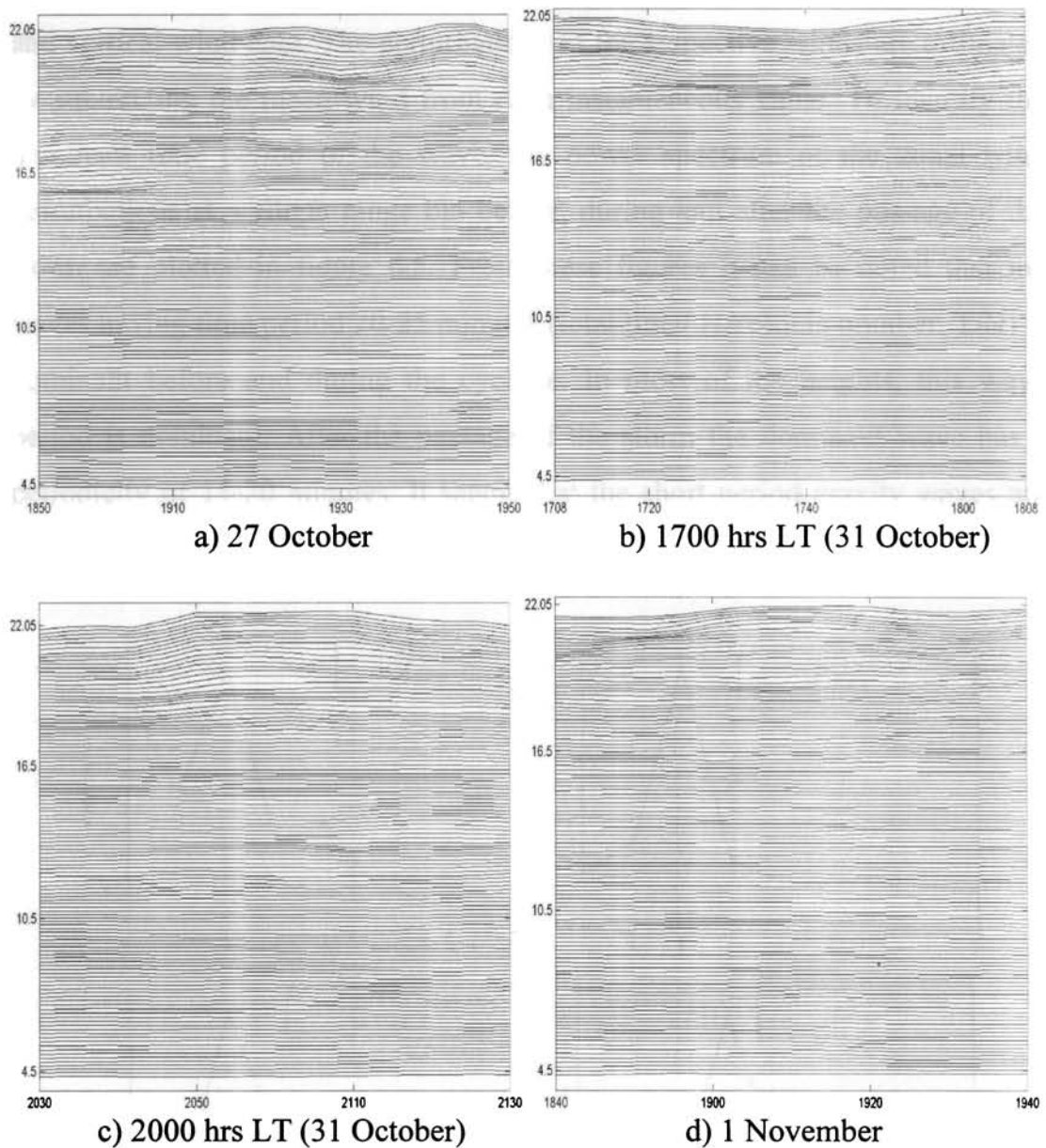


Figure 6.4. Time series of vertical wind with height

From all these profiles we can find the presence of waves in the troposphere and lower stratosphere during the cyclone passage. The wave features are more dominant in zonal wind.

#### **6.4.1c Determination of the periodicity of gravity waves**

Power spectra analysis has been performed on wind velocity components to detect the gravity waves generated during the passage of

cyclone. For that Fourier analysis has been carried out on the zonal, meridional and vertical wind data. The perturbations of the respective winds are estimated by subtracting the mean wind from each instantaneous value. To identify the dominant time period of the wave, the power spectrum of the zonal wind perturbations at a single range bin before, during and after the passage of the storm are plotted in figure 6.5. From these figures it can be noted that the waves having time period 20-25 minutes (total time/ Harmonic number, T/N) is dominant before and during the cyclone. In most of the heights, this wave period is dominant. After the passage of the storm the dominant wave has a periodicity of 15-20 minutes. It seems that the short period gravity waves are generated in the atmosphere during the overhead passage of a cyclonic storm.

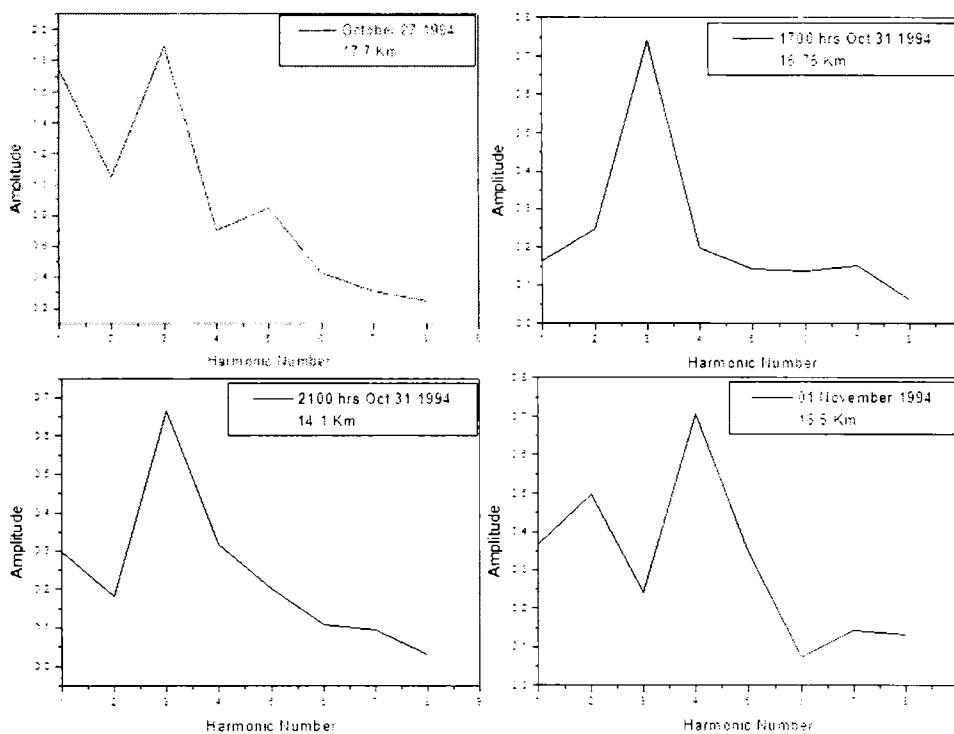


Figure 6.5. Power spectrum of zonal wind perturbations

#### 6.4.1d Characteristics of gravity waves generated due to storm passage

To estimate the direction of propagation of the gravity wave and vertical wavelength, hodograph analysis has been carried out. Figure 6.6 represents the hodographs for three days before, 4 hours, 8 hours and 21 hours

after the passage of the storm. In each case, two height regions are selected, one in the lower/middle troposphere and the other in the upper troposphere/lower stratosphere to find the source region of gravity waves. An ellipse is fitted to the data by least square method. From this the direction of propagation of wave can be understood. Figures 6.6a and b represents the hodographs for the two regions mentioned above, three days before the cyclone passage. It can be noted that the ellipse is rotating anticlockwise in the middle troposphere and clockwise in the stratosphere. If the ellipse is rotating in clockwise direction, the phase is propagating downwards and the energy is propagating upwards and *vice versa*. The source region of gravity waves is thus located between 10 and 17 km. From figures 6.6 a and b, it is evident that the direction of propagation of the wave in the troposphere is from southwest to northeast (SW-NE) and in the stratosphere, it is from west to east (W-E). The vertical wavelength of the observed oscillation is found to be around 1.35 km in the middle troposphere and around 0.75 km in the lower stratosphere.

Figure 6.6 c & d represent the hodographs 4 hours after the overhead passage of the cyclonic storm. Since the rotation of the ellipse is clockwise in both the lower and upper troposphere, the source region cannot be identified. The direction of propagation is noted from south to north in the lower/middle troposphere and southwest to northeast in the upper troposphere/lower stratosphere. The vertical wavelengths of the oscillations are noted to be 0.6 km and 0.9 km, respectively.

Figure 6.6 e and f shows the hodographs for 8 hours after the cyclone passage. The ellipse rotating in the anticlockwise direction in the lower troposphere and clockwise direction in the lower stratosphere, indicating that the source region is located around 10-12 km region. The direction of propagation is noted to be from southwest to northeast in upper troposphere. The vertical wavelengths of the observed oscillations are found to be around 0.75 km and 1.35 km in the lower and upper troposphere, respectively.

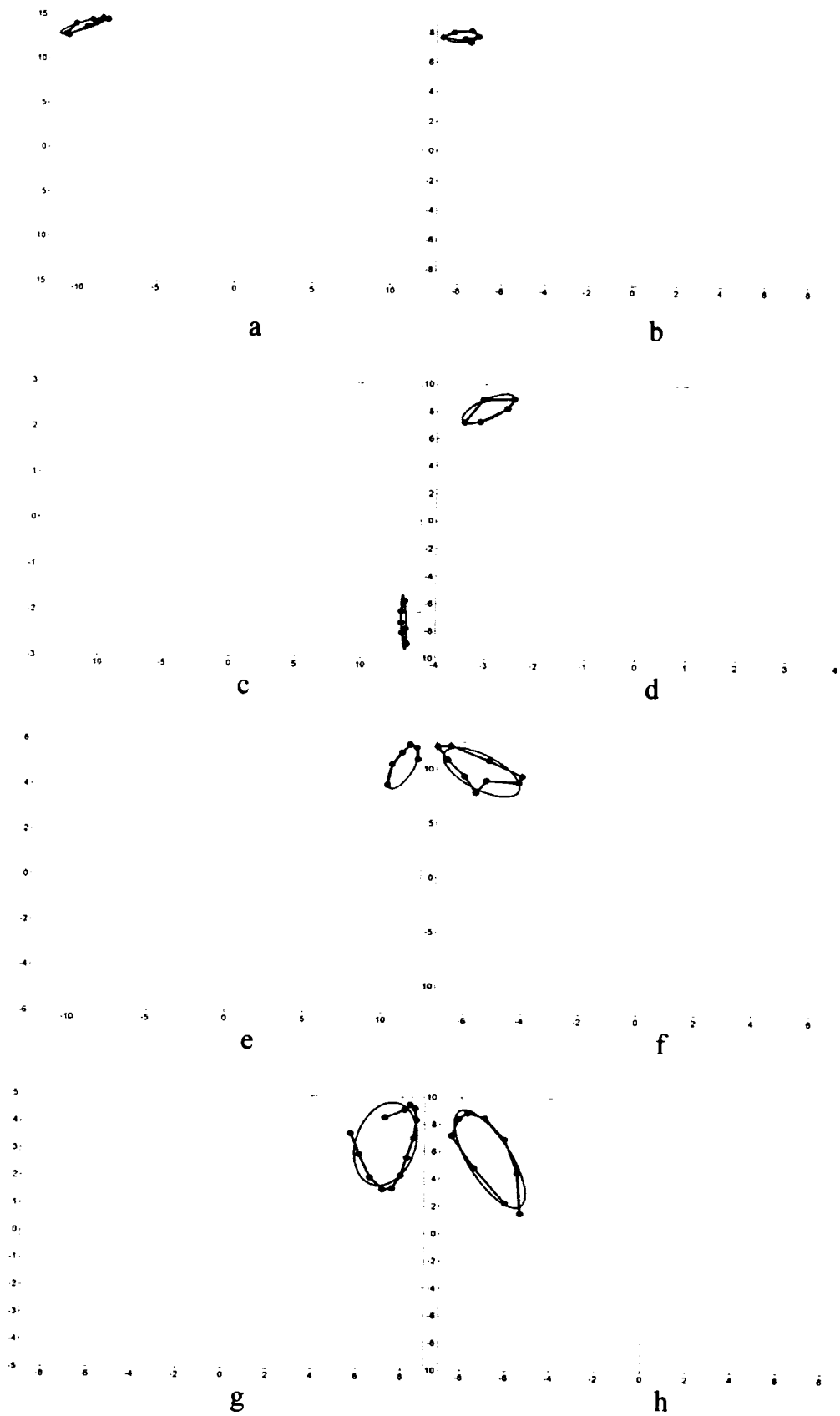


Figure 6.6. Hodograph Analysis before, on the day and after the overhead passage of the cyclonic storm (left panel –LT/MT, right panel – UT/LS)

On 1<sup>st</sup> November, 1994 the source region is located below that observed on the previous day, i.e., the day of overhead passage of cyclone (see figure 6.6g and h). It can be noted that the ellipse is rotating anticlockwise in the lower/middle troposphere and clockwise in the upper troposphere/lower stratosphere. The vertical wavelengths are 1.8 km and 1.2 km respectively for the oscillations observed in these height regions. The direction of propagation is noted to be from southwest to northeast (SW-NE) in the lower troposphere and from southeast to northwest (SE-NW) in the upper troposphere.

#### **6.4.2. Generation of gravity waves during the nearby cyclone passage**

In October 2001 the cyclone formed in the Bay of Bengal during 14 –17 October passed overhead of the radar station on 16<sup>th</sup> October. Continuous special observations were taken during this cyclone.

##### ***6.4.2a Disturbances in mean wind distribution***

Figure 6.7a -c show the height profiles of mean zonal, meridional and vertical wind one day before, during and just after the nearest passage of the storm. One day before the passage of storm, the entire atmosphere from 4 to 22 km comprises of easterly wind with a maximum around 16 km. Just after the passage of the storm, the wind changes its direction to westerly in lower levels. The easterly wind with maximum strength is noted between 15 and 18 km.

One day before and during the passage of the storm, the meridional wind is northerly in the troposphere (see figure 6.7b). Just after the passage of the storm, reversal of wind direction is noted in the 6-12 km region. The wind speed decreases between 4 and 20 km at all altitudes except around 16 km. Very strong northerlies are observed around 16 km. In the lower regions the northerly wind gives way to southerly wind, while in the upper troposphere the southerly wind changes to northerly.

In the case of vertical wind, the wind is mostly upward one day prior the passage of the cyclonic storm. During the nearest passage of the cyclonic storm, decrease in wind strength is noted and at some altitudes the upward wind changes to downward. Strong downward wind is noted around 5 km. Soon after the passage of the cyclonic storm, strong downward wind is noted below 8 km and upward above.

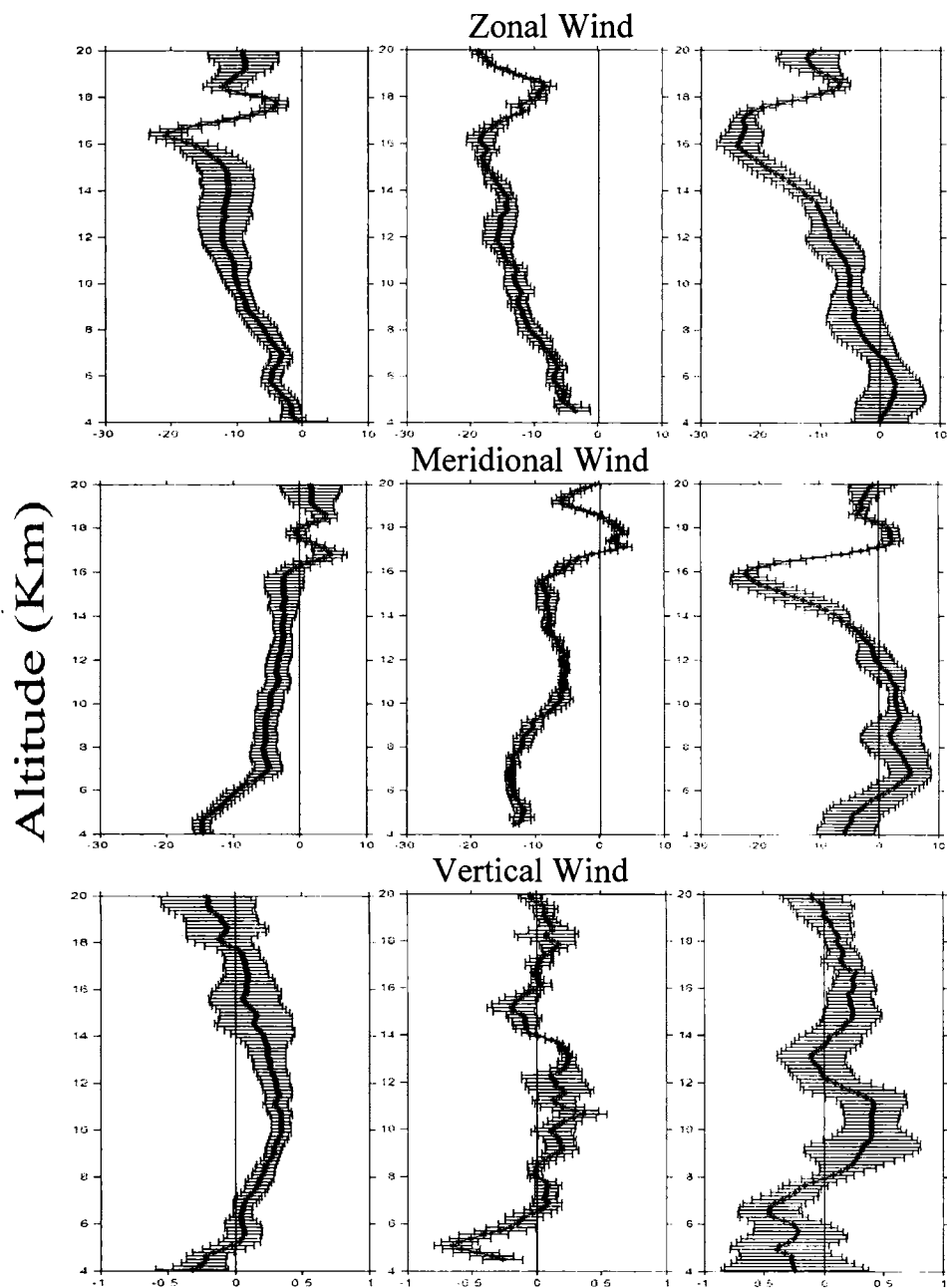


Figure 6.7. Vertical profiles of mean a) zonal, b) meridional and c) vertical wind

#### ***6.4.2b Detection of wave generation***

Figure 6.8 is the time series data of zonal, meridional and vertical winds in the troposphere and lower stratosphere associated with the nearby passage of tropical cyclone. Continuous observations were taken at 4 minute interval for 5 hours during the previous day and for 2 hours and 30 minutes during the time of the nearest passage of the storm. From the zonal wind time series, wave features are prominently seen in the lower stratosphere (fig. 6.8 a & b). On the day of the nearest passage of tropical cyclone, well defined oscillations are present in the troposphere. These oscillations are believed to be excited by the cyclone associated disturbances in the middle troposphere. Wave activity is also noted in the meridional wind (fig. 6.8 c & d).

It can be noted that on the previous day of nearest passage of the cyclone, the wave activity is dominant in the lower stratosphere, while on the day of cyclone passage, wave activity is more prominent in the troposphere. The time series plots of vertical wind show well -defined oscillations in the lower stratosphere. It can also be noted that the wave activity is more prominent in the lower stratosphere one day before the cyclone, whereas on the day of cyclone, the wave activity is present in both troposphere and lower stratosphere.

#### ***6.4.2c Determination of the periodicity of gravity waves***

These time series data of zonal, meridional and vertical winds are subjected to power spectrum analysis to further investigate the wave activity associated with the passage of the cyclone over the radar site. The time series of the wind components during the nearby passage of the cyclone are not included as they are of short duration. The data presented here is that of the wind components before and just after the nearest passage of the cyclonic storm.

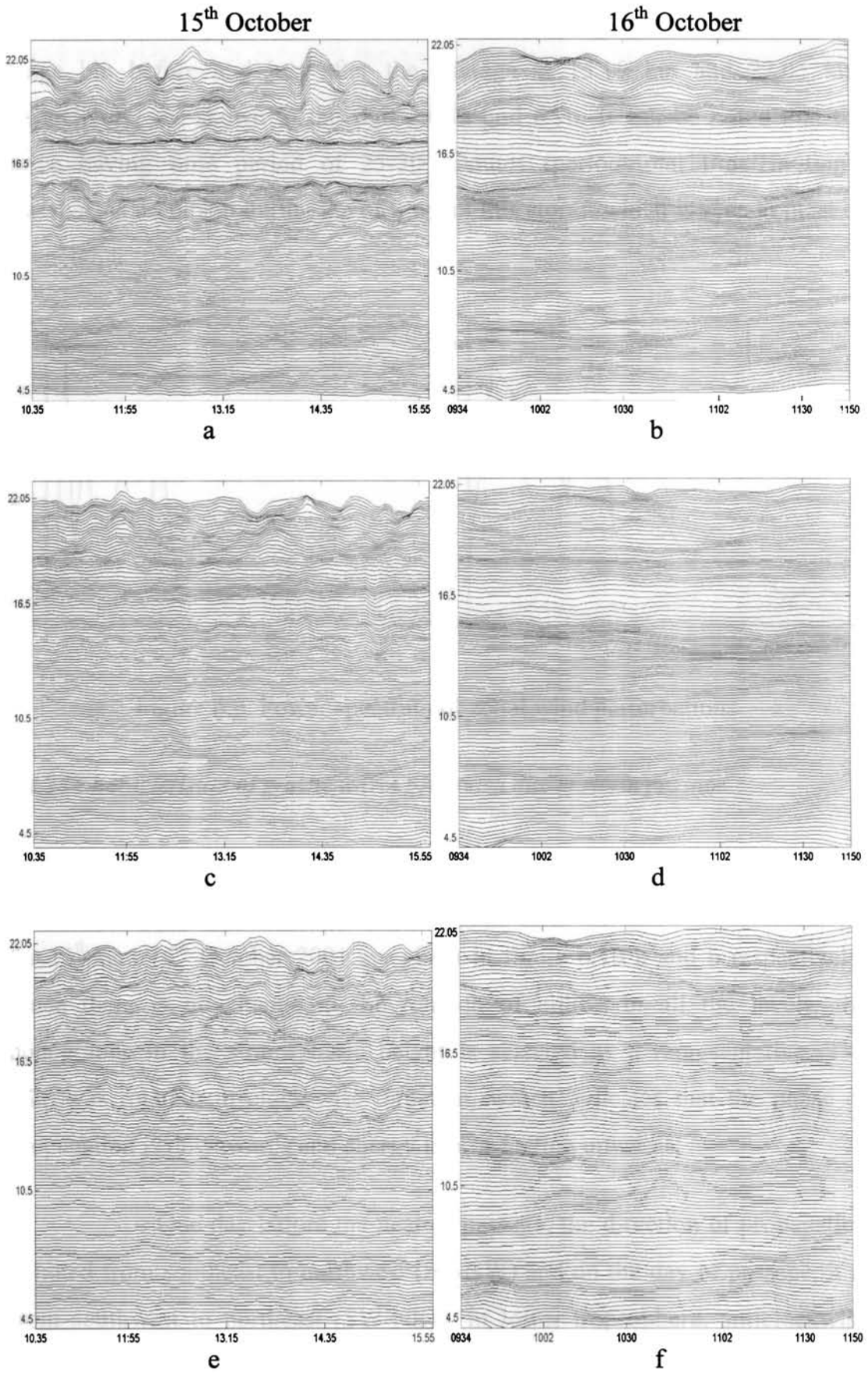


Figure 6.8. Time series with height of zonal, meridional and vertical wind



The power spectrum of the zonal wind perturbations at a single range bin before and just after the passage at 15.15 km and 22.05 km, respectively, are shown in the figure 6.9a and 6.9b. It can be noted that the wave having time period of 25-30 minutes (period=total time/Harmonic Number) is dominant during the passage of this storm, which is seen at most of the heights.

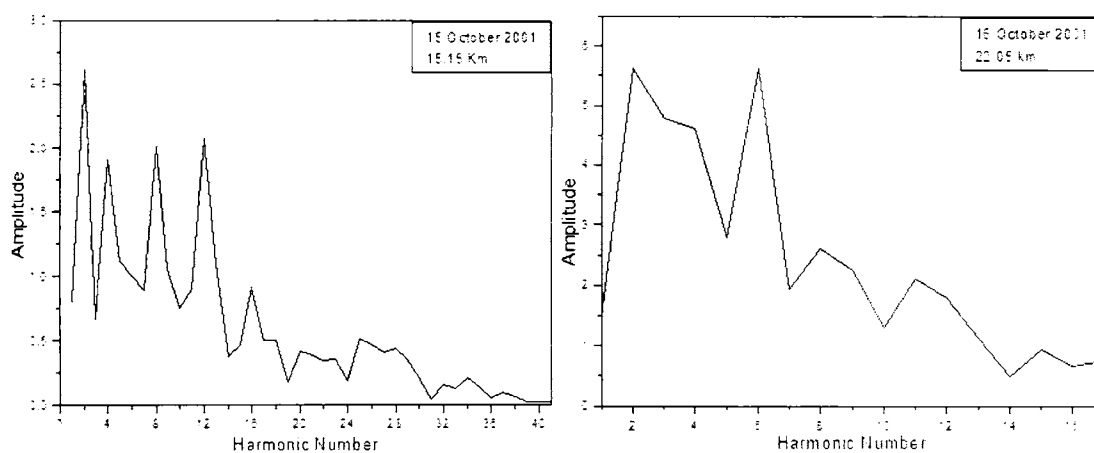


Figure 6.9. Power spectrum of zonal wind perturbations

#### 6.4.2d Characteristics of gravity waves generated due to storm passage

To estimate the direction of propagation of the gravity wave and vertical wavelength, hodograph analysis has been carried out. The hodograph for 15<sup>th</sup> and 16<sup>th</sup> October 2001 are given in figure 6.10 a and b respectively. Since there is no change in the rotation of ellipse in all the levels, the hodographs in the stratospheric height is selected as a representative. The ellipse is rotating in clock-wise direction, which indicates that the phase of propagation is downwards and energy is propagating upwards.

One day before the nearest passage, the direction of propagation is noted from southeast to northwest (SE-NW) and on the day of passage, it is from southwest to northeast (SW-NE). In lower troposphere, anticlockwise rotation is noted on 15<sup>th</sup> October suggesting that the source region of gravity waves is somewhere in the middle troposphere. But on 16<sup>th</sup> October only

clockwise rotation is noted in the entire troposphere and lower stratosphere. The vertical wavelength of the observed oscillation is noted to be  $\sim 1.35$  km on previous day, whereas it is  $\sim 3.45$  km on the day of nearest passage.

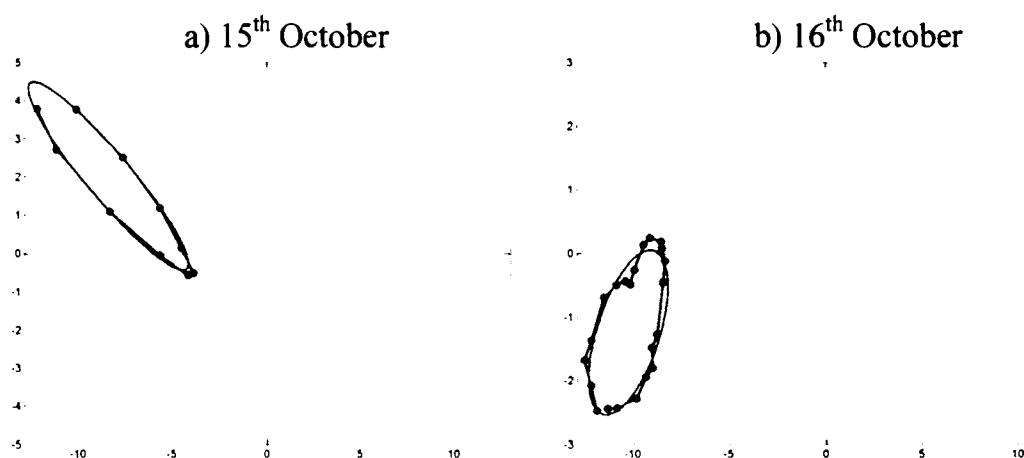


Figure 6.10. Hodograph Analysis

### 6.4.3. Wave observations during far away passage

Several observations were taken associated with the far away passage of tropical cyclone developed in Bay of Bengal on 23<sup>rd</sup> November, 2002. The cyclonic storm was most nearer to the radar site in the early morning hours of 24<sup>th</sup> November. The results of the observed waves during the passage of the cyclone are described as follows.

#### 6.4.3a Disturbances in the mean wind distribution

Figures 6.11-c show the mean height profiles of horizontal and vertical wind before, during and after the passage of the storm. From figure 6.11a, it can be noted that the wind is easterly at all altitudes from 4 to 20 km, with a peak around 14 km before the passage of the storm. As the cyclone passes by, considerable changes in the zonal wind were not observed, except the strengthening of wind around 6 km and 14 km. Just after the nearest passage of the storm, reversal of wind is observed between 7 and 11 km. The easterly wind at 14 km becomes very strong after the passage of the cyclone.

The meridional wind is southerly from 4 to 22 km except in the region from 4 to 6 km before the approach of the cyclone. After that a decreasing trend in windspeed is noted in the lower and middle troposphere. Soon after the passage of the cyclonic storm northerly winds in the lower region extend upward. The vertical wind does not show much variation throughout the observation period. The winds are very weak. During the nearest passage of the cyclonic storm upward wind of the order of  $\sim 0.5 \text{ ms}^{-2}$  is noted around 14 km.

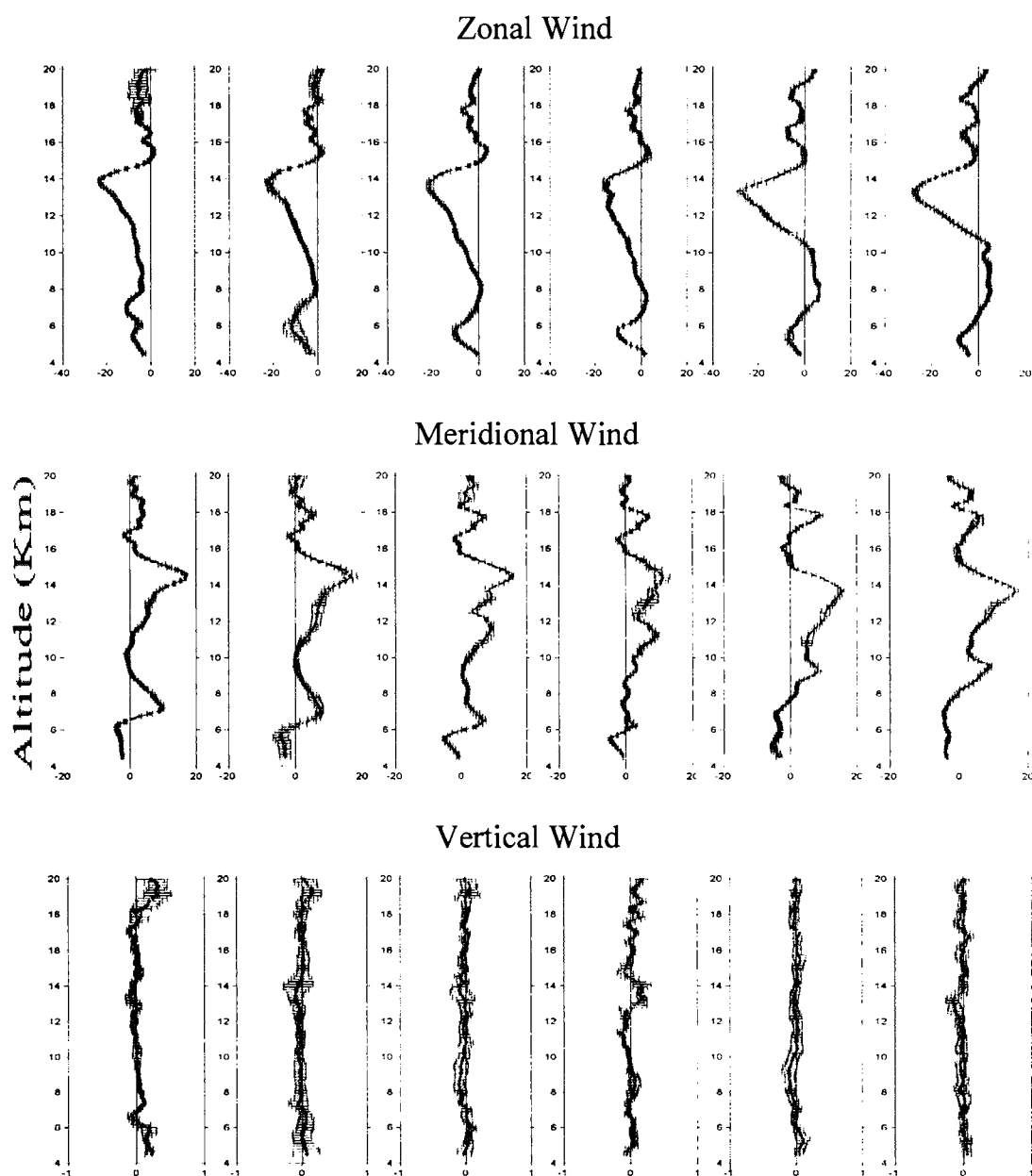


Figure 6.11. Mean height profiles of zonal, meridional and vertical wind

### 6.4.3b Detection of wave generation

Figures 6.12 are the time series data of wind components in the troposphere and lower stratosphere, before (on 23<sup>rd</sup> November) and just after (24<sup>th</sup> November) the passage of the cyclonic storm. Wave features can be detected before the passage of the storm in the troposphere and lower stratosphere. The waves become weak after the passage of the storm. Wave features present in meridional wind are similar to that in the zonal wind (figure 6.12c and d). But lower stratospheric waves in meridional wind can be more easily identified than the tropospheric waves. The wave features are also prominent in the vertical wind (See figure 6.12e and f). Before the cyclone passage waves can be identified at all altitude regions from 4 to 22 km.

### 6.4.3c Determination of the periodicity of gravity waves

The power spectra of the zonal wind perturbations at a single range bin (in upper tropospheric/lower stratospheric heights) were taken and they are plotted in figure 6.13 a-d. From these figures it can be noted that the wave having time period of 15-20 minutes is dominant before and after the storm passage.

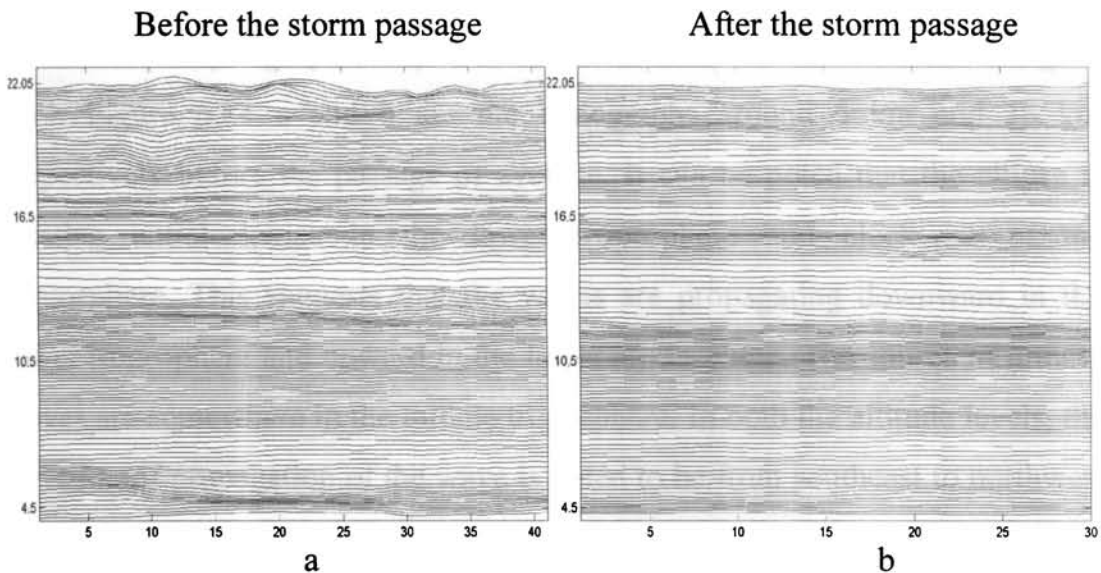


Figure 6.12. Time series of zonal wind with height

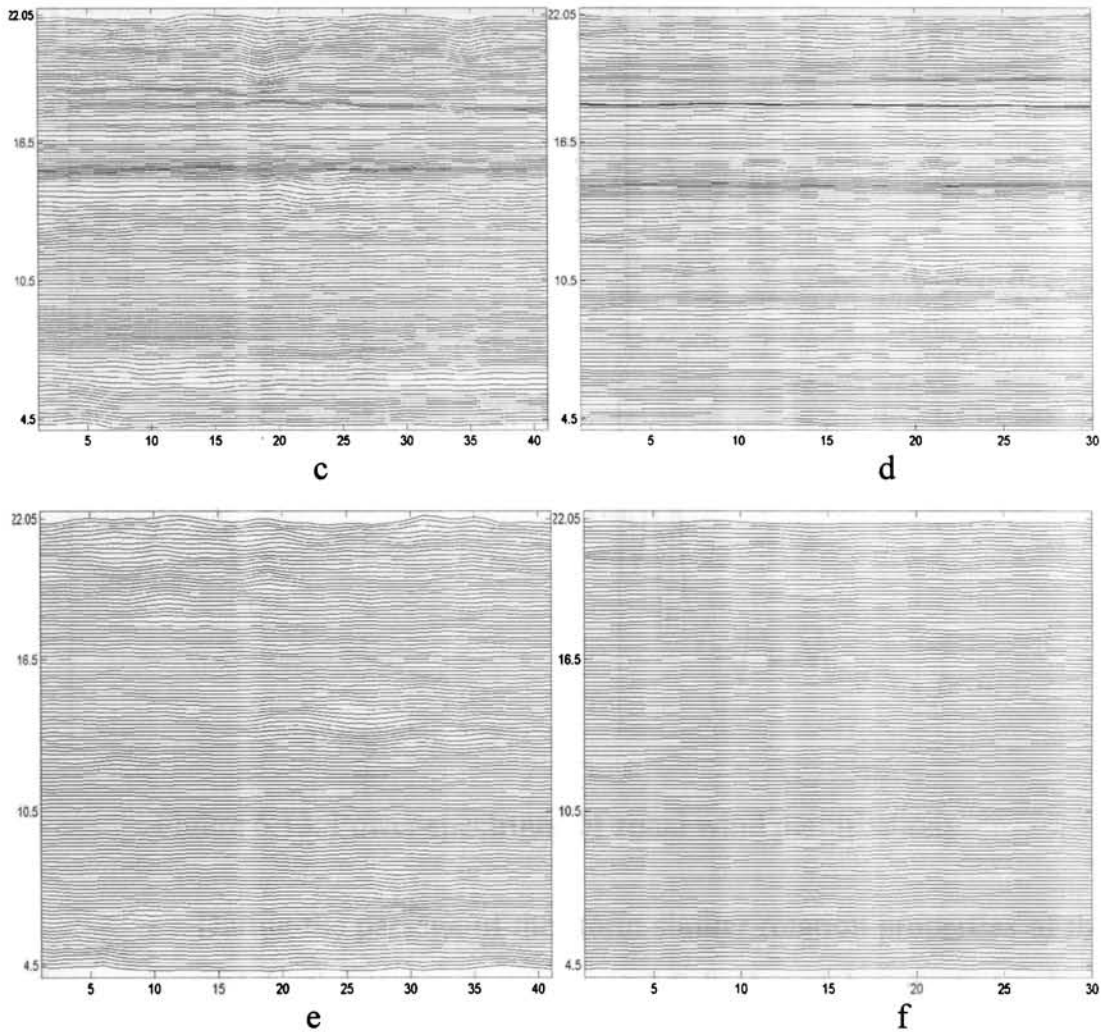


Figure 6.12. Time series with height of meridional (c&d) & vertical wind (e&f)

#### **6.4.3d Characteristics of gravity waves generated due to storm passage**

Hodograph analysis has been carried out and is shown in figure 6.14. Figure 6.14 a and b are the hodographs around 6 km and 18 km respectively before the passage of cyclone. It can be noted that the ellipse is rotating anticlockwise in the lower troposphere and clockwise in the stratosphere. This suggests that the waves are propagating downward in the lower troposphere and upward in the lower stratosphere. The source of gravity waves are somewhere in the middle troposphere. In both the altitude levels, the direction of propagation of the wave is noted to be from southeast to northwest (SE-NW). The vertical wavelength of the oscillations is noted to be 0.8 km and 0.6 km respectively.

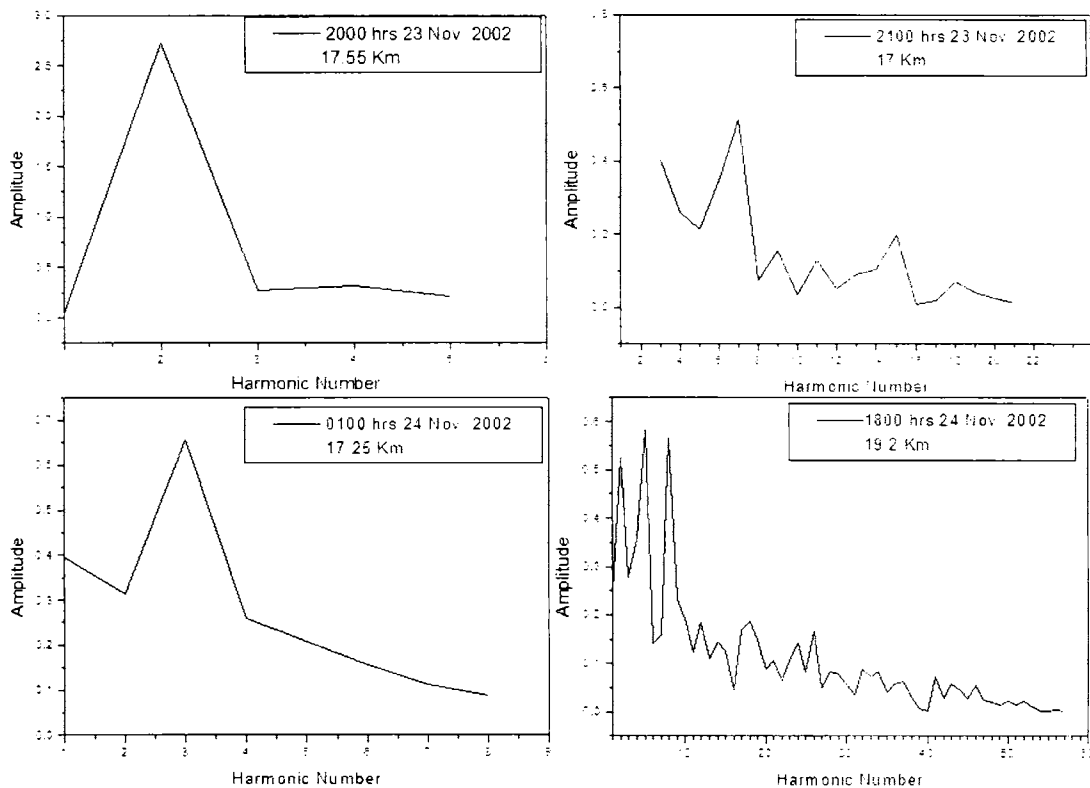


Figure 6.13. Power spectra of zonal wind perturbations

During the passage of the storm similar rotation properties of the ellipse are noted in the troposphere (around 8 km) and lower stratosphere (around 18 km) (figure 6.14 c and d). The source region is located in the upper troposphere. An important factor to be noted is the change in the direction of propagation in the lower levels. The waves are propagating from southwest to northeast (SW-NE) in the lower levels and from southeast to northwest (SE-NW) in the upper levels. The vertical wavelengths of the oscillations are similar to that observed on the previous day.

Figures 6.14 e and f shows the hodographs around 6 km and 14 km soon after the passage of the cyclone. In these figures we can note that ellipse is rotating clockwise in both troposphere and lower stratosphere, which suggests that the waves are propagating upward. The direction of propagation of the waves is similar to that observed during the passage of the storm. The vertical wavelength of the oscillations has increased to 3.9 km in the upper troposphere and to 1.8 km in the lower levels.

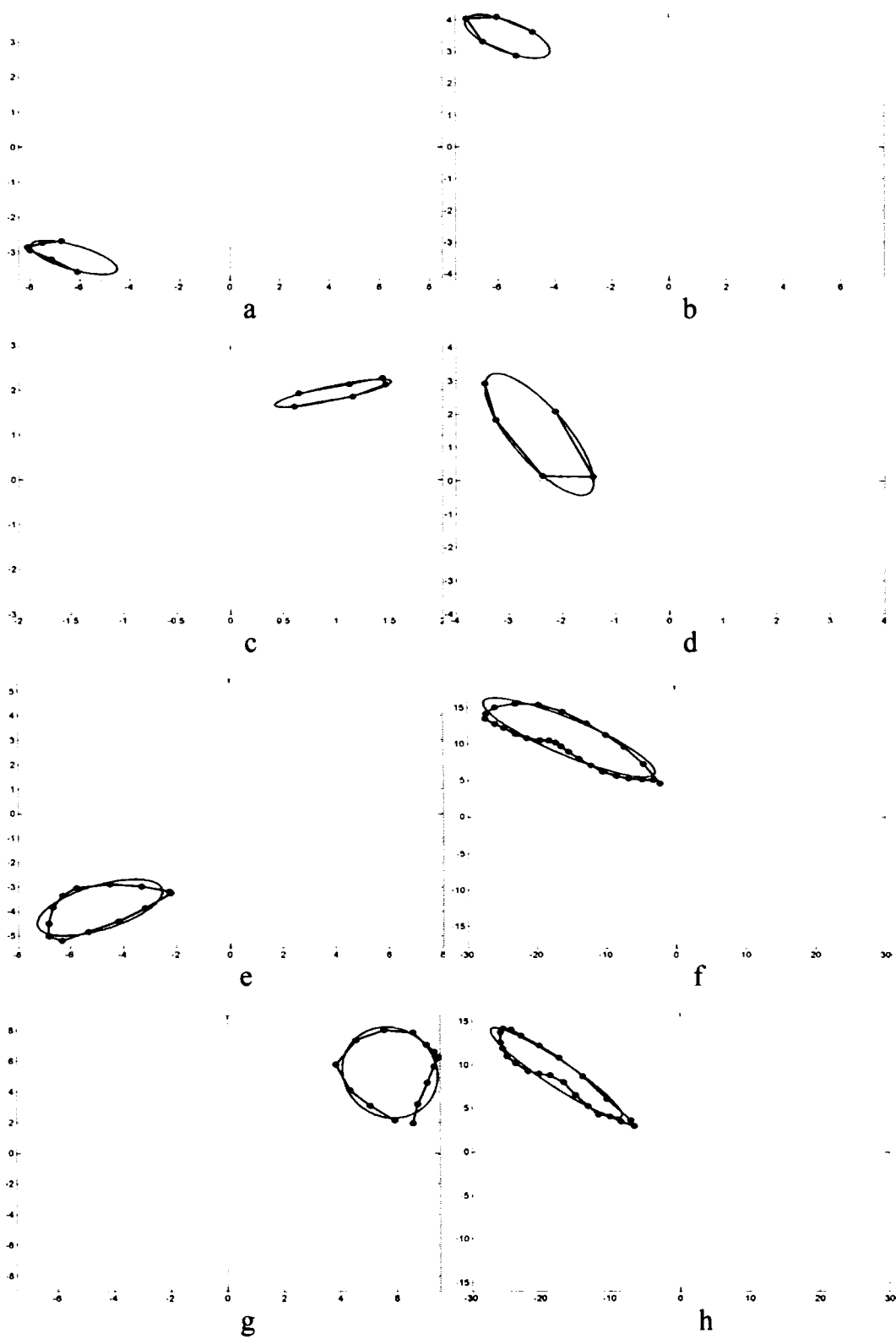


Figure 6.14. Hodograph analyses before, during and after the nearest passage of the cyclone during 23- 24 November 2002 (left and right panel for the same day at different height regions)

After the passage of the storm, the ellipse is rotating anticlockwise in the lower height and clockwise in the upper height region (see fig 6.14 g & h). This suggests that the waves are propagating downward in the lower levels and upward in the upper regions. The source region is in the upper troposphere. The hodographs after this period also look similar (figures not shown). The waves are propagating from southeast to northwest (SE-NW). The vertical wavelength of the oscillations in the upper troposphere is 3.3 km, while that in the lower levels has increased to 2 km.

### **6.5. Concluding Remarks**

The generation of gravity waves during the passage of cyclone is identified from the case studies. Mainly, short period gravity waves having period ranging from 15 to 30 minutes are observed during the passage of tropical cyclones. It has also been observed that before the passage of the storm the source region of gravity waves is in the upper troposphere and tropopause region. During and just after the passage, the source region is in the lower troposphere. After the passage of the storm, the source region of gravity waves is seen shifting upwards. The vertical wavelength of the waves is found variable.



Chapter # 7

*Troposphere-Stratosphere Exchange During  
Tropical Cyclones*

## 7.1. Introduction

Dynamical, chemical and radiative coupling between the stratosphere and troposphere are among the many important processes that must be understood for the prediction of global change. Of special significance is the transport of trace chemical species, natural and anthropogenic between the stratosphere and the troposphere. For instance, anthropogenic species transported from the troposphere into the stratosphere initiate much of the chemistry responsible for stratospheric ozone depletion. Conversely, downward transport from the stratosphere, not only constitutes the main removal mechanism for many stratospheric species including those involved in ozone depletion, but also represents a significant input of ozone and other reactive species into the tropospheric chemical system. Chemical effects from stratosphere-troposphere exchange (STE) can influence the radiative flux balance in the troposphere and lower stratosphere (e.g., *Ramaswamy et al.*, 1992; *Toumi et al.*, 1994). Stratosphere –Troposphere Exchange can therefore have a significant role in the radiative forcing of global climate change. The vertical transport of air and chemical species through the depth of the troposphere can occur on timescales as short as a few hours *via* moist convection, and on timescales of days *via* baroclinic eddy motions in middle latitudes. By contrast, vertical transport through a similar altitude range in the stratosphere takes months, a year or more in the lower stratosphere and this vertical transport must be accompanied by radiative heating or cooling.

However global exchange rate is not determined by details of near-tropopause phenomena such as penetrative cumulus convection or small-scale mixing associated with upper level fronts and cyclones. These smaller scale processes must be considered in order to understand the finer details of exchange. Stratospheric air finds its way back into the troposphere through a vast variety of irreversible eddy exchange phenomena, including tropopause

folding and the formation of so-called tropical upper-tropospheric troughs and consequent irreversible exchange. Thus, in order to understand the physics and chemistry of the upper troposphere and lowermost stratosphere, quantitative information on the mass and property transports between these two regions is required.

A tropical cyclone is characterized by extremely violent horizontal winds, convergent in the cyclonic direction in the lower layers, divergent in the anticyclonic direction in the upper troposphere. By continuity and conservation of mass, secondary vertical circulations are induced. Disturbances in the tropopause above the most active cloud masses can be the origin of transfer from the upper troposphere to the lower stratosphere. When the cyclone is particularly strong, its influence can extend to the outer environment of the cyclone, where mesoscale stratosphere troposphere exchange is possible.

The internal gravity waves generated due to cyclonic disturbance contribute to the small-scale turbulence assumed to be omnipresent in the deduction of the net flow into the stratosphere (*Danielson, 1993*). Slower ascending motions lift the tropopause and lower stratosphere, creating a strong thermal inversion layer above the cirrus cloud. The large stability in this layer resists penetrations; therefore any small-scale inhomogeneities in vertical velocities will also lift and lower the layer, generating internal gravity waves. These waves, in turn, generate small-scale turbulence and their diffusive transport plays a critical role in the tropical cyclone's troposphere to stratosphere transport. The STEP/Tropical experiment clearly showed that convective exchange in the tropics can transport tropospheric air upward and dehydrate it at the same time (*Holton et al., 1995*). A succession of overshooting and detraining convective turrets has produced a region of weak stability that is a mixture of stratospheric and tropospheric air.

## 7.2. Momentum Flux, Mass Flux and Body Force

The vertical flux of horizontal momentum associated with the upward propagating waves is very important, because its vertical divergence is connected with a body force acting on the mean flow. However, there was no direct method for the measurement of momentum flux until *Vincent and Reid* (1983) developed a method using Doppler radars. Direct measurements of wave momentum fluxes were performed over Adelaide, Australia, using a multiple-beam configuration of a MF radar (*Vincent and Reid*, 1983; *Fritts and Vincent*, 1987; *Reid and Vincent*, 1987). *Fukao et al.* (1988) measured momentum flux with three and four-beam methods and reported that the vertical transport of momentum is mainly by the longer-period fluctuations. *Fritts et al.* (1990) observed fluxes of  $u'w' \sim -0.1$  to  $-1.0 \text{ m}^2\text{s}^{-2}$ , with a mean of  $-0.2 \text{ m}^2\text{s}^{-2}$ , in the upper troposphere and lower stratosphere with the MU radar. A zonal drag of  $1\text{-}2 \text{ ms}^{-1}\text{d}^{-1}$  was also observed, which is sufficient to balance the momentum in large-scale models.

*Vincent and Reid* (1983) first measured the vertical flux of horizontal momentum using dual complementary coplanar Doppler beams of the MF radar located near Adelaide. This method uses the fact that the momentum flux is proportional to the difference between the variances of the radial velocities in two opposite directions. According to this method the momentum flux is measured by two off-zenith radar beams symmetric with respect to the vertical direction.

If  $\bar{V}_E$  and  $\bar{V}_W$  are the average velocities in the east and west beams, respectively then average zonal velocity is

$$\bar{u}' = (\bar{V}_E - \bar{V}_W)/2 \text{ Sin}\theta \quad \text{--- 7.1}$$

where,  $\theta$  is the tilt angle.

Mean vertical velocity is

$$\bar{w}' = (\bar{V}_E + \bar{V}_W)/2 \cos\theta \quad \text{--- 7.2}$$

Then the vertical flux of zonal momentum per unit mass at any given height is

$$(\overline{u'w'}) = (\bar{V}_E^2 - \bar{V}_W^2)/2\sin 2\theta \quad \text{--- 7.3}$$

Similarly, the vertical flux of meridional momentum per unit mass at a given height is given by

$$(\overline{v'w'}) = (\bar{V}_N^2 - \bar{V}_S^2)/2\sin 2\theta \quad \text{--- 7.4}$$

where  $\bar{V}_N$  and  $\bar{V}_S$  are average radial velocities from north and south beams, respectively.

The mass flux transport is given by

$$\text{Mass flux} = \rho w \Delta \quad \text{--- 7.5}$$

The zonal and meridional body forces per unit mass are estimated using

$$F_U = - (1/\rho)(\partial/\partial z (\overline{\rho u' w'})) \quad \text{--- 7.6}$$

$$F_V = - (1/\rho)(\partial/\partial z (\overline{\rho v' w'})) \quad \text{--- 7.7}$$

Where,  $\rho$  is the density. The density for the present study is taken from the MSIS model.

### 7.3. Experimental Approach

Observations were made using 6 beams (East 10, West 10, North 10, South 10, Zx and Zy) and single beam with a pulse width of  $16\mu\text{s}$  (coded) during tropical cyclone passage in various years. In 1994 there was no continuous data. This case was considered, as it was the only case of overhead

passage of cyclone over the radar site. The observations were taken from 4 – 21 km with an altitude resolution of 150 m. Details of the cyclone cases considered and associated synoptic features are already mentioned in the thesis.

## **7.4. Stratosphere – Troposphere Exchange during Tropical Cyclones**

### **7.4.1. Case I – Overhead passage**

In 1994, the cyclone formed in the Bay of Bengal during 28<sup>th</sup> October – 2<sup>nd</sup> November passed overhead of the radar site when it was in the form of a severe cyclonic storm. The storm was overhead of the station around 1300 hrs LT of 31<sup>st</sup> October 1994.

#### ***7.4.1a Zonal and meridional momentum flux***

Figures 7.1a – c show the zonal momentum fluxes on 27<sup>th</sup> October, 31<sup>st</sup> October and 1<sup>st</sup> November representing before, during and after the passage of the storm, respectively. From figure 7.1a, we can see that the momentum flux is upward in the lower and middle troposphere and downward in the upper troposphere and lower stratosphere. In the first half of the observation period there is upward transport from 4 to 10 km and downward transport above. As time progresses the upward transport in the lower levels strengthens, while the downward transport in the upper troposphere and lower stratosphere weakens. In the lower altitudes the transport is upward throughout the observation period. In the lower levels downward transport is seen initially and it changes to upward afterwards during the passage of the cyclone (Figure 7.1b). Upward flow around 12 km is seen spreading downward as time progresses. Strong upward flow is noted around 8 and 15 km. Above 10 km mostly downward transport prevails. After the passage of the cyclone, the momentum flux transports are very little and downward transport is seen (Figure 7.1c). Strong upward transport is noted in lower stratospheric levels.

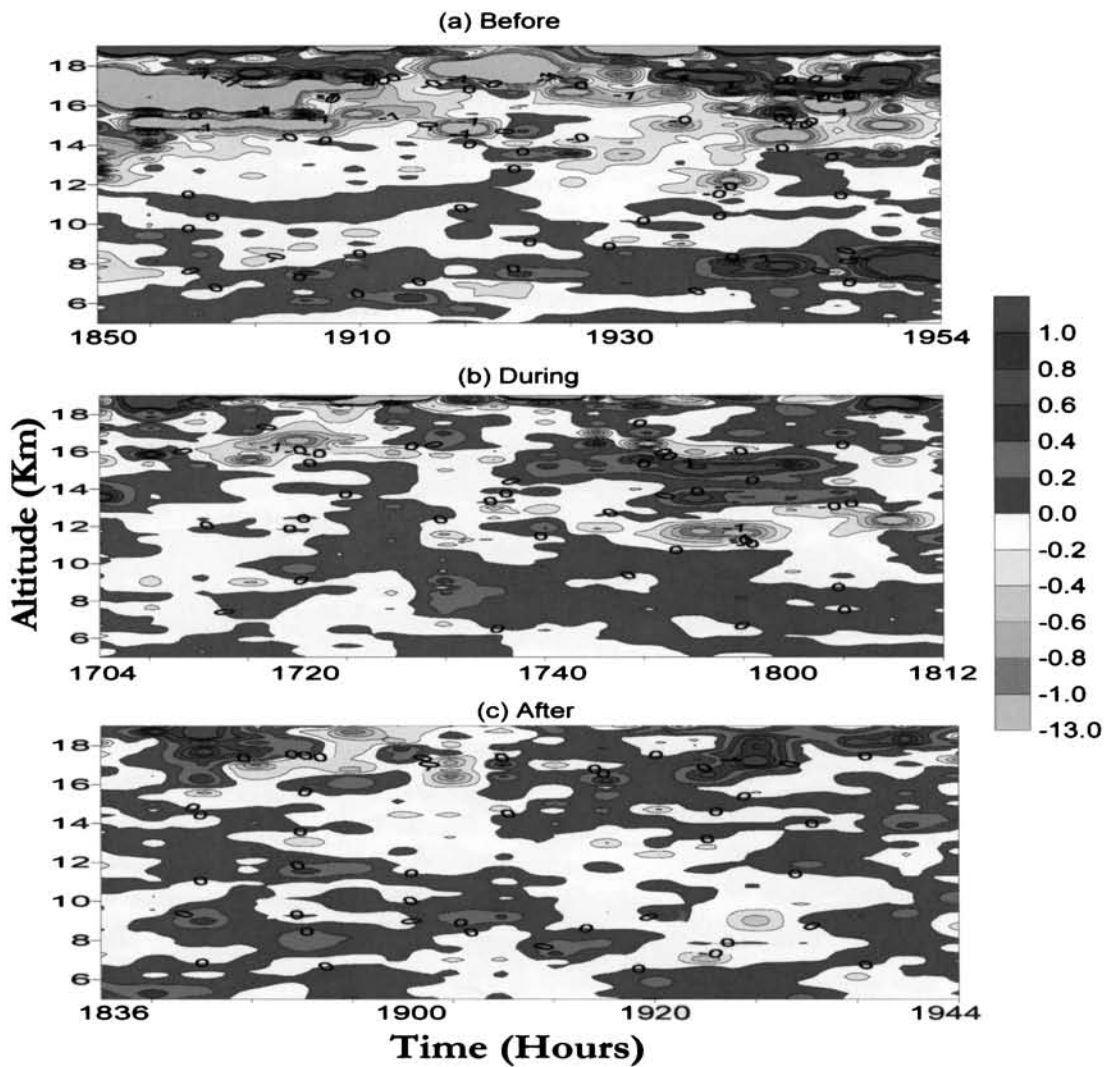


Figure 7.1. Contour plots of zonal momentum flux

Figures 7.2a – c show the meridional momentum fluxes before, during and after the storm passage. The important feature noted in figure 7.2a is the strong upward flow noted around 17 km during the first half of the observation period changed to downward in the second half. In lower levels, the transport is downward and it is generally upward in upper levels. Strong upward transport is noted around 10 km at 1900 hrs LT, three days prior to the passage of cyclone. In figure 7.2b, we can see that in the lower levels the transport becomes upward. Strong upward transport of meridional momentum flux is noted around 16 km near the tropopause level. The transport is downward around 12 km. On 1<sup>st</sup> November, the transport is very less in the case of meridional momentum transport (figure 7.2c).

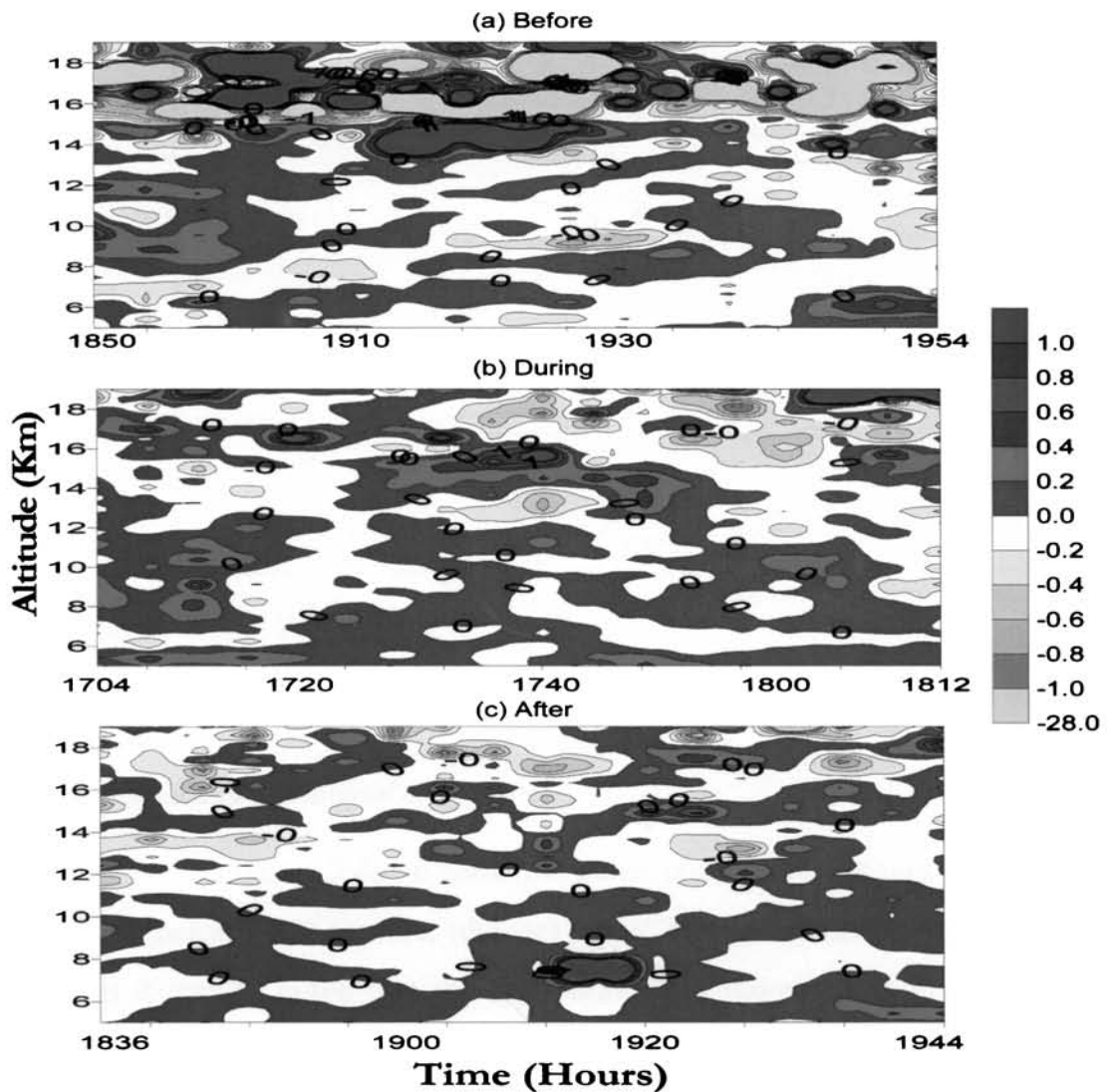


Figure 7.2. Contour plots of meridional momentum flux on a) before, b) during and c) after the storm passage

#### 7.4.1b Mass flux transport

Figure 7.3 illustrates the transport of mass flux before, during and after the storm passage. Strong downward transport of mass flux is noted around 8 km three days before the passage of storm. The transport is generally weak and upward above 10 km. During the storm, strong upward flow is noted from 11 to 14 km. The transport is downward below 6 km and between 8 and 11 km. Downward transport is noted from 8 to 11 km. After the passage of the storm the transport becomes weak and downward at all altitudes between 4 and 22 km.



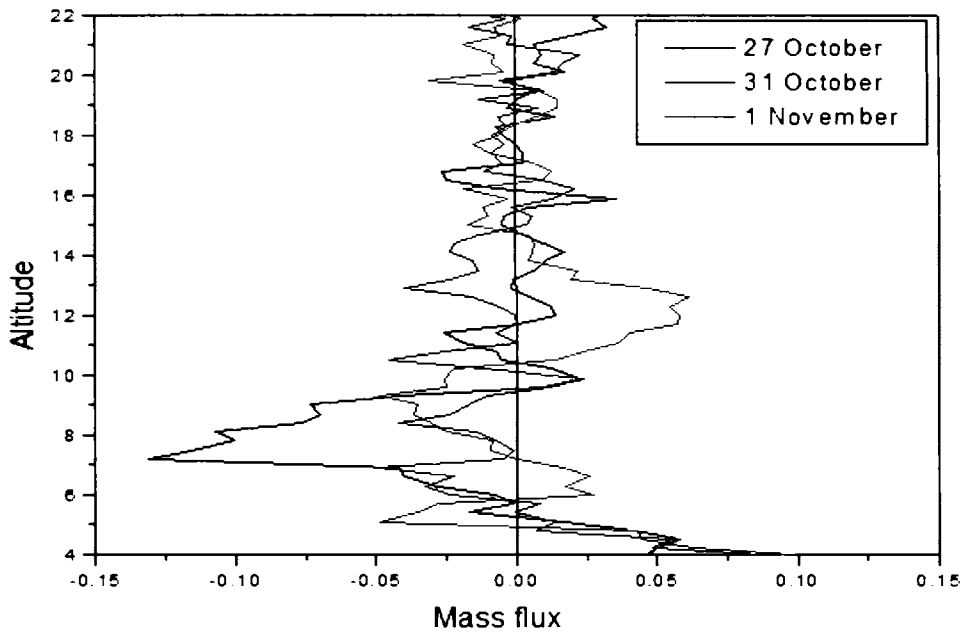


Figure 7.3. Mass flux transport before, during and after the passage of the storm

#### 7.4.1c Zonal and meridional body forces

Figures 7.4a –c show the zonal body force per unit mass on 27<sup>th</sup> October (before), 31<sup>st</sup> October (during) and 1<sup>st</sup> November (after). From all these figures it can be noted that the fluctuations are more before and during the passage of the storm than after the passage. Before the overhead passage, the body force is mostly strong and westward. Fluctuations are more in the lower and upper troposphere. The body force is weak and eastward during the passage. One day after the storm passage the body force is negligible.

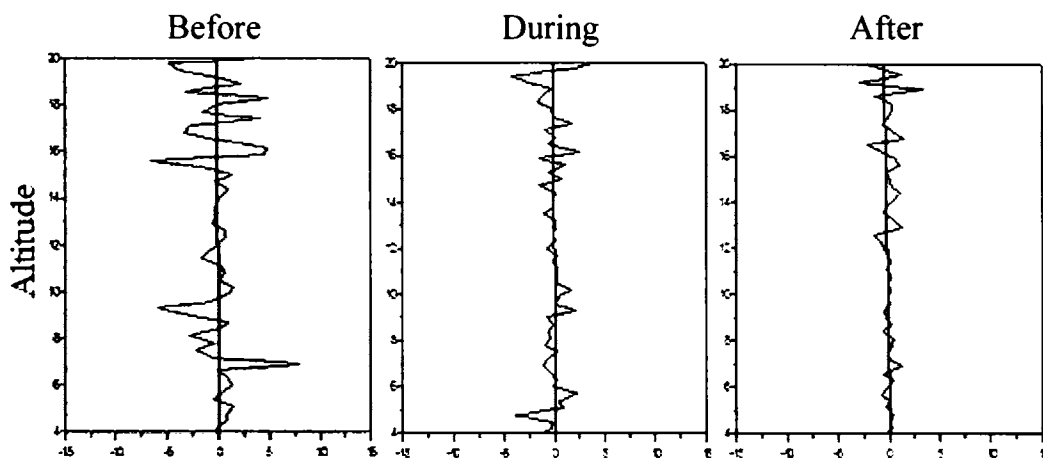


Figure 7.4. Zonal body force before, during and after the storm passage

Figures 7.5a –c show the vertical distribution of meridional body force per unit mass. Fluctuations are large above the tropopause. Fluctuations in the lower levels are more pronounced during the time of storm passage. In all the cases the body force is generally northward.

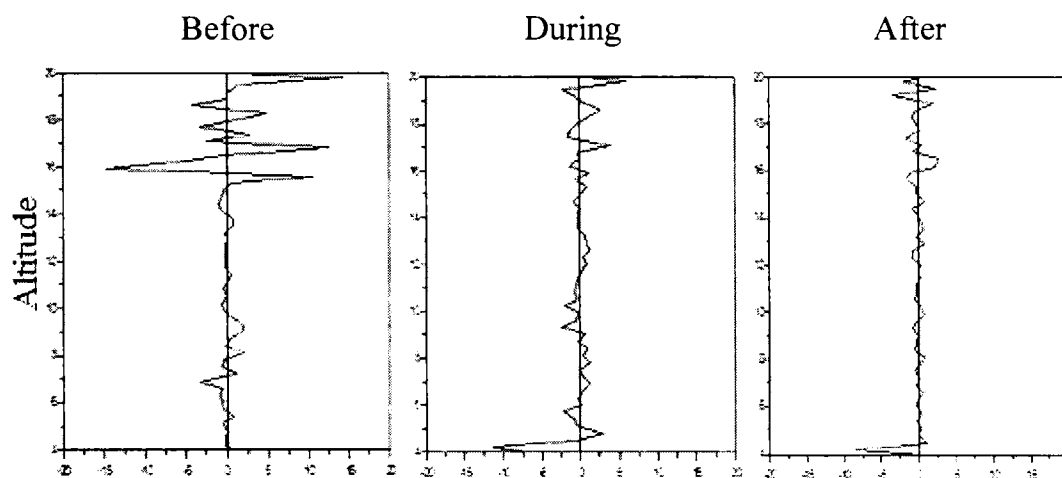


Figure 7.5. Meridional body force before, during and after the storm passage

#### 7.4.2. Case II – Nearby passage

A case of very nearby passage of a tropical cyclone was observed in October 2001. This cyclone was most nearer to the radar site on 16<sup>th</sup> October 2001 at 0500 hrs LT. The distance of the cyclone centre from the radar site at this time was approximately 60 km.

##### 7.4.2a Zonal and meridional momentum fluxes

Figure 7.6 shows the zonal momentum for 32 hours at 1-hour interval from 0930 hrs LT on 15<sup>th</sup> October to 1630 hrs LT on 16<sup>th</sup> October. This figure covers the zonal momentum flux transport before, during and after the nearby passage. The box in the figure shows the time of nearest passage of cyclone. The transport is generally downward during the observation period. Strong downward flow is noted from 10 to 12 km just before the passage of the storm. Upward transport is noted between 8 and 15 km from 0300 hrs to 0530

hrs LT on 16<sup>th</sup> October. Strong upward transport of zonal momentum flux is noted around 12 km during the passage of the storm. After the passage strong downward motion is noted around 6 km.

Meridional momentum flux transport is illustrated in figure 7.7. Before the passage of the storm, the transport is generally weak and downward. Upward transport is noted in the lower levels for 7 hours from 2030 hrs LT on 15<sup>th</sup> October. It can be noted that the transport is mostly upward during the passage. In the lower layers of the troposphere intense downward transport of momentum flux is noted, while strong upward transport is seen in the middle troposphere. After the crossing of the cyclone, intense downward transport is noted in the lower levels.

#### ***7.4.2b Mass flux transport***

Figure 7.8 indicates the transport of mass flux on 15<sup>th</sup> October, one day before the passage of the storm and on 16<sup>th</sup> October during the cyclone passage. It can be seen that the transport is generally upward one day before the passage of the storm. Strong upward transport of mass flux is noted from 6 to 10 km. During the cyclone passage remarkable changes occur in the mass flux transport. The upward transport around 6 km changes to downward and the downward transport between 12 and 14 km become stronger. Minor variations are noted at other altitudes also.

#### ***7.4.2c Zonal and meridional body forces***

Figure 7.9 shows the zonal body force per unit mass associated with the cyclone passage. Minor fluctuations are present in the atmosphere from 4 to 16 km. More fluctuations are noted above the tropopause. During the cyclone passage fluctuations becomes more in the troposphere. Body force is generally eastward during the passage of the storm. Figure 7.10 shows the meridional body force per unit mass. Before the passage of the storm the

fluctuations are very little in the troposphere. It is interesting to note that the fluctuations become stronger during the passage of the storm. Fluctuations are more prominent below the tropopause during the passage of the storm. The body force is generally northward in direction. In the case of meridional body force the fluctuations are more compared to zonal body force.

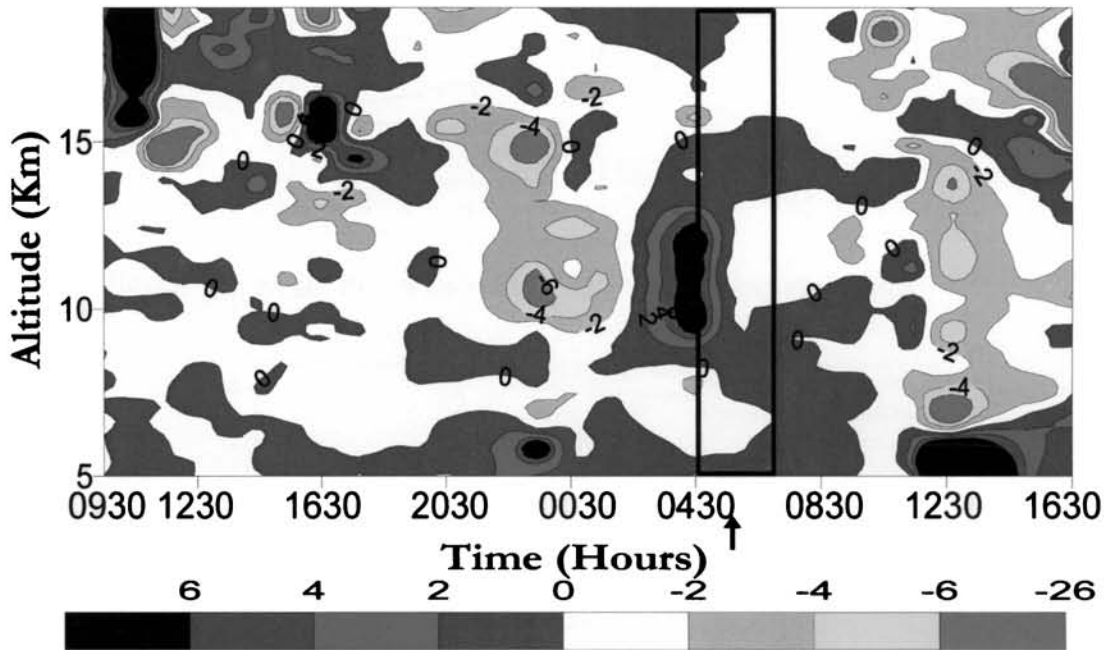


Figure 7.6. Zonal momentum flux from 0930 hrs LT on 15th October

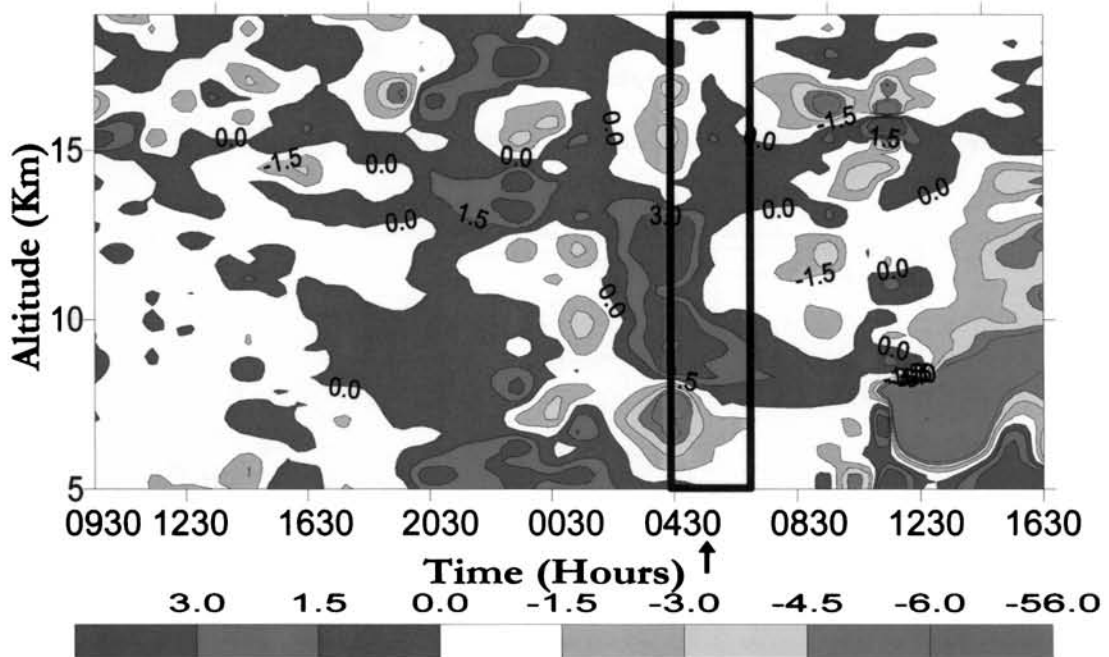


Figure 7.7. Meridional momentum flux for 32 hours

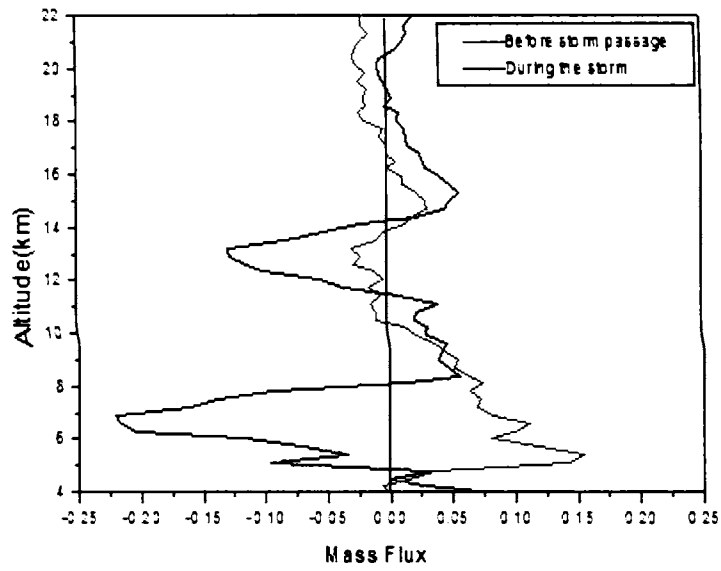


Figure 7.8. Mass flux transport before and during the storm

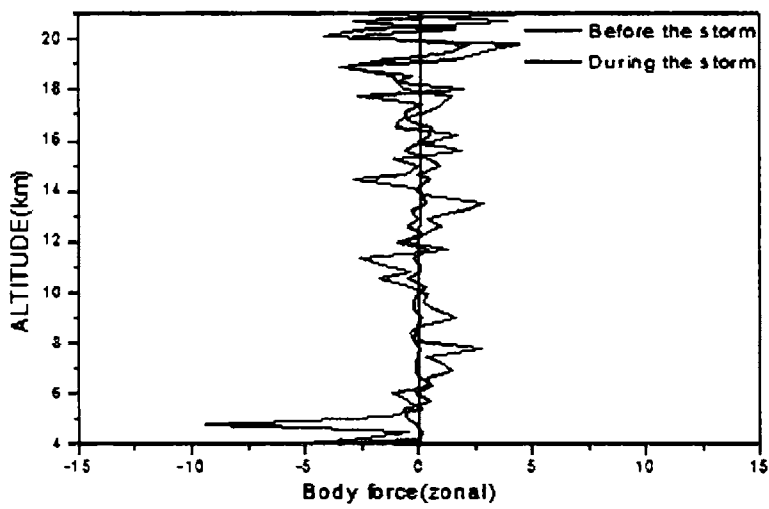


Figure 7.9. Zonal body forces before and during the cyclone passage in 2001

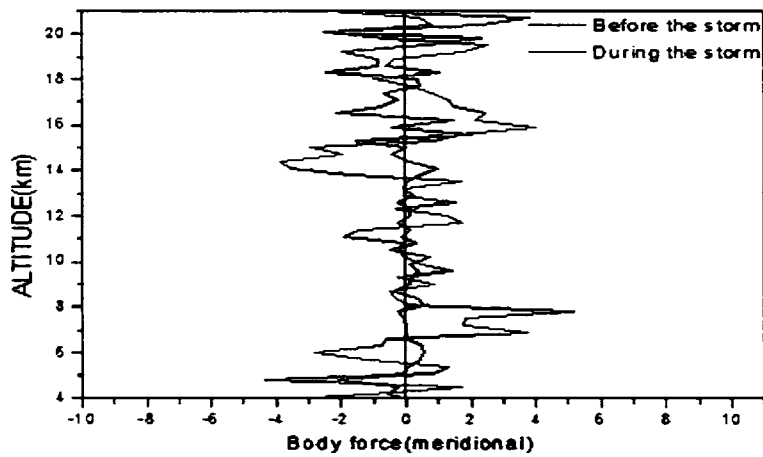


Figure 7.10. Meridional body forces before and during the cyclone passage

### **7.4.3. Case III- Far away passage**

During the cyclone formation in Bay of Bengal during 23 – 28 November 2002, special experiments were carried out using the MST radar to understand the characteristics of the atmosphere when the cyclone is far away. This cyclone passed approximately 700 km away from the radar site.

#### ***7.4.3a Zonal and meridional momentum fluxes***

Figures 7.11a - c show the zonal momentum flux in the case of far away passage of the cyclone. Before the passage, the transport is weak and variable. As the cyclone moves nearer strong upward transport is noted in the 13-15 km altitude, where the transport was downward before. During the passage of the storm, generally upward transport is observed. Strong upward transport is noted around 13 km. After the passage, the transport became weak. In the lower levels downward transport prevails, while in the upper levels upward transport is present.

Figures 7.12a - c show the meridional momentum fluxes before, during and after the cyclone passage. Before the passage, strong upward transport is seen below 8 km. Downward transport noted around 10 km is seen extending upwards. During the passage of the storm, lower and middle troposphere is characterised by the downward transport of meridional momentum flux. Strong upward transport is noted in the upper troposphere. After the passage of the storm, the transport becomes weak and variable.

#### ***7.4.3b Mass flux transport***

Figure 7.13 indicates the transport of mass flux before, during and after the far away passage. Before the passage, the transport is upward nearly at all altitudes and strong upward transport is seen in the lower levels. Downward transport of mass is noted around 8 km. As time progresses the transport pattern changes. Strong upward transport is noted from 5 to 15 km

except between 10-12 km. It is interesting to note that the nearest passage of cyclone occurred around this time. As the cyclone moved away from the station the mass flux transport became weak. Downward transport is noted from 6 to 10 km.

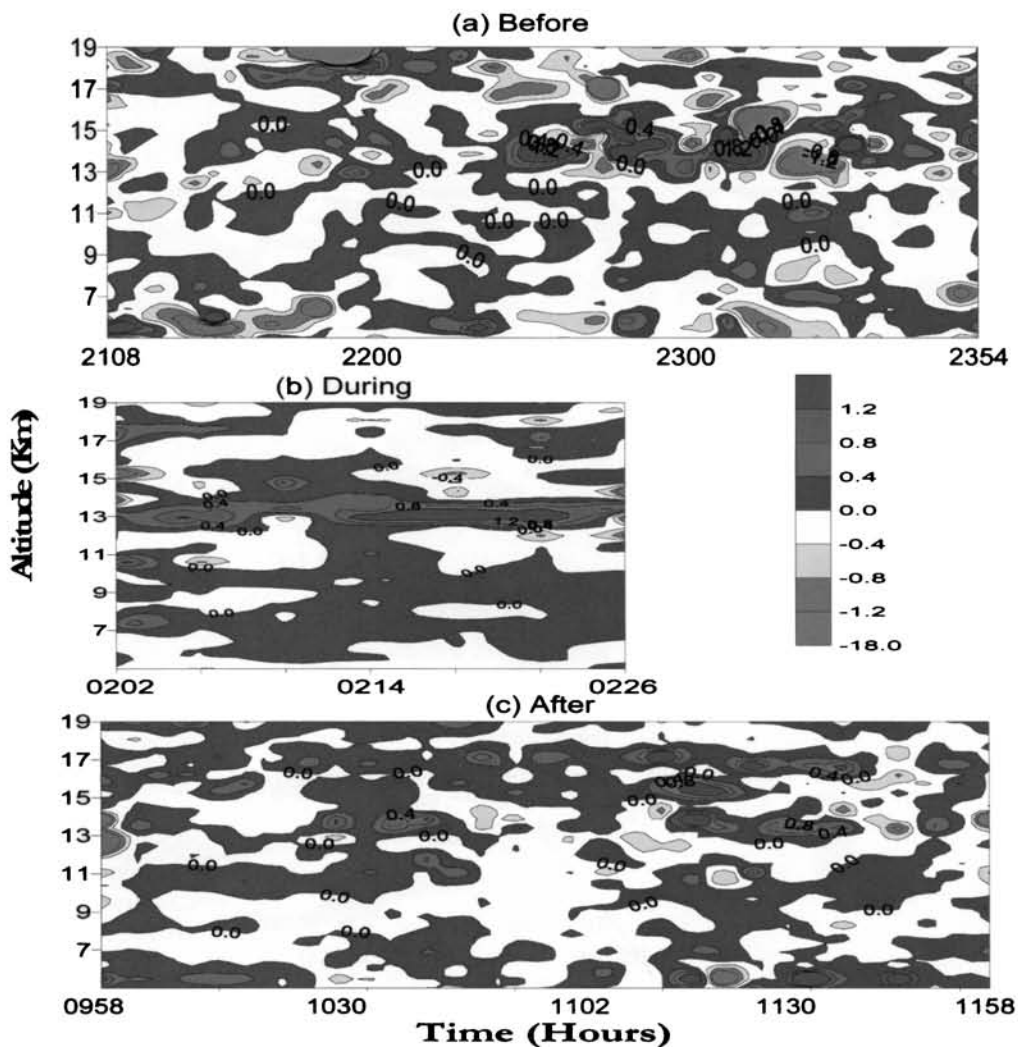


Figure 7.11. Zonal momentum fluxes before, during and after storm passage

#### 7.4.3c Zonal and meridional body forces

Figures 7.14 show the zonal body force per unit mass. Before the passage of the storm the zonal body force is generally weak with sharp fluctuation between 6 and 8 km. During the passage of the storm, sharp fluctuations appear in the middle troposphere. The fluctuations disappeared after the passage of the storm.

Figure 7.15 show the meridional body force per unit mass. Before the passage of the storm large fluctuations are noted around 4 to 8 km. Fluctuations are also seen in the upper troposphere and lower stratosphere. During the passage of the storm, sharp fluctuations are observed only around 12 to 16 km region. After the passage of the storm weak fluctuations are noted in the entire altitude range.

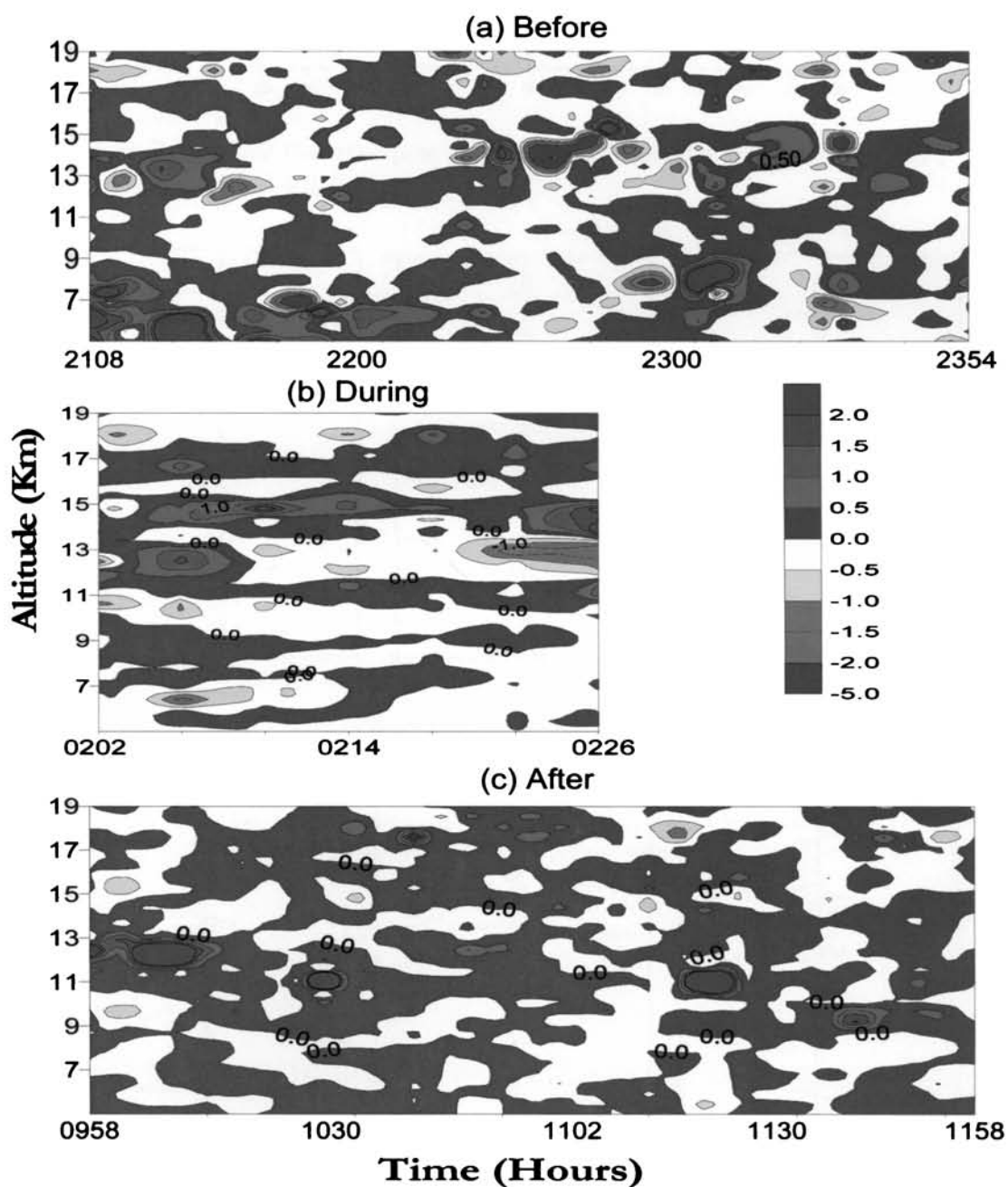


Figure 7.12. Meridional momentum fluxes before, during and after storm passage



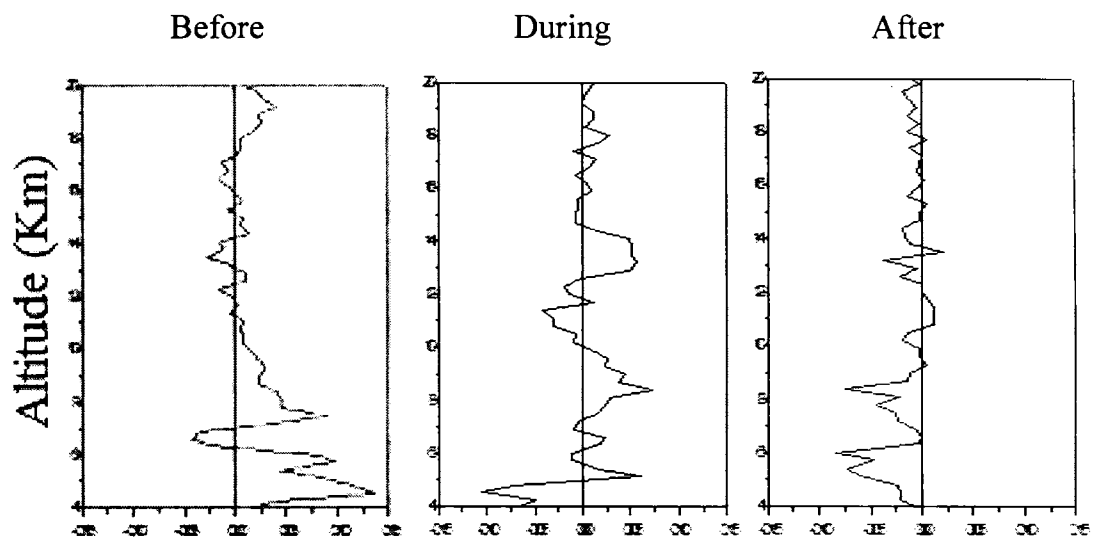


Figure 7.13. Mass flux transport before, during and after the storm passage (from 4 to 20 Km)

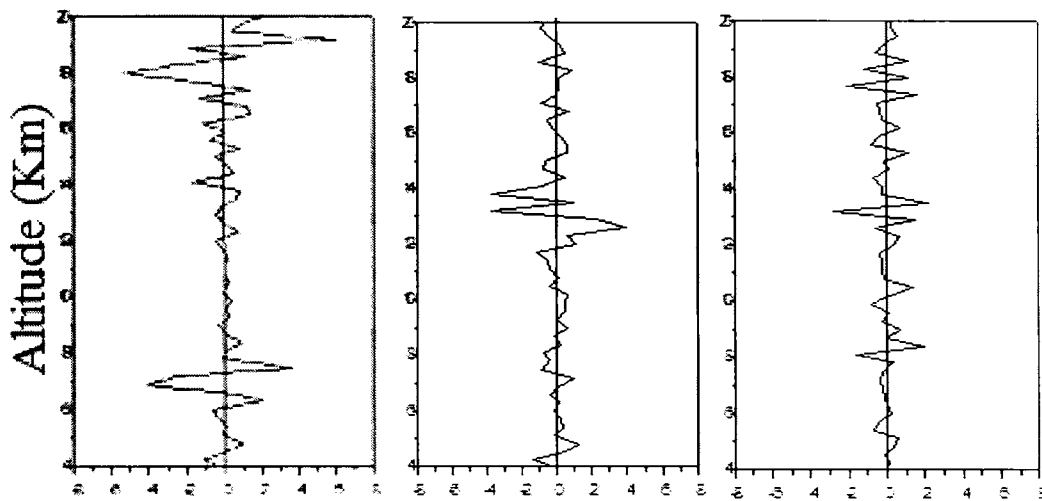


Figure 7.14. Zonal body force for the far away passage (4-20 km)

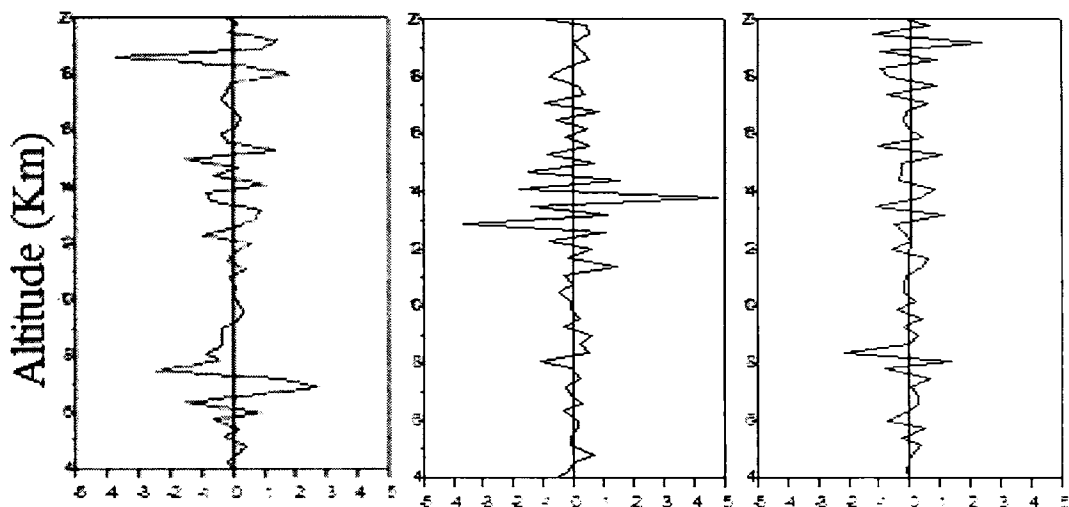


Figure 7.15. Meridional body force during 23-24 November 2002 (4-20 km)

It is seen that in the case of overhead and nearby passage, no change in the direction of zonal momentum flux transport occur below 8 km, but the downward transport changed to upward in the far away passage. In the 8-16 km region, the downward transport changed to upward in all the three cases. Above the tropopause, downward transport is noted. In the case of overhead passage, the downward transport of meridional momentum flux before the passage changed to upward during the passage below 8 km. In the middle and upper troposphere, the transport changed in the opposite direction. Thus momentum flux divergence is noted around 8 km. This result is in accordance with the finding of *Sato* (1993). Above the tropopause downward transport noted during the passage persists thereafter. After the passage, in all the three cases downward transport is observed in the altitude range between 5 and 19 km.

*Sato* (1993) observed changes in the vertical momentum flux associated with typhoon passage using MU radar in Japan. She found that the disturbances in the middle troposphere were associated with divergence of vertical momentum flux corresponding to a forcing to decelerate the cyclonic wind of typhoon.

In the case of overhead passage, strong downward transport of mass flux noted around 7 km before the passage, weakens a little and shifts upward during the passage. The transport is upward in the 10-12 km region. After the passage, the transport becomes very weak. The upward transport observed below 8 km changed to downward during the nearby passage of the storm. In the case of far away passage, the upward flux transport below 8 km weakened and changed to downward as the cyclone crosses the station. Much change is not observed above 8 km associated with the passage of the storm.

In the case of overhead passage, fluctuations are more prominent in the zonal body force before the passage of the storm. Both the zonal and

meridional body forces weaken as the cyclone moves over and away from the station. In the case of nearby passage, just the reverse is noted. i.e., the fluctuations are more during the passage of the storm. The fluctuations are more in meridional body force during the nearby passage. The fluctuations in zonal body force are more before the passage than during and after the passage of the storm in the case of faraway passage.

### **7.5. Concluding Remarks**

In both the overhead and nearby passage, the downward transport of both zonal and meridional momentum fluxes changed to upward in the upper troposphere during the passage of the storm. After the passage of the storm generally downward transport is observed. The downward transport of meridional momentum flux observed below 10 km changed to upward in overhead passage. During far away passage, considerable change is not seen associated with the passage of the storm. In the case of mass flux transport, strong downward transport is noted around 7 km during the period of overhead and nearby passage. Strong upward transport of mass flux is noted before the far away passage of the storm. Fluctuations are seen in both the zonal and meridional body force. After the storm passage, fluctuations are generally weak.

## Chapter #8

*Summary and Conclusions*

### **8.1. Major Outcome of the Study**

The characteristics of the troposphere and lower stratosphere during the passage of tropical cyclones have been studied in detail using the Indian MST radar located at Gadanki (13.5°N, 79.2°E), India. The major results obtained from the present study are given as follows.

Tropical cyclones are occasionally very severe in the North Indian Ocean, especially in Bay of Bengal. The Indian MST radar located at Gadanki is an ideal instrument to study the structure and dynamics of the atmosphere during the time of cyclones when it passes overhead of the radar site. Special cyclone experiments were carried out by us (CUSAT team) during 2001- 2004 period, to study the cyclone characteristics over Gadanki. Two cyclone cases were chosen from the five cyclones observed during this period, taking into account of the data quality and the position and intensity of the cyclones. A rare case of overhead passage reported in 1994 is also considered for the present study. These three cases are classified as *overhead*, *nearby* and *far away passage*.

The winds in the troposphere and lower stratosphere are greatly affected by the passage of cyclones. Lower and middle tropospheric winds showed signs of reversal, while strengthening of winds are noted in the upper troposphere and lower stratosphere during the passage of cyclones. In the case of overhead and nearby passage, wind reversed from northeasterly to southwesterly, suggesting that the direction of movement of the cyclones were from southeast to northwest of the radar site. In the case of far away passage, the change in wind direction is from southeasterly to southwesterly. This implies that the cyclone moved from south to north of the radar site. The wind speed increased considerably in the upper troposphere and lower stratosphere. Strong winds are noted around 16 km in the case of overhead and nearby passage, whereas the strong wind region is shifted downwards to 14 km in the case of far away passage.

The vertical wind showed marked variations only when the cyclone is closest to the station. The variation is more pronounced in the case of overhead and nearby passage. During the passage of the storm, strong updraft is noted around 12 km, both in the overhead and nearby passage, the level of maximum convective outflow. Below 6 km, strong updraft and downdraft regions are noted in all the three cases suggesting convective activities associated with the storm passage.

The presence of high reflectivity layers below the tropopause suggests the passage of severe weather systems. In all the three cases considered in the thesis, high reflectivity layers are noted below the tropopause in addition to the layers observed at the tropopause and above. These layers exist for longer duration in the case of overhead and nearby passage. A broad layer of high SNR is noted above the tropopause during the far away passage, indicating the presence of a highly stable layer. When the periphery of the nearby cyclone is over the station, the broader layer is noted below the tropopause. But in the case of overhead passage, a number of thin high reflectivity layers are noted below the tropopause.

Fluctuations in tropopause height are noted in all the three cases, the fluctuations being more prominent when the cyclones are nearer to the radar site. In the case of overhead passage, lowering of the tropopause is noted when the periphery of the cyclone is above the radar site. Afterwards, the tropopause is seen swinging back to its normal position or even goes beyond that height level. In the case of nearby passage, the tropopause raised when the cyclone centre was very near to the radar and then lowered when the periphery of the cyclone was over the radar site. The tropopause is seen rising back again after the passage of the storm and it is seen overshooting the mean position. The tropopause is seen lowering when the cyclone is far away from the radar, i.e., when the outer edge of the cyclone is over the radar station. It is also seen swinging back to the normal position soon after the passage of the cyclone.

The mean wind distribution reveals marked changes associated with the passage of the storm. The strengthening and reversal of the wind is noted in all the three cases considered. It is also seen that in the case of far away passage, though the cyclone centre is 700 km away from the radar, the atmosphere is well affected by the cyclone passage. Wave generations are noted associated with the overhead, nearby and far away passage of tropical cyclones. The wave features are more prominent in the upper troposphere and lower stratosphere. Waves in the zonal wind are more dominant than waves present in the other wind components. Short period gravity waves are seen generated during the passage of tropical cyclones. These waves have periodicities between 20 and 30 minutes. The vertical wavelengths of these gravity waves are variable in the three cases. The period and vertical wavelength of the gravity waves generated during far away passage were slightly higher than that observed during the other cases. The propagation of these waves is downward in the lower troposphere and upward in the upper troposphere. Thus the source region of gravity waves is located in the middle/upper troposphere. During the passage of the storm, upward propagation of gravity waves are noted from the middle troposphere to lower stratosphere, suggesting that the source region is in the lower troposphere.

The downward transport of momentum fluxes noted before the storm in the middle and upper troposphere, changed to upward just after the passage. Below 10 km the upward transport of zonal momentum flux did not change during the storm passage. But the downward transport of meridional momentum flux changed to upward in overhead passage. After the passage of the storm generally downward transport is observed. Not much change in the direction of momentum flux transport is noted associated with the far away passage of the storm.

In all the three cases, strong downward transport of mass flux is noted in the lower and upper troposphere during the passage of the storm. In

the middle troposphere the mass flux transport is upward. The upward transport observed below 8 km changed to downward during the nearby passage of the storm. The transport of mass flux is more pronounced in the case of overhead and nearby passage. Fluctuations are seen in both the zonal and meridional body forces. Strong meridional body force is noted during nearby passage of the storm.

## **8.2. Scope of Future Studies**

The present study could bring forward some of the characteristics of the troposphere and lower stratosphere during the passage of tropical cyclones. The study can be extended further to understand the circulation and dynamics of the atmosphere associated with the passage of tropical cyclones. The Lower Atmospheric Wind Profiler (LAWP) available at Gadanki, if operated together with the MST radar can provide continuous information from ground to 25 km altitude. To get a deep insight into the structure of the cyclones, supplementary data from satellites, meteorological rockets, radiosondes, GPS sondes and Doppler weather radar have to be used.

The gravity wave generation and its characteristics during the passage of storms is another important aspect to be studied in detail. For this study the radar should operate continuously. These special experimental observations along with the supplementary data are expected to provide all the necessary information for a better understanding of gravity wave dynamics.

Stratosphere – Troposphere Exchange (STE) is now gaining more and more importance in the science community. STE during cyclones are studied for hurricanes mainly and to a less extent for typhoons. STE during tropical cyclones in Indian region is not yet studied in detail. MST radar along with LAWP can give valuable inputs to such a study as it provides continuous data with high resolution in altitude and time.



## *References*

- Abdullah, A. J.**, 1966: The spiral bands of a hurricane: A possible dynamic explanation, *J. Atmos. Sci.*, **23**, 367–375.
- Alexander, M. J. and L. Pfister**, 1995: Gravity wave momentum flux in the lower stratosphere over convection, *Geophys. Res. Lett.*, **22**, 2029-2032.
- Alexander, M. J., J. R. Holton and D. R. Durran**, 1995: The gravity wave response above deep convection in a squall line simulation. *J. Atmos. Sci.*, **52**, 2212-2226.
- Alexander, M. J. and J. R. Holton**, 1997: A model study of zonal forcing in the equatorial stratosphere by convectively induced gravity waves, *J. Atmos. Sci.*, **54**, 408-419.
- Alexander, M. J.**, 1998: Interpretations of observed climatological patterns in stratospheric gravity wave variance, *J. Geophys. Res.*, **103**, 8627-8640.
- Alexander, M. J., T. Tsuda and R. A. Vincent**, 2002: On the latitudinal variations observed in gravity waves with short vertical wavelengths, *J. Atmos. Sci.*, **59**, 1394-1404.
- Allen, S. J. and R. A. Vincent**, 1995: Gravity wave activity in the lower atmosphere: Seasonal and latitudinal variations, *J. Geophys. Res.*, **100**, 1327-1350.
- Anandan, V. K.**, 1996: *The Atmospheric Data processor, Technical and User Reference Manual*, National MST Radar Facility, Department of Space, Govt. of India, Gadanki-517112, AP, India.
- Andrews, D. G., J. R. Holton and C. B. Leovy**, 1987: *Middle Atmospheric Dynamics*, Academic Press, Orlando.
- Appenzeller, C. and H. C. Davies**, 1992: Structure of stratospheric intrusions into the troposphere, *Nature*, **358**, 570-572.
- Appenzeller, C., J. R. Holton and K. H. Rosenlof**, 1996: Seasonal variation of mass transport across the tropopause, *J. Geophys. Res.*, **101**, 15071-15078.
- Balsley, B. B., W. L. Ecklund, D. A. Carter and P. E. Johnston**, 1980: The MST radar at Poker Flat, Alaska, *Radio Sci.*, **15**, 213-223.
- Baray, J. -L., G. Ancellet, T. Randriambelo and S. Baldy**, 1999: Tropical cyclone Marlene and stratosphere-troposphere exchange, *J. Geophys. Res.*, **104**, 13953-13970.
- Basher, R. E. and X. Zheng**, 1995: Tropical cyclones in the southwest Pacific: spatial patterns and relationships to the Southern Oscillation and sea surface temperature, *J. Climate*, **8**, 1249-1260.

- Beres, J. H., M. J. Alexander and J. R. Holton**, 2002: Effects of tropospheric wind shear on the spectrum of convectively generated gravity waves, *J. Atmos. Sci.*, **59**, 1805-1824.
- Black, P.G.**, 1977: Some aspects of tropical storm structure revealed by handheld camera photographs from space, *Skylab Explores the Earth*, NASA Johnson Space Flight Center, 417–461.
- Black, P.G.**, 1983: Ocean temperature change induced by tropical cyclones, *Ph.D. Dissertation*, Pennsylvania State University, University Park, 278 pp.
- Bleck, R. and C. Mattocks**, 1984: A preliminary analysis of the role of potential vorticity in Alpine lee cyclogenesis, *Contrib. Atmos. Phys.*, **57**, 357-368.
- Booker, H. G. and W. E. Gordon**, 1950: A theory of radio scattering in the troposphere, *Proc. Inst. Radio. Eng.*, **38**, 401-412.
- Boyle, J. S. and L. F. Bosart**, 1986: Cyclone–anticyclone couplets over North America. Part II: Analysis of a major cyclone event over the eastern United States, *Mon. Wea. Rev.*, **114**, 2432–2465.
- Bretherton, F.**, 1969a: Momentum transport by gravity waves, *Quart. J. Roy. Meteor. Soc.*, **95**, 213-243.
- Bretherton, F.**, 1969b: On the mean motion induced by internal gravity waves, *J. Fluid Mech.*, **36**, 758-803.
- Brewer, A. M.**, 1949: Evidence for a world circulation provided by the measurements of Helium and water vapor distribution in the stratosphere, *Quart. J. Roy. Meteor. Soc.*, **75**, 351-363.
- Brigham, E. O.**, 1988: *The Fast Fourier Transform and Its Applications*, Prentice-Hall, Englewood Cliffs, NJ.
- Burpee, R. W. and M. L. Black**, 1989: Temporal and spatial variations of rainfall near the center of two tropical cyclones, *Mon. Wea. Rev.*, **117**, 2204-2218.
- Butchart, N. and A. A. Scaife**, 2001: Removal of CFCs through increased mass exchange between the stratosphere and troposphere in a changing climate, *Nature*, **410**, 799-801.
- Caccia, J. L., B. Bench and V. Klaus**, 1997: Space-time description of nonstationary trapped lee waves using ST radar, aircraft and constant volume balloons during the PYREX experiment, *J. Atmos. Sci.*, **14**, 1821-1833.
- Caccia, J. L. and J. P. Cammas**, 1998: VHF-ST radar observations of an upper-level front using vertical and oblique-beam CN2 measurements, *Mon. Wea. Rev.*, **126**, 483-501.

- Cadet, D. and H. Teitelbaum**, 1979: Observational evidence of internal inertia-gravity waves in the tropical stratosphere, *J. Atmos. Sci.*, **36**, 892-907.
- Chane-Ming, F., F. Molinaro, J. Leveau, P. Keckhut and A. Hauchecorne**, 2000: Analysis of gravity waves in the tropical middle atmosphere over La Reunion Island (21°S, 55°E) with lidar using wavelet techniques, *Ann. Geophys.*, **18**, 485–498.
- Chane-Ming, F., G. Roff, L. Robert and J. Leveau**, 2002: Gravity wave characteristics over Tromelin Island during the passage of cyclone Hudah, *Geophys. Res. Lett.*, **29**, 1094, doi: 10.1029/2001GL013286.
- Chang, P., L. Ji and H. Li**, 1997: A decadal climate variation in the tropical ocean from thermodynamic air-sea interactions, *Nature*, **385**, 516-518.
- Chanin, M. L. and A. Hauchecorne**, 1981: Lidar observation of gravity and tidal waves in the stratosphere and mesosphere, *J. Geophys. Res.*, **86**, 9715-9721.
- Chanin, M. L. and A. Hauchecorne**, 1984: Lidar studies of temperature and density using Rayleigh scattering. *Handbook for MAP*, SCOSTEP Secr., University of Illionis, Ill., Urbana, **13**, 7.
- Chao, J. K., F. S. Kuo, Y. S. Chu, I. J. Fu, J. Rottger and C. H. Liu**, 1986: The first operation and results of the Chung-Li VHF radar, *Handbook for MAP*, SCOSTEP Secr., University of Illionis, Ill., Urbana, **20**, 359.
- Chilson, P. B., C. W. Ulbrich, M. F. Larsen, P. Perillat and J. E. Keener**, 1993: Observations of a tropical thunderstorm using a vertically pointing, dual frequency, collinear beam Doppler radar, *J. Atmos. Oceanic Technol.*, **10**, 663-673.
- Cifelli, R., S. A. Rutledge, D. J. Boccippio and T. Matejka**, 1996: Horizontal divergence and vertical velocity retrievals from Doppler radar and wind profiler observations in tropical convection, *J. Atmos. Oceanic Technol.*, **13**, 948-966.
- Collis, P. N., M. T. Rietveld, J. Rottger and W. K. Hocking**, 1992: Turbulence scattering layers in the middle-mesosphere observed by the EISCAT 224-MHz radar, *Radio Sci.*, **27**, 97-107.
- Connor, L. N. and S. K. Avery**, 1996: A three-year gravity wave climatology of the mesosphere and lower thermosphere over Kauai, *J. Geophys. Res.*, **101**, 4065-4077.
- Czechowsky, P., J. Klostermeyer, J. Rottger, R. Ruster, G. Schmidt and R. F. Woodman**, 1976: The SOUSY-VHF-radar for tropospheric, stratospheric and mesospheric sounding, *Preprints, 17<sup>th</sup> Radar Meteorology Conf.*, Seattle WA, American Meteorological Society, 349-353.
- Danielsen, E. F.**, 1968: Stratospheric-tropospheric exchange based upon radioactivity, ozone and potential vorticity, *J. Atmos. Sci.*, **25**, 502-518.

- Danielsen, E. F., R. S. Hipskind, W. L. Starr, J. F. Vedder, S. E. Gaines, D. Kley and K. K. Kelly**, 1991: Irreversible transport in the stratosphere by internal waves of short vertical wavelength, *J. Geophys. Res.*, **96**, 17433–17452.
- Danielsen, E. F.**, 1993: In situ evidence of rapid, vertical, irreversible transport of lower tropospheric air into the lower tropical stratosphere by convective cloud turrets and by larger-scale upwelling in tropical cyclones, *J. Geophys. Res.*, **98**, 8665-8868.
- Dewan, E. M., R. H. Picard, R. R. O'Neil, H. A. Gardiner, J. Gibson, J. D. Mill, E. Richards, M. Kendra and W. O. Gallery**, 1998: MSX satellite observations of thunderstorm-generated gravity waves in midwave infrared images of the upper stratosphere, *Geophys. Res. Lett.*, **25**, 939-942.
- Dhaka, S. K., P. K. Devarajan, Y. Shibagaki, R. K. Choudhary and S. Fukao.**, 2001: Indian MST radar observations of gravity wave activities associated with tropical convection, *J. Atmos. Solar Terr. Phys.*, **63**, 1631-1642.
- Dhaka, S. K., R. K. Choudhary, S. Malik, Y. Shibagaki, M. D. Yamanaka and S. Fukao.**, 2002: Observable signatures of a convectively generated wave field over the tropics using Indian MST radar at Gadanki (13.5°N, 79.2°E), *Geophys. Res. Lett.*, **29**, 1872- 1875.
- Dhaka, S. K., M. Takahashi, Y. Shibagaki, M. D. Yamanaka and S. Fukao.**, 2003: Gravity wave generation in the lower stratosphere due to passage of the typhoon 9426 (Orchid) observed by the MU radar at Shigaraki (34.85°N, 136.10°E), *J. Geophys. Res.*, **108**, 4595, doi:10.1029/2003/JD003489.
- Dickinson, M. J. and J. Molinari.**, 2002: Mixed Rossby-gravity waves and Western Pacific tropical cyclogenesis Part I: Synoptic evolution, *J. Atmos. Sci.*, **59**, 2183-2196
- Dobson, G. M. B.**, 1956: Origin and distribution of polyatomic molecules in the atmosphere, *Proc. Roy. Soc. London*, **236A**, 187–193.
- Dunkerton, T. J.**, 1982: Wave transience in a compressible atmosphere. Part III: The saturation of internal gravity waves in the mesosphere, *J. Atmos. Sci.*, **39**, 1042-1051.
- Dunkerton, T. J.**, 1984: Inertia-gravity waves in the stratosphere, *J. Atmos. Sci.*, **41**, 3396-3404.
- Dunkerton, T. J. and N. Butchart.**, 1984: Propagation and selective transmission of internal gravity waves in a sudden warming, *J. Atmos. Sci.*, **41**, 1443-1460.
- Dutta, G., B. Bapiraju, P. Balasubrahmanyam and H. Aleem Basha**, 1999: VHF radar observations of gravity waves at a low latitude, *Ann. Geophys.*, **17**, 1012-1019.

- Dvorak, V.F.**, 1975: Tropical cyclone intensity analysis and forecasting from satellite imagery, *Mon. Wea. Rev.*, **103**, 420-430.
- Eckermann S. D.**, 1995: Effect of background winds on vertical wavenumber spectra of atmospheric gravity waves, *J. Geophys. Res.*, **100**, 14097-14 112.
- Eckermann, S. D., I. Hirota and W. K. Hocking**, 1995: Gravity wave and equatorial wave morphology of the stratosphere derived from long-term rocket soundings. *Quart. J. Roy. Meteor. Soc.*, **121**, 149-186.
- Ecklund, W. L., D. A. Carter and B. B. Balsley.**, 1979: Continuous measurement of upper atmospheric winds and turbulence using a VHF Doppler radar: preliminary results, *J. Atmos. Terr. Phys.*, **41**, 983-994.
- Eliassen, A. and E. Palm**, 1960: On the transfer of energy in stationary mountain waves, *Geophys. Norv.*, **22**, 1-23.
- Elliot, R. S.**, 1985: *Antenna, Theory and Design*, Prentice-Hall, Eaglewood Cliffs, NJ.
- Emanuel, K. A.**, 1987: The dependence of hurricane intensity on climate, *Nature*, **326**, 483-485.
- Evans, J. L. and R. J. Allen**, 1992: El Nino/Southern Oscillation modification to the structure of the monsoon and tropical activity in the Australian region, *Int. J. Climatol.*, **12**, 611-623.
- Farley, D. T.**, 1985: On-line data processing techniques for MST radars, *Radio Sci.*, **20**, 1177-1184.
- Fovell, R., D. Durran and J. R. Holton**, 1992: Numerical simulations of convectively generated stratospheric gravity waves, *J. Atmos. Sci.*, **49**, 1427-1442.
- Friend, A. W.**, 1949: Theory and practice of tropospheric sounding by radar, *Proc. IEEE*, **37**, 116-138.
- Frisch, A. S., B. L. Weber, R. G. Strauch and D. A. Merritt.**, 1986: The altitude coverage of the Colorado Wind Profilers at 50, 405, and 915 MHz, *J. Atmos. Oceanic Technol.*, **3**, 680-692.
- Fritts D. C.**, 1984: Gravity wave saturation in the middle atmosphere: A review of theory and observations, *Rev. Geophys. Space Phys.*, **22**, 275-308.
- Fritts, D. C., M. A. Geller, B. B. Balsley, M. L. Chanin, I. Hirota, J. R. Hotton, S. Kato, R. S. Lindzen, M. R. Schoeberl, R. A. Vincent and R. F. Woodman**, 1984: Research status and recommendations from the Alaska workshop on gravity waves and turbulence in the middle atmosphere, *Bull. Amer. Meteor. Soc.*, **65**, 149-159.

- Fritts, D. C. and P. K. Rastogi**, 1985: Convective and dynamical instabilities due to gravity wave motions in the lower and middle atmosphere: Theory and observations, *Radio Sci.*, **20**, 1247–1277.
- Fritts, D. C. and R. A. Vincent**, 1987: Mesospheric momentum flux studies at Adelaide, Australia: Observations and a gravity wave/tidal interaction model. *J. Atmos. Sci.*, **44**, 605-619.
- Fritts, D. C., T. Tsuda, T. E. VanZandt, S. A. Smith, T. Kato, S. Fukao and S. Kato**, 1990: Studies of velocity fluctuations in the lower atmosphere using MU radar:II Momentum flux and energy densities, *J. Atmos. Sci.*, **47**, 51-66.
- Fritts, D. C. and G. D. Nastrom**, 1992: Sources of mesoscale variability of gravity waves. Part II: frontal, convective and jet stream excitation, *J. Atmos. Sci.*, **49**, 111-127.
- Fukao, S., T. Sato, T. Tsuda, S. Kato, K. Wakasugi and T. Makahira**, 1985a: The MU radar with an active phased array system: 1. Antenna and power amplifiers, *Radio Sci.*, **20**, 1155-1168.
- Fukao, S., K. Wakasugi, T. Sato, S. Morimoto, T. Tsuda, I. Hirota, I. Kimura and S. Kato**, 1985b: The MU radar with an active phased array system: 2. In-house equipment, *Radio Sci.*, **20**, 1169-1176.
- Fukao, S., T. Tsuda, T. Sato, S. Kato, K. Wakasugi and T. Makahira**, 1985c: Direct measurement of air and precipitation particle motion by very high frequency Doppler radar, *Nature*, **316**, 712-714.
- Fukao, S., T. Sato, T. Tsuda, S. Kato, M. Inaba and I. Kimura**, 1987: VHF Doppler radar determination of the momentum flux in the upper troposphere and lower stratosphere: Comparison between the three and four-beam methods, *J. Atmos. Oceanic. Technol.*, **5**, 57-69.
- Fukao, S., M. D. Yamanaka, T. Sato, T. Tsuda and S. Kato**, 1988: Three-dimensional air motions over the Baiu front observed by a VHF band Doppler radar: A case study, *Mon. Wea. Rev.*, **116**, 281-292.
- Fukao, S., M. D. Yamanaka, H. Matsumoto, T. Sato, T. Tsuda and S. Kato**, 1989: Wind fluctuations near a cold vortex-tropopause funnel system observed by the MU radar, *Pure Appl. Geophys.*, **130**, 463–479.
- Fukao, S., T. Tsuda, T. Sato and S. Kato**, 1990: Equatorial radar system, *Space Res.*, **10**, 151-154.
- Gage, K. S. and J. L. Green**, 1978: Evidence for specular reflection from monostatic VHF radar observations of the stratosphere, *Radio Sci.*, **13**, 991-1001.
- Gage, K. S. and J. L. Green**, 1979: Tropopause detection by partial specular reflection using VHF radar, *Science*, **203**, 1238-1240.

- Gage, K. S. and B. B. Balsley**, 1980: On the scattering and reflection mechanisms contributing to clear air radar echoes from the troposphere, stratosphere and mesosphere, *Radio Sci.*, **15**, 243-257.
- Gage, K. S. and J. L. Green**, 1982a: An objective method for the determination of tropopause height from VHF radar observation, *J. Appl. Meteor.*, **21**, 1150–1154.
- Gage, K. S., and J. L. Green.**, 1982b: A technique for determining temperature profile from VHF radar observations, *J. Appl. Meteor.*, **21**, 1146–1149.
- Gage, K. S., W. L. Ecklund and B. B. Balsley**, 1985: A modified Fresnel scattering model for the parameterization of Fresnel returns, *Radio Sci.*, **20**, 1493-1501.
- Gage, K. S., W. L. Ecklund, A. C. Riddle and B. B. Balsley.**, 1986: Objective tropopause height determination using low-resolution VHF radar observations, *J. Atmos. Oceanic Technol.*, **3**, 248-254.
- Gage, K. S. and G. C. Reid**, 1987: Longitudinal variations in tropical tropopause properties in relation to tropical convection and ENSO events, *J. Geophys. Res.*, **92**, 14197-14203.
- Garcia, R. R. and S. Solomon**, 1985: The effect of breaking gravity waves on the dynamical and chemical composition of the mesosphere and lower thermosphere, *J. Geophys. res.*, **90**, 3850-3868.
- Gardner, C. S. and D. G. Voelz**, 1987: Lidar studies of the night sodium layer over Urbana, Illinois. 2. Gravity waves, *J. Geophys. Res.*, **92**, 4673-4694.
- Ghosh, A. K., V. Sivakumar, K. Kishore Kumar and A. R. Jain**, 2001: VHF radar observation of atmospheric winds, associated shears and  $Cn^2$  at a tropical location: interdependence and seasonal pattern, *Ann. Geophys.*, **19**, 965-973.
- Ghosh, A. K., A. R. Jain and V. Sivakumar**, 2003: Simultaneous MST radar and radiosonde measurements at Gadanki (13.5°N, 79.2°E) 2. Determination of various atmospheric turbulence parameters, *Radio Sci.*, **38**, 1014, doi: 10.1029/2000RS002528.
- Gossard, E. E.**, 1962: Vertical flux of energy into the lower ionosphere from internal gravity waves generated in the troposphere, *J. Geophys. Res.*, **67**, 745-757.
- Gossard, E. E.**, 1988: Measuring drop-size distributions in clouds with a clear-air-sensing Doppler radar, *J. Atmos. Ocean. Technol.*, **5**, 640-649.
- Gossard, E. E., D. E. Wolfe, K. P. Moran, R. A. Paulus, K. D. Anderson and L. T. Rogers**, 1998: Measurement of clear-air gradients and turbulence properties with radar wind profilers, *J. Atmos. Ocean. Technol.*, **15**, 321-342.
- Graham, N. E. and T. P. Barnett**, 1987: Sea surface temperature, surface wind divergence, and convection over tropical oceans, *Science*, **238**, 657-659.



- Gray, W. M. and D. J. Shea**, 1973: The hurricane's inner core region. II. Thermal stability and dynamics characteristics, *J. Atmos. Sci.*, **30**, 1565-1576.
- Gray, W. M.**, 1979: Hurricanes: Their formation, structure and likely role in the tropical circulation. *Meteorology over the tropical oceans*, Roy. Meteor. Soc., James Glaisher House, Grenville Place, Bracknell, Berkshire, RG12 1BX, 155.
- Gray, W. M.**, 1991: Comments on "Gradient balance in tropical cyclones", *J. Atmos. Sci.*, **48**, 1201-1208.
- Green, J. L., J. M. Warnock, R. H. Winkler and T. E. VanZandt**, 1975: Studies of winds in the upper troposphere with a sensitive VHF radar, *Geophys. Res. Lett.*, **2**, 19-21.
- Green, J. L. and K. S. Gage**, 1980: Observations of stable layers in the troposphere and stratosphere using VHF radar, *Radio Sci.*, **15**, 395-405.
- Gyakum, J. R.**, 1983: On the evolution of the QE II storm. Part I: Synoptic aspects, *Mon. Wea. Rev.*, **111**, 1137-1155.
- Hamilton, K.**, 1991: Climatological statistics of stratospheric intertigravity waves deduced from historical rocketsonde wind and temperature data, *J. Geophys. Res.*, **96**, 20831-20839.
- Hansen A. R., G. D. Nastrom, J. A. Otkin and F. D. Eaton**, 2002: MST radar observations of gravity waves and turbulence near thunderstorms, *J. Appl. Meteor.*, **41**, 298-305.
- Hardy, K. R. and K. S. Gage.**, 1990: The history of radar studies of the clear atmosphere, *Radar in Meteorology*, Amer. Meteor. Soc., 130.
- Hauchecorne, A., M. -L. Chanin, P. Keckhut and D. Nedeljkovic**, 1992: LIDAR monitoring of the temperature in the middle and lower atmosphere, *App. Phys.*, **B55**, 29-34.
- Haurwitz, B.**, 1935: The height of tropical cyclones and the eye of the storm, *Mon. Wea. Rev.*, **63**, 45-49.
- Hawkins, H. F. and D. T. Rubsam**, 1968: Hurricane Hilda, 1964. II. Structure and budgets of the hurricane on October 1, 1964, *Mon. Wea. Rev.*, **104**, 418-442.
- Haynes, P. H., C. J. Marks, M. E. McIntyre, T. G. Shepherd and K. P. Shine**, 1991: On the "downward control" of extratropical diabatic circulations by eddy-induced mean zonal forces, *J. Atmos. Sci.*, **48**, 651-678.
- Highwood, E.J. and B. J. Hoskins**, 1998: The tropical tropopause, *Q. J. Roy. Meteor. Soc.*, **124**, 1579-1604.

- Hilderbrand, P. H. and R. S. Sekhon**, 1974: Objective determination of the noise level in Doppler spectra, *J. Appl. Meteor.*, **13**, 808-811.
- Hines, C. O.**, 1960: Internal atmospheric gravity waves at ionospheric heights, *Can. J. Phys.*, **38**, 1441-1481.
- Hints, E. J., K. A. Boering, E. M. Weinstock, J. G. Anderson, B. L. Gary, L. Pfister, B. C. Daube, S. C. Wofsy, M. Loewenstein, J. R. Podolske, J. J. Margitan and T. P. Bui**, 1998: Troposphere to stratosphere transport in the lowermost stratosphere from measurements of H<sub>2</sub>O, CO<sub>2</sub>, N<sub>2</sub>O and O<sub>3</sub>, *Geophys. Res. Lett.*, **25**, 2655-2658.
- Hirota, I.**, 1984: Climatology of gravity waves in the middle atmosphere, *J. Atmos. Terr. Phys.*, **46**, 767-773.
- Hirota, I. and T. Niki**, 1986: Inertia-gravity waves in the troposphere and stratosphere observed by the MU radar, *J. Meteor. Soc., Japan*, **64**, 995-999.
- Hocking, W. K.**, 1979: Angular and temporal characteristics of partial reflections from the D-region of the ionosphere, *J. Geophys. Res.*, **84**, 845-851.
- Hocking, W. K.**, 1985: Measurement of turbulent energy dissipation rates in the middle atmosphere by radar techniques: A review, *Radio Sci.*, **20**, 1403-1422.
- Hocking, W. K.**, 1996: An assessment of the capabilities and limitations of radars in measurements of upper atmosphere turbulence, *Adv. Space. Res.*, **17**, 37-47.
- Hocking, W. K.**, 1997: Strengths and limitations for MST radar measurements of middle atmosphere winds, *Ann. Geophys.*, **15**, 1111-1122.
- Hoinka, K.P.**, 1999: Temperature, humidity, and wind at the global tropopause, *Mon. Wea. Rev.*, **127**, 2248-2265.
- Holton, J. R.**, 1975: *The Dynamic Meteorology of the Stratosphere and Mesosphere*, American Meteorological Society, Boston.
- Holton, J. R.**, 1982: The role of gravity wave induced drag and diffusion in the momentum budget of the mesosphere, *J. Atmos. Sci.*, **39**, 791-799.
- Holton, J. R., P. H. Haynes, M. E. McIntyre, A. R. Douglass, R. B. Rood and L. Pfister**, 1995: Stratosphere-troposphere exchange, *Rev. Geophys.*, **33**, 403-439.
- Hooper, D. A. and L. Thomas**, 1995: Aspect sensitivity of VHF scatterers in the troposphere and stratosphere from comparisons of power in off-vertical beams, *J. Atmos. Terr. Phys.*, **57**, 655-663.
- Hoskins, B. J., M. E. McIntyre and A. W. Robertson**, 1985: On the use and significance of isentropic potential vorticity maps, *Quart. J. Roy. Meteor. Soc.*, **111**, 877-946.

- Hung, R. J., Y. D. Tsao, D. L. Johnson, A. J. Chen, C. H. Lin, J. M. Cheng and C. M. You.**, 1988: VHF radar remote sensing of atmospheric parameters over Taiwan during the time period of typhoon Wayne, *Int. J. Remote Sensing*, **9**, 477-493.
- Jain, A. R., Y. J. Rao, P. B. Rao, V. K. Anandan, S. H. Damle, P. Balamuralidhar, A. Kulkarni and G. Viswanathan**, 1995: Indian MST radar 2. First scientific results in ST mode, *Radio Sci.*, **30**, 1139-1158.
- Jain, A. R., Y. J. Rao and P. B. Rao.**, 1997: Aspect sensitivity of the received radar backscatter at VHF: Preliminary observations using the Indian MST radar, *Radio Sci.*, **32**, 1249-1260.
- Jain, A. R., A. K. Ghosh, V. Sivakumar and K. Kishore Kumar**, 2003: Simultaneous MST radar and radiosonde measurements at Gadanki (13.5°N, 79.2°E), 1, Causative mechanism and characteristics of radar backscatterers at VHF, *Radio Sci.*, **38**, 1013, doi:10.1029/2000RS002527.
- Jaya Rao, Y., A. R. Jain, V. K. Anandan, P. B. Rao, G. Viswanathan and R. Arvindan**, 1994: Some observations of tropical tropopause using ST made of the Indian MST radar: Multiple stable layer structure, *Indian J. Radio Space Phys.*, **23**, 75– 85.
- Jordan, C. L. and E. S. Jordan.**, 1954: On the mean thermal structure of tropical cyclones, *J. Meteor.*, **11**, 440-448.
- Kato, S., T. Ogawa, T. Tsuda, T. Sato, I. Kimura and S. Fukao**, 1984: The middle and upper atmosphere radar: First results using a partial system, *Radio. Sci.*, **19**, 1475-1484.
- Keckhut, P., M. L. Chanin and A. Hauchecorne**, 1990: Stratosphere temperature measurement using Raman lidar, *Appl. Opt.*, **29**, 5182-5186.
- Kley, D., A. L. Schmeltekopf, K. Kelly, R. H. Winkler, T. L. Thompson and M. McFarland**, 1982: Transport of water through the tropical tropopause, *Geophys. Res. Lett.*, **9**, 617-620.
- Knollenberg, R. G., A. J. Dascher and D. Huffman**, 1982: Measurements of the aerosol and ice crystal populations in tropical stratospheric cumulonimbus anvils, *Geophys. Res. Lett.*, **9**, 613-616.
- Kobayashi, T., A. Adachi, T. Nagai and S. Asano**, 1999: Detection of cirrus clouds with UHF wind profiling radar, *J. Atmos. Ocean. Tech.*, **16**, 298-304.
- Koteswaram, P.**, 1967: On the structure of hurricanes in the upper troposphere and lower stratosphere, *Mon. Wea. Rev.*, **95**, 541-564.

- Krishna Murthy, B. V., K Satheesan, K. Parameswaran, M. N. Sasi, Geetha Ramkumar, Y. Bhavanikumar, K. Raghunath and M. Krishnaiah**, 2002: Equatorial waves in temperature in the altitude range 4 to 70 km, *Quar. J. Roy. Meteor. Soc.*, **128**, 819–837.
- Kumar, K., S. Singh, K. K. Mahajan and N. K. Sethi**, 1994: A study of tropopause and stable layers in the lower atmosphere from the Indian MST Radar, *Indian J. Radio Space Phys.*, **23**, 71-74.
- Kuo, F. S. and H. Y. Lue**, 1994: Effect of the wave-shear interaction on gravity wave activity in the lower and middle atmosphere, *J. Atmos. Terr. Phys.*, **56**, 1147-1155.
- Kurihara, Y.**, 1976: On the development of spiral bands in a tropical cyclone, *J. Atmos. Sci.*, **33**, 940–958.
- Lander, M. A.**, 1994: An exploratory analysis of the relationship between tropical storm formation in the western North Pacific and ENSO, *Mon. Wea. Rev.*, **122**, 6636-6651.
- Lane, T. P., M. J. Reeder and T. L. Clark**, 2001a: Numerical modeling of gravity wave generation by deep tropical convection, *J. Atmos. Sci.*, **58**, 1249–1274.
- Lane, T. P., M. J. Reeder and T. L. Clark**, 2001b: Modeling the generation of gravity waves by a maritime continent thunderstorm. *Quart. J. Roy. Meteor. Soc.*, **127**, 2705–2724.
- Larsen, M. F., R. F. Woodman, T. Sato and M. K. Davis**, 1986: Power spectra of oblique velocities in the troposphere and lower stratosphere observed at Arecibo, Puerto Rico, *J. Atmos. Sci.*, **43**, 2230-2240.
- Larsen, M. F. and J. Rottger**, 1982: VHF and UHF Doppler radars as tools for synoptic research, *Bull. Amer. Meteor. Soc.*, **63**, 996-1008.
- Larsen, M.F. and J. Rottger**, 1983: Comparison of tropopause height and frontal boundary locations based on radar and radiosonde data. *Geophys. Res. Lett.*, **10**, 325-328.
- Larsen, M. F. and J. Rottger**, 1987: Observations of thunderstorm reflectivities and Doppler velocities measured at VHF and UHF, *J. Atmos. Oceanic. Tech.*, **4**, 151-159.
- Larsen M. F., J. Rottger and T. S. Dennis.**, 1988: A comparison of operational analysis and VHF wind profiler vertical velocities, *Mon. Wea. Rev.*, **116**, 48-59.
- Larsen, M. F., I. S. Mikkelsen, J. W. Meriwether, R. Niciejewski and K. Vickery**, 1989: Simultaneous observations of neutral winds and electric fields at spaced locations in the dawn auroral oval, *J. Geophys. Res.*, **94**, 17235–17243.

- Lelieveld, J. and F. Dentener**, 2000: What controls tropospheric ozone?, *J. Geophys. Res.*, **105**, 3531-3551.
- Lesicar, D., W. K. Hocking and R. A. Vincent.**, 1994: Comparative studies of scatterers observed by MF radars in the Southern Hemisphere mesosphere. *J. Atmos. Terr. Phys.*, **56**, 581-591.
- Levy II, H., J. D. Mahlman and W. J. Moxim.**, 1980: A stratospheric source of reactive nitrogen in the unpolluted troposphere, *Geophys. Res. Lett.*, **7**, 441-444.
- Lindzen, R. S.**, 1981: Turbulence and stress owing to gravity wave and tidal breakdown, *J. Geophys. Res.*, **86**, 9707-9714.
- Ma, M. T.**, 1998: *Theory and Application of Antenna Arrays*, John Wiley, New York.
- Maguire, W. B. and S. K. Avery**, 1994: Retrieval of raindrop size distributions using two Doppler wind profilers: Model sensitivity testing, *J. Appl. Meteor.*, **33**, 1623-1635.
- Mandal. T. K., J. Y. N. Cho, P. B. Rao, A. R. Jain, S. K. Peshin, S. K. Srivastva, A. K. Bohra and A. P. Mitra**, 1998: Stratosphere-troposphere ozone exchange observed with the Indian MST radar and simultaneous balloon-borne ozonesonde, *Radio Sci.*, **33**, 861-893.
- Matsuno, T.**, 1982: A quasi one-dimensional model of the middle atmosphere circulation interacting with internal gravity waves, *J. Meteor. Soc. Japan.*, **60**, 215-226
- Matsumoto, S. and H. Okamura**, 1985: The internal gravity wave observed in the Typhoon T8124 (Gay), *J. Meteor. Soc. Japan.*, **63**, 37-51.
- Maynard, R.H.**, 1945: Radar and weather, *J. Meteor.*, **2**, 214-226.
- McLandress, C.**, 1998: On the importance of gravity waves in the middle atmosphere and their parameterization in general circulation models, *J. Atmos. Solar Terr. Phys.*, **60**, 1357-1383.
- Mc Afee, J. R., B. B. Balsley and K. S. Gage**, 1989: Momentum flux measurements over mountains: problems associated with the symmetric two-beam radar technique, *J. Atmos. Oceanic. Technol.*, **6**, 500-508.
- Metcalf, J. I.**, 1975: Gravity waves in a low-level inversion, *J. Atmos. Sci.*, **32**, 351-361
- Miyahara, S., Y. Hayashi and J.D. Mahlman**, 1986: Interactions between gravity waves and the planetary scale flow simulated by the GFDL "SKYHI" general circulation model, *J. Atmos. Sci.*, **43**, 1844-1861.

- Molina, M. J. and F. S. Rowland**, 1974: Stratospheric sink for chlorofluoromethanes: Chlorine atom catalyzed destruction of ozone, *Nature*, **249**, 810-812.
- Mote, P. W., K. H. Rosenlof, J. S. Holton, R. S. Harwood and J. W. Waters**, 1995: Seasonal variations of water vapor in the tropical lower stratosphere, *Geophys. Res. Lett.*, **22**, 1093–1096.
- Mote, P. W., K. H. Rosenlof, M. E. McIntyre, E. S. Carr, J. C. Gille, J. R. Holton, J. S. Kinnnersley, H. C. Pumphrey, J. M. Russel III and J. W. Waters**, 1996: An atmospheric tape recorder: The imprint of tropical tropopause temperatures on stratospheric water vapor, *J. Geophys. Res.*, **101**, 3989–4006.
- Muschinski, A., P. B. Chilson, S. Kern, J. Nielinger, G. Schmidt and T. Prensil**, 1999: First frequency- domain interferometry observations of large-scale vertical motion in the atmosphere, *J. Atmos. Sci.*, **56**, 1248-1258.
- Nakamura, T., T. Tsuda, M. Yamamoto, S. Fukao, S. Kato and R. A. Vincent**, 1993: Comparison of the mesospheric gravity waves observed with the MU radar (35 °N) and the Adelaide MF radar (35 °S), *Geophys. Res. Lett.*, **20**, 803-806.
- Nastrom, G. D., B. B. Balsley and D. A. Carter**, 1982: Mean meridional winds in the mid- and high-latitude summer mesosphere, *Geophys. Res. Lett.*, **9**, 139-142.
- Nastrom, G. D., W. L. Ecklund and K. S. Gage**, 1985: Direct measurement of large-scale vertical velocities using clear-air Doppler radars, *Mon. Wea. Rev.*, **113**, 708-718.
- Nastrom, G. D., K. S. Gage and W. L. Ecklund**, 1986: Variability of turbulence, 4–20 km, in Colorado and Alaska from MST radar observations, *J. Geophys. Res.*, **91**, 6722–734.
- Nastrom, G. D., M. R. Peterson, J. L. Green, K. S. Gage and T. E. VanZandt**, 1989: Sources of gravity wave activity seen in the vertical velocities observed by the Flatland VHF radar, *J. Appl. Meteor.*, **29**, 783-792.
- Nastrom, G. D. and D. C. Fritts.**, 1992: Sources of mesoscale variability of gravity waves. Part I: Topographic excitation, *J. Atmos. Sci.*, **49**, 101-110.
- Nastrom, G. D., W. L. Clark, K. S. Gage, T. E. VanZandt, J. M. Warnock, R. Creasey and P.M. Pauley**, 1994: Case studies of the vertical velocity seen by the Flatland radar compared with indirectly computed values, *J. App. Meteor.*, **11**, 14–21.
- Nastrom G. D. and T. E. VanZandt**, 1996: Biases due to gravity waves in wind profiler measurements of winds, *J. App. Meteor.*, **35**, 243–257.
- Nastrom, G. D., R. Ruester and G. Schmidt**, 1998: The coupling of vertical velocity and signal power observed with the SouSy VHF radar, *J. Appl. Meteor.*, **37**, 114-119.

- Newell, R. E. and S. Gould-Stewart**, 1981: A stratospheric fountain?, *J. Atmos. Sci.*, **38**, 2789- 2796.
- O'Sullivan, D. and T. J. Dunkerton**, 1995: Generation of inertia-gravity waves in a simulated life cycle of baroclinic instability, *J. Atmos. Sci.*, **52**, 3695±3716.
- Palmen, E. H.**, 1948: On the formation and structure of tropical cyclones. *Geophysica* , Univ. of Helsinki, **3**, 26-38.
- Palmer, T. N., G. J. Shutts, and R. Swinbank**, 1986: Alleviation of a systematic westerly bias in general circulation and numerical weather prediction models through an orographic gravity wave drag parameterization. *Quart. J. Roy. Meteor. Soc.*, **112**, 1001-1039
- Parrish, J. R., R. W. Burpee, F. D. Marks, Jr. and R. Grebe**, 1982: Rainfall patterns observed by digitized radar during the landfall of hurricane Frederic (1979), *Mon. Wea. Rev.*, **110**, 1933-1944.
- Pekeris, C. L.**, 1947: Note on the scattering of radiation in an inhomogeneous medium, *Phy. Rev.*, **71**, 268-269.
- Penn, S.**, 1965: Ozone and temperature structure in a hurricane, *J. App. Meteor.*, **4**, 212-216.
- Petzold, K., B. Naujokat and K. Neugebahren**, 1994: Correlation between stratospheric temperature, total ozone and tropospheric weather systems, *Geophys. Res. Lett.*, **21**, 1203 - 1206.
- Plumb, R. A.**, 1996: A “tropical pipe” model of stratospheric transport, *J. Geophys. Res.*, **101**, 3957–3972.
- Powell, M. D.**, 1982: The transition of the hurricane Frederic boundary-layer wind fields from the open Gulf of Mexico to landfall, *Mon. Wea. Rev.*, **110**, 1912-1932.
- Powell, M. D.**, 1987: Changes in the low-level kinematic and thermodynamic structure of Hurricane Alicia (1983) at landfall, *Mon. Wea. Rev.*, **115**, 75–99.
- Prichard, I. T. and L. Thomas**, 1993: Radar observations of gravity-wave momentum fluxes in the troposphere and lower stratosphere, *Ann. Geophys.*, **11**, 1075-1083.
- Prichard, I. T., L. Thomas and R.M. Worthington**, 1995: The characteristics of mountain waves observed by radar near the west coast of Wales, *Ann. Geophys.*, **13**, 757-767.
- Raja, R. V. M. K., G. C. Asnani, P. S. Sewekar, A. R. Jain, D. N. Rao, S. V. Rao, P. Kishore and M. Hareesh**, 1999: Layered clouds in the Indian monsoon region, *Proc. Indian Acad. Sci. (Earth & Planet. Sci.)*, **108**, 287-295.

- Rajopadhyaya, D. K., P. T. May and R. A. Vincent**, 1993: A general approach to the retrieval of raindrop size distributions from wind profiler Doppler spectra: Modeling results, *J. Atmos. Oceanic Technol.*, **10**, 710–717.
- Ralph, M. F., P. J. Neiman and D. Ruffieux.**, 1996: Precipitation identification from radar wind profiler spectral moment data: Vertical velocity histogram, velocity variance and signal power vertical velocity correlations, *J. Atmos. Oceanic Technol.*, **13**, 545–559.
- Ramanatham, R., I. Subbaramayya, N. J. Rao and J. K. Patnaik**, 1969: Tropopause over India, *Pure Appl. Geophys.*, **75**, 355-364.
- Ramaswamy, V., M. D. Schwarzkopf and K. P. Shine**, 1992: Radiative forcing of climate from halocarbon-induced global stratospheric ozone loss, *Nature*, **355**, 810-812.
- Rao, P. B., A. R. Jain, P. Kishore, P. Balamuralidhar, S. H. Damle and G. Viswanathan**, 1995: Indian MST radar: 1. System description and sample wind measurements in ST mode, *Radio Sci.*, **30**, 1125-1138.
- Rao, D. N., P. Kishore, T. N. Rao, S. V. B. Rao, K. K. Reddy, M. Yarraiah and M. Harish**, 1997: Studies of refractivity structure constant, eddy dissipation rate and momentum flux at a tropical latitude, *Radio Sci.*, **32**, 1375-1389.
- Rastogi P. K. and J. Rottger.**, 1982: VHF radar observations of coherent reflections in the vicinity of the tropopause, *J. Atmos. Terr. Phys.*, **44**, 461-469.
- Rechou, A., V. Barabash, P. Chilson, S. Kirkwood, T. Savitskaya and K. Stebel**, 1999: Mountain wave motions determined by the Esrange MST radar, *Ann. Geophys.*, **17**, 957-970.
- Reddy, K. K., T. Kozu, Y. Ohno, K. Nakamura, A. Higuchi, K. Madhu Chandra Reddy, V. K. Anandan, P. Srinivasulu, A. R. Jain, P. B. Rao, R. Ranga Rao, G. Viswanathan and D. N. Rao**, 2002: Planetary boundary layer and precipitation studies using lower atmospheric wind profiler over tropical India, *Radio Sci.*, **37**, No.4, 1061, doi:10.1029/2000RS002538.
- Reid, G. C. and K. S. Gage**, 1985: Interannual variations in the height of the tropical tropopause, *J. Geophys. Res.*, **90**, 5629–5635.
- Reid, G. C. and K. S. Gage**, 1996: The tropical tropopause over the western Pacific: wave driving, convection, and the annual cyclone, *J. Geophys. Res.*, **101**, 21233–21341.
- Reid, I. M. and R. A. Vincent**, 1987: Measurements of mesospheric gravity wave momentum fluxes and mean flow accelerations at Adelaide, Australia, *J. Atmos. Terr. Phys.*, **49**, 443-460.



- Revathy, K., S. R. P. Nayar and B. V. Krishna Murthy**, 1996: Deduction of temperature profile from MST radar observations of vertical wind, *Geophys. Res. Lett.*, **23**, 285–288.
- Riddle, A. C.**, 1983: Parameterization of spectrum, *Handbook for MAP*, SCOSTEP Secretariat, University of Illinois, Ill., Urbana, **9**, 546.
- Riddle, A. C., K. S. Gage and B.B. Balsley**, 1983: An algorithm to monitor continuously the tropopause height using a VHF radar, *21<sup>st</sup> Conf. On Radar meteorology*, Am. Meteor. Soc., Boston.
- Riddle, A. C., K. S. Gage and B.B. Balsley**, 1984: Practical use of a tropopause height determination algorithm on an MST radar data set, *Handbook for MAP*, SCOSTEP Secretariat, University of Illinois, Ill., Urbana, **14**, 69.
- Rossa, A.M., H. Wernli and H.C. Davies**, 2000: Growth and decay of an extra-tropical cyclone's PV-tower, *Meteor. Atmos. Phys.*, **73**, 139-156.
- Rosenlof, K. H.**, 1995: The seasonal cycle of the residual mean meridional circulation in the stratosphere, *J. Geophys. Res.*, **100**, 5173-5191.
- Rothermel, J., C. Kessinger and D.L. Davis**, 1985: Dual Doppler lidar measurement of winds in the JAWS experiment. *J. Atmos. Oceanic Technol.*, **2**, 138-147.
- Rottger, J. and C. H. Liu**, 1978: Partial reflection and scattering of VHF radar signal from the clear air atmosphere, *Geophys. Res. Lett.*, **5**, 357–360.
- Rottger, J.**, 1980: Reflection and scattering of VHF radar signals from atmospheric reflectivity structures, *Radio Sci.*, **15**, 259-276.
- Rottger, J., P. Czechowsky and G. Schmidt**, 1981: First low-power VHF radar observations of tropospheric, stratospheric and mesospheric winds and turbulence at the Arecibo Observatory, *J. Atmos. Terr. Phys.*, **43**, 789– 800.
- Rottger, J., C. H. Liu, J. K. Chao, A. J. Chen, C. J. Pan and I-J. Fu**, 1990: Spatial interferometer measurements with the Chung-Li VHF radar, *Radio Sci.*, **25**, 503-515.
- Rottger, J., C. J. Pan, C. H. Liu and S.Y. Su**, 1991: Wind field and reflectivity variations investigated with the Chung – Li VHF radar during typhoon passage, *Proceedings of International Conference on Mesoscale Meteorology and TAMEX*, The Meteorological Society of Republic of China, Taiwan and the American Meteorological Society, Taipei, 373 – 379.
- Rottger, J., C. H. Liu, C. J. Pan and S. Y. Su.**, 1995: Characteristics of lightning echoes observed with VHF ST radar, *Radio Sci.*, **30**, 1085-1097.
- Rottger, J.**, 2000: ST radar observations of atmospheric waves over mountainous areas: a review, *Ann. Geophys.*, **18**, 750–765.

- Sarkar, B. K., P. B. Tole and A. Agarwal**, 1988: Feeder network for the Indian MST radar, *Handbook for MAP*, SCOSTEP Secr., University of Illionis, Ill., Urbana, **28**, 523.
- Sato, K.**, 1990: Vertical wind disturbances in the troposphere and lower stratosphere observed by the MU radar, *J. Atmos. Sci.*, **47**, 2803-2817.
- Sato, K.**, 1993: Small-scale wind disturbances observed by the MU radar during the passage of Typhoon Kelly, *J. Atmos. Sci.*, **50**, 518-537.
- Sato, K. and T. J. Dunkerton**, 2002: Layered structure associated with low potential vorticity near the tropopause seen in high-resolution radiosondes over Japan, *J. Atmos. Sci.*, **59**, 2782-2800.
- Sato, T. and R. F. Woodman.**, 1982: Fine altitude resolution observations of stratospheric turbulent layers by the Arecibo 430-MHz radar, *J. Atmos. Sci.*, **39**, 2546-2552.
- Sato, T.**, 1989: Radar principles, *Handbook for MAP*, SCOSTEP Secr., University of Illionis, Ill., Urbana, **30**, 19.
- Sato, T., H. Doji, H. Iwai, I. Kimuar, S. Fukao, M. Yamamoto, T. Tsuda and S. Kato**, 1990: Computer processing for deriving drop-size distributions and vertical air velocities from VHF Doppler radar spectra, *Radio Sci.*, **25**, 961-973.
- Sato, T., N. Ao, M. Yamamoto, S. Fukao, T. Tsuda and S. Kato**, 1991: A typhoon observed with the MU radar, *Mon. Wea. Rev.*, **199**, 755-768.
- Senn, H. V. and H. W. Hiser**, 1957: Tracking hurricanes with radar, *Proceedings of 6<sup>th</sup> Weather Radar Conference*, 165-170.
- Shapiro, M. A.**, 1980: Turbulent mixing within tropopause folds as a mechanism for the exchange of chemical constituents between the stratosphere and the troposphere, *J. Atmos. Sci.*, **37**, 994-1004.
- Sherwood, S. C. and A. E. Dessler**, 2000: On the control of stratospheric humidity, *Geophys. Res. Lett.*, **27**, 2513-2516.
- Sherwood, S. C. and A. E. Dessler**, 2001: A model for transport across the tropical tropopause, *J. Atmos. Sci.*, **58**, 765-79.
- Shibagaki, Y., M. D. Yamanaka, S. Shimizu, H. Uyeda, A. Watanabe, Y. Maekawa and S. Fukao**, 2000: Meso- $\beta$  to - $\gamma$  scale wind circulations associated with precipitating clouds near Baiu Front observed by the MU and meteorological radars, *J. Meteor. Soc. Japan*, **78**, 69-91.
- Shibata, T., T. Fukuda and M. Maeda**, 1986: Density fluctuations in the middle atmosphere over Fukuoka observed by a XeF Rayleigh lidar, *Geophys. Res. Lett.*, **13**, 1121-1124.

- Sienkiewicz, M. E., and T. Gal-Chen**, 1989: Application of MST data to numerical weather prediction, *Handbook for MAP*, SCOSTEP Secr., University of Illinois, Ill., Urbana, **28**, 17.
- Smith, S. A., G. J. Romick and K. Jayaweera**, 1983: PokerFlat MST radar observations of shear induced turbulence, *J. Geophys. Res.*, **88**, 5265-5271.
- Stohl, A. and T. Trickl**, 1999: A textbook example of long-range transport: Simultaneous observation of ozone maxima of stratospheric and North American origin in the free troposphere over Europe, *J. Geophys. Res.*, **104**, 30445-30462.
- Takahashi, M.**, 1999: Simulation of the quasibiennial oscillation in a general circulation model, *Geophys. Res. Lett.*, **26**, 1307-1310.
- Tatarski, V.I.**, 1961: *Wave propagation in a turbulent medium*, McGraw-Hill, New York.
- Thuburn, J. and G.C. Craig**, 1997: GCM tests of theories for the height of the tropopause, *J. Atmos. Sci.*, **54**, 869-82.
- Toumi, R., S. Bekki and K. S. Law**, 1994: Indirect influence of ozone depletion on climate forcing by clouds, *Nature*, **372**, 348-351.
- Tsuda, T., K. Hirose, S. Kato and M. P. Sulzer**, 1985: Some finding on correlation between the stratospheric echo power and the wind shear observed by the Aericoibo UHF radar, *Radio Sci.*, **20**, 1503- 1508.
- Tsuda, T.**, 1988: *Data acquisition and processing*, Lecture notes, International school on atmospheric radar, Kyoto, Japan, Nov. 24-28.
- Uccellini, L. W. and S. E. Koch**, 1987: The synoptic setting and possible energy sources for mesoscale wave disturbances, *Mon. Wea. Rev.*, **115**, 721-729.
- VanZandt, T. E., J. L. Green, K. S. Gage and W. L. Clark**, 1978: Vertical profiles of refractivity turbulence structure constant: comparison of observations by the Sunset radar with a new theoretical model, *Radio Sci.*, **13**, 819-829.
- Vaughan, G. and C. Timmis**, 1998: Transport of near-tropopause air into the lower midlatitude stratosphere, *Quart. J. Roy. Meteor. Soc.*, **124**, 1559-1578.
- Vincent, R. A., W. G. Elford and B. H. Briggs**, 1982: A VHF radar for atmospheric studies, *Aust. Physicist*, **19**, 70-73.
- Vincent, R. A. and I. M. Reid**, 1983: HF Doppler measurements of mesospheric gravity wave momentum fluxes, *J. Atmos. Sci.*, **40**, 1321-1333.
- Vincent, R. A.**, 1984: MF/HF radar measurements of the dynamics of the mesopause region: a review, *J. Atmos. Terr. Phys.*, **46**, 961-976.

- Vincent, R. A., P. T. May, W. K. Hocking, W. G. Elford, B. H. Candy and B. H. Briggs**, 1987: First results with the Adelaide VHF radar: spaced antenna studies of tropospheric winds, *J. Atmos. Terr. Phys.*, **39**, 353-366.
- Vincent R. A.**, 1990: Gravity waves in the middle atmosphere of the southern hemisphere: A review of observations, *Dynamics transport and photochemistry in the middle atmosphere of the southern hemisphere*, Kluwer Academic Publishers, Netherlands, 171.
- Wakasugi, K, A. Mizutani, M. Matsuo, S. Fukao and S. Kato**, 1986: A direct method for deriving drop-size distribution and vertical air velocities from VHF Doppler radar spectra, *J. Atmos. Oceanic Technol.*, **3**, 623-629.
- Warnock, J. M., T. E. Van Zandt, W. L. Clark, S. J. Franke, H. S. Kim, G. D. Nastrom and P. E. Johnston**, 1994: Measurements of synoptic-scale vertical velocities by two nearby VHF Doppler radars in very flat terrain, *J. Atmos. Oceanic Technol.*, **11**, 5-13.
- Waugh, D. W.**, 1996: Seasonal variation of isentropic transport out of the tropical stratosphere, *J. Geophys. Res.*, **101**, 4007-4023.
- Wexler, H.**, 1947, Structure of hurricanes as determined by radar, *Ann. N.Y. Acad. Sci.*, **48**, 821-844.
- Wilczak, J. M., T. W. Christian, D. E. Wolfe, R. J. Zamora and B. B. Stankov**, 1992: Observations of a Colorado tornado. Part I: Mesoscale environment and tornadogenesis, *Mon. Wea. Rev.*, **120**, 497-520.
- Willoughby, H. E.**, 1979: Forced secondary circulations in hurricanes, *J. Geophys. Res.*, **84**, 3173-3183.
- Willoughby, H. E., J. A. Clos and M. G. Shoreibah**, 1982: Concentric eye walls, secondary wind maxima, and the evolution of the hurricane vortex, *J. Atmos. Sci.*, **39**, 395-411.
- Willoughby, H. E., F. D. Marks and R. J. Feinberg**, 1984: Stationary and propagating convective bands in asymmetric hurricanes, *J. Atmos. Sci.*, **41**, 3189-3211.
- Willoughby, H. E.**, 1990a: Temporal changes of the primary circulation in tropical cyclones, *J. Atmos. Sci.*, **47**, 242-264.
- Willoughby, H.E.**, 1990b: Gradient balance in tropical cyclones, *J. Atmos. Sci.*, **47**, 265-274.
- Willoughby, H.E.**, 1991: Reply, *J. Atmos. Sci.*, **48**, 1209-1212.

- Willoughby, H. E.**, 1992: Linear motion of a shallow water barotropic vortex as an initial value problem, *J. Atmos. Sci.*, **49**, 2015-2031.
- Willoughby, H.E.**, 1995: *Mature structure and evolution*, Global perspectives on tropical cyclones, World Meteorological Organization, TCP-38, Geneva, 62 pp.
- Wirth, V., H. Borth, J. -F. Lopez, W. -G. Panhans, M. Riemer and T. Szabo**, 2005: Dynamics in the extratropical tropopause region: a case of transition between dynamically active and passive tracer advection? , *Q. J. Roy. Meteor. Soc.* **131**, 247-258.
- World Meteorological Organisation (WMO)**, 1995: *Scientific Assessment of Ozone Depletion 1994*, WMO 37, Geneva, Switzerland.
- Woodman, R.F.**, 1985: Spectral moments estimation in MST radars, *Radio Sci.*, **20**, 1185-1195.
- Woodman, R. F. and A. Guillen**, 1994: Radar observations of winds and turbulence in the stratosphere and mesosphere, *J. Atmos. Sci.*, **31**, 493-505.
- Worthington, R. M.**, 1999: Alignment of mountain wave patterns above Wales: A VHF radar study during 1990-1998, *J. Geophys. Res.*, **104**, 9199-9212.
- Xu, Q.**, 1983: Unstable spiral inertial gravity waves in typhoons, *Sci. Sin.*, **26**, 70-80.
- Yamamoto, R.**, 1963: A dynamical theory of spiral rain band in tropical cyclones, *Tellus*, **15**, 153-161.
- Yamanaka, M. D., S.-Y. Ogino, S. Kondo, T. Shimomai, S. Fukao, Y. Shibagaki, Y. Maekawa and I. Takayabu**, 1996: Inertio-gravity waves and subtropical multiple tropopauses: Vertical wavenumber spectra of wind and temperature observed by the MU radar, radiosondes and operational rawinsonde network, *J. Atmos. Terr. Phys.*, **58**, 785-805.
- Yamasaki, M.**, 1986: A three-dimensional tropical cyclone model with parameterized cumulus convection, *Papers Meteor. Geophys.*, **37**, 205-234.
- Zangl, G. and V. Wirth**, 2002: Synoptic-scale variability of the polar and subpolar tropopause: Data analysis and idealized PV inversions, *Quart. J. Roy. Meteor. Soc.*, **128**, 2301-2315.
- Zeng, G. and J. A. Pyle**, 2005: Influence of El Nino Southern Oscillation on stratosphere/troposphere exchange and the global tropospheric ozone budget, *Geophys. Res. Lett.*, **32**, L01814, doi:10.1029/2004GL021353.
- Zhou, X.L.**, 2000: *The tropical cold point tropopause and stratospheric water vapor*. Ph.D. dissertation, State University of New York at Stony Brook, 121 pp.

## PAPERS PUBLISHED IN JOURNALS & PROCEEDINGS

1. Parameswaran, K., M. N. Sasi, Geetha Ramkumar, Prabha. R. Nair, V. Deepa, B. V. Krishnamurthy, S. R. Prabhakaran Nair, K. Revathy, **G. Mrudula**, K. Satheesan, Y. Bhavani Kumar, V. Sivakumar, K. Raghunath, T. RajendraPrasad, and M. Krishnaiah: *Altitude profiles of temperature from 4 to 80 Km over the tropics from MST Radar and Lidar*, *J. Atmos. Solar Terr. Phys.*, **62**, 1327-1337, 2000.
2. Krishnamurthy, B.V., S. R. Prabhakaran Nair, K. Revathy, **G. Mrudula**, K. Satheesan, A. R. Jain: *Signature of the passage of ITCZ on wind profiles from MST Radar at Gadanki*, *Indian J. Radio Space Phys.*, **29**, 199-202, 2000.
3. Krishnamurthy, B.V., S. R. Prabhakaran Nair, K. Revathy, **G. Mrudula**, K. Satheesan, K. Parameswaran, M. N. Sasi, Prabha. R. Nair, Geetha Ramkumar, V. Deepa, Y. Bhavani Kumar, V. Sivakumar, K. Raghunath, T. RajendraPrasad, M. Krishnaiah: *Preliminary results of Equatorial Wave Experiment conducted from 18 January 1999 to 5 March 1999 with Lidar at Gadanki*, *Indian J. Radio Space Phys.*, **29**, 231-234, 2000.
4. Krishnamurthy, B.V., S. R. Prabhakaran Nair, K. Revathy, **G. Mrudula**, K. Satheesan, K. Parameswaran, M. N. Sasi, Prabha. R. Nair, Geetha Ramkumar, V. Deepa, Y. Bhavani Kumar, V. Sivakumar, K. Raghunath, M. Krishnaiah: *Equatorial Wave Experiment of 1999 Winter*, Proceedings of the Fifth User Scientists' Workshop, 61-62, 2001.
5. Revathy, K., **G. Mrudula**, S. R. Prabhakaran Nair and B. V. Krishnamurthy, *Diurnal evolution of temperature profile of troposphere and lower stratosphere using MST Radar*, *Indian J. Radio Space Phys.*, **30**, 315- 318, 2001.
6. **Mrudula G.**, and K Mohan Kumar, *Stratosphere – troposphere exchange during the passage of a tropical cyclone*, Dynamical Coupling in the Equatorial Atmosphere – Ionosphere System (DYCEAIS – 2002) (Extended Abstracts), Tirunelveli, 2002.
7. **Mrudula, G.**, K Mohan Kumar and K. Kishore Kumar, *Wind Characteristics of the Troposphere and Lower Stratosphere during the Passage of a Tropical Cyclone*, *J. Atmos. Solar Terr. Phys.*, Submitted after revision, 2005.
8. **Mrudula, G.**, K Mohan Kumar and Siddarth Shankar Das, *Lowering of the Tropopause Height Associated with a Tropical Cyclone Passage*, *Geophys. Res. Lett.*, Submitted, 2005.

## PAPERS PRESENTED IN SEMINARS

1. Krishnamurthy, B.V., S. R. Prabhakaran Nair, K. Revathy, **G. Mrudula**, K. Satheesan, A.R. Jain: *Signature of the passage of ITCZ on wind profiles from MST Radar at Gadanki*, Presented at *Third User Scientist's Workshop*, NMRF, Tirupati, 1999.
2. Krishnamurthy, B.V., S. R. Prabhakaran Nair, K. Revathy, **G. Mrudula**, K. Satheesan, K. Parameswaran, M. N. Sasi, Prabha. R. Nair, Geetha Ramkumar, V. Deepa, Y. Bhavani Kumar, V. Sivakumar, K. Raghunath, T. Rajendra Prasad, M. Krishnaiah: *Preliminary results of Equatorial Wave Experiment conducted from 18 January 1999 to 5 March 1999 with Lidar at Gadanki*, Presented at *Third User Scientist's Workshop*, NMRF, Tirupati, 1999.
3. Revathy, K., **G. Mrudula**, S. R. Prabhakaran Nair and B. V. Krishnamurthy, *Diurnal evolution of temperature profile of troposphere and lower stratosphere using MST Radar*, Presented at *Third User Scientist's Workshop*, NMRF, Tirupati, 1999.
4. Revathy, K., **G. Mrudula**, S. R. Prabhakaran Nair and B. V. Krishnamurthy, *Evaluation of temperature profile and its diurnal and seasonal variation*, Accepted for presentation at the *Ninth International Workshop on Technical and Scientific Aspects of MST Radar (MST 9)*, Toulouse, France, 2000 (INTERNATIONAL).
5. Revathy, K., **G. Mrudula**, S. R. Prabhakaran Nair and B. V. Krishnamurthy, *Evaluation of temperature profile using MST Radar - An automatic evaluation program*, Accepted for presentation at the *Ninth International Workshop on Technical and Scientific Aspects of MST Radar (MST 9)*, Toulouse, France, 2000 (INTERNATIONAL).
6. **Mrudula, G.**, K. Mohan Kumar, K. Kishore Kumar, A. R. Jain and D. N. Rao, *Wind characteristics of the troposphere and lower stratosphere during the passage of a tropical cyclone using MST radar*, Participated and presented at the workshop on *Studies of Tropical Mesoscale Convective System*, NMRF, Tirupati, 2002.
7. **Mrudula, G.**, and K. Mohan Kumar, *Stratosphere – troposphere exchange during the passage of a tropical cyclone*, Participated and presented at the Workshop on *Dynamical Coupling in the Equatorial Atmosphere – Ionosphere System (DYCEAIS – 2002)*, Tirunelveli, 2002.
8. Rajesh, J., **G. Mrudula** and K. Mohan Kumar, *Three dimensional wind characteristics in the troposphere and lower stratosphere over Gadanki during the 1996 monsoon*, Participated and presented at the Workshop on *Dynamical Coupling in the Equatorial Atmosphere – Ionosphere System (DYCEAIS – 2002)*, Tirunelveli, 2002.

9. **Mrudula, G., K. Mohan Kumar and K. Kishore Kumar, *A study on the tropospheric and lower stratospheric wind characteristics associated with the passage of a tropical cyclone over Gadanki***, Participated and presented at *Sixth User Scientists' Workshop* at **NMRF, Tirupati**, 26-27 February 2003.
10. **Mrudula, G., K. Mohan Kumar and Siddarth Sankar Das, *Tropical cyclone induced fluctuations in the height of the tropopause***, Participated and presented at *Sixth User Scientists' Workshop* at **NMRF, Tirupati**, 26-27 February 2003.
11. **Mrudula, G., K. Mohan Kumar and Siddarth Sankar Das, *Tropopause fluctuations during the passage of a tropical cyclone***, Participated and presented at *tenth international workshop on technical and scientific aspects of MST radar (MST10)* at **Piura, Peru**, 13- 20 May 2003 (INTERNATIONAL).
12. **Mrudula, G., K. Mohan Kumar and K. Kishore Kumar, *Three dimensional wind characteristics of troposphere and lower stratosphere during the passage of a tropical cyclone***, Participated and presented at the *IUGG General Assembly* at **Sapporo, Japan**, June 30 –July 11, 2003 (INTERNATIONAL).
13. **Mrudula, G., and K Mohan Kumar, *Troposphere- stratosphere interaction during a tropical cyclone passage over India***, Participated and presented at the *IUGG General Assembly* at **Sapporo, Japan**, June 30 –July 11, 2003 (INTERNATIONAL).
14. **Mrudula, G., K. Mohan Kumar and S. Abhilash, *Gravity wave observation during the passage of a tropical cyclone over India***, Participated and presented at the *Chapman Conference on Gravity Waves Processes and Parameterization* at **Hawaii, USA**, January 10 – 14, 2004 (INTERNATIONAL).
15. **Mohan Kumar, K., G. Mrudula and S. Abhilash, *Gravity wave generation associated with indian summer monsoon***, Participated and presented at the *Chapman Conference on Gravity Waves Processes and Parameterization* at **Hawaii, USA**, January 10 – 14, 2004 (INTERNATIONAL).
16. **Abhilash, S., G. Mrudula and K. Mohan Kumar, *Gravity wave observations and it's properties associated with tropical convection***, Participated and presented at the *Chapman Conference on Gravity Waves Processes and Parameterization* at **Hawaii, USA**, January 10 – 14, 2004 (INTERNATIONAL).
17. **Mrudula, G., and K Mohan Kumar, *Tropical cyclone and associated Stratosphere – Troposphere Exchange***, Participated and presented at the *SPARC General Assembly* at **Victoria, Canada**, August 1 – 7, 2004 (INTERNATIONAL).
18. **Mohan Kumar, K., and G. Mrudula, *Stratosphere – Troposphere Exchange during southwest and Northeast monsoon***, Participated and presented at the *SPARC General Assembly* at **Victoria, Canada**, August 1 – 7, 2004 (INTERNATIONAL).



G9410

19. Abhilash, S., K. Mohan Kumar, **G. Mrudula**, Siddarth Shankar Das, and K Kishore Kumar, *VHF radar observations on prominent features of gravity waves and weakening of tropopause associated with tropical convection*, Participated and presented at the *SPARC General Assembly at Victoria, Canada*, August 1 – 7, 2004 (INTERNATIONAL).
20. **Mrudula, G.** and K Mohan Kumar, *VHF radar observations of monsoon depressions in the Bay of Bengal*, Accepted for presentation in *Chapman Conference on Tropical-Extratropical Climatic Tele-connections, A Long-Term Perspective* At Hawaii, USA, February 1-8, 2005 (INTERNATIONAL).
21. **Mrudula, G.** and K Mohan Kumar, *Indian Summer Monsoon and Associated Dynamics Using VHF Radar Observations*, Accepted for presentation in *IAMAS 2005* at Beijing, China, August 2-11, 2005 (INTERNATIONAL).

